Mechanistical insights into the role of importin-α7 and ANP32 proteins on influenza A virus replication and pathogenicity in mammals

Doctoral Thesis

University of Hamburg

Faculty of Mathematics, Informatics and Natural Sciences

Department of Chemistry

Submitted by

Sebastian Beck

Hamburg, April 2020

Reviewer:	Prof. Dr. Gülşah Gabriel
Second Reviewer:	Prof. Dr. Michael Kolbe
Third Reviewer:	Prof. Dr. Martin Schwemmle

Date of Thesis Defense:	July 3, 2020
Approval for Publication:	July 3, 2020

Die vorliegende Arbeit mit dem Titel „Mechanistical insights into the role of importin-α7 and ANP32 proteins on influenza A virus replication and pathogenicity in mammals“ wurde im Zeitraum vom 01. Juni 2016 – 06. April 2020 am Heinrich-Pette-Institut, Leibniz-Institut für Experimentelle Virologie (Abteilung 61: *Virale Zoonosen – One Health*) in Hamburg angefertigt.

List of publications

1. **Beck, S.[#]**, Zickler, M., Pinho dos Reis, V., Günther, T., Grundhoff, A., Reilly, P.T., Mak, T.W., Stanelle-Bertram, S., and Gabriel, G. *ANP32B Deficiency Protects Mice From Lethal Influenza A Virus Challenge by Dampening the Host Immune Response.* Front Immunol, 2020. **11**: p. 450.

2. Thiele, S., Stanelle-Bertram, S., **Beck, S**., Mounogou Kouassi, N., Zickler, M., Müller, M., Tuku, B., Resa-Infante, P., van Riel, D., Alawi, M., Günther, T., Rother, F., Hügel, S., Reimering, S., McHardy, A., Grundhoff, A., Brune, W., Osterhaus, A., Bader, M., Hartmann, E., and Gabriel, G. *Cellular importin-α3 expression dynamics in the lung regulate antiviral response pathways against influenza.* Cell Reports (*accepted*), 2020.

3. Tuku, B., Stanelle-Bertram, S., Sellau, J., **Beck, S**., Bai, T., Mounogou Kouassi, N., Preuß, A., Hoenow, S., Renné, T., Lotter, H., and Gabriel, G., *Testosterone protects against severe influenza by reducing pro-inflammatory cytokine response in the murine lung.* Frontiers in Immunology (*accepted*), 2020.

4. Resa-Infante, P., Bonet, J., Thiele, S., Alawi, M., Stanelle-Bertram, S., Tuku, B., **Beck, S.**, Oliva, B., and Gabriel, G. *Alternative interaction sites in the influenza A virus nucleoprotein mediate viral escape from the importin-alpha7 mediated nuclear import pathway.* FEBS J, 2019. **286**(17): p. 3374-3388.

5. Koc, C., Gerlach, D., **Beck, S.**, Peschel, A., Xia, G., and Stehle, T. *Structural and enzymatic analysis of TarM glycosyltransferase from Staphylococcus aureus reveals an oligomeric protein specific for the glycosylation of wall teichoic acid.* J Biol Chem, 2015. **290**(15): p. 9874-85.

[#] publication contains parts of the work presented in this thesis

Manuscripts *in preparation*

1. **Beck, S.[#]**, Zickler, M., Hoffmann, J., Thiele, S., Sohst, V., Buck, F., Klingen, T., McHardy, A., Krisp, C., Schlüter, H., Stanelle-Bertram, S., Gabriel, G. *The importin-α7 interactome as a platform to study molecular mechanisms of human-type influenza A virus replication and pathogenicity in mammals.* Molecular and Cellular Proteomics (*in preparation*), 2020.

2. Bai, T.*, Chen, Y.*, **Beck, S.***, Stanelle-Bertram, S., Chen, T., Yang, J., Wang, L., Dong, J., Wang, D., Shu, Y., Gabriel, G., *Reduced testosterone levels in males correlate with increased immune responses and severe H7N9 influenza A virus infection.* Lancet Infectious Diseases (*in preparation*), 2020.

[#] manuscript contains parts of the work presented in this thesis

* shared first authorship

I. Table of contents

I. Table of contents 1

II. List of Abbreviations 7

III. List of Figures 13

IV. List of Tables 17

1. Zusammenfassung 21

2. Abstract 22

3. Introduction 23

3.1 Influenza A Viruses (IAV) 23

3.1.1 Taxonomy 23

3.1.2 Virion structure and genome organization 23

3.1.3 The viral replication cycle 26

3.1.3.1 Host cell attachment, receptor-mediated endocytosis and uncoating 27

3.1.3.2 Nuclear transport of the viral genome 28

3.1.3.3 Transcription and replication of the viral genome, synthesis of viral proteins 28

3.1.3.4 Trafficking of vRNPs, maturation of IAV membrane proteins, and budding from the cell membrane 30

3.1.4 Ecology, evolution and host spectrum 31

3.1.5 Avian influenza viruses 33

3.1.5.1 Low-pathogenic AIV (LPAIV) 33

3.1.5.2 Highly-pathogenic AIV (HPAIV) 34

3.1.5.3 AIV pathogenicity in humans and pandemic potential 34

3.1.6 Epidemiology 35

3.1.6.1 Epidemics 35

3.1.6.2 Pandemics 36

3.1.7 IAV pathogenesis in humans 37

3.1.8 Prevention and treatment of influenza in humans 38

3.1.8.1 Vaccines 38

3.1.8.2 Anti IAV therapeutics 39

3.1.9 Viral determinants of IAV species specificity and pathogenesis in mammals 41

3.1.9.1 The viral hemagglutinin 41
3.1.9.2 The viral polymerase 43
3.1.9.3 The viral neuraminidase 43
3.1.9.4 The viral non-structural protein 1 44
3.1.9.5 Other viral determinants of pathogenicity 45
3.1.10 Host determinants of IAV species specificity and pathogenesis in mammals 45
3.1.10.1 Importin-α isoforms 46
3.1.10.2 ANP32 proteins 48
3.2 Nucleocytoplasmic transport *50*
3.2.1 The importin-α protein family 50
3.2.1.1 Classification of importin-α isoforms 50
3.2.1.2 Structure of importin-α isoforms 50
3.2.1.3 Functional diversity of importin-α isoforms 52
3.2.2 Nucleocytoplasmic transport in the cell 52
3.2.2.1 The classical importin-α/importin-β_1 mediated nuclear import pathway 54
3.3 Aim of this study *55*
4. Materials and Methods 56
4.1 Materials *56*
4.1.1 Chemicals and disinfectants 56
4.1.2 Buffers and solutions 59
4.1.3 Manufactured solutions, reagents and reaction systems (kits) 63
4.1.4 Antibodies 65
4.1.5 Enzymes 67
4.1.6 Plasmids and vectors 68
4.1.7 DNA oligonucleotides (Sanger Sequencing, PCR, Genotyping) 72
4.1.8 DNA oligonucleotides (qRT-PCR) 75
4.1.9 RNA oligonucleotides (siRNA) 77
4.1.10 Narcotics and supplements 78
4.1.11 Bacterial strains 78
4.1.12 Media and supplements for bacterial cell culture 78
4.1.13 Eukaryotic cell lines 79
4.1.14 Media and supplements for eukaryotic cell culture 80
4.1.15 Virus strains 83

4.1.16 Experimental mouse lines 84
4.1.17 Consumables 85
4.1.18 Safety gear 87
4.1.19 Laboratory equipment 88
4.1.20 Software 91
4.2 Methods *93*
4.2.1 Microbiological techniques 93
4.2.1.1 Cultivation of bacteria 93
4.2.1.2 Preparation of plasmid DNA 93
4.2.2 Cell culture techniques 93
4.2.2.1 Cultivation of eukaryotic cells 93
4.2.2.2 Freezing and thawing of eukaryotic cells 94
4.2.2.3 Authentication of human cell lines 94
4.2.2.4 Mycoplasma PCR 95
4.2.3 Nucleic acid techniques 95
4.2.3.1 Analytical digestion of plasmid DNA 95
4.2.3.2 Agarose gel electrophoresis 96
4.2.3.3 Isolation of total RNA from eukaryotic cells or murine tissue 96
4.2.3.4 Polymerase chain reaction (PCR) 96
4.2.3.5 Site-directed mutagenesis PCR and digestion with DpnI 97
4.2.3.6 Reverse transcription PCR (RT-PCR) 98
4.2.3.7 Purification of PCR products 99
4.2.3.8 Preparative digestion of PCR products with restriction endonucleases 100
4.2.3.9 Gel extraction of plasmid DNA 100
4.2.3.10 Ligation of DNA fragments into expression vectors 100
4.2.3.11 Transformation of chemically-competent *E. coli* bacteria 101
4.2.3.12 Sanger sequencing of plasmid DNA 102
4.2.3.13 Quantitative real-time reverse transcription PCR (qRT-PCR) 102
4.2.3.14 Next generation sequencing (NGS) 104
4.2.3.15 Transfection of eukaryotic cells 105
4.2.4 Protein biochemical methods 106
4.2.4.1 Protein knockdown in eukaryotic cells using specific siRNAs 106
4.2.4.2 Generation of eukaryotic knockout cell lines using CRISPR/Cas 107
4.2.4.3 Preparation of total protein lysates from eukaryotic cells 107

4.2.4.4 SDS-PAGE and Western blot 108
4.2.4.5 Co-immunoprecipitation and SILAC mass spectrometry 109
4.2.4.6 vRNP reconstitution assay (vRNP-RA) 113
4.2.4.7 Multiplex immunoassay 114
4.2.5 Virological techniques 114
4.2.5.1 Generation of recombinant influenza A viruses using reverse genetics 114
4.2.5.2 Propagation of influenza A virus on MDCK cells 116
4.2.5.3 Hemagglutination assay with chicken erythrocytes 116
4.2.5.4 Infection of eukaryotic cells with influenza A viruses 116
4.2.5.5 Determination of viral titers by plaque test (PT) 117
4.2.6 Histological techniques 118
4.2.6.1 Preparation of murine lung tissue for histology 118
4.2.6.2 Hematoxylin and eosin (H/E) staining of murine lung tissue 120
4.2.6.3 Immunohistochemical (IHC-P) staining of viral antigen in murine lung tissue 120
4.2.7 Microscopy techniques 122
4.2.7.1 Confocal fluorescence microscopy 122
4.2.7.2 Visualization of H/E or IHC-P stained murine lung tissue 123
4.2.8 Animal experiments 123
4.2.8.1 Generation, breeding and genotyping of ANP32 knockout mice 123
4.2.8.2 Narcosis, infection and euthanization of mice 125
4.2.8.3 Weight loss and survival experiments 125
4.2.8.4 Harvesting of blood and organs 126
4.2.8.5 Isolation and culturing of murine lung fibroblasts 126
4.2.9 *In silico* analyses 127
4.2.9.1 Visualization of importin-α7 – ANP32A interaction using *Pymol* 127
4.2.9.2 Evaluation of pre-processed mass spectrometry data 127
4.2.9.3 Visualization of MS-derived interactome data using *STRING* and Cytoscape software 128
4.2.9.4 Visualization of NGS-derived transcriptomic data using *ClustVis* 128
4.2.9.5 Gene ontology analyses using the ToppGene Suite 128
4.2.9.6 Alignment of nucleic and amino acid sequences 128
4.2.10 Statistical evaluations 129

5. Results 130

5.1 The importin-α interactome as a platform to study molecular mechanisms of IAV replicative fitness in human cells 130

5.1.1 Establishment of a SILAC-based mass spectrometry approach to identify importin-α interaction partners in human cells 130

5.1.2 The importin-α interactome in uninfected or influenza infected human cells 133

5.1.3 Importin-α7 interacting cellular factors and their role in influenza infection 138

5.2 Interplay of importin-α7 and ANP32A in promoting human-type IAV replicative fitness in human cells 142

5.2.1 Nuclear transport of ANP32A occurs via the importin-α pathway 142

5.2.2 Importin-α7 promotes $PB2_{627K}$ IAV polymerase activity independently of ANP32A ... 146

5.2.3 ANP32A promotes IAV replicative fitness independently of importin-α7 148

5.3 Role of ANP32 proteins on $PB2_{627K}$ IAV replication and pathogenicity in mammals 152

5.3.1 Phylogenetic analysis of human and murine ANP32 proteins 152

5.3.2 ANP32B, but not ANP32A promotes IAV pathogenicity in mice 152

5.3.2.1 Confirmation of ANP32 knockout in the murine lung and brain 152

5.3.2.2 IAV pathogenesis in $ANP32A^{+/+}$ and $ANP32A^{-/-}$ mice 153

5.3.2.3 IAV pathogenesis in $ANP32B^{+/+}$ and $ANP32B^{-/-}$ mice 154

5.3.3 ANP32B is required for IAV replication in mice and in murine cells 155

5.3.3.1 Viral replication in the lung and brain of $ANP32A^{+/+}$ and $ANP32A^{-/-}$ mice 155

5.3.3.2 Viral replication in the lung and brain of $ANP32B^{+/+}$ and $ANP32B^{-/-}$ mice 156

5.3.3.3 Viral replication and cell tropism in the lung of infected $ANP32A^{-/-}$ and $ANP32B^{-/-}$ mice 157

5.3.3.4 Viral replication in murine cells lacking the ANP32A or ANP32B genes 158

5.3.4 ANP32B contributes to IAV replicative fitness in human cells 159

5.3.5 Pro-inflammatory immune response is reduced in ANP32B-deficient mice 161

5.3.6 Transcriptome in infected $ANP32B^{-/-}$ mice reveals global changes in pro-inflammatory gene expression 163

6. Discussion 169

6.1 The role of importin-α-mediated nuclear transport in human health and disease 169

6.1.1 Diverse cargo binding specificities are a hallmark of importin-α function 170

6.1.2 Comprehensive analysis of importin-α7 interacting cellular factors in influenza infected human cells 170

6.1.3 Dual role of importin-α7 interacting cellular factors during influenza infection 173

6.2 The importin-α7 interactome as platform to study molecular mechanisms of IAV replication and pathogenesis 175

6.2.1 ANP32A uses the classical importin-α/importin-β_1 pathway for nuclear import 176

6.2.2 Importin-α7 and ANP32A promote high-level IAV replicative fitness by functionally-independent and spatially-separated mechanisms 177

6.2.3 The molecular mechanism underlying importin-α7 function during IAV infection – Current theories and concepts 181

6.3 Species-dependent ability of ANP32 proteins to promote IAV replication and pathogenesis in mammals 184

6.3.1 Differential role of ANP32A and ANP32B during influenza infection in mammalian hosts 184

6.3.2 Is ANP32B as a novel key regulator of inflammation and immunity in mice? 188

6.4 Conclusion 189

7. Literature 190

8. Appendix 212

8.1 List of hazardous substances according to GHS classification 212

8.2 Supplemental information accompanying chapter 5.1 217

8.3 Supplemental information accompanying chapter 5.3 250

9. Danksagung 263

10. Affidavit 266

II. List of Abbreviations

The abbreviations of amino acids, chemical elements/compounds (e.g. NaCl, sodium chloride) and SI units are considered to be known according to common literature and are therefore not listed here.

°C	degree Celsius
µg	microgram
µl	microliter
5'-m7G-cap	5'-N7-methylguanosin cap
AA	amino acid
ACN	acetonitrile
ADs	adamantanes
AIV	avian influenza virus
Amp	ampicillin
ANP32	acidic leucine-rich nuclear phosphoprotein 32
APS	ammonium peroxidisulfate
ARDS	acute respiratory distress syndrome
ARM	armadillo
ATP	adenosine triphosphate
avANP32A/B	avian ANP32A/B
BCS	basic cleavage site
BGH	bovine growth hormone
bp	base pair
BSA	bovine serum albumin
BSL	biosafety level
C-	carboxy-terminal
C/C	cytokines and chemokines
CAS	cellular apoptosis susceptibility
Cas9	CRISPR-associated protein 9
CBC	cap-binding complex
cDNA	complementary DNA
CMV	cytomegalovirus

CO_2	carbon dioxide
CoIP	co-immunoprecipitation
CRISPR	clustered regularly interspaced short palindromic repeats
Crm1	chromosome maintenance 1
cRNA	complementary RNA
cRNP	complementary ribonucleoprotein
CTD	carboxy-terminal domain
Ctrl	control
d p.i.	days post infection
DDA	data-dependent acquisition
ddH_2O	double distilled H_2O
DMEM	Dulbecco's Modified Eagle's Medium
DMSO	dimethylsulfoxide
DNA	deoxyribonucleic acid
dNTP	2'-deoxynucleotide-5'-triphosphate
DTT	dithiotreitol
E. coli	Escherichia coli
e.g.	example given
EDTA	ethylendiamine tetraacetate
ER	endoplasmic reticulum
FBS	fetal bovine serum
FD	fast digest
FG	phenylalanine – glycine
fwd	forward
g	gram
GAPDH	glycerinealdehyde 3'-phosphate dehydrogenase
GC	guanine – cytosine
GFP	green fluorescent protein
GO	gene ontology
GTP	guanosine triphosphate
h	hour
h p.i.	hours post infection
h p.t.	hours post transfection

H_2O	water
HA_0	hemagglutinin precursor protein
HA_1	hemaggluttinin subunit 1
HA_2	hemaggluttinin subunit 2
hANP32A/B	human ANP32A/B
HF	high fidelity
HPAIV	highly pathogenic avian influenza virus
HPD	host pathogenicity determinant
HPI	Heinrich Pette Institute
HRP	horse radish peroxidase
HSV	herpes simplex virus
i.e.	id est
i.p.	interperitoneal
IAA	iodoacetamide
IAV	influenza A virus
IBB	importin-β_1 binding domain
IBV	influenza B virus
INHAT	inhibitor of acetyl transferase
kb	kilo base pairs
kDa	kilodalton
KPNA	karyopherin
L	liter
LB	Luria broth
LCAR	low-complexity acidic region
Log2FC	log_2FoldChange
LPAIV	low pathogenic avian influenza virus
LRR	leucine-rich repeat
LRT	lower respiratory tract
M	molar
M1/2	matrix protein 1/2
mANP32A/B	murine ANP32A/B
MEM	Minimum Essential Medium
mg	milligram

min	minute
Mio.	million
ml	milliliter
mLF	murine lung fibroblasts
mM	millimolar
MOI	multiplicity of infection
mRNA	messenger RNA
N-	amino-terminal
NA	neuraminidase
NAIs	neuraminidase inhibitors
NCBP1/2	nuclear cap-binding protein 1/2
NEP	nuclear export protein
NF-κB	nuclear factor κB
NLS	nuclear localization signal
nm	nanometer
nM	nanomolar
NP	nucleoprotein
NPC	nuclear pore complex
NS1	non-structural protein 1
NUP	nucleoporin
OD_{600}	optical density at wavelength 600 nm
ON	over night
ORF	open reading frame
P/S	penicillin – streptomycin
PA	polymerase acidic protein
PB1/2	polymerase basic protein 1/2
PBS	phosphate buffered saline
PBS-T	PBS, supplemented with Tween-20
PCR	polymerase chain reaction
PEI	polyethylenimine
PFA	paraformaldehyde
PFU	plaque-forming units
PLB	passive lysis buffer

pmol	picomol
PMSF	phenylmethylsulfonylfluoride
POM	membrane pore protein
PT	plaque test
qRT-PCR	quantitative reverse transcription PCR
Ran	Ras-related nuclear protein
RanBP5	Ran binding protein 5
RBS	receptor binding site
RdRp	RNA-dependent RNA polymerase
rev	reverse
RNA	ribonucleid acid
RNAP I/II	RNA polymerase I/II
RNP	ribonucleoprotein
RP	reversed phase
rpm	rounds per minute
RT	reverse transcriptase
RT	room temperature
RT-PCR	reverse transcription PCR
S & G	Stop & Glo
SA	sialic acid
SD	standard deviation
SDM	site-directed mutagenesis
SDS	sodium dodecylsulfate
SDS-PAGE	SDS polyacrylamide gel electrophoresis
sec	second
siRNA	small-interfering RNA
SNP	single nucleotide polymorphism
snRNA	small nuclear RNA
SOP	standard operating procedure
STAT	signal transducer and activator of transcription
SUMO	small ubiquitin-like modifier
SV 40	simian virus 40
TAE	tri-acetate-EDTA

TBS	tris buffered saline
TEMED	tetramethylethylendiamine
TF	transfection
TK	thymidine kinase
T_M	melting temperature
TMD	transmembrane domain
Tris	tris(hydroxymethyl)aminomethane
U	unit (enzymatic activity)
URT	upper respiratory tract
V	volt
VPD	viral pathogenicity determinant
vRNA	viral RNA
vRNP	viral RNP
vRNP-RA	vRNP reconstitution assay
WB	Western blot
WHO	world health organization
WL/S	weight loss and survival
WT	wild type
x g	gravity
β_1	importin-β_1
ΔIBB	deleted importin-β_1 binding domain

III. List of Figures

Figure 1: Structure of the influenza A virion. 24

Figure 2: Schematic diagram of the influenza A virus replication cycle. 27

Figure 3: Influenza A virus genome replication and transcription. 30

Figure 4: Interspecies transmission of IAV. 32

Figure 5: Drugs approved for prevention and treatment of uncomplicated or severe influenza disease. 40

Figure 6: Structural and functional characteristics of mammalian importin-α isoforms. 51

Figure 7: The classical, importin-α/β-mediated nuclear import cycle. 53

Figure 8: A co-immunoprecipitation coupled with SILAC mass spectrometry approach to determine the importin-α interactome in human cells. 131

Figure 9: Confirmation of efficient importin-α pulldown in co-immunoprecipitated samples from SILAC-MS experiments....132

Figure 10: The combined importin-α1, -α5 and -α7 interactome in uninfected HEK293T cells....135

Figure 11: The combined importin-α1, -α5 and -α7 interactome in influenza infected HEK293T cells....137

Figure 12: The combined importin-α7 interactome in uninfected and influenza infected HEK293T cells....138

Figure 13: Confirmation of the importin-α7 – ANP32A interaction by Western blotting. 141

Figure 14: The C-terminus of ANP32A comprises a bona fide NLS motif. 142

Figure 15: Localization of GFP- or FLAG-tagged WT and mutNLS ANP32A variants in HEK293T cells....143

Figure 16: Mutation of the NLS motif in ANP32A disrupts its binding to importin-α5 and -α7....144

Figure 17: Modelling of the interaction of ANP32A with importin-α7 *in silico*. 145

Figure 18: Importin-α7 promotes IAV polymerase activity in the context of a balanced and functional nuclear transport machinery.....146

Figure 19: Importin-α7 promotes IAV polymerase activity independently of ANP32A. 148

Figure 20: ANP32A variants with mutations in the NLS motif retain their ability to promote high-level viral polymerase activity in human cells. 149

Figure 21: ANP32A promotes viral polymerase activity in human cells independently of importin-α7.....150

Figure 22: Confirmation of ANP32 protein knockout in the lung and brain of ANP32A$^{-/-}$ and ANP32B$^{-/-}$ mice. 153

Figure 23: Influenza A virus pathogenesis is not affected in ANP32A$^{-/-}$ mice.....154

Figure 24: Improved survival in ANP32B$^{-/-}$ mice challenged with human influenza isolates. 155

Figure 25: ANP32B deficiency impairs influenza A virus replication in mice. 156

Figure 26: ANP32B deficiency impairs influenza A virus replication in bronchial and alveolar murine lung tissue at 3 days post infection.....157

Figure 27: Establishment of murine lung fibroblast cell lines deficient for ANP32 proteins. 158

Figure 28: H3N2 and H5N1 virus replication is severely reduced in murine lung fibroblast cells derived from ANP32B$^{-/-}$ mice. 159

Figure 29: Generation of human HeLa cells with a deleted ANP32B gene. 159

Figure 30: H3N2 and H5N1 IAV replication is reduced in human HeLa cells lacking ANP32B. 160

Figure 31: Reduced cytokine and chemokine response in IAV infected ANP32B$^{-/-}$ mice. 162

Figure 32: Gene ontology analysis of disregulated genes in ANP32B$^{+/+}$ mice during influenza infection. 164

Figure 33: Global expression profile of inflammatory genes in ANP32B$^{+/+}$ mice during influenza infection. 165

Figure 34: Gene ontology analysis of disregulated genes in ANP32B$^{+/+}$ vs. ANP32B$^{-/-}$ mice during influenza infection. 166

Figure 35: Global expression profile of inflammatory genes in ANP32B$^{+/+}$ vs. ANP32B$^{-/-}$ mice during influenza infection. 167

Figure 36: Viral replication in infected ANP32B$^{+/+}$ and ANP32B$^{-/-}$ mice. 168

Figure 37: Virus-induced cytokine responses are reduced in ANP32B$^{-/-}$ mice. 168

Figure 38: Importin-α7 and ANP32A promote human-type IAV replicative fitness by functionally-independent and spatially-separated mechanisms. 180

Figure 39: The molecular mechanism underlying importin-α7 function during influenza infection – Current theories and concepts. 182

Figure 40: Molecular mechanisms of IAV pathogenesis in ANP32B deficient mice. 187

Figure 41: Hazard pictograms. 216

Figure 42: Identification of importin-α1 interaction partners in influenza infected cells using a SILAC-based mass spectrometry approach. 217

Figure 43: Identification of importin-α5 interaction partners in influenza infected cells using a SILAC-based mass spectrometry approach. 227

Figure 44: Identification of importin-α7 interaction partners in influenza infected cells using a SILAC-based mass spectrometry approach. 239

Figure 45: Gene ontology (GO) enrichment analysis of clusters of importin-α1, -α5 and -α7 interacting cellular proteins in uninfected cells. 248

Figure 46: Gene ontology (GO) enrichment analysis of clusters of importin-α1, -α5 and -α7 interacting cellular proteins in influenza infected cells. 249

Figure 47: Knockout of ANP32A does not affect influenza A virus replication in mice. 250

Figure 48: Absence of ANP32A does not affect viral replication or cell tropism in the murine lung. 250

Figure 49: H3N2 IAV replication in ANP32A$^{+/+}$ and ANP32A$^{-/-}$ murine lung fibroblast cells 251

Figure 50: Viral nucleoprotein expression is reduced in ANP32B knockout human HeLa cells.....251

Figure 51: Comparable cytokine and chemokine response in IAV infected ANP32A$^{+/+}$ and ANP32A$^{-/-}$ mice. 252

Figure 52: Differentially regulated genes in influenza A virus infected ANP32B$^{+/+}$ mice. 253

Figure 53: Differentially regulated genes in influenza A virus infected ANP32B$^{+/+}$ versus ANP32B$^{-/-}$ mice. 258

IV. List of Tables

Table 1: Overview of the influenza A virus genome. 25

Table 2: Influenza pandemics since 1918. 36

Table 3: STR profile of authenticated human cell lines. 94

Table 4: Digestion of plasmid DNA with endonucleases. 95

Table 5: Setup of the PCR reaction (including cycling parameters). 97

Table 6: Setup of the PCR reaction for SDM (including cycling parameters). 98

Table 7: Setup of RT reaction for cDNA synthesis. 99

Table 8: Setup of preparative digestion of PCR products with restriction endonucleases. 100

Table 9: Setup of the T4 ligation reaction. 101

Table 10: Setup of Sanger sequencing reaction. 102

Table 11: Setup of cDNA synthesis using a random nonamer (p9) primer mix. 103

Table 12: Setup of quantitative amplification reaction using SYBR Green reagent. 103

Table 13: Usage of PEI and Lipofectamine 2000 (Lipo2k) for transfection of eukaryotic cells. 105

Table 14: Detailed parameters of transfection experiments. 106

Table 15: Preparation of SDS gels (4x). 108

Table 16: Summary of CoIP transfection conditions for SILAC MS using one representative combination of SILAC media. 112

Table 17: Summary of transfection conditions for the vRNP reconstitution assay. 113

Table 18: Summary of transfection for IAV A/WSN/33 (H1N1) rescue using reverse genetics. 115

Table 19: Parameters of PT in different multi-well formats. 117

Table 20: Dehydration and paraffin embedding procedure for histology. 118

Table 21: Deparaffinization and rehydration of FFPE sections prior to staining procedures. 119

Table 22: H/E staining procedure for murine lung tissue. 120

Table 23: Demasking of viral antigen in FFPE sections with Citrate Plus Buffer. 121

Table 24: Transfection of HEK293T cells for confocal fluorescence microscopy. 122

Table 25: Genotyping of ANP32A mice by PCR and agarose gel electrophoresis. 124

Table 26: Importin-α7 interacting cellular proteins and their role during influenza infection. 139

Table 27: Amino acid sequence similarity [%] of human and murine ANP32A and ANP32B proteins. 152

Table 28: List of hazardous substances according to GHS classification. 212

Table 29: Cellular proteins specifically precipitated with importin-α1 in uninfected cells (Mock). 218

Table 30: Cellular proteins specifically precipitated with importin-α1 in influenza (A/WSN/33, $PB2_{627K}$) infected cells (H1N1). 220

Table 31: Gene Ontology (GO) enrichment analysis of importin-α1 (WT, ΔIBB) interaction partners in uninfected cells (Mock). 223

Table 32: Gene Ontology (GO) enrichment analysis of importin-α1 (WT, ΔIBB) interaction partners in influenza (A/WSN/33, $PB2_{627K}$) infected cells. 225

Table 33: Cellular proteins specifically precipitated with importin-α5 in uninfected cells (Mock). 228

Table 34: Cellular proteins specifically precipitated with importin-α5 in influenza (A/WSN/33, $PB2_{627K}$) infected cells (H1N1). 232

Table 35: Gene Ontology (GO) enrichment analysis of importin-α5 (WT, ΔIBB) interaction partners in uninfected cells (Mock). 236

Table 36: Gene Ontology (GO) enrichment analysis of importin-α5 (WT, ΔIBB) interaction partners in influenza (A/WSN/33, $PB2_{627K}$) infected cells. 237

Table 37: Cellular proteins specifically precipitated with importin-α7 in uninfected cells (Mock). 240

Table 38: Cellular proteins specifically precipitated with importin-α7 in influenza (A/WSN/33, $PB2_{627K}$) infected cells (H1N1). 242

Table 39: Gene Ontology (GO) enrichment analysis of importin-α7 (WT, ΔIBB) interaction partners in uninfected cells (Mock). 245

Table 40: Gene Ontology (GO) enrichment analysis of importin-α7 (WT, ΔIBB) interaction partners in influenza (A/WSN/33, $PB2_{627K}$) infected cells. 246

Table 41: Significantly upregulated genes (Top20) in PBS vs. H3N2 infected $ANP32B^{+/+}$ mice at 3 days post infection, sorted by log2FoldChange (log2FC). 254

Table 42: Significantly downregulated genes (Top20) in PBS vs. H3N2 infected $ANP32B^{+/+}$ mice at 3 days post infection, sorted by log2FoldChange (log2FC). 255

Table 43: Significantly upregulated genes (Top20) in PBS vs. H5N1 infected $ANP32B^{+/+}$ mice at 3 days post infection, sorted by log2FoldChange (log2FC). 256

Table 44: Significantly downregulated genes (Top20) in PBS vs. H5N1 infected $ANP32B^{+/+}$ mice at 3 days post infection, sorted by log2FoldChange (log2FC). 257

Table 45: Significantly upregulated genes (Top20) in H3N2 infected $ANP32B^{+/+}$ vs. $ANP32B^{-/-}$ mice at 3 days post infection, sorted by log2FoldChange (log2FC). 259

Table 46: Significantly downregulated genes (Top20) in H3N2 infected $ANP32B^{+/+}$ vs. $ANP32B^{-/-}$ mice at 3 days post infection, sorted by log2FoldChange (log2FC). 260

Table 47: Significantly upregulated genes (Top20) in H5N1 infected $ANP32B^{+/+}$ vs. $ANP32B^{-/-}$ mice at 3 days post infection, sorted by log2FoldChange (log2FC). 261

Table 48: Significantly downregulated genes (Top20) in H5N1 infected ANP32B$^{+/+}$ vs. ANP32B$^{-/-}$ mice at 3 days post infection, sorted by log2FoldChange (log2FC) 262

1. Zusammenfassung

Influenza-A-Viren (IAV) können mittels Interspeziestransmission von ihrem natürlichen Reservoir über Zwischenwirte auf Menschen übergehen, wo das Virus schwere oder sogar tödliche Atemwegserkrankungen verursachen kann. Die Analyse der komplexen und dynamischen Virus-Wirt-Wechselwirkungen ist daher für die Entwicklung wirksamer Medikamente zur Behandlung einer schweren Influenza beim Menschen sowie für die Vorbereitung auf Pandemien von entscheidender Bedeutung. Die vorliegende Studie zielte daher darauf ab, mechanistische Einblicke in die Funktion von zwei Wirtszellfaktoren zu liefern, welche hauptsächlich zur Interspeziestransmission und Pathogenese von IAV in Säugetieren beitragen: Importin-α7, eine Komponente der zellulären Kernimportmaschinerie, sowie ANP32-Proteine.

Für Importin-α7 wurde zuvor postuliert, dass es indirekt die Polymeraseaktivität von human-adaptierten ($PB2_{627K}$) IAV fördert, indem es die subzelluläre Lokalisation anderer Wirtszellfaktoren reguliert. Zur Überprüfung dieser Hypothese wurde in dieser Studie das humane Importin-α7-Interaktom mittels Massen-Spektrometrie bestimmt. Mit Hilfe von Fluoreszenz-Mikroskopie konnte schließlich ANP32A als ein zelluläres Protein identifiziert werden, welches spezifisch Importin-α7 für den Kernimport nutzt. Unter Verwendung eines neu-etablierten Assays zur Bestimmung der viralen Polymeraseaktivität konnte jedoch gezeigt werden, dass Importin-α7 und ANP32A die replikative Fitness von $PB2_{627K}$-adaptierten IAV in humanen Zellen sowohl funktionell als auch räumlich unabhängig voneinander regulieren.

Bis heute ist unbekannt, ob die ANP32-Proteine, welche bisher primär in Zellkultur studiert wurden, auch die Replikation und Pathogenese von IAV *in vivo* unterstützen. In dieser Studie konnte jetzt gezeigt werden, dass der Knockout von ANP32A in der Maus keinen Einfluss hat auf den Virustropismus, die Immunantwort oder den Krankheitsverlauf. Im Gegensatz dazu führte die Infektion von ANP32B-defizienten Mäusen mit saisonalen H3N2 oder hoch-pathogenen H5N1 IAV zu einer signifikant verringerten Viruslast, einer stark reduzierten Immunantwort und in der Folge eine erhöhte Überlebensrate der infizierten Mäuse. Genomweite Transkriptomanalysen konnten außerdem zeigen, dass der Knockout von ANP32B das Immunsystem in einen anti-inflammatorischen Zustand versetzt. Dies deutet darauf hin, dass ANP32B eine bisher unbekannte Schlüsselfunktion bei der Regulation der antiviralen Immunität in Mäusen und möglicherweise auch im Menschen einnehmen könnte.

Zusammenfassend legen die hier vorgestellten Ergebnisse nahe, dass Importin-α7, ANP32B sowie deren regulierte Signalwege neue Ziele für die therapeutische Behandlung von schweren Influenza-Infektionen im Menschen darstellen könnten.

2. Abstract

Influenza A viruses (IAV) occasionally transmit from their natural reservoir via intermediate hosts to mammals, including humans. Here, the virus can cause severe and even fatal respiratory disease, posing a major health threat to the human population. Thus, deciphering the complex and dynamic virus-host interactions is essential for the development of effective countermeasures to prevent severe influenza in humans, as well as for pandemic preparedness. This study aimed to provide mechanistical insights in the function of two major host factors that have been implicated to drive IAV interspecies transmission and pathogenicity in mammals: Importin-α7, a member of the cellular nuclear import machinery, and ANP32. Importantly, the detailed mode-of-action underlying the function of these key host factors during influenza infection is still largely unknown.

For importin-α7, it was proposed before that it indirectly promotes human-type ($PB2_{627K}$) polymerase activity by regulating the subcellular localization of other host cell factors. To address this hypothesis, the human importin-α7 interactome was determined in this study using an unbiased proteomic approach. Coupled with fluorescence microscopy, ANP32A was identified as a cellular cargo protein that uses specifically importin-α7 for nuclear import. However, using a combined gain- and loss-of-function viral polymerase activity assay, it could be demonstrated that importin-α7 and ANP32A unfold functionally-independent and spatially-separated mode of actions in promoting $PB2_{627K}$ IAV replicative fitness in human cells.

Importantly, the role of ANP32 proteins during influenza infection has been mostly studied using *in vitro* cell culture systems. To address the question whether these host cell factors also promote human-type IAV replication and pathogenicity *in vivo*, a genetically modified knockout mouse model was used. Surprisingly, virus tropism, innate immune responses or disease outcome was not affected in IAV infected ANP32A knockout mice, compared to their wild type littermates. On the other hand, infection of mice lacking the ANP32B gene ($ANP32B^{-/-}$) with seasonal H3N2 or highly-pathogenic avian H5N1 IAV resulted in significantly reduced viral loads, pro-inflammatory immune responses and, in turn, increased survival upon otherwise lethal IAV challenge. Genome-wide transcriptome analyses further uncovered a global switch towards an anti-inflammatory state in IAV infected $ANP32B^{-/-}$ mice, indicating that ANP32B might be a novel key regulator of inflammation and immunity in mice, and perhaps also in humans.

In conclusion, the findings presented here suggest that targeting importin-α7, ANP32B or their regulated cellular pathways might present a novel approach to treat severe influenza in humans, by inhibiting viral replication and/or preventing virus-induced immunopathology.

3. Introduction

3.1 Influenza A Viruses (IAV)

3.1.1 Taxonomy

Phylogenetically, the family of *Orthomyxoviridae* comprises seven genera, including influenza A virus (IAV), influenza B virus (IBV), influenza C virus, influenza D virus, Thogotavirus, Quarjavirus and Isavirus [1, 2]. Since IAV are the main focus of this study, their biological, epidemiological and molecular characteristics will be described in more detail below.

IAV are classified according to their major surface glycoproteins, hemagglutinin (HA) and neuraminidase (NA), which also represent the antigenic part of the virus. To this date, 18 HA and 11 NA subtypes have been described, while H17 and H18 as well as N10 and N11 were only found in bats by sequence analyses [3, 4]. All subtypes, except for H17N10 and H18N11, have been detected in aquatic waterfowl which is therefore considered the natural reservoir of IAV [5]. The nomenclature of IAV includes the genus, the species from which it was isolated (unless human), the place of isolation, the number of the isolate, the year when it was isolated, and the virus subtype in brackets [6]. Two exemplary virus strains are: *A/Duck/Alberta/35/76 (H1N1)*, a virus isolated from Ducks, or *A/Vietnam/1194/04 (H5N1)*, a human isolate from a fatal case in Vietnam in 2004.

3.1.2 Virion structure and genome organization

Influenza a viruses are pleomorphic, and the virions can adopt either spherical or filamentous shapes of about 80 to 120 nm in diameter. In electron microscopy, the viral surface proteins HA and NA are visible as spike-like structures which are embedded into the host cell derived viral lipid bilayer membrane [7, 8]. The viral M2 (*matrix 2*) protein is also integrated into the membrane, while the inner part of the membrane is coated with the viral M1 (*matrix 1*) protein (**Figure 1**). Stoichiometrically, HA is the most abundant protein in the envelope, followed by NA and M2 [9]. Furthermore, host cell proteins are also incorporated into the virion during the budding process, but whether this has a functional consequence remains to be investigated [10].

Protected by the envelope and the inner M1 protein shell, the single-stranded, negative-sensed, segmented viral genome of about 13.6 kb in size lies within the viral particle as ribbon-like, superhelical structures (**Figure 1**). Each of the eight viral RNA (vRNA) segments of different length is associated via their conserved, semi-complementary 5'- and 3'-ends with a trimeric polymerase complex composed of PB1 (*polymerase basic protein 1*), PB2 (*polymerase basic*

protein 2) and PA (*polymerase acidic protein*), forming hairpin-shaped viral ribonucleoprotein complexes (vRNPs) [11-13]. Pre-association of the viral genome with the viral polymerase allows rapid transcription and replication upon infection of a host cell. Furthermore, the vRNAs are encapsulated by multiple copies of the viral NP (*nucleoprotein)* protein which has both structural and biological functions throughout the viral replication cycle. The non-coding 5'- and 3'-ends within each vRNA comprise regulatory promoter sequences for transcription [14, 15]. Furthermore, they regulate polyadenylation of viral mRNAs and coordinate the incorporation of complete viral genomes, composed of eight different vRNPs, into newly formed virions.

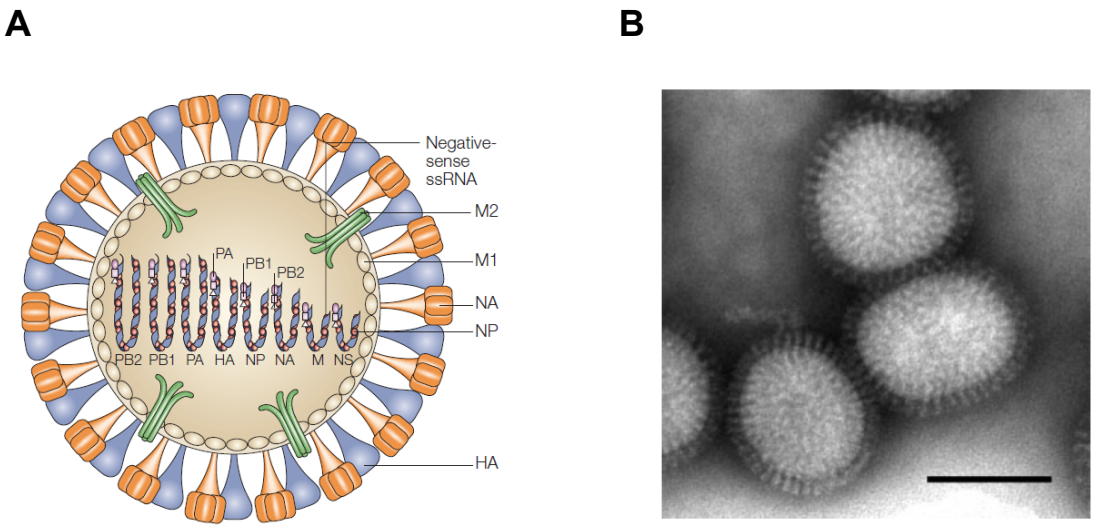

Figure 1: Structure of the influenza A virion. A, Schematic diagram of the influenza A virus. Each of the viral RNAs (vRNAs) is encapsulated by multiple copies of the viral nucleoprotein (NP) and associated with the viral polymerase heterotrimer (PB1, PB2, PA), forming superhelical viral ribonucleoprotein (vRNP) complexes. They are surrounded by a matrix, formed by the M1 matrix protein, and a lipid bilayer envelope, in which the viral glycoproteins hemagglutinin (HA) and neuraminidase (NA) as well as the M2 ion channel are inserted (adapted from [16]). **B,** Influenza A virions of the H1N1 subtype, visualized by electron microscopy. The HA and NA proteins appear as spike-like structures on the surface of the virion (adapted from [8]).

Via alternative splicing, ribosomal frameshifting or overlapping open reading frames (ORFs), the eight vRNAs encode for at least 18 proteins. All gene products and their respective functions are summarized in **Table 1**.

Table 1: Overview of the influenza A virus genome. Shown are the eight viral RNA segments and their encoded gene products with their respective functions (adapted from [6, 17-26]).

Segment	Length (bp)	Protein(s)	Size (kDa)	Protein function
1	2342	PB2	80	*Polymerase basic protein 2* Subunit of viral polymerase; 5'-cap recognition of cellular mRNAs
		PB2-S1	55	*Polymerase basic protein 2, variant S1* Localizes to mitochondria; inhibits Rig-I dependent interferon signaling; no effect on pathogenicity in mice
2	2341	PB1	90	*Polymerase basic protein 1* Subunit of viral polymerase; RNA elongation
		PB1-F2	10	*Polymerase basic protein 1, variant F2* Pro-apoptotic activity; interferon antagonism
		PB1-N40	82	*Polymerase basic protein 1, variant N40* Function unknown
3	2233	PA	83	*Polymerase acidic protein* Subunit of viral polymerase; endonuclease activity; serine protease activity
		PA-X	29	*Polymerase acidic protein, variant X* Modulation of host immune response; endonuclease activity
		PA-N155	62	*Polymerase acidic protein, variant N155* Function unknown
		PA-N182	60	*Polymerase acidic protein, variant N182* Function unknown

4	1778	HA	77	*Hemagglutinin* Surface glycoprotein; major antigen; receptor binding and fusion activities
5	1565	NP	55	*Nucleoprotein* RNA binding protein; synthesis of RNA; regulation of nuclear import of vRNPs
6	1413	NA	56	*Neuraminidase* Surface glycoprotein; major antigen; sialidase activity for virus release
7	1027	M1	28	*Matrix protein 1* vRNP interaction; vRNP nuclear export; viral budding
		M2	15	*Matrix protein 2* Transmembrane ion channel; release of vRNPs from endosomes; virus assembly
		M42	11	Matrix protein 42 Localization to Golgi; function unknown
8	890	NS1	26	*Non-structural protein 1* Interferon antagonism; regulation of host gene expression
		NEP/NS2	11	*Nuclear export protein / Non-structural protein 2* Nuclear export of vRNPs
		NS3	22	*Non-structural protein 3* Provides replicative gain-of-function

3.1.3 The viral replication cycle

The viral replication cycle (**Figure 2**) can be divided into four major parts, i.e. i) attachment to the host cell, receptor-mediated endocytosis and uncoating; ii) nuclear transport of the viral genome;

iii) transcription and replication of the viral genome, synthesis of viral proteins; and iv) trafficking of vRNPs, maturation of IAV membrane proteins, and budding from the cell membrane [27].

3.1.3.1 Host cell attachment, receptor-mediated endocytosis and uncoating

The cellular plasma membrane is the first barrier that IAV need to overcome. Here, glycoconjugates containing N-acetylneuraminic (sialic) acid (SA) residues that are present on the cell surface were identified as the primary receptors for the viral hemagglutinin [28]. While avian IAV preferentially use α2,3-linked SAs, mammalian-adapted IAV use α2,6-linked SAs. In the human respiratory tract, both α2,3- and α2,6-linked SA are present, with α2,3-linked SA mainly expressed in the lower respiratory tract (LRT) and α2,6-linked SA most prevalent in the upper respiratory tract (URT). The presence of α2,3-linked SA in the LRT might explain why humans can be infected with avian IAV, albeit with overall lower efficiency and reduced potential for airborne transmission [29-32].

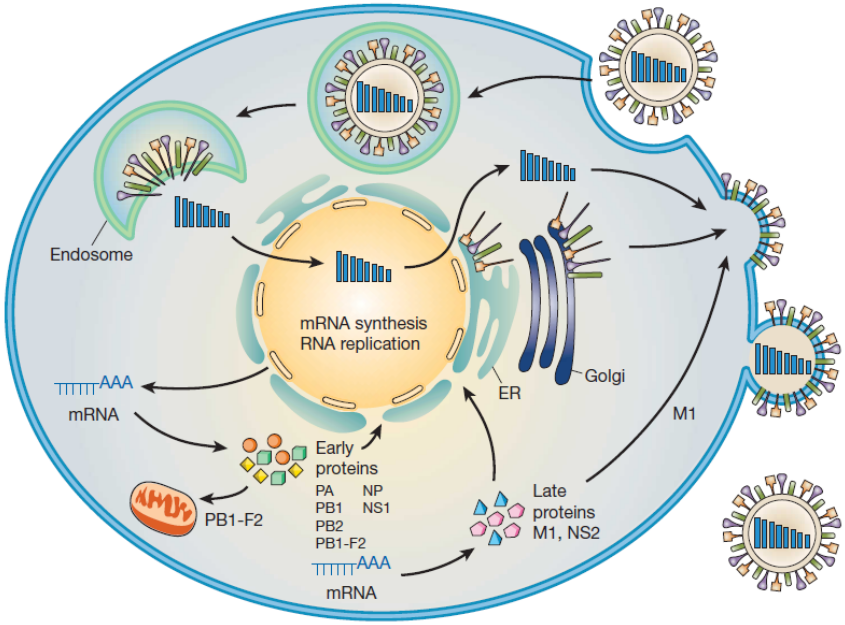

Figure 2: Schematic diagram of the influenza A virus replication cycle. After initial attachment to the cell, receptor-mediated endocytosis, and uncoating, the vRNP complexes are imported into the nucleus for replication and transcription of the viral genome. The early viral proteins (PA, PB1, PB2, NP) are transported back to the nucleus. Newly synthesized vRNPs are exported from the nucleus, mediated by the viral M1/NEP proteins, and transported to the apical site of the cell. Here, vRNPs are packaged and budding from the cell membrane is initiated via the viral surface proteins HA, NA, and M2. Through the sialidase function of NA, newly synthesized virions are released from the cell (adapted from [27]).

In most instances, IAV particles released from cells are already equipped with a proteolytically-activated HA protein composed of the larger subunit HA_1 and the smaller subunit HA_2, both of which are essential for the productive infection of a new cell [33, 34]. First, the virus attaches to the host cell by binding of HA_1 to SAs on the cell membrane. This binding triggers internalization of the virus, which can either occur via clathrin-dependent endocytosis [35, 36] or macropinocytosis [37, 38], and trafficking via the endosomal pathway until the virus particle resides in the late endosome [39]. Inside the endosome, the acidic environment leads to activation of the ion channel M2, an influx of protons and further acidification of the endosome [40, 41]. This has two functional consequences: i) the interaction of the vRNPs with the M1 protein shell is weakened [42, 43], and ii) the subunit HA_2 exposes a fusion peptide that after multiple conformational changes triggers the fusion of the viral and endosomal membranes [33, 34]. Finally, the vRNPs are released into the cytoplasm.

3.1.3.2 Nuclear transport of the viral genome

Once released from the endosome, the vRNPs need to gain access to the host cell nucleus where viral replication and transcription take place. Nuclear import in the cell is a tightly regulated process that is crucial to maintain cellular homeostasis. Detailed characteristics of this pathway are further discussed in chapter 3.2 (*Nucleocytoplasmic Transport*). Cellular proteins with a size larger than ~ 40 kDa cannot simply diffuse through the nuclear pores but rather require certain transport factors, one group of which is termed karyopherins (KPNAs) or importin-α isoforms [44]. Herein, importin-α binds to a cargo protein in the cytoplasm, recruits the co-receptor importin-β_1 and the heterotrimeric complex is translocated into the nucleus. Nuclear import of vRNPs has been shown to be primarily dependent on an unconventional nuclear localization sequence (NLS) in the viral NP protein [45, 46]. However, in-depth studies over the last decades have also revealed that each of the viral polymerase subunits contains NLS motifs and can therefore also be individually imported into the nucleus [47-49]. Interestingly, divergence of importin-α isoforms between different species was shown to be a key driver of IAV adaptation and interspecies transmission [50]. This phenomenon is further discussed in chapter 3.1.10.1.

3.1.3.3 Transcription and replication of the viral genome, synthesis of viral proteins

After transport of the incoming vRNPs into the nucleus, transcription of the viral genome is initiated first to ensure that high amounts of viral proteins are synthesized for all subsequent steps in the viral replication cycle, including genome replication and transcription (PB1, PB2, PA, NP), cellular export of viral mRNAs (M1/NEP), inhibition of the host immune response (NS1), and release of new infectious virions (HA, NA, M2).

Transcription of the viral genome is a primer-dependent process which in general is more efficient than unprimed viral replication as outlined below [51]. Both transcription and replication are performed by the viral RNA-dependent RNA polymerase (RdRP), composed of PB2, PB1 and PA [52]. Additionally, the viral nucleoprotein is essential for viral replication, either due to its intrinsic RNA binding activity or because it functions as an adapter molecule for host cell factors [53]. The primer for transcription is obtained through a process termed *cap snatching*. Herein, the PB2 subunit, through a direct interaction with the cellular RNA polymerase II carboxy-terminal domain (CTD) [54-56], binds to the 5'-N7-methylguanosin cap (5'-m7G-cap) structures of nascent cellular mRNAs or snRNAs (*small nuclear RNAs*) which in turn are cleaved off by the endonuclease activity residing in the PA subunit [25, 57]. This further inhibits host gene expression, aiding viral transcription. After positioning of the 5'-cap into the catalytic center of the PB1 subunit, it serves as template for viral mRNA synthesis [58]. In contrast to cellular polyadenylation via a specific poly(A)-polymerase, the polyA tail of viral mRNAs is directly encoded as a stretch of 5 to 7 uridine residues in the vRNAs. Most likely, a multi-step process of dissociation, repositioning and reannealing of the mRNA to this region of the vRNA is responsible for generating a polyA tail of sufficient length for nuclear export [59, 60].

Newly generated viral mRNAs are exported into the cytoplasm for the translation of the early viral proteins (PB1, PB2, PA, NP and NS1) on cytoplasmic ribosomes. Interestingly, the viral surface proteins HA, NA and M2, which later are required in the budding process, are synthesized and processed on endoplasmic reticulum (ER)-associated ribosomes [61]. Via cellular-like splice donor and acceptor sites, the primary M and NS mRNA transcripts are further processed by the cellular spliceosome to generate the M1/M2 and NS1/NEP transcripts, respectively [62-65]. Subsequently, the polymerase subunits are imported back into the nucleus for further transcription and genome replication. While NP and PB2 are imported via their individual NLS sequences following the classical importin-α/importin-β_1 pathway, PA and PB1 are transported to the nucleus as a heterodimer using the importin-β_1 homologue RanBP5 as shuttling factor [49]. The viral NS1 protein is also transported to the nucleus to inhibit interferon signaling, promoting efficient viral replication [66].

Replication of the negative-sensed vRNA is performed by the RdRP in an unprimed manner via a positive-sensed cRNA (*complementary RNA*) intermediate. This process relies on spontaneous annealing of free nucleoside triphosphates (NTPs; usually GTP or ATP) to the 3'-end of the vRNA, resulting in the formation of an A-G dinucleotide primer that initiates cRNA biosynthesis [52, 67-69]. In analogy to vRNPs, the generated cRNAs are coated by viral nucleoprotein and associate with the trimeric polymerase to form a cRNP intermediate. Finally,

multiple copies of vRNA are generated from the cRNPs. Both processes, viral transcription and genome replication, are illustrated in **Figure 3**.

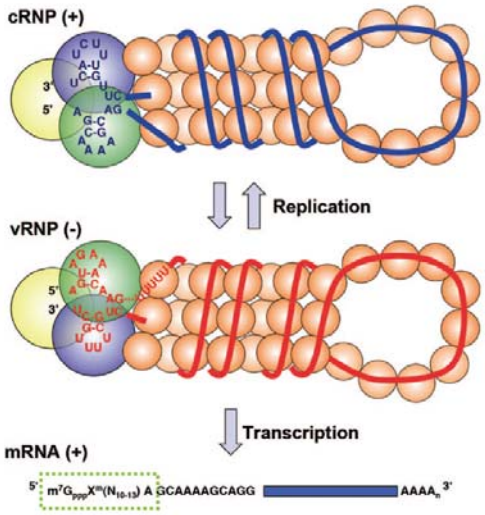

Figure 3: Influenza A virus genome replication and transcription. The incoming vRNPs are imported to the host cell nucleus for transcription and replication. First, transcription is initiated using 5'-cap structures from cellular mRNAs as primers (depicted in green box). 5'-capped and polyadenylated viral mRNAs are transported to the cytoplasm for translation on cytosolic (PB1, PB2, PA, NP, NS1, NEP, M1) or ER-associated (HA, NA, M2) ribosomes. Replication of the viral genome occurs via a cRNA intermediate in a primer-independent fashion. Spontaneous formation of an A-G dinucleotide initiates cRNA biosynthesis. After association with NP and a polymerase trimer, the resulting cRNP molecules are transcribed into multiple copies of vRNA (adapted from [70]).

The nuclear export of vRNPs is mediated via the cellular Crm1 (*chromosomal maintenance 1*) pathway. Herein, a current model suggests that the viral nuclear export protein (NEP) binds simultaneously to vRNPs, using M1 as an adapter protein, and cellular Crm1 to promote vRNP export [71-73].

3.1.3.4 Trafficking of vRNPs, maturation of IAV membrane proteins, and budding from the cell membrane

Once exported from the nucleus, the vRNPs are trafficked towards the plasma membrane by interacting with the microtubule-associated protein Rab11 [74]. Via intrinsic ER targeting sequences (i.e., the cleavage site in HA, and the transmembrane domains (TMDs) in NA and M2), the membrane proteins HA, NA and M2 are co-translationally directed to the ER lumen for

further processing and maturation (e.g. attachment of glycans) [75-80]. After oligomerization of HA and NA [81, 82], all three membrane proteins are transported to the plasma membrane via the *trans-Golgi* network. HA exits the ER as a fusion incompetent precursor protein (termed HA_0) and must be proteolytically activated, either by proteases residing in the *Golgi* network (e.g. Furin or TMPRSS2) or by proteases localized in the plasma membrane (e.g. HAT) [33, 83, 84]. The characteristic cleavage site in the HA_0, which can either be of mono- or multibasic nature, is an important pathogenicity determinant of avian influenza viruses (AIV) and will be discussed in detail in chapters 3.1.5 and 3.1.9.1 [85].

In order to assemble infectious virions, IAV have to target their membrane proteins (HA, NA, M2), vRNPs, and M1 protein to the same apical budding site on the plasma membrane. Most likely, this is a multi-factorial process involving several interactions of the viral proteins with each other as well as with components in the plasma membrane [61]. Likewise, the viral budding and scission process is likely based on an interplay between HA, NA, M1 and M2, all of which have been described to possess membrane-bending properties [61]. During budding, the sialidase activity of the homotetrameric NA protein facilitates virus release by local removal of SAs on the cell surface, thereby preventing HA binding and re-attachment to the cell [86-88]. Finally, infectious virus particles are released from the cell.

3.1.4 Ecology, evolution and host spectrum

The natural reservoir of IAV is aquatic waterfowl of the families *Anseriformes* and, to lesser extent, *Charadriformes* and *Laridae* [5, 89]. These families comprise a large number of different bird species, including geese, gulls, ducks, mallards, and ducks. IAV are highly adapted to this reservoir and rarely cause disease. All influenza virus subtypes (except for H17N10 and H18N11 which circulate in bats) have been observed and isolated from aquatic birds [5, 16]. Importantly, within the reservoir and particularly in ducks, IAV show a high genetic stability, suggesting an evolutionary stasis and no need for further adaptation [90]. Transmission of IAV between different bird species is believed to occur via the oral-fecal route by the uptake of contaminated food and water. Ducks, for instance, have been shown to shed high amounts of virus in the feces for up to 21 days after the initial infection [5, 91].

Occasionally, IAV can transmit from their natural reservoir to other species, including domestic poultry, pigs, horses, marine animals and humans, where they can cause severe and even fatal disease (**Figure 4**) [5, 92, 93]. Within the new host, a selective pressure drives adaptation and evolution of influenza viruses. During this process, adaptive mutations are selected that i) increase the replicative fitness of the virus (i.e., in the viral polymerase), ii) that enable efficient

transmission within a particular species (i.e., in the HA protein), and iii) that promote escape from the host immune system (i.e., in the antigenic surface glycoproteins, HA and NA) [94]. If these mutations are maintained, a new virus lineage is established [5]. The absence of a proof-reading activity in the viral RdRP (1 error/10^4 bases) is the basis for these mutations [95-97]. This process, which is termed *antigenic drift*, is the basis for the annual updates of the influenza vaccine [98]. However, even despite vaccination, mismatches in the vaccine to the currently circulating strains, risk factors (e.g. age or pregnancy) or genetic predispositions cause the seasonal influenza epidemics with up to 500.000 deaths every year (chapter 3.1.6.1) [99].

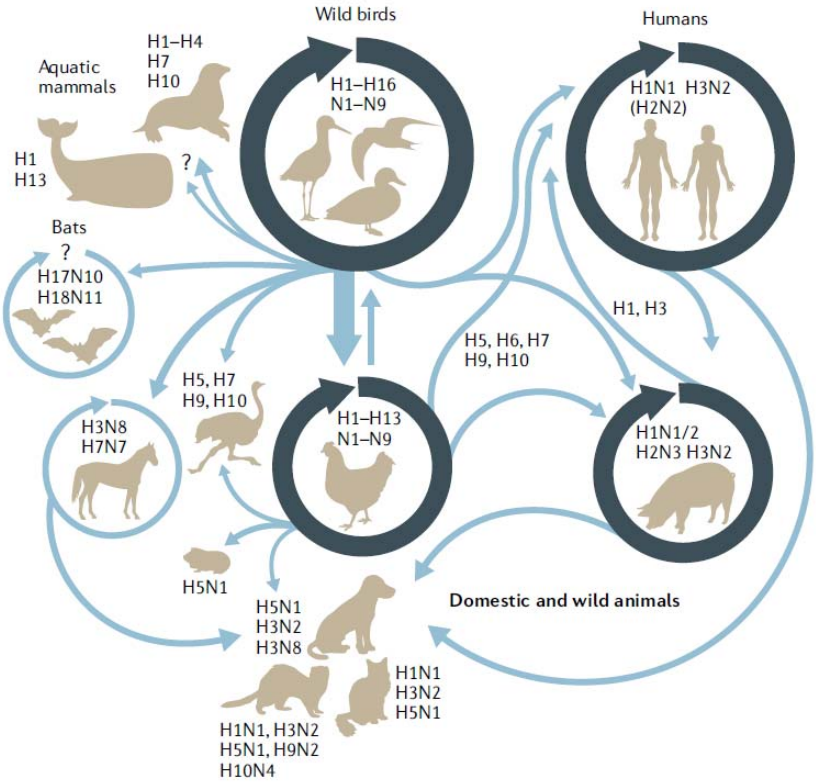

Figure 4: Interspecies transmission of IAV. The natural reservoir of IAV is aquatic waterfowl, comprising all HA and NA subtypes (H1-H16, N1-N9). From here, IAV occasionally transmit to other species, including domestic poultry, pigs and humans (black circles), but also domesticated animals (e.g. cats and dogs), bats (H17N10, H18N11), and even marine mammals. Transmission occurs either directly from the wild bird reservoir or via intermediate hosts. Three major subtypes have been or are still circulating in humans (H1N1, H2N2, H3N2), all of which have caused pandemics in the 20th and 21st century. Avian influenza viruses (e.g. H5 or H7) have been transmitted to humans via contact with infected poultry, causing high mortality rates, but currently lack sustained human-to-human transmission (adapted from [94]).Avian influenza viruses (AIV) are naturally restricted in mammalian cells [100].

However, in the rare event that a single mammalian cell is co-infected with an AIV and a mammalian-adapted strain, reassortment of viral genes can take place [27]. The pig, for example, has been described as a *mixing vessel* that promotes co-infection with viruses bearing avian- and mammalian-type HAs based on the presence of both α2,3- and α2,6-linked SAs on the cell surface [16, 101]. After reassortment, the newly formed virions might possess a highly productive mammalian-type polymerase, but at the same time maintain their avian-type viral surface antigens. If the HA acquires further mutations that promote airborne transmission and HA stability, these new viruses can jump-start a pandemic in an immunologically naïve human population [94]. This rapid reprogramming of viral genomes by reassortment is referred to as *antigenic shift*.

The human population faced four major influenza pandemics in the 20th and 21st century [102]. In chapter 3.1.6.2, the molecular and epidemiological characteristics of these pandemics are further discussed in detail.

3.1.5 Avian influenza viruses

Avian influenza viruses (AIV) can be distinguished into low-pathogenic (LPAIV) and highly-pathogenic (HPAIV) strains, based on differential virulence in birds and chickens due to distinct properties of the viral HA glycoprotein [16].

3.1.5.1 Low-pathogenic AIV (LPAIV)

The HA glycoprotein of influenza viruses, which mediates entry into the host cell via binding to sialic acids on the cell surface [16, 94], is an important determinant of viral pathogenicity, transmission and species specificity. This function highly depends on the post-translationally proteolytic activation of the HA_0 precursor protein by cellular proteases, residing either in the *Golgi* network, at the plasma membrane, or in the extracellular space (chapter 3.1.3.4) [33, 83, 84]. The cleavage site in the HA_0 protein further determines which proteases are able to cleave the HA_0 precursor into the active HA_1 and HA_2 subunits. LPAIV as well as seasonal IAV strains possess a mono-basic cleavage site (mono-BCS), characterized by a single arginine residue at the critical position [85]. In the avian host, proteases that cleave the mono-BCS are localized in the respiratory and intestinal tract. This restricts virus replication to a limited number of organs and thus causes only mild or even asymptomatic infections [16, 85]. In domestic poultry, symptoms after infection with LPAIV can include crouching, depression, reduced intake of food and water, weight reduction, diarrhea, mild respiratory symptoms, and a drop in egg production [103].

3.1.5.2 Highly-pathogenic AIV (HPAIV)

HPAIV, including the H5 and H7 subtypes, are characterized by a multi-BCS containing a series of basic amino acid residues at the cleavage site. In chickens, ubiquitously expressed proteases like furin or PC6 (*proprotein convertase 6*) are able to cleave and activate the HA_0 protein, leading to systemic virus replication, hemorrhages, multiple organ failure and often death within a couple of days after the initial infection [83, 104-106]. The molecular mechanisms underlying the switch from an avirulent AIV to a HPAIV by acquiring a multi-BCS are only poorly understood. However, available experimental data suggest two possible mechanisms: i) homologous recombination of the HA with ribosomal RNAs or non-homologous recombination with other IAV gene segments [106-112], and ii) polymerase slippage at purine-rich arginine or lysine codons, leading to the successive addition of basic amino acids [113-115].

HPAIV pose an enormous burden to the poultry industry as outbreaks usually require culling of entire flocks to control the infection.

3.1.5.3 AIV pathogenicity in humans and pandemic potential

Avian influenza viruses are highly adapted to their avian reservoir and thus direct interspecies transmission to humans and other mammals was considered a rare event. However, this dogma was challenged in 1997 when a H5N1 HPAIV was directly transmitted from birds to humans [116, 117]. After a major outbreak of H5N1 in Asian countries in 2003/2004, by the end of 2019, the World Health Organization (WHO) reported a cumulative number of 861 human infections with H5N1, including 455 deaths, which represents a mortality rate of approximately 52% [118]. Clinical and pathological symptoms of human H5N1 infection include high fever, destruction of alveolar tissue, and multiple organ failure, most likely due to hypercytokinemia which is characterized by a massive induction of pro-inflammatory cytokine and chemokine expression [119-121]. Although H5N1 viruses are not yet airborne transmissible, given the high mortality rates in humans, reassortment with seasonal IAV or acquisition of adaptive mutations that enable efficient human-to-human transmission might lead to the next influenza pandemic with a predicted devastating outcome for the human population [122-124]. Indeed, two studies showed that only a few mutations can cause H5N1 to become airborne transmissible between ferrets, highlighting the importance of continuous surveillance of circulating H5N1 viruses for pandemic preparedness [125, 126].

In addition to human infections with H5N1, in 2013, a new AIV of the subtype H7N9 emerged in mainland China causing five epidemic waves of human infections [127, 128]. As of September 2018, a total of 1657 human H7N9 infections and 615 associated deaths have been reported (mortality rate: 37%) [129]. While the H7N9 virus that caused the first four epidemic waves was

classified as a LPAIV based on the presence of a mono-BCS, during the fifth wave (2016/2017) an H7N9 HPAIV with a multi-BCS emerged that showed increased virulence and broader tissue tropism, but still no sustained human-to-human transmission [130, 131]. In the experimental setting, however, this H7N9 HPAIV has been shown to be transmissible between ferrets via respiratory droplets [132]. Therefore, as with H5N1, close monitoring of H7N9 HPAIV circulation and evolution in poultry is essential to assess the risk of it becoming a human pandemic virus in the future [133].

3.1.6 Epidemiology

3.1.6.1 Epidemics

As discussed in chapter 3.1.4, influenza viruses rapidly evolve through a mechanism termed *antigenic drift*, which is due to the error-prone viral polymerase [95]. This phenomenon is the basis for the seasonal influenza epidemics that usually occur during the winter months in the Northern hemisphere [134]. Albeit extensively studied, the mechanisms underlying influenza seasonality in temperate regions of the world are still not completely understood. However, it is generally accepted that low temperature as well as low relative and absolute humidity promote survival of viral particles in respiratory droplets, thereby increasing the rates of viral transmission [135, 136]. Additionally, social behavior in the winter season like indoor crowding could enhance contact transmission of IAV, particularly in the setting of primary schools [137]. On the molecular level, seasonal changes in the expression of certain metabolites with immune-regulatory functions (e.g. melatonin or vitamin D) might increase susceptibility to influenza [138, 139]. In the tropical and subtropical regions, the basis for influenza seasonality is even less well defined, with multiple peaks that coincide with the rainy seasons. Importantly, this needs to be considered in terms of vaccination timing and vaccine formulation in these climate zones [140, 141].

According to the WHO, three to five million people are infected with seasonal influenza viruses every year, of which 250.000 to 500.000 people die due to the infection or secondary complications [142]. Since influenza disease can last up to 14 days, it further places a substantial burden on worldwide economy. In 2015 in the United States, for instance, influenza disease caused an estimated average burden of $11.2 billion to health care systems and society [143]. Once more, these data highlight the importance of annual vaccination against influenza (chapter 3.1.8.1).

3.1.6.2 Pandemics

In addition to the annual influenza epidemics, global changes in the viral genome (*antigenic shift*), either due to accumulation of mutations or reassortment or a combination thereof, can lead to the emergence of antigenetically new viruses to which the human population has no existing immunity [27]. In general, the receptor binding properties of the viral HA protein are most critical for starting a pandemic. Herein, binding to human-type α-2,6-linked SAs, which are dominantly expressed in the URT of humans, is essential for efficient virus transmission via aerosols [31, 32]. Furthermore, in order to produce sufficient progeny virions for viral transmission, the viral polymerase needs to acquire adaptive mutations that confer high replicative fitness in human cells [144].

Table 2 summarizes the key molecular and epidemiological characteristics of the four major influenza pandemics of the 20th and 21st century.

Table 2: Influenza pandemics since 1918. Shown are the main molecular and epidemiological characteristics of the four major influenza pandemics of the 20th and 21st century (adapted from [102] and other references, as indicated).

Pandemic	Years	IAV subtype	Number of reported deaths	Molecular and epidemiological characteristics; [Reference]
Spanish flu	1918-1919	H1N1	40 – 50 million	Avian-like H1H1 precursor virus [145] High mortality in young age groups [145, 146] Often complications with secondary bacterial infections [147] Mono-BSC and thus infection largely confined to the respiratory tract [145, 148, 149] HA, the viral polymerase, NS1, and PB1-F2 contributed to high virulence, whereas HA and PB2 promoted transmissibility [150-157]
Asian flu	1957-1958	H2N2	1 – 2 million	Human/avian reassorted virus: HA, NA and PB1 of avian origin, while the remaining gene segments are from the 1918 lineage [16, 102, 158, 159] High mortality in younger age groups [102, 160]

Hong Kong flu	1968-1969	H3N2	0.5 – 2 million	Likely derived from reassortment of the 1957 H2N2 virus with an H3Nx AIV [161, 162] High mortality in younger age groups [102]
Swine flu	2009-2010	H1N1	up to 575.000	First and only pandemic of the 21st century, also known as *Mexican flu* or *New flu* [102] Rapid spread across the world, affecting over 122 countries in just 6 weeks [102] Originated from reassortment of North American H3N2 and H1N2 swine viruses with Eurasian avian-like swine viruses [27] High mortality in children, young healthy adults, and pregnant women [163] Since the 2009 pandemic, the WHO recommends to vaccinate pregnant women with highest priority [164] The 2009 pandemic H1N1 virus is nowadays circulating as a seasonal IAV in the human population [165]

3.1.7 IAV pathogenesis in humans

Influenza A viruses, the causative agents of the classical flu, are highly contagious and can be transmitted via droplets/aerosols, contact or smear infection. The infection is initiated by binding of the viral hemagglutinin to epithelial cells in the upper respiratory tract. After an incubation time of one to five days, the first symptoms include high fever, headache, muscle pain, and chills, all of which are due to the initial immune reaction towards the viral infection [166-168]. During the course of infection, other symptoms include loss of appetite, sore throat and dry cough. Also, diarrhea and nausea have been described as flu-associated symptoms [168, 169]. In healthy adults, the symptoms disappear after 7 to 10 days, although complete recovery may take days or even weeks, placing an enormous burden on health care systems and economy [168].

The most severe complication of influenza is primary viral pneumonia [169], which can occur even in healthy individuals but often manifests in high-risk groups, including pregnant women [170], immuno-compromised patients (e.g. after organ transplantation) [171], the elderly generation [172, 173], children below the age of two [174], and patients with chronic underlying

diseases (e.g. asthma) [142, 175, 176]. After the typical course of infection as outlined above, these patients suffer from breathing difficulties, caused by destruction of the lung epithelium layer. This is rapidly followed by hemorrhages, edema and, if untreated, progression to ARDS (*acute respiratory distress syndrome*), lung failure and hypoxia-induced death of the patient [169]. Increased permeability in the lung might also promote virus dissemination and lead to viremia [177, 178]. The causative IAV subtype can be a seasonally circulating strain, but particularly pandemic strains and HPAIV (e.g. H5N1 or H7N9) have been shown to induce high levels of pro-inflammatory cytokines (‘*cytokine storm’*) that ultimately cause the destruction of lung tissue and ARDS [27, 120, 179, 180]. Furthermore, HPAIV are able to replicate systemically and even reach the brain where they can cause encephalopathies in the central nervous system [181, 182].

In addition to viral pneumonia, other severe complications associated with IAV infection have been observed in the clinics, including myocarditis [183, 184], conjunctivitis [185], croup (often in children) [186], Reye’s syndrome [187, 188], and bacterial co-infections [189-191], for example caused by *S. pneumonia*, *S.aureus* or *H. influenzae*. The weakened immune system allows these pathogenic bacteria to colonize virus-infected tissue and organs, resulting in secondary bacterial pneumonia and even sepsis if the bacteria enter the blood stream.

Although differentiation from the common cold is difficult, the sudden onset of symptoms in combination with high fever (38-41 °C) is a reliable diagnostic marker for an influenza virus infection during a winter period [192]. However, only laboratory tests based on detection of viral antigen or viral RNA are able to clearly diagnose an influenza infection [166].

3.1.8 Prevention and treatment of influenza in humans

The annual flu vaccine is the most effective measure to prevent severe influenza complications, especially in risk groups like pregnant women, and spread of the infection to the community. However, these vaccines might not confer adequate protection against HPAIV or future pandemic IAV strains. Therefore, it is also essential to develop and stockpile larger portfolios of effective antivirals to combat life-threatening influenza. The following chapters summarize the current status on influenza vaccines and anti-influenza drugs.

3.1.8.1 Vaccines

Influenza vaccines are either produced using egg- or cell culture-based technologies. Since the 1950s, egg-derived vaccine viruses were the gold standard for vaccine production. However, in recent years, cell-grown vaccine viruses have proven to be a valuable alternative over egg-

derived vaccines which present several drawbacks [193], including: i) the availability of eggs within a short time window, for example in case of a pandemic [194]; ii) the fact that some human-adapted viruses, particularly the recent H3N2 strains, do not grow well in embryonated hen eggs [195]; iii) the higher mutation frequency after serial passaging in eggs, especially in the HA receptor binding site [195, 196]; and iv) the allergenic properties of the vaccine, even despite an extensive purification process. In contrast, cell culture (e.g. MDCK)- based vaccines overcome most of these drawbacks and were shown to be at least as safe and immunogenic as egg-based vaccines [197-199].

Currently circulating influenza strains are genotyped by WHO reference laboratories all over the world (e.g. the Robert-Koch-Institut in Berlin, Germany), which then report back to the WHO. Based on these data, the WHO announces which IAV strains should be used for vaccine production for a particular flu season. These influenza vaccines can be either of trivalent (i.e., two IAV subtypes plus one IBV subtype) or quadrivalent (i.e., trivalent vaccine plus one additional IBV subtype) composition [200]. In Germany, however, due to an unexpectedly high number of influenza-associated complications and death caused by a mismatched IBV strain in the trivalent vaccine of the 2017/2018 season [201, 202], only quadrivalent vaccines are available since the 2018/2019 influenza season [203].

3.1.8.2 Anti IAV therapeutics

The available spectrum of drugs to treat severe influenza is limited and novel treatment strategies are urgently required. **Figure 5** illustrates which drugs are currently used or in clinical trials for treatment and prophylaxis of influenza infections (adapted and modified from [204]).

First, adamantane derivatives (ADs; amantadine, rimantadine) are used to inhibit the viral uncoating process by disabling the M2 ion channels [41]. Second, neuraminidase inhibitors (NAIs; zanamivir, oseltamivir) are employed to block viral release from the cell [205]. A novel NAI, peramivir, is currently licensed for use in Japan, China, South Korea and the US, but the overall efficacy was shown to be not substantially different from oseltamivir [206]. Importantly, due to the high mutation frequency of IAV, increased emergence of AD- and/or NAI-resistant strains has been reported, highlighting the urgent demand for novel anti-influenza therapeutics [207-209].

Although extensive work has been carried out for decades in order to identify and develop new therapeutic intervention strategies to combat influenza, this task proved to be very challenging and many potential drug candidates failed in clinical studies [204]. One promising candidate, however, is *favipiravir*, also named *T-705*, which is a nucleoside analogue that after processing in the cell selectively and potently inhibits the viral RNA polymerase, shutting down virus

replication [210]. Due to this function, T-705 was shown to be also active against a wide range of other RNA viruses, including hemorrhagic fever viruses, like Ebola [210, 211]. Potential teratogenic effects of T-705 have been reported, but this requires further investigation.

Another drug recently licensed in Japan and in the US to treat uncomplicated influenza is *baloxavir marboxil* (BAM; Roche). The mode-of-action is inhibition of the cap-dependent endonuclease activity of the viral PA protein, thereby inhibiting *cap snatching*, viral transcription and shut-down of cellular gene expression [212, 213]. BAM-resistant IAV strains have been already detected in patients treated with the drug, particularly in children, and thus further emergence of resistant strains needs to be closely monitored in the future [213-216].

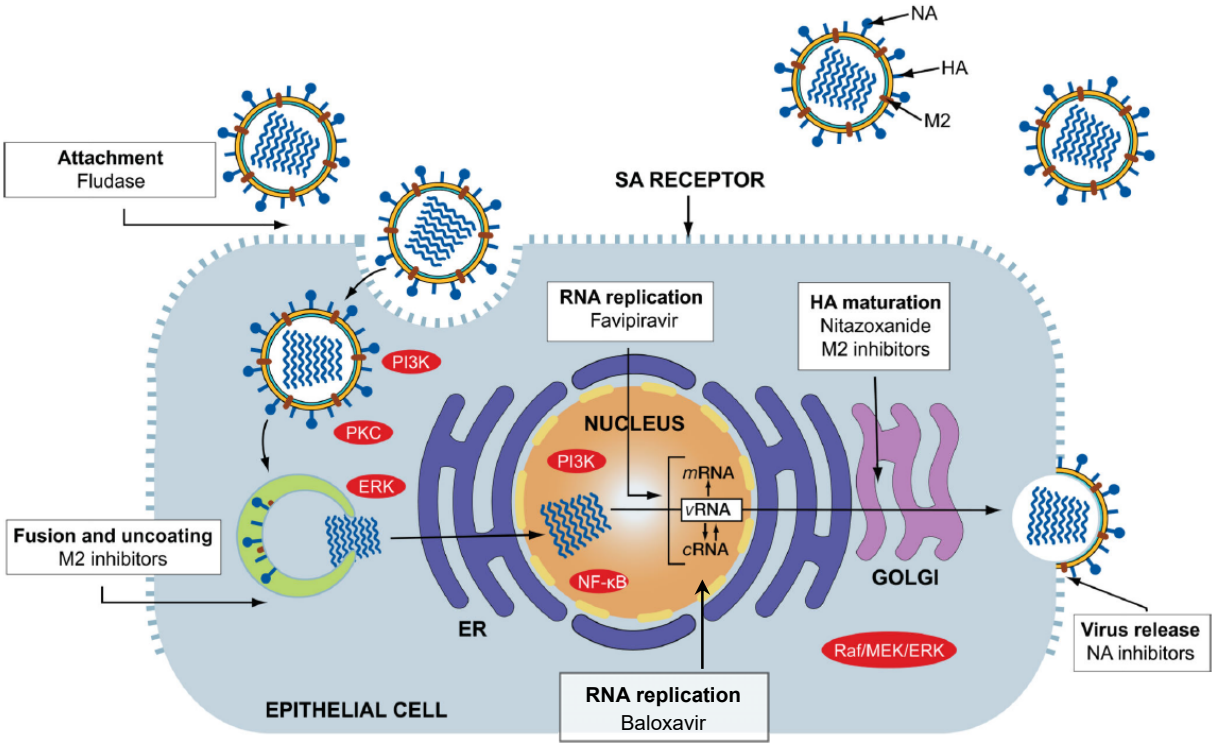

Figure 5: Drugs approved for prevention and treatment of uncomplicated or severe influenza disease. Shown are the anti-influenza therapeutics that are currently licensed in at least one country for clinical use, and their respective modes-of-action. *Fludase* inhibits attachment of viral particles to the cell by removing sialic acids; *adamantane derivatives* (M2 inhibitors) prevent viral uncoating by disabling the M2 ion channels; *favipiramir* and *baloxavir* block viral RNA replication; maturation of hemagglutinin (HA) in the Golgi network is inhibited by *nitazoxandide* as well as *M2 inhibitors*; and *neuraminidase inhibitors* (oseltamivir, peramivir) prevent release of virions from the host cell (adapted and modified from [204]).

In addition to the development of new antivirals to inhibit essential steps of the viral replication cycle, other concepts are currently discussed to treat severe influenza in humans. These include i) targeting host factors rather than viral proteins to prevent the emergence of drug-resistant strains [217, 218], and ii) modulating the patient's immune system to generate a controlled, more beneficial immune response that clears the virus infection without causing too much harm to tissue and organs [204, 219]. For these approaches, however, it is crucial to obtain a better understanding of the diverse virus-host interactions that drive IAV interspecies transmission and pathogenicity in mammals.

3.1.9 Viral determinants of IAV species specificity and pathogenesis in mammals

Influenza A viruses present an ongoing threat to human health due to their ability to cross species barriers and infect humans where they can cause severe and even fatal respiratory disease. In the natural reservoir, IAV are highly adapted and rarely cause disease [5]. In the new host, however, a selection pressure drives adaptation of IAV that leads to the emergence of human-adaptive signatures (i.e. mutations in the viral genome), particularly in the HA, NA, NS1 and polymerase proteins [220]. This selection pressure is believed to be based on differences in identity, functionality, and/or expression patterns of certain host cell factors between different species [94]. The selected mutations can support the virus throughout its replication cycle, including entry into the host cell, replication and transcription of the viral genome, inhibition of cellular innate immune signaling, and release of virus progeny. The viral proteins in which these adaptive signatures arise after host switch are termed *viral pathogenicity determinants* (VPDs) [221]. These VPDs not only drive virus evolution, but they also largely contribute to viral pathogenicity in the new host, as well as to inter- and intraspecies transmission [221]. Likewise, host factors that support viral replication, pathogenicity and transmission are termed *host pathogenicity determinants* (HPDs) [94]. The following chapters summarize the current knowledge on how VPDs and HPDs regulate IAV species specificity, pathogenesis and transmission in and between mammalian hosts.

3.1.9.1 The viral hemagglutinin

Along with the viral polymerase (chapter 3.1.9.2), the viral HA protein is probably one of the most characterized VPDs to this day [85, 222]. It initiates entry into the host cell by binding to SAs on the cell surface, and thereby it affects organ tropism and pathogenicity, but also transmission of the virus [125, 126].

As outlined in chapter 3.1.3.1, epithelial cells in the human URT contain mostly α2,6-linked SAs (i.e., the receptor for human-type IAV), while the human LRT is rich in α2,3-linked SAs (i.e., the receptor for avian-type IAV) [28, 30, 31]. Upon adaptation of AIVs to mammals, mutations arise in the receptor binding site (RBS) of the HA protein that enable the HA to bind to α2,6-linked SAs, allowing replication in the URT and efficient human-to-human transmission by coughing and sneezing [125, 126, 223-225]. Based on the HA subtype, these mutations include: $HA_{E190D/G225D}$ (in *H1* viruses); $HA_{Q226L/G228S}$ or $HA_{N224K/Q226L}$ (in *H3* viruses); and $HA_{Q222L/G224S}$ (in *H5* viruses). The crystal structures of human-type HAs suggest that these adaptive mutations create a wider RBS that is able to accommodate SAs with the more bulky α2,6 conformation [226]. In contrast, mutations HA_{H103Y} and HA_{T156A} (*H3* nomenclature) were associated with increased binding to α2,3-linked SAs, but further promote α2,6-linked SA binding in the presence of the human-adaptive $HA_{Q222L/G224S}$ mutations [125, 126]. Finally, it was shown that the mutation HA_{T156A} as well as an adjacent amino acid substitution (HA_{N158D}) leads to a loss of an N-glycosylation at this site, which could alter receptor binding [125, 227-229].

In addition to receptor binding, the HA mediates fusion of viral and endosomal membranes which is required for release of the vRNPs from the late endosomes into the cytoplasm [230]. This process is highly dependent on the acidification of the endosome, and HA stability under these acidic conditions is crucial for the fusion event. The HA mutations $HA_{N224K/Q226L}$ and $HA_{N224K/Q226L/N2158D}$ enable the virus to bind to the human-type receptors, but simultaneously they reduce the stability of the HA protein, thereby negatively affecting its fusion ability [126]. However, this seems to be counteracted by another mutation at position 318 (HA_{T318I}), which increases HA stability [126].

AIV are distinguished into LPAIV and HPAIV, based on the proteolytic cleavage site in the precursor HA_0 protein (chapter 3.1.5) [16]. While the HA_0 protein of LPAIV and human IAV strains contains a mono-BCS and is cleaved by lung tissue-specific proteases (e.g. HAT or TMPRSS2) [85], the multi-BCS in the HA_0 of HPAIV (H5, H7) can be activated by ubiquitously expressed proteases, like furin or PC6 [16, 104]. These characteristics promote systemic spread of the virus to other organs, leading to increased pathogenicity [16]. Interestingly, in the case of a bacterial co-infection, bacterial proteases were shown to also induce HA activation, either directly or by activation of cellular proteases, and thereby might contribute to viral pathogenicity and spread [231-233]. Although repeatedly observed (e.g. in AIV of the H7 subtype) [132, 234], the detailed molecular mechanisms that could turn a mono-BCS into a multi-BCS are still not fully understood (chapter 3.1.5.2) [85].

3.1.9.2 The viral polymerase

Replication and transcription of the IAV RNA genome is carried out in the nucleus of the host cell by the viral RdRP, composed of subunits PB1, PB2 and PA. This trimeric polymerase complex is an important determinant of IAV species specificity, pathogenesis and transmission in mammals [94, 221]. Upon animal-to-man transmission, it is believed that the selection pressure in the new host drives the emergence of human-type polymerase signatures, particularly in the PB2 protein. Among the most characterized signatures are mutations at positions 627 ($PB2_{E627K}$) and 701 ($PB2_{D701N}$) in the viral PB2 protein [235, 236]. Herein, it is important to note that the $PB2_{D701N}$ mutation is often accompanied by a mutation in the viral nucleoprotein at position 319 (NP_{D319K}) [237, 238]. The fact that the $PB2_{E627K}$ and $PB2_{D701N}$ mutations have not been detected together in a single virus isolate suggests functional redundancy of these mutations, at least to some degree [235, 239]. Both of these mutations have been associated with increased viral replicative fitness [236, 238, 240-243] and, as a result, high pathogenicity in mammalian hosts [127, 179, 240, 243-246]. More importantly, they mediate high-level virus replication in the URT of mammals, a prerequisite for efficient inter- and intraspecies transmission [125, 239, 243, 247, 248]. Interestingly, neither 627 nor 701 adaptive signatures were observed in the PB2 protein of the 2009 pH1N1 virus. Instead, alternative amino acid substitutions in PB2 ($PB2_{G590S/Q591R}$) that are adjacent to the 627 residue are believed to have compensatory effects [249].

To this day, the underlying molecular mechanisms of PB2 627 and 701 mediated host switch are not completely understood. However, both $PB2_{E627K}$ and $PB2_{D701N}$ seem to mediate adaptation, at least in part, to mammalian host importin-α isoforms [50, 237, 250, 251]. Moreover, in a recent publication, ANP32 (*acidic leucine rich nuclear phosphoprotein 32*) proteins were identified as another family of host cell factors that support avian-type polymerases (i.e. with avian-type signatures) in a species-specific manner, thereby driving virus adaptation [252]. Since both, importin-α isoforms and ANP32 proteins, are the subject of this study, the current knowledge on how they mediate IAV adaptation to mammals is further discussed in chapter 3.1.10.

Other adaptive mutations in the polymerase complex (e.g. $PB2_{H357N}$, $PB1_{L598P}$, or PA_{K615E}; increase in polymerase activity), in the nucleoprotein (e.g. NP_{L283P}; escape from Mx1 restriction) and in the nuclear export protein (e.g. NEP_{E75G}; increase in polymerase activity) have been described that are repeatedly selected to overcome restriction of avian-type polymerases in mammalian cells, but a detailed mechanistical understanding is still missing [235, 253, 254].

3.1.9.3 The viral neuraminidase

Compared to the viral HA protein, adaptive mutations in the viral neuraminidase (NA) occur less frequently and their role in IAV interspecies transmission is not completely understood. Often,

mutations arise in the NA protein after selection pressure posed by NAIs that are used in the clinics to treat severe influenza disease [255]. One characteristic mutation is located at position 292 (NA_{R292K}), which was shown to mediate resistance of an H7N9 AIV to the NAI oseltamivir [256].

The neuraminidase cleaves SAs at the budding site on the plasma membrane, preventing HA re-attachment which would hamper efficient release of progeny virions [86, 88]. Therefore, the NA represents an important determinant of viral pathogenicity and transmission [221, 257]. In some NA proteins, two SA binding sites have been identified, but it is believed that only one site is catalytically active. The exact function of the second SA binding pocket remains unknown. However, it was speculated that it might potentiate HA binding to SAs, or even take over HA function [258, 259]. Undoubtedly, the balance of HA binding to SAs and the NA catalytic activity needs to be finetuned for efficient viral replication and transmission [260-263]. Interestingly, upon transmission of AIVs from aquatic waterfowl to domestic poultry, mutations are selected that lead to the expression of NA variants with shorter stalk domains. Viruses bearing these shorter NA proteins are more pathogenic in poultry as well as in mammalian hosts [264, 265], but transmission between ferrets is limited [266].

3.1.9.4 The viral non-structural protein 1

Influenza viruses efficiently block the host immune system, thereby creating optimal conditions for high-level virus replication. A key player in this process is the viral NS1 protein, a multi-functional effector protein which main task is to disable the defense mechanisms of the host cell [267]. In addition to targeting specifically antiviral host factors (e.g. PKR or RIG-I/DDX58) [268, 269], a general shut-off of cellular gene expression by inhibition of CPSF30 (*cleavage and polyadenylation specificity factor 30 kDa subunit*; involved in RNA processing) predominantly contributes to the immunomodulatory function of NS1 [267, 270]. In line, mutations that lead to increased or decreased binding of NS1 to CPSF30 were shown to affect the host's interferon response and, in turn, viral pathogenicity [271]. For example, the 2009 pH1N1 virus only weakly binds to CPSF30 [272], while recent H5 HPAIV (since 1998), seasonal and other pandemic IAV strains very efficiently bind to and inhibit CPSF30 function [271, 273, 274]. The potent ability of the 1918 IAV NS1 protein to block interferon signaling by disabling CPSF30 likely contributed to its high virulence [150].

An aspartate-to-glutamate mutation at position 92 ($NS1_{D92E}$), located in the PDZ ligand domain of NS1, was identified in H5 HPAIV and 1918 IAV that further increased virulence of these viruses in mice [275]. Other adaptive mutations in NS1 (e.g. $NS1_{P213S}$) have been associated with increased potential for airborne transmission between ferrets [276, 277].

3.1.9.5 Other viral determinants of pathogenicity

The genomic repertoire of IAV allows expression of two additional viral proteins with immunoregulatory functions.

PB1-F2, which is expressed via an alternative ORF from the PB1 encoding gene segment, contributes to the high virulence of pandemic IAV and H5N1 HPAIV by blocking the interferon response and thereby allowing uncontrolled viral replication [17, 18, 152]. An amino acid mutation at position 66 (PB1-F2$_{N66S}$) was shown to be critical for this phenotype [18]. Furthermore, PB1-F2 has been attributed pro-apoptotic functions by localizing to mitochondria where it inhibits the function of MAVS (*mitochondrial antiviral-signaling protein*) [17, 278]. Finally, presence of PB1-F2$_{N66S}$ was shown to increase NS1-mediated inhibition of cellular immune responses, suggesting a functional relationship [278]. Further research is required to decipher the exact role and interplay of the different PB1-F2 modes-of-action, depending on the viral subtype (e.g. avian- vs. human-type IAV) as well as the cell type that is infected (e.g. epithelial cells vs. immune cells).

Another viral protein that is expressed by ribosomal frameshifting from genome segment 3, PA-X, was shown to inhibit immune responses by shutting down host gene expression [21, 279], particularly by targeting cellular RNA processing proteins [280]. Both, truncation of PA-X as well as specific amino acids substitutions (e.g. at positions P28 and S68), were linked to the ability of PA-X to exert its function [281, 282].

3.1.10 Host determinants of IAV species specificity and pathogenesis in mammals

Influenza viruses, like other RNA viruses, rely on host cell factors to support replication and transcription of the viral genome. Two families of these cellular proteins, namely importin-α isoforms and ANP32 proteins, have been identified as key determinants of IAV replicative fitness, species specificity and pathogenicity. The following chapters summarize the current knowledge on the function of these host factors during influenza infection.

By contrast, certain host factors restrict virus replication in a species-dependent manner, for example by sequestering viral proteins or by induction of intracellular signaling cascades leading to immune activation [94]. However, these negative-regulatory host proteins are not the main subject of this study and therefore will not be further discussed.

3.1.10.1 Importin-α isoforms

In the last two decades, substantial evidence has emerged that importin-α proteins, key mediators of nuclear transport in the cell, drive IAV interspecies transmission and pathogenesis in mammals [94]. As outlined above, IAV replicate and transcribe their genome in the nucleus of the host cell. On the one hand, this allows the virus to hide from major cytoplasmic RNA sensors (e.g. RigI) and thereby evade the immune system [283]. On the other hand, IAV need to get access to the nucleus. This is achieved by hijacking the nuclear import machinery of the cell. This machinery is fundamentally important for maintaining cellular homeostasis through tightly controlling the cytoplasmic-nuclear shuttling of host cell proteins, such as transcription factors or components of the splicing machinery [284, 285]. In the cytoplasm, importin-α proteins bind to the NLS (*nuclear localization signal*) of a cargo protein. This allows recruitment of the transport co-receptor importin-β_1, and the heterotrimeric complex is subsequently translocated through the nuclear pore in an energy-dependent fashion [44]. The detailed characteristics of this process are discussed in chapter 3.2.

Differential nuclear transport pathways are utilized by influenza viruses to transport their vRNPs as well as the three polymerase subunits into the nucleus [237]. Nuclear import of entire vRNPs is mediated by direct binding of NP to importin-α and nuclear translocation following the classical importin-α/importin-β_1 pathway (chapter 3.2.2.1) [46, 49]. This predominantly occurs via an N-terminal unconventional NLS motif in NP [45]. Furthermore, monomeric NP and PB2 are recognized by importin-α via their respective NLS motifs and individually transported into the nucleus [45, 47, 250]. In contrast, PB1 and PA form a heterodimer that uses the importin-β_1 homologue and transport factor RanBP5 (*Ran binding protein 5)* for nuclear import [49, 286]. Of note, the cellular chaperone Hsp90 was also implicated in the nuclear import of PB1-PA or PB1-PB2 heterodimers [287].

Human-type signatures in the viral polymerase, particularly $PB2_{E627K}$ and $PB2_{D701N}$/NP_{D319K}, were shown to mediate adaptation of IAV to host importin-α isoforms in a species-specific manner [50]. Herein, the divergence between avian and mammalian importin-α proteins was proposed to drive virus evolution [50]. Human-type PB2 and NP proteins carrying the $PB2_{D701N}$ and NP_{D319K} mutations, respectively, showed increased binding to mammalian but not avian importin-α isoforms, particularly to importin-α1 [250, 288]. Structural analyses further revealed that the aspartate-to-arginine mutation at position 701 dissolves a salt bridge between residues 701D and 753R, which exposes the C-terminal NLS motif in PB2 [47]. As a result, increased access to importin-α likely promotes nuclear localization of PB2 and NP in mammalian cells [250, 289].

In contrast to $PB2_{D701N}$, the $PB2_{E627K}$ mutation did not affect binding of individual polymerase subunits to importin-α, but rather increased affinity of entire vRNPs to importin-α1, -α5 and -α7

isoforms, possibly mediated by NP [251]. The generation of a '*basic patch'* on the surface of the PB2 protein, caused by the glutamate-to-lysine mutation at position 627, likely contributes to increased binding to acidic importin-α, but probably also to other host cell factors [290]. Interestingly, modulation of the PB2 627 identity did not affect subcellular localization of vRNPs, indicating that alternative, nuclear transport independent mechanisms underlying importin-α function might exist [237, 251, 288].

In-depth studies over the last years could show that avian and human influenza viruses possess differential preferences for importin-α isoforms in human lung cells [50]. While growth of avian influenza viruses depends on importin-α3, human influenza viruses depend on importin-α7. Both, avian- and human-type IAV require importin-α1 for efficient viral replication [50, 251]. Thus, a switch from importin-α3 to importin-α7 dependency seems to be a key characteristic of IAV avian-mammalian adaptation. Interestingly, in a mini-replicon system, importin-α3 was shown to restrict the activity of $PB2_{627E}$ and $PB2_{627K}$ adapted polymerases [251]. Recent data further showed that this inhibitory effect is maintained during avian-type ($PB2_{701D}$), but not mammalian-type ($PB2_{701N}$) IAV replication, suggesting that mammalian-adapted viruses have evolved mechanisms to circumvent importin-α3 mediated restriction in mammalian cells, particularly during later stages of infection [291]. Indeed, this hypothesis is supported by the key finding that $PB2_{627K}$ or $PB2_{701N}/NP_{319K}$ adapted IAV efficiently downregulate importin-α3 expression in the murine and human respiratory tract. The antiviral effects of importin-α3 on avian-type IAV replication could also be recapitulated in mice deficient for the importin-α3 gene. Here, IAV pathogenicity was dramatically increased compared to the wild type littermates [291].

Importantly, the importin-α7 isoform was identified as a positive-regulatory host cell factor for mammalian-adapted IAV ($PB2_{627K}$ or $PB2_{701N}/NP_{319K}$), affecting polymerase activity, replication and pathogenicity of both seasonal IAV as well as HPAIV strains [50, 251, 292, 293]. Interestingly, mice expressing an importin-α7 variant with a deleted importin-β_1 binding domain (ΔIBB) were also (partially) protected from lethal influenza challenge, indicating that importin-α7 acts on viral replication inside the nucleus and in dependency of its IBB domain [50]. Although a molecular mechanism beyond nuclear transport has been proposed for importin-α7 function [251], the exact mode-of-action during influenza infection remains unknown to this day. Nevertheless, in line with the current concept of targeting host factors rather than viral proteins to treat severe influenza (chapter 3.1.8.2), down-regulation of importin-α7 expression levels or blocking its interaction with the viral polymerase might present a future strategy with therapeutic potential. This, however, has to be carefully evaluated since IAV might acquire adaptive mutations that enable them to replicate efficiently even in the absence of importin-α7, as recently demonstrated using an *in vivo* IAV adaptation model [294, 295].

3.1.10.2 ANP32 proteins

For almost a decade, species-specific differences in the nuclear transport machinery, particularly in the importin-α transport proteins, have been the only known host determinants of influenza adaptation to mammals [50]. In 2016, however, the ANP32 protein family has been identified as another key driver of IAV interspecies transmission [252]. ANP32 proteins, including the family members ANP32A, ANP32B and ANP32E, are master regulators in the cell, acting alone or as part of large cellular machineries on gene expression, mRNA export, apoptosis, and various other processes [296]. ANP32 proteins share a characteristic whip-like structure, composed of five N-terminal leucine-rich repeats (LRRs) and a C-terminal low complexity acidic region (LCAR) [296].

As demonstrated by Long and colleagues, an avian-type ($PB2_{627E}$) polymerase, which is highly restricted in mammalian cells [297], can be rescued by co-expression of the avian ANP32A (avANP32A) protein [252]. Amino acid sequence alignments further revealed that mammalian including human ANP32A (huANP32A) proteins are lacking a stretch of 33 amino acids compared to the avian homologue, and that these differences account for the inability of the avian polymerase to use huANP32A for high-level virus replication, likely due to weakened interaction with huANP32A [252, 298].

After the initial discovery, the focus in influenza research has shifted in order to identify the molecular mechanisms underlying avANP32A function. For example, it has been shown that various ANP32A splicing variants exist in birds that all differ in their ability to support avian-type polymerase activity, both in avian as well as in mammalian cell lines [299-301]. Moreover, a SUMO (*small ubiquitin-related modifier*) interacting motif has been identified in the aforementioned 33 amino acid sequence of avANP32A that was critical for its function [302]. Interestingly, avian ANP32B (avANP32B) did not support avian-origin polymerase activity, neither in avian nor in mammalian cells, suggesting that it has lost its function throughout evolution [303]. In another recent study, the authors showed that the absence of murine ANP32A (muANP32A) could also affect the *in vivo* emergence of human-type signatures in an H7N9 AIV bearing the $PB2_{627E}$ signature [304]. Here, $PB2_{E627K}$-mediated adaptation, as also often detected in human H7N9 isolates [127], shifted towards $PB2_{D701N}$-mediated adaptation after infection of mice lacking the muANP32A protein [304]. Importantly, ANP32A deficiency in avian cells significantly reduces avian-type virus replication [303]. This led to a new concept of genetically altered poultry as a measure to prevent virus transmission from these intermediate hosts to humans. Although this approach is certainly interesting and might bear some future potential to counteract IAV interspecies transmission, it is equally important to understand the role of the mammalian ANP32 proteins on human-type influenza virus replication and

pathogenicity in mammals. However, to this day, only a few studies have addressed this question by investigating IAV replication in ANP32 silenced or knockout cancer cell lines, raising a concern for the significance of these data [218, 305-307]. Furthermore, the results from recent studies using knockout cells lines are, at least in part, contradictive to the initial observations obtained after siRNA silencing of individual ANP32 members, particularly for the role of huANP32A [252, 305]. Therefore, there is an urgent need for knockout mouse models that would allow analyses on human-type IAV replication and pathogenicity *in vivo*. Nevertheless, the homology between the ANP32 family members of one particular species as well as species-specific differences between avian, murine and human ANP32A and ANP32B proteins need to be carefully considered before drawing major conclusions from these *in vivo* experiments.

3.2 Nucleocytoplasmic transport

Eukaryotic cells are divided into compartments, which are separated from each other by membrane structures. One of the most important compartments is the nucleus which harbors the genome of the cell, tightly packaged into chromosomes. Cellular homeostasis largely depends on the coordinated trafficking of transcription factors as well as other proteins associated with gene expression and chromatin remodeling between the cytoplasm and the nucleus (e.g. RNA/DNA polymerases, histones, splicing factors) [308, 309]. Accordingly, dysregulation of nuclear transport is linked to a large variety of human diseases, including various carcinomas, neuropathological and developmental disorders, and susceptibility to bacterial or viral infections [284, 310-313].

3.2.1 The importin-α protein family

3.2.1.1 Classification of importin-α isoforms

In the cell, nuclear transport is mainly mediated by the family of importin-α transport factors, also termed karyopherins (KPNAs). To this date, seven importin-α isoforms have been described in higher eukaryotes which are all highly conserved throughout evolution [314]. They are further divided into three subgroups based on their amino acid sequence similarity: the importin-α1 (importin-α5, -α6, -α7), importin-α2 (importin-α1, -α8) and importin-α3 (importin-α3, -α4) subgroup [315]. Importin-α isoforms are ubiquitously expressed, with the exception of importin-α6 which is only found in testis. However, they show differential tissue-, cell- and organ-specific expression patterns [316, 317]. Importantly, recent data from our laboratory further revealed that the different importin-α isoforms are expressed as gradient throughout the human and murine respiratory tract, with the highest expression levels found in the LRT [291].

3.2.1.2 Structure of importin-α isoforms

The importin-α protein structure can be divided into 3 functional domains, i.e. i) the N-terminal importin-β1 binding (IBB) and autoinhibition domain, ii) the NLS-cargo binding site, which is characterized by 10 armadillo (*ARM*) repeats, and iii) the C-terminal domain for the interaction with the export co-receptor CAS (*cellular apoptosis susceptibility*) (10th ARM repeat) (**Figure 6A and B**) [314].

The IBB domain carries out two important functions: First, as the name implies, this domain mediates binding of importin-α to importin-β_1, generating the heterotrimeric nuclear import complex (interaction *in trans*) [44]. Secondly, it masks the importin-α binding site in the absence

of a cargo protein (interaction *in cis*), a process called *autoinhibition*. This mechanism ensures that nuclear import only takes place when a cargo protein is available, thereby minimizing the loss of energy due to inefficient transport. Moreover, it promotes the release of the cargo protein into the nucleus [44].

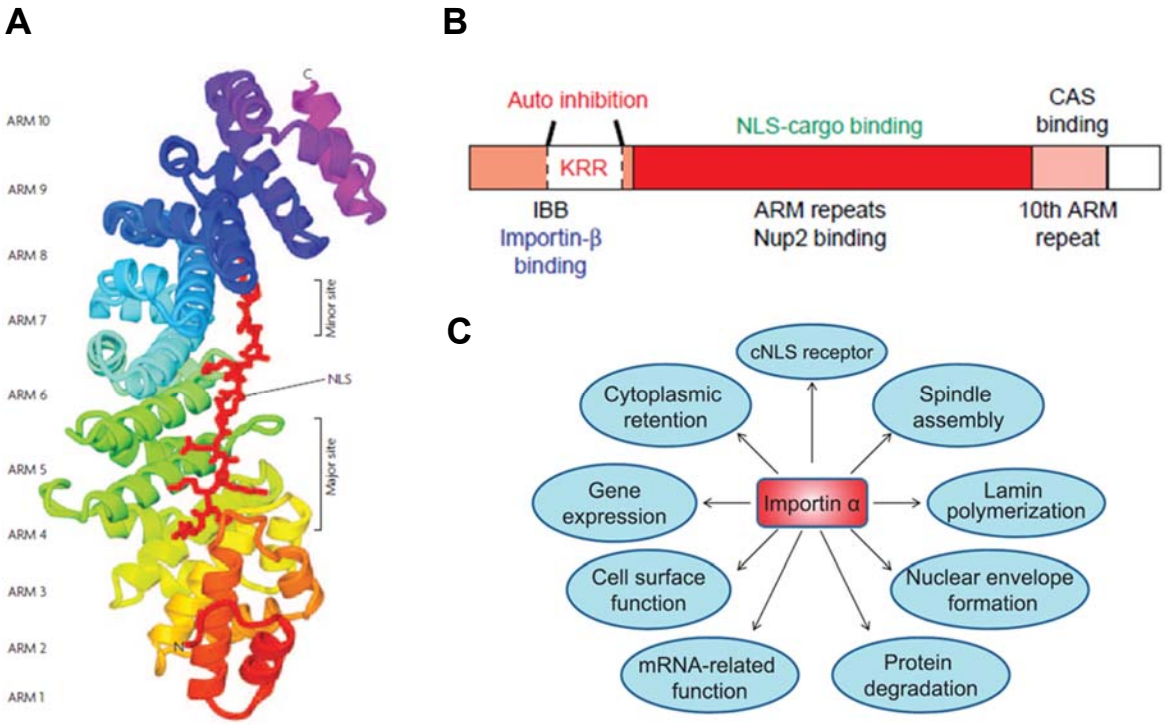

Figure 6: Structural and functional characteristics of mammalian importin-α isoforms. A and B, The importin-α protein structure is composed of 10 armadillo (*ARM*) repeats (colored) which mediate binding to an NLS-containing cargo protein (major and minor site, ARM 3-8) or to the export co-receptor CAS (ARM 10). Further, importin-α contains an N-terminal importin-β_1 binding (IBB) domain (adapted from [44, 314]). **C,** The major function of the importin-α proteins is to mediate nuclear transport of cytoplasmic cargo proteins presenting an NLS motif. However, increasing body of evidence suggests that importin-α proteins are involved in various cellular processes, including chaperone-like functions, mRNA export, regulation of gene expression and even modes-of-actions on the cell surface (adapted from [318]).

The ARM repeats comprise the recognition and binding sites for NLS motifs on cytoplasmic cargo proteins. Importin-α proteins are able to bind two different classes of NLS, which are characterized by either one (monopartite; e.g. SV40 large T antigen) or two (bipartite; e.g. nucleoplasmin) clusters of basic amino acids [319]. While monopartite NLSs interact with the major binding site on the importin-α adapter protein, bipartite NLSs interact with both the major

and the minor binding site [320, 321]. Importantly, binding of a cargo protein to importin-α is not only determined by the NLS, but also by the conformation and the three-dimensional structure of the entire cargo protein [322, 323]. The 10th ARM repeat comprises the binding site on importin-α for the recycling factor CAS that transports importin-α back to the cytoplasm in conjunction with RanGTP as energy source [44, 324].

3.2.1.3 Functional diversity of importin-α isoforms

As outlined above, the main task of importin-α isoforms is to mediate translocation of cytoplasmic NLS-containing cargoes across the nuclear membrane into the nucleus (chapter 3.2.2.1) [44]. However, accumulating evidence suggests that their functions range beyond nuclear import, highlighting the global role of importin-α isoforms in maintaining cellular metabolism and homeostasis (**Figure 6C**) [318]. For example, importin-α1 has been implicated in carcinogenesis [325, 326]. Furthermore, importin-α isoforms have been associated with the modulation of gene expression and the mRNA quality control pathway [327, 328]. Finally and most importantly, recent evidence suggests that several human pathogenic viruses (e.g. influenza A virus, Zaire Ebola virus, Hepatitis C virus, Severe Acute and Middle East Respiratory Syndrome Coronavirus (SARS- and MERS-CoV, respectively), and Dengue virus) have evolved mechanisms to interact with importin-α proteins in order to manipulate the innate immune response of the host cell or to ensure efficient viral replication ([50, 251, 329-337]; and *unpublished data*). Undoubtedly, with the advances in cell and molecular biology techniques, even more diverse importin-α functions will be discovered in the next years [318].

3.2.2 Nucleocytoplasmic transport in the cell

The transport of cargo molecules across the nuclear membrane occurs through the nuclear pore complexes (NPC). These large protein complexes of up to 60 MDa in size are composed of nucleoporins (NUPs), which are further divided into structural NUPs, membrane pore proteins (POMs) and FG-NUPs, i.e. nucleoporins characterized by multiple phenylalanine-glycine (FG) repeats [338, 339]. While small molecules can pass the pore complex via simple diffusion, larger molecules (≥ 40 kDa) depend on transport receptors which actively translocate through the NPC in an energy-dependent process using the FG-repeats as '*steppingstones*' [309, 340].

The largest group of transport receptors is the importin-β protein family. Here, the importin-β proteins either directly bind to a cargo (e.g. RanBP5) or, in case of importin-β_1, use a member of the importin-α family as an adapter protein (chapter 3.2.1) [314, 341]. The energy required for

nuclear transport is provided by a RanGDP/RanGTP gradient. Furthermore, this gradient is crucial for maintaining the directionality of the transport process [342].

Nuclear import is divided into the classical and non-classical pathway [44]. Since the importin-α isoforms, key players in the classical importin-α/importin-β_1-dependent pathway, are major determinants of IAV species-specificity and pathogenicity (chapter 3.1.10.1) [50], this pathway will be described in more detail below (**Figure 7**).

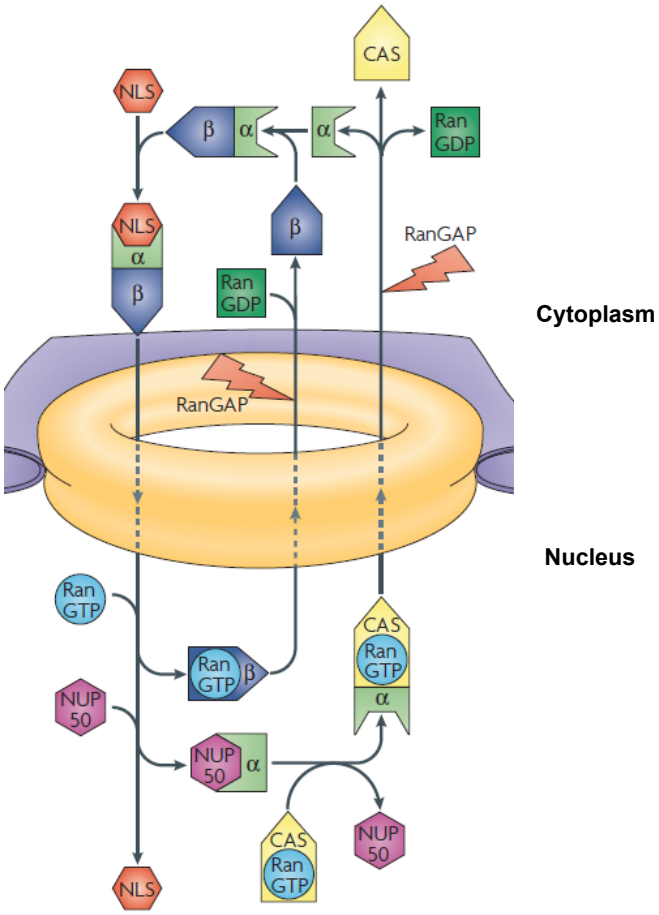

Figure 7: The classical, importin-α/β-mediated nuclear import cycle. In the cytoplasm, the heterotrimeric complex composed of importin-α, importin-β_1 and a cargo protein is formed and translocated through the nuclear pore complex (NPC). Upon binding of RanGTP to importin-β_1, the complex dissociates and importin-β_1 is recycled into the cytoplasm. By contrast, importin-α actively forms a trimer with RanGTP and its export co-receptor CAS (*cellular apoptosis susceptibility*) and the complex is transported back into the cytoplasm. Here, hydrolysis of GTP provides the energy for the release of importin-α and importin-β_1 from the Ran protein so that both proteins are available for another import cycle (modified after [44]).

3.2.2.1 The classical importin-α/importin-β_1 mediated nuclear import pathway

Cargo proteins that are imported into the nucleus generally possess an NLS motif, although also NLS- and importin-α-independent transport has been described [319, 343]. Upon recognition and binding of a cargo by an importin-α protein via the NLS motif, the transport receptor importin-β_1 is recruited and the ternary complex is translocated through the NPC in an energy-dependent fashion [44, 344]. Inside the nucleus, release of the cargo and the importin-α protein from the complex is mediated by binding of RanGTP to importin-β_1 [345, 346]. RanGTP alone is further sufficient for nuclear export of importin-β_1. In contrast, importin-α actively forms a heterotrimer with RanGTP and its export receptor CAS, which is then transported back to the cytoplasm [44, 324]. Here, hydrolysis of GTP leads to a conformational change in the Ran protein which provides free importin-α and importin-β_1 proteins for the next import cycle [44]. **Figure 7** illustrates a schematic representation of the importin-α/importin-β_1 nuclear import pathway.

3.3 Aim of this study

Despite advances in vaccine and drug development, influenza A viruses (IAV) continue to pose a major threat to human health due to their ability to transmit from the avian reservoir to mammals, including humans. Here, the virus can cause severe and even fatal respiratory disease. According to a report published in *The Lancet*, the next influenza pandemic may claim up to 80 million deaths worldwide, and the WHO recently announced that it is only a matter of time until the next pandemic strikes [123, 347]. For pandemic preparedness, it is crucial to obtain a better, more detailed understanding of the diverse interactions of key viral and cellular factors that facilitate IAV animal-to-man transmission.

This study aimed to provide mechanistical insights into the function and interplay between two major families of host cell factors that were shown to drive IAV interspecies transmission and pathogenicity in mammals: Importin-α7 and ANP32 proteins.

Specifically, the following questions and tasks should have been addressed:

1. Provide novel insights into the molecular function of importin-α7 during human-type IAV infection by determining its interactome in human cells.
2. Analyze, whether a functional relationship exists between importin-α7 and ANP32A, both proposed positive regulators of viral replication.
3. Using transgenic knockout mouse models, investigate the role of ANP32A and ANP32B on human-type IAV replication and pathogenicity *in vivo.*

4. Materials and Methods

4.1 Materials

4.1.1 Chemicals and disinfectants

Chemical	Manufacturer
2-mercaptoethanol	FlukaBiochemika
2-propanol	Sigma-Aldrich/Merck
3,3'-diamnobenzidin (DAB)	Zytomed
4-(2-hydroxyethyl)-1-piperazine ethane sulfonic acid (HEPES)	Biomol
Acetonitrile	Sigma-Aldrich/Merck
Agarose	Serva
Ammonium bicarbonate	Sigma-Aldrich/Merck
Ammoniumperoxodisulfate (APS)	Carl Roth
Ampicillin sodium-salt	Serva
Avicel	FMC BioPolymer
Bacto-Agar	BD Biosciences
Bovine serum albumin (BSA)	Sigma-Aldrich/Merck
Bromophenol blue	Carl Roth
Coomassie Brilliant Blue G-250	Sigma-Aldrich/Merck
Crystal violet	Merck
Diethylpyrocarbonate (DEPC)	Sigma-Aldrich/Merck

Dimethylsulfoxide (DMSO)	Sigma-Aldrich/Merck
Dithiothreitol (DTT)	Serva
Ethanol (denatured), for disinfection	Geyer Th. GmbH & Co.KG
Ethanol (pure)	Merck
Eukitt	Kindler
Formaldehyde (37%)	Merck
Formic acid	Sigma-Aldrich/Merck
Glacial acetic acid	Merck
Glycerol (ultra-pure)	Invitrogen
Glycine	AppliChem
Hematoxylin	Shandon
Hydrochloric acid (37 %)	Merck
Hydrogen peroxide	Merck
Igepal (NP 40)	Sigma-Aldrich/Merck
Iodoacetamide	Sigma-Aldrich/Merck
Magnesium chloride ($MgCl_2$)	Merck
Methanol	ChemSolute
Ottix Plus	DiaPath
Ottix Shaper	DiaPath
Paraffin (low-melting)	DCS

Paraformaldehyde (PFA)	AppliChem
Peptone	AppliChem
Phenylmethanesulfonyl fluoride (PMSF)	Sigma-Aldrich/Merck
Polyethylene glycol 8000	FlukaBiochemika
Polyethylenimine (PEI)	Polysciences
Potassium dihydrogene phosphate	Merck
Pursept-A Xpress, for disinfection	SCHÜLKE & MAYR AG
Rotiphorese Gel 30	Carl Roth
Sodium chloride	ChemSolute
Sodium dodecylsulfate (SDS)	Sigma-Aldrich/Merck
Sodium hydrogene phosphate	Merck
Sodium hydroxide (NaOH)	Merck
Sterilium, for hand disinfection	Bode
Tetramethylethylenediamine (TEMED)	Carl Roth
Tris (hydroxymethyl) amino methane	Merck
Triton X-100	Sigma-Aldrich/Merck
Trizol Reagent	Ambion RNA
Tween-20 (pure)	Serva
Virkon S, for disinfection (BSL-3 work)	DuPont
Xylol	Merck

Yeast extract	AppliChem

4.1.2 Buffers and solutions

Buffers and solutions were prepared in double-distilled H_2O (ddH_2O), if not otherwise noted.

Description	Composition/Preparation notes
4x Laemmli loading dye (*SDS-PAGE*)	0.2 M Tris-HCl pH 6.8 8 % SDS 40 % glycerol Trace of bromophenol blue 40 mM DTT (→add shortly before usage)
APS (10%)	10 % APS →filter sterilize (0.22µm)
Avicel solution	2.5 % Avicel →autoclave
Blocking Buffer (*Western Blot*)	1x PBS-T 3 % BSA
Blocking Buffer (I*mmunofluorescence*)	D-PBS 3 % BSA
Blotting Buffer (10x) (*Western Blot*)	250 mM Tris base 1,92 M glycine →autoclave
Blotting Buffer (1x) (*Western Blot)*	Diluted from 10 x Blotting Buffer 20% methanol
Coomassie destaining solution	40 % methanol 10 % glacial acetic acid

Coomassie staining solution	45 % methanol 10 % glacial acetic acid 2.5g / L Coomassie Brilliant Blue G250
Crystal violet solution	270 ml 37 % formaldehyde 1 g crystal violet ad 1L ddH_2O
DEPC-ddH_2O	0.1 % DEPC, in ddH_2O →soluble overnight at RT or >12h at 37°C →autoclave
DEPC-ethanol (70%)	100 % ethanol (pure) →dilute to 70% ethanol with DEPC-ddH_2O
DTT (1M)	1 M DTT
Glycerol (80%)	Diluted from 100 % glycerol
H_2O_2 solution *(IHC-P)*	3 % H_2O_2, in methanol
Lysis Buffer (*SDS-PAGE*)	50 mM HEPES (pH 8.0) 200 mM NaCl 0.5 % Igepal (NP40) 25 % Glycerol 1 mM PMSF 0.07 µl/ml β-mercaptoethanol 1 x HALT Protease & Phosphatase Inhibitor (100x; including EDTA, 100x →add shortly before usage)

Lysis Buffer (*Genotyping*)	100 mM Tris HCl pH 8.5 5 mM EDTA 0.2 % SDS 200 mM NaCl 100 µg/ml Proteinase K
Mass Spectrometry Buffer A	0.1 % formic acid
Mass Spectrometry Buffer B	0.1 % formic acid, in acetonitrile
PFA (4%)	4% PFA, in PBS →soluble at approx. 50°C for >6h
Phosphate buffered saline (PBS) (1x)	Diluted from 10x PBS →autoclave
PBS (10x)	1.37 M NaCl 26.8 mM NaCl 51.3 mM Na_2HPO_4 x $2H_2O$ 17.6 mM KH_2PO_4 pH 7.2-7.4 →autoclave
Pre-incubation Blocking Buffer *(IHC-P)*	1x PBS 10 % donkey serum
SDS resolving gel buffer (4x) (*SDS-PAGE*)	1.5 M Tris base 0.4 % SDS pH 8.8
SDS Running Buffer (10x) (*SDS-PAGE)*	250 mM Tris base 1.92 M glycine 1 % SDS →autoclave

SDS Running Buffer (1x) (*SDS-PAGE)*	Diluted from 10x SDS Running Buffer
SDS stacking gel buffer (4x) (*SDS-PAGE*)	0.5 M Tris base 0.4 % SDS pH 6.8
SDS (10 %)	5 g ad 50 ml ddH_2O
Sodium chloride buffer (0.9 %)	0.9 % NaCl, in ddH_2O
TAE Buffer (1x)	Diluted from 50x TAE buffer
TAE Buffer (50x)	2 M Tris base 1 M glacial acetic acid 0.05 M EDTA pH 8.0
TBS Buffer (1x)	50 mM Tris base 150 mM NaCl pH 7.6
Triton X-100 buffer (*Immunofluorescence*)	0.1 % Triton X-100, in ddH_2O
TSS Buffer (1x)	5 g PEG 8000 0.30 g $MgCl_2$ x $6H_2O$ 2.5 ml DMSO ad 50 ml LB medium →filter sterilize (0.22µm)
Washing Buffer *(IHC-P)*	1x PBS 0.5 % Tween-20
Washing Buffer (PBS-T) (*Western Blot*)	1x PBS 0.1% Tween-20

4.1.3 Manufactured solutions, reagents and reaction systems (kits)

Description	Manufacturer
3x FLAG peptide	Sigma-Aldrich
Agilent DNA 1000 Kit	Agilent Technologies
Agilent RNA 6000 Nano Kit	Agilent Technologies
Avidin/Biotin Blocking Kit SP2001	Biozol
Chicken whole blood, with citrate	Lohmann Tierzucht
Citrate Plus Buffer (10x)	DCS
DNase/RNase-free ddH_2O	Gibco/Life Technologies
dNTP mix (10 mM)	Life Technologies
Donkey serum	Jackson ImmunoResearch
DTT (0.1M) (part of *Superscript™ III Reverse Transcriptase Kit*)	Invitrogen/Life Technologies
Dual-Luciferase® Reporter Assay System	Promega
Eosin-Y solution	Merck
Ethidium bromide solution (10 mg/ml)	Roth
Ezview Red ANTI-FLAG M2 affinity gel	Sigma-Aldrich
FastStart Essential DNA Green Master (MasterMix for SYBR Green I-based qRT-PCR)	Roche
FD Green Buffer (10x)	Thermo Scientific

First Strand Buffer (5x) (part of *Superscript™ III Reverse Transcriptase Kit*)	Invitrogen/Life Technologies
Halt™ Protease & Phosphatase Inhibitor Cocktail (including 0.5M EDTA; 100x)	Thermo Scientific
HF Buffer (5x)	Thermo Scientific
innuprep RNA Mini Kit	Analytik Jena
Lipofectamine 2000	Invitrogen
MassRuler DNA Ladder Mix	Thermo Scientific
MassRuler DNA Loading Dye	Thermo Scientific
Mayer's hemalum solution	Merck
Multiplex mouse immunoassay, custom-designed (IL-1b, IL6, TNF-a, IL-10, IFN-a, MCP-1, IL-17A, IL21)	Invitrogen
NEBNext Poly(A) mRNA Magnetic Isolation Module	New England Biolabs
NEXTflex rapid Directional qRNA-Seq Kit	Bio Scientific
NextSeq 500/550 High Output Kit v2.5	Illumina
NucleoBond Xtra Maxi	Macherey-Nagel
Passive Lysis Buffer (5x)	Promega
Poly-L-Lysin solution	Sigma-Aldrich/Merck
Precision Plus Protein™ Dual Core Standards	Bio-Rad
Pursept-A Xpress	Merz Hygiene GmbH
QIAprep Spin Miniprep Kit	Qiagen

QIAquick Gel Extraction Kit	Qiagen
QIAquick PCR Purification Kit	Qiagen
Ribolock RNase Inhibitor (40U/µl)	Fermentas/Thermo Scientific
RNAlater RNA Stabilization Reagent	Qiagen
RNase-Free DNase Set	Qiagen
Superscript™ III Reverse Transcriptase Kit	Invitrogen/Thermo Scientific
Super Signal West Femto Maximum Sensitivity Substrate	Thermo Scientific
SuperBlock T20 (TBS)	Thermo Scientific
T4 DNA Ligase buffer	New England Biolabs
Venor®GeM Classic Mycoplasma PCR Detection Kit	Minerva Biolabs GmbH
ZytoChemPlus (HRP) Broad Spectrum (DAB) Kit	Zytomed

4.1.4 Antibodies

Primary antibodies were prepared in Superblock T20 (Thermo Scientific), while secondary antibodies were prepared in Western blot blocking buffer, if not otherwise stated.

Primary Antibody	**Species/Dilution**	**Application/Manufacturer/Catalogue number**
Anti-ANP32A	Goat 1:1.000	Primary antibody for Western Blot Santa Cruz #sc-5652
Anti-ANP32B	Goat 1:1.000	Primary antibody for Western Blot Santa Cruz #sc-68219

Anti-FLAG	Rabbit 1:6.000	Primary antibody for Western Blot Sigma-Aldrich/Merck #F7425
Anti-GAPDH	Rabbit 1:1.000	Primary antibody for Western Blot Cell Signaling #2118
Anti-Importin-α5/α7	Rabbit 1:4.000	Primary antibody for Western Blot Kind gift from Prof. Dr. E Hartmann, University of Lübeck, Lübeck, Germany
Anti-NCBP1	Rabbit 1:1.000	Primary antibody for Western Blot Abcam #ab42389
Anti-nucleoprotein	Mouse 1:1.000	Primary antibody for Western Blot Abcam #ab128193
Anti-nucleoprotein	Rabbit 1:10.000	Antibody for IHC-P, prepared in Citrate Plus Buffer (DCS) Life Technologies #PA5-32242
Anti-phospho-ANP32B	Rabbit 1:1.000	Primary antibody for Western Blot Kind gift from PD Dr. Jan Chemnitz, Heinrich Pette Institute, Hamburg, Germany

Secondary Antibody	**Origin/Dilution**	**Application/Manufacturer/Catalogue number**
Anti-goat-HRP	Rabbit 1:20.000	Secondary antibody for Western Blot Sigma-Aldrich/Merck #A5420

Anti-mouse-HRP	Goat 1:20.000	Secondary antibody for Western Blot Sigma-Aldrich/Merck #A4416
Anti-rabbit-HRP	Goat 1:20.000	Secondary antibody Western Blot Sigma-Aldrich/Merck #A8275
Biotin donkey anti-rabbit	Donkey 1:200	Secondary antibody for IHC-P, prepared in 1x PBS supplemented with 2 % donkey serum Jackson ImmunoResearch # 711-066-152

4.1.5 Enzymes

Enzyme	**Manufacturer**
DpnI	New England Biolabs
FD BamHI	Fermentas
FD NotI	Fermentas
Phusion High Fidelity (HF) DNA Polymerase	Thermo Scientific
Proteinase K	Proteinase K
SuperScript III Reverse Transcriptase (part of *Superscript™ III Reverse Transcriptase Kit;*)	Invitrogen/Life Technologies
T4 DNA Ligase	New England Biolabs
Taq DNA polymerase	Qiagen

4.1.6 Plasmids and vectors

Plasmid/Vector	Application/Description/Reference
ANP32A CRISPR/Cas9 KO Plasmid (h)	All-in-one vector to deliver a pool of three guide RNAs targeting human ANP32A and the Cas9 protein into eukaryotic cells; expresses GFP *Santa Cruz (#sc-402988)*
Control CRISPR/Cas9 plasmid	All-in-one vector to deliver a non-targeting guide RNA and the Cas9 protein into eukaryotic cells; expresses GFP *Santa Cruz (#sc-418922)*
Importin-α7 (KPNA6) CRISPR/Cas9 Plasmid	All-in-one vector to deliver a guide RNA targeting human importin-α7 (KPNA6) and the Cas9 protein into eukaryotic cells; expresses GFP; guide RNA sequence: GTGTTGATAACTTCATCTAT *GenScript (#SC1678)*
pcDNA3.1	pcDNA3.1 empty vector *Generated by P. Resa-Infante, Institut de Reserca de la Sida, Barcelona, Spain*
pcDNA3.1-ANP32A	Expresses human ANP32A WT protein *This study*
pcDNA3.1-ANP32A-C-FLAG	Expresses human ANP32A WT protein with a C-terminal FLAG tag *This study*
pcDNA3.1-ANP32A-mutNLS1	Expresses human ANP32A protein with a mutated NLS sequence (KRKR →AAKR) *This study*
pcDNA3.1-ANP32A-mutNLS1-C-FLAG	Expresses human ANP32A protein with a mutated NLS sequence (KRKR →AAKR) and a C-terminal FLAG tag *This study*

pcDNA3.1-ANP32A-mutNLS2	Expresses human ANP32A protein with a mutated NLS sequence (KRKR →AAAA) *This study*
pcDNA3.1-ANP32A-mutNLS2-C-FLAG	Expresses human ANP32A protein with a mutated NLS sequence (KRKR →AAAA) and a C-terminal FLAG tag *This study*
pcDNA3.1-CAS	Expression vector for human CAS (*cellular apoptosis susceptibility)* protein *[348]*
pcDNA3.1-C-FLAG	pcDNA3.1 vector expressing C-FLAG only *Generated by P. Resa-Infante, Institut de Reserca de la Sida, Barcelona, Spain*
pcDNA3.1-Importin-α1-C-FLAG	Expresses human importin-α1 (KPNA2) protein with a C-terminal FLAG tag *[348]*
pcDNA3.1-Importin-α1-ΔIBB-C-FLAG	Expresses human importin-α1 (KPNA2) protein with a deleted IBB domain and a C-terminal FLAG tag *[348]*
pcDNA3.1-Importin-α5-C-FLAG	Expresses human importin-α5 (KPNA1) protein with a C-terminal FLAG tag *[348]*
pcDNA3.1-Importin-α5-ΔIBB-C-FLAG	Expresses human importin-α5 (KPNA5) protein with a deleted IBB domain and a C-terminal FLAG tag *[348]*
pcDNA3.1-Importin-α7	Expresses human importin-α7 (KPNA6) protein [349]

pcDNA3.1-Importin-α7-C-FLAG	Expresses human importin-α7 (KPNA6) protein with a C-terminal FLAG tag *Generated by P. Resa-Infante, Institut de Reserca de la Sida, Barcelona, Spain*
pcDNA3.1-Importin-α7-ΔIBB-C-FLAG	Expresses human importin-α7 (KPNA6) protein with a deleted IBB domain and a C-terminal FLAG tag *[348]*
pcDNA3.1-Importin-β1	Expression vector for human importin-β_1 (KPNB1) protein *[348]*
pcDNA3.1-WSN-NP	Expression vector for A/WSN/33 NP protein *Kind gift from Ervin Fodor, Oxford University, Oxford, United Kingdom*
pcDNA3.1-WSN-PA	Expression vector for A/WSN/33 PA protein *Kind gift from Ervin Fodor, Oxford University, Oxford, United Kingdom*
pcDNA3.1-WSN-PB1	Expression vector for A/WSN/33 PB1 protein *Kind gift from Ervin Fodor, Oxford University, Oxford, United Kingdom*
pcDNA3.1-WSN-PB2	Expression vector for A/WSN/33 PB2 protein *Kind gift from Ervin Fodor, Oxford University, Oxford, United Kingdom*
pEGFP	Expression vector for enhanced green fluorescent protein (EGFP) *Clontech*
pEGFP-ANP32A	Expresses human ANP32A WT protein with a C-terminal GFP tag *This study*

pEGFP-ANP32A-mutNLS1	Expresses human ANP32A protein with a mutated NLS sequence (KRKR →AAKR) and a C-terminal GFP tag *This study*
pEGFP-ANP32A-mutNLS1	Expresses human ANP32A protein with a mutated NLS sequence (KRKR →AAAA) and a C-terminal GFP tag *This study*
pHW2000	pHW2000 empty vector, used for reverse genetics [350]
pHW2000-WSN-HA	Rescue of A/WSN/33 virus using reverse genetics *Kind gift from Hans-Dieter Klenk, University of Marburg, Marburg, Germany*
pHW2000-WSN-M	Rescue of A/WSN/33 virus using reverse genetics *Kind gift from Hans-Dieter Klenk, University of Marburg, Marburg, Germany*
pHW2000-WSN-NA	Rescue of A/WSN/33 virus using reverse genetics *Kind gift from Hans-Dieter Klenk, University of Marburg, Marburg, Germany*
pHW2000-WSN-NP	Rescue of A/WSN/33 virus using reverse genetics *Kind gift from Hans-Dieter Klenk, University of Marburg, Marburg, Germany*
pHW2000-WSN-NS	Rescue of A/WSN/33 virus using reverse genetics *Kind gift from Hans-Dieter Klenk, University of Marburg, Marburg, Germany*
pHW2000-WSN-PA	Rescue of A/WSN/33 virus using reverse genetics *Kind gift from Hans-Dieter Klenk, University of Marburg, Marburg, Germany*

pHW2000-WSN-PB1	Rescue of A/WSN/33 virus using reverse genetics *Kind gift from Hans-Dieter Klenk, University of Marburg, Marburg, Germany*
pHW2000-WSN-PB2	Rescue of A/WSN/33 virus using reverse genetics; human-adaptive PB2-627K signature *Kind gift from Hans-Dieter Klenk, University of Marburg, Marburg, Germany*
pPol-I-NP-Luc, human	Firefly luciferase reporter construct (Photinus pyralis); luciferase gene (GenBANK: AF053462) is under the control of the RNA Pol I promoter and flanked by the 3' and 5' non-coding regions of the A/WSN/33 (H1N1) virus (GenBank: M30746) [238]
pRenilla-TK	Renilla luciferase reporter construct (Renilla reniformis); luciferase gene under the control of the constitutively expressed CMV promoter *Promega*

4.1.7 DNA oligonucleotides (Sanger Sequencing, PCR, Genotyping)

DNA oligonucleotide	**Sequence (5'-3')/Application/Reference**
ANP32A-C-FLAG-for	5'-GCGGATCCACCATGGAGATGGGCAGACGGATTCAT TTAGAGCTGCG-3' Cloning of ANP32A ORF with a C-terminal FLAG tag into pcDNA3.1 vector; BamHI restriction site (5')
ANP32A-C-FLAG-rev	5'-GCGCGGCCGCTTACTTATCGTCGTCATCCTTGTAA TCGTCATCATCTTCTCCCTCATCTTCAGGTTCTCGTTTTCG-3' Cloning of ANP32A ORF with a C-terminal FLAG tag into pcDNA3.1 vector; NotI restriction site (3'); contains FLAG sequence
ANP32A-C-GFP-for	5'-GCCTCGAGACCATGGAGATGGGCAGACGGATTCAT TTAGAGC-3' Cloning of ANP32A ORF with a linker sequence into the pEGFP vector (*Clontech*), generating a C-terminal GFP tag on ANP32A

ANP32A-C-GFP-rev	5'-GCGGATCCGAGCCGCCGCCGCCCGAGCCGCCGCC GCCGTCATCATCTTCTCCCTCATCTTCAGGTTC-3' Cloning of ANP32A ORF with a linker sequence into the pEGFP vector (*Clontech*), generating a C-terminal GFP tag on ANP32A; contains linker sequence (Gly-Gly-Gly-Gly-Ser, x2)
ANP32A-for	5'-GCGGATCCACCATGGAGATGGGCAGACGGATTCAT TTAGAGCTGCG-3' Cloning of ANP32A ORF into pcDNA3.1 vector
ANP32A-mutNLS1-for	5'-GAAAGGGGTCAGGCGGCAAAACGAGAACCTGAAG ATGAGG-3' Mutation of ANP32A NLS sequence in pcDNA3.1-ANP32A expression vector (WT, "KRKR" → mutNLS1, "AAKR")
ANP32A-mutNLS1-rev	5'-CCTCATCTTCAGGTTCTCGTTTTGCCGCCTGACCCC TTTC-3' Mutation of ANP32A NLS sequence in pcDNA3.1-ANP32A expression vector (WT, "KRKR" → mutNLS1, "AAKR")
ANP32A-mutNLS2-for	5'-GAAAGGGGTCAGGCGGCAGCAGCAGAACCTGAAGA TGAGG-3' Mutation of ANP32A NLS sequence in pcDNA3.1-ANP32A expression vector (WT, "KRKR" → mutNLS2, "AAAA")
ANP32A-mutNLS2-rev	5'-CCTCATCTTCAGGTTCTGCTGCTGCCGCCTGACCCC TTTC-3' Mutation of ANP32A NLS sequence in pcDNA3.1-ANP32A expression vector (WT, "KRKR" → mutNLS2, "AAAA")
ANP32A-NeoRev	5'-CTACCGGTGGATGTGGAATGTGTGCG-3' Genotyping of ANP32A$^{+/+}$, ANP32A$^{+/-}$ and ANP32A$^{-/-}$ mice [351]
ANP32A-ScPr fwd	5'-CTAATCCCTCTTCAGAGAACTGCCCTGTTCAAG-3' Genotyping of ANP32A$^{+/+}$, ANP32A$^{+/-}$ and ANP32A$^{-/-}$ mice [351]

ANP32A-WtRev	5’-GAATGAGGTGAGAGGTCAAGATTCAGCTGC-3’ Genotyping of ANP32A$^{+/+}$, ANP32A$^{+/-}$ and ANP32A$^{-/-}$ mice [351]
ANP32B-allele-P1	5’-GGTTTTGTTTAATTTTGGGAGAGCACTAAACTTA-3’ Genotyping of ANP32B$^{+/+}$, ANP32B$^{+/-}$ and ANP32B$^{-/-}$ mice [352]
ANP32B-allele-P2	5’-GAAAATGATGAACTCTAAGCACAGAAAGGATTCT-3’ Genotyping of ANP32B$^{+/+}$, ANP32B$^{+/-}$ and ANP32B$^{-/-}$ mice [352]
ANP32B-Cre-for	5’-CTCTAGAGCCTCTGCTAACC-3’ Genotyping of ANP32B$^{+/+}$, ANP32B$^{+/-}$ and ANP32B$^{-/-}$ mice [352]
ANP32B-Cre-rev	5’-CCTGGCGATCCCTGAACATGTCC-3’ Genotyping of ANP32B$^{+/+}$, ANP32B$^{+/-}$ and ANP32B$^{-/-}$ mice [352]
ANP32A-rev	5’-GCGCGGCCGCTTAGTCATCATCTTCTCCCTCATCTT CAGGTTCTCGTTTTCG-3’ Cloning of ANP32A ORF into pcDNA3.1 vector
BGH-rev	3’-TAGAAGGCACAGTCGAGG-5’ Sanger sequencing of pcDNA3.1 and pHW2000 vectors, amplifies BGH terminator sequence
CMV-for	5’CGCAAATGGGCGGTAGGCGTG-3’ Sanger sequencing of pcDNA3.1 and pHW2000 vectors, amplifies CMV promoter sequence
Oligo p(dN)9 Random nonamers	Gene Link

4.1.8 DNA oligonucleotides (qRT-PCR)

Primer/Gene (m, *Mus musculus*)	Accession No./Sequence 5'-3'/Amplified DNA fragment
A/WSN/33-NP-fwd	CY034135.1 5'-AGGGTCAGTTGCTCACAAGTCC-3' 124 bp
A/WSN/33-NP-rev	CY034135.1 5'- TTTGAAGCAGTCTGAAAGGGTCTA-3' 124 bp
mCXCL10-for	NM_021274.2 5'- ATCATCCCTGCGAGCCTATCCT-3' 134 bp
mCXCL10-rev	NM_021274.2 5'- GACCTTTTTTGGCTAAACGCTTTC -3' 134 bp
mIFN-β1-for	NM_010510.1 5'- CCAGCTCCAAGAAAGGACGA-3' 216 bp
mIFN-β1-rev	NM_010510.1 5'- GTCTCATTCCACCCAGTGCT -3' 216 bp
mIL-1β-for	NM_008361.4 5'-GCACTACAGGCTCCGAGATGAAC-3' 147 bp
mIL-1β-rev	NM_008361.4 5'- TTGTCGTTGCTTGGTTCTCCTTGT -3' 147 bp

mIL-6-for	NM_031168.2 5’- CTCCCAACAGACCTGTCTATAC-3’ 129 bp
mIL-6-rev	NM_031168.2 5’- GTGCATCATCGTTGTTCATAC -3’ 129 bp
mIRF-7-for	NM_016850.3 5’-CAGCGAGTGCTGTTTGGAGAC-3’ 351 bp
mIRF-7-rev	NM_016850.3 5’-AAGTTCGTACACCTTATGCGG-3’ 351 bp
mMCP-1 (CCL-2)-for	NM_011333.2 5’- TGATCCCAATGAGTAGGCTGGAG-3’ 132 bp
mMCP-1 (CCL-2)-rev	NM_011333.2 5’- ATGTCTGGACCCATTCCTTCTTG-3’ 132 bp
mMx1-for	NM_010846.1 5’- GGGGAGGAAATAGAGAAAATGAT-3’ 275 bp
mMx1-rev	NM_010846.1 5’- GTTTACAAAGGGCTTGCTTGCT-3’ 275 bp

mRPS9-for	NM_029767.2 5’-CCGCCTTGTCTCTCTTTGTC-3’ 177 bp
mRPS9-rev	NM_029767.2 5’-CCGGAGTCCATACTCTCCAA-3’ 177 bp
mTNF-α-for	NM_013693.3 5’-TCGTAGCAAACCACCAAGTG-3’ 207 bp
mTNF-α-rev	NM_013693.3 5’- AGATAGCAAATCGGCTGACG -3’ 207 bp

4.1.9 RNA oligonucleotides (siRNA)

Primer/Gene (h, *Homo sapiens*)	**Sequence 5’-3’/Manufacturer/Reference**
Allstars Negative Control siRNA	Qiagen
hANP32A siRNA	5’-CAAUCGCAAACUUACCAAA**AG**-3’ (sense) 5’-UUUGGUAAGUUUGCGAUUG**AG**-3’ (antisense) Sigma-Aldrich/Merck
hImportin-α7 siRNA	5’-AGAGCCUAGUCCUCCAAUA**UU**-3’ (sense) 5’-UAUUGGAGGACUAGGCUCU**UU-3’** (antisense) Sigma-Aldrich/Merck [50]

4.1.10 Narcotics and supplements

Description	Manufacturer
Forene/Isofluorane (100%)	Abbott
Ketamine (100 mg/ml)	WDT
Sodium chloride (NaCl) (0.9%)	B. Braun Melsungen AG
Xylazine (20 mg/ml)	WDT

4.1.11 Bacterial strains

Species	Strain/Genotype
Escherichia coli (E. coli)	XL1 Blue Δ(*mcrA*)*183* Δ(*mcrCB-hsdSMR-mrr*)*173 endA1 supE44 thi-1 recA1* gyrA96 relA1 lac *[F'* proABlac^{q}Z *Δ*M15*Tn(Tet^{r})]*

4.1.12 Media and supplements for bacterial cell culture

Bacterial growth media were autoclaved after preparation, and antibiotics were added prior to usage as sterile-filtered solutions at 1:1.000 dilution.

Medium	Composition
Ampicillin (100 mg/ml)	5 g ampicillin ad 50 ml ddH_2O
Cryoconservation medium	700 µl bacterial overnight culture 30 % glycerol
Luria Broth (LB) agar	LB medium 1.5 % Bacto-Agar

Luria Broth (LB) medium	10 g Trypton (Pepton) 5 g Yeast extract 10 g NaCl ad 1 L ddH_2O pH 7.5

4.1.13 Eukaryotic cell lines

Cell line	Description/Origin/Reference
C57BL/6J ANP32A$^{-/-}$ murine lung fibroblasts (mLF)	Immortalized murine lung fibroblast cell line, isolated from ANP32A$^{-/-}$ mice (♂) *This study*
C57BL/6J ANP32A$^{+/+}$ murine lung fibroblasts (mLF)	Immortalized murine lung fibroblast cell line, isolated from ANP32A$^{+/+}$ mice (♂) *This study*
C57BL/6J ANP32B$^{-/-}$ murine lung fibroblasts (mLF)	Immortalized murine lung fibroblast cell line, isolated from ANP32B$^{-/-}$ mice (♂) *This study*
C57BL/6J ANP32B$^{+/+}$ murine lung fibroblasts (mLF)	Immortalized murine lung fibroblast cell line, isolated from ANP32B$^{+/+}$ mice (♂) *This study*
HeLa (ANP32B KO #1)	Immortalized human HeLa cell line (♀) Knockout of ANP32B using CRISPR/Cas (clone #1) *Kind gift from PD Dr. Jan Chemnitz, Heinrich Pette Institute, Hamburg, Germany*
HeLa (ANP32B KO #2)	Immortalized human HeLa cell line (♀) Knockout of ANP32B using CRISPR/Cas (clone #2) *Kind gift from PD Dr. Jan Chemnitz, Heinrich Pette Institute, Hamburg, Germany*

HeLa (ANP32B Control)	Immortalized human HeLa cell line (♀) CRISPR/Cas control cell line, treated with non-targeting guide RNA *Kind gift from PD Dr. Jan Chemnitz, Heinrich Pette Institute, Hamburg, Germany*
Human Embryonic Kidney 293T (HEK293T)	Immortalized human HEK293T cell line (♀) *Leibniz Institute DSMZ (ACC 635)*
Madin-Darby Canine Kidney (MDCK)	Immortalized canine MDCK cell line (♀) *ATCC (CCL-34)*

4.1.14 Media and supplements for eukaryotic cell culture

Medium	Manufacturer
Bovine serum albumin solution (BSA; 35%, in D-PBS)	Sigma-Aldrich/Merck
Cryoconservation medium	FBS 10 % DMSO
Dulbecco's Modified Eagle's Medium (DMEM)	Sigma-Aldrich/Merck
Dulbecco's Modified Eagle's Medium (DMEM), SILAC R0K0 (non-labeled arginine and lysine)	Gemini Biosciences
Dulbecco's Modified Eagle's Medium (DMEM), SILAC R10K8 (13C/15N labeled arginine and lysine)	Gemini Biosciences
Dulbecco's Modified Eagle's Medium (DMEM), SILAC R6K4 (13C labeled arginine and 2D labeled lysine)	Gemini Biosciences
Dulbecco's Phosphate Buffered Saline (D-PBS)	Sigma-Aldrich/Merck
FBS, dialyzed, US origin (for SILAC experiments)	Sigma-Aldrich/Merck

Fetal bovine serum (FBS) superior	Biochrom GmbH
HEK293T/HeLa growth medium	DMEM 10 % FBS 1 % L-Glutamine 1 % Penicillin & Streptomycin (P/S)
HEK293T transfection medium (DMEM-TF)	DMEM 10 % FBS 1 % L-Glutamine
Infection medium (HEK293T)	SILAC-DMEM 1 % L-Glutamine 1 % P/S 2 % dialyzed FBS 0.2 % BSA
Infection medium (HeLa)	DMEM 1 % L-Glutamine 1 % P/S 0.1 % FBS 0.2 % BSA 1:1.000 TPCK trypsin, if necessary
Infection medium (MDCK)	MEM 1 % L-Glutamine 1 % Penicillin & Streptomycin (P/S) 0.2 % BSA 1:1000 TPCK trypsin, if necessary (2 % FBS, for A/WSN/33 virus rescue only)

Infection medium (mLF)	DMEM
	1 % L-Glutamine
	1 % P/S
	1 % NEAA
	1 % Na-pyruvate
	0.1 % FBS
	0.2 % BSA
	1:1.000 TPCK trypsin, if necessary
Inoculation medium (MDCK)	MEM
	1 % L-Glutamine
	1 % Penicillin & Streptomycin (P/S)
Inoculation medium (HEK293T, HeLa)	DMEM (HeLa) or SILAC-DMEM (HEK293T)
	1 % L-Glutamine
	1 % P/S
Inoculation medium (mLF)	DMEM
	1 % L-Glutamine
	1 % P/S
	1 % NEAA
	1 % Na-pyruvate
L-Glutamine (200 mM)	Sigma-Aldrich/Merck
MDCK growth medium	MEM
	10 % FBS
	1 % L-Glutamine
	1 % Penicillin & Streptomycin (P/S)
Minimum Essential Medium (MEM)	Sigma-Aldrich/Merck

mLF growth medium	DMEM 10 % FBS 1 % L-Glutamine 1 % P/S 1 % NEAA 1 % Na-pyruvate
Modified Eagle Medium 2x (2x MEM), without Phenol Red	Sigma-Aldrich/Merck
Non-essential amino acid solution (NEAA; 10 nM)	Biozym Scientific GmbH
OptiMEM I medium (1x)	Gibco by Life Technologies
Overlay medium for plaque test	2x MEM (2 % L-Glu, 2 % P/S, 0.4 % BSA) *and* 2.5% Avicel in ddH_2O (*1:1 mixture*)
Penicillin-Streptomycin (P/S)	Sigma-Aldrich/Merck
Sodium pyruvate solution (Na-pyruvate; 100 mM)	Sigma-Aldrich/Merck
Trypsin from bovine pancreas, TPCK-treated (TPCK trypsin)	Sigma-Aldrich/Merck
Trypsin-EDTA	Sigma-Aldrich/Merck

4.1.15 Virus strains

Virus strain	**Origin/Description/References**
A/WSN/33 (H1N1)	Generated by reverse genetics; carries the human-adaptive $PB2_{627K}$ signature [353]

A/Vietnam/1194/04 (H5N1)	Isolate from a fatal human case in Vietnam in 2004; carries the human-adaptive $PB2_{627K}$ signature *Kind gift from Hans-Dieter Klenk, University of Marburg, Marburg, Germany*
A/WSN/33(H1N1) – A/Aichi/2/68 (H3N2)	Generated by reverse genetics; 6+2 virus, i.e. HA and NA are derived from the 1968 pandemic Aichi lineage and all remaining gene segments from the WSN strain; virus was shown to be pathogenic in mice, in contrast to currently circulating H3N2 variants; carries the human-adaptive $PB2_{627K}$ signature [353, 354]

4.1.16 Experimental mouse lines

Mouse line	Background	Description/Reference
$ANP32A^{-/-}$	C57BL/6J	Littermates of $ANP32A^{+/+}$ mice, knockout of the ANP32A protein was confirmed by genotyping and Western blotting (lung, brain) Generated using sperm purchased from the EMMA repository (originally deposited by Tak W Mak, University Health Network, Toronto, Canada) and embryo transfer at the University Medical Center Hamburg-Eppendorf, Hamburg, Germany [351]
$ANP32A^{+/+}$	C57BL/6J	Littermates of $ANP32A^{-/-}$ mice expressing the ANP32A protein as confirmed by genotyping and Western blotting (lung, brain) Generated using sperm purchased from the EMMA repository (originally deposited by Tak W Mak, University Health Network, Toronto, Canada) and embryo transfer at the University Medical Center Hamburg-Eppendorf, Hamburg, Germany [351]

ANP32B$^{-/-}$	C57BL/6J	Littermates of ANP32B$^{+/+}$ mice, knockout of the ANP32B protein was confirmed by genotyping and Western blotting (lung, brain) Generated using the Cre recombinase approach and provided by PD Dr. Jan Chemnitz, Heinrich Pette Institute, Hamburg, Germany [352]
ANP32B$^{+/+}$	C57BL/6J	Littermates of ANP32B$^{-/-}$ mice expressing the ANP32B protein as confirmed by genotyping and Western blotting (lung, brain) Generated using the Cre recombinase approach and provided by PD Dr. Jan Chemnitz, Heinrich Pette Institute, Hamburg, Germany [352]

4.1.17 Consumables

Consumable	Manufacturer
12-well tissue culture plate	Greiner bio-one Cellstar
24-well tissue culture plate	Falcon / BD Biosciences
6-well tissue culture plate	Falcon / BD Biosciences
96-well conical bottom microwell plate	Nunc
96-well lockwell plate (white)	Nunc
96-well tissue culture plate	Sarstedt
Cannula Microlance™ 3 (25G x 1'', 0.5x25 mm)	BD Microlance
Cannula Microlance™ 3 (26G x 3/8'', 0.45x10 mm)	BD Microlance
Cannula Microlance™ 3 (27G x ¾'', 0.4x19 mm)	BD Microlance
Capillary/EDTA tubes for blood collection (200 µl)	Kabe Labortechnik GmbH

Cryo vials (1ml)	Sarstedt
Glass beads (ø 0.50-0.75 mm)	RETSCH (#22.222.0003)
Ibidi glass-bottom dishes	Ibidi GmbH
Metal beads (ø 2.0 mm)	RETSCH (#22.455.0010)
Nitrocellulose membrane Hybond-C Extra	Amersham Biosciences
PCR tubes (8-stripes)	Sarstedt
Petri dishes (100mm)	Falcon / BD Biosciences
Pipette tips, with filter (10, 100, 1000 µl)	Sarstedt
Pipette tips, without filter (100, 100, 1000 µl)	Brandt
Precision wipe tissue	Kimtech Science
Reaction tubes (1.5 ml, 2.0 ml)	Sarstedt
SafeSeal reaction tubes (+screw caps)	Sarstedt
Scalpel	BRAUN
Syringe Omnifix® (10 ml / Luer Lock Solo)	B. Braun Melsungen AG
Syringe Omnifix® (20 ml / Luer Lock Solo)	B. Braun Melsungen AG
Syringe Omnifix® (3 ml / Luer Lock Solo)	B. Braun Melsungen AG
Syringe TERUMO®, without needle, U-100 Insulin (1 ml, 6 % Luer)	TERUMO Cooperation
T25 cell culture flask	Falcon / BD Biosciences
T75 cell culture flask	Sarstedt
Tissue culture dish (100 mm)	Falcon / BD Biosciences

Transfer pipettes (5, 10, 25 ml)	Sarstedt
Whatman paper	A. Hartenstein

4.1.18 Safety gear

Safety gear	Manufacturer
Duct tape *Extra Universal*	TESA
Filter/respirator mask, type 9332 FFP3 ventil	3M
Gloves *Biogel*	3M
Gloves Latex	Kimberly-Clark
Gloves Purple Nitrile	Kimberly-Clark
Lab coat	Leiber
Lab shoes Unisex	Suecos
OP mask	Mölnlycke Health Care
OP Nurse Cap	Mölnlycke Health Care
OP pants (green)	Sattelmacher
Overalls (blue)	ProFit
Safety goggles	UVEX
Shoe covers (blue)	Ansell Health Care
TYVEK® boot covers	DuPont
TYVEK® overalls	DuPont

4.1.19 Laboratory equipment

Laboratory equipment	Manufacturer
Animal scale	Kern
Biological safety cabinet *HeraSafe KS12*	Thermo Scientific
Biological safety cabinet *HeraSafe KS18*	Thermo Scientific
Centrifuge *Avanti J-E*	Beckham Coulter
Centrifuge *Centrifuge 5417R*	Eppendorf
Centrifuge *Varifuge 3.0R*	Thermo Scientific
Cryo conservation container *Mr. Frosty*	Nalgene
Documentation System *Imagequant LAS 4000 GE*	Amersham Biosciences
Double door system autoclave (BSL-3 laboratory)	MMM
Electrophoresis system *Mini Trans-Blot Cell*	Bio-Rad
FACS Aria-Fusion (5-laser, 18-fluorescence system)	BD Biosciences
Gel documentation system *Gel Doc XR*	Bio-Rad
Gel electrophoresis system *Mini-PROTEAN Tetra Cell*	Bio-Rad
Gel electrophoresis system *Sub-Cell GT (15 x 15 cm)*	Bio-Rad
Heraeus temperature-controlled CO_2 incubator *B6120*	Kendro
Heraeus temperature-controlled CO_2 incubator *BBD 6220*	Thermo Scientific
Heraeus temperature-controlled CO_2 incubator Heracell 150	Thermo Scientific

Intelli-Mixer (overhead mixer for falcon tubes)	NeoLab
Isoflurane vaporizer	UNO
LightCycler® 96	Roche
Luminometer *TriStar LB 94*	Berthold Technologies
Magnetic stirrer *MR3001* (with heating element)	Heidolph
Microliter pipettes *Eppendorf Reference* (1-10, 10-100, 100-1000 µl)	Eppendorf
Microplate reader *Tecan Safire2*	Tecan
Microwave *Supratomic M754*	Miele
Mikrotom HM325	Microm
Mixer mill *MM 400*	RETSCH
Multichannel pipettes (8 channel; 5-50 µl; 20-200 µl)	Brand
Neubauer counting chamber, bright light	Marienfeld
NextSeq500	Illumina
Nikon Eclipse 80i upright light microscope, coupled with Color Camera Nikon DS-Ri2	Nikon (Japan)
Nikon Eclipse Ti-E spinning disc microscope	Nikon (Japan)
Overhead shaker	Heidolph
Paraffin embedding center *EG1160*	Leica Biosystems
PCR cycler *GeneAmp PCR System 9700*	Applied Biosystems
pH calculation device *pHenomenal*®	VWR

Pipetus	Hirschmann Laborgeräte
Power Pac HC Power Supply	Bio-Rad
Precision scale *Extend ED224S*	Sartorius
Precision scale *ExtendED3202S-CW*	Sartorius
Quadrupole ion trap orbitrap mass spectrometer *Fusion*	Thermo Scientific
Roche LightCycler ® 96	Roche
Roller Mixer SRT9	Stuart
Shaker *MaxQ 6000*	Thermo Scientific
Shaker *WT 17*	Biometra
Shaking waterbath*SW22*	Julabo
Small centrifuge (1.5 reactions tubes)	Biozym
Small centrifuge (PCR 8-stripes)	Biozym
Sonicator *UP100H*	Heidolph
Spectrophotometer *NanoDrop 1000*	Peqlab
Spectrophotometer *Spectronic Genesys 10 Bio*	Thermo Scientific
Surgical forceps (for organ harvesting)	F.S.T.
Surgical scissors (for organ harvesting)	F.S.T.
Thermomixer *TMix 220V*	Analytik Jena
ThermoMixer® C, including Thermoblock	Eppendorf
Thermostat *Precitherm PFV*	Labora Mannheim

Tissue infiltration system ASP300	Leica Biosystems
Transmitted-light microscope	Zeiss
Ultrapure water system *Milli Q Aca*	Millipore
UPLC system Dionex Ultimate 3000	Thermo Scientific
Vacuum centrifuge	Eppendorf
Vortex-Mixer *7-2020*	neoLab

4.1.20 Software

Software	**Manufacturer/Reference**
Adobe Photoshop CS4	Adobe Systems Inc.
BD FACS Diva™ Software v.8.0.1	BD Biosciences
Clone Manager Professional 9	Sci-Ed Software
ClustVis	[355]
Cytoscape	[356]
DeSeq2	[357]
GraphPadPrism v.5.03	GraphPad Software Inc.
ImageJ	National Center for Biotechnology Information
Inkscape v.0.92.3	https://inkscape.org
LightCycler® 96 software, V 1.1.0.1320	Roche
MaxQuant (v. 1.6.2.10)	Max Plank Institute for Biochemistry

Microsoft Office	Microsoft
Mikrowin2000 software v.4.41	Berthold Technologies / Mikrotek Laborsysteme GmbH
Nikon NIS-Elements Advanced Research 4.51	Nikon (Japan)
Pymol 2.3 (by Schrödinger)	https://pymol.org/2/
Search Tool for the Retrieval of Interacting Genes/Proteins (STRING)	https://string-db.org [358]
STAR	[359]
ToppGene Suite	https://toppgene.cchmc.org/ [360]

4.2 Methods

4.2.1 Microbiological techniques

4.2.1.1 Cultivation of bacteria

Bacterial strains used for preparation of plasmid DNA or cloning approaches were either cultivated on LB agar plates or in LB medium at 37°C, supplemented with the appropriate antibiotics. Glycerol stocks of bacteria were prepared by mixing 700 µl of a bacterial culture and 300 µl of 80% glycerol (final glycerol concentration: 25 %) and stored at -80 °C.

4.2.1.2 Preparation of plasmid DNA

All plasmid DNA preparations were carried out in LB bacterial growth medium freshly supplemented with appropriate antibiotics.

Maxi plasmid DNA for transfection of eukaryotic cells was prepared from a bacterial cell culture using the *Nucleobond Xtra Maxi* kit (Macherey & Nagel). Briefly, a 5 ml LB medium culture was inoculated with a scratch from a glycerol stock and incubated for 8 h at 37 °C (210 rpm). Then, a 250 ml LB medium culture was inoculated with 1 ml of the first culture and further incubated overnight (approx. 16 h) at 37 °C (160 rpm). Plasmid DNA was subsequently isolated according to manufacturer's instructions. The DNA concentration was measured using *NanoDrop1000*, adjusted to 1 µg/µl and stored at -20 °C. Plasmid identity was confirmed by analytical digestion with restriction enzymes (chapter 4.2.3.1) and agarose gel electrophoresis (chapter 4.2.3.2).

Mini plasmid DNA was prepared using the *MiniPrep Spin Kit* (Qiagen) according to manufacturer's instructions. Therefore, a 5 ml LB medium culture was inoculated with a single bacterial colony from plate and incubated overnight (approx. 16 h) at 37 °C (210 rpm). Plasmid DNA was eluted from columns with 50 µl of ddH_2O and stored at 4 °C (short term) or -20 °C (long-term) until further processing.

4.2.2 Cell culture techniques

4.2.2.1 Cultivation of eukaryotic cells

HEK293T and HeLa cell lines were cultivated in Dulbecco's Modified Eagles Medium (DMEM), supplemented with 10 % fetal bovine serum (FBS), 1 % L-Glutamine (L-Glu) and 1 % penicillin/streptomycin (P/S). MDCK cells were maintained in Minimal Essential Medium (MEM), supplemented with 10 % FBS, 1 % L-Glu and 1 % P/S. Isolated murine lung fibroblasts (mLF) were cultivated in DMEM medium, supplemented with 10 % FBS, 1 % L-Glu, 1 % P/S, 1 % non-

essential amino acids (NEAA) and 1 % sodium pyruvate. All cell lines were maintained in a temperature-controlled incubator at 37 °C, 5 % CO_2 and 95 % relative humidity (rH).
Human cell lines (HEK293T, HeLa) were verified by STR analysis (chapter 4.2.2.3) and regularly checked for mycoplasma contamination (chapter 4.2.2.4).

4.2.2.2 Freezing and thawing of eukaryotic cells

Eukaryotic cell lines were stored in liquid nitrogen or at -80 °C (short-term). To prepare cryo-conserved stocks, a confluent T75 flask was trypsinized, cells were pelleted by centrifugation (1.000 x g, 5 min, at room temperature), resuspended in 3 ml of a 10 % DMSO solution (in FBS), aliquoted à 1 ml into cryo vials, and stored at -80°C until transfer into liquid nitrogen.
Cells were re-introduced into cell culture by thawing at 37°C, followed by a washing step in growth medium to remove residual traces of DMSO (centrifugation: 300 x g, 5 min). Pelleted cells were then resuspended in growth medium, seeded into T25 cell culture flasks and incubated further at 37 °C, 5 % CO_2, 95 % rH.

4.2.2.3 Authentication of human cell lines

Human cell lines (HEK293T, HeLa) were authenticated by short-tandem repeat (STR) analysis through the external service provider *Eurofins Genomics* (**Table 3**).

Table 3: STR profile of authenticated human cell lines.

STR marker	HEK293T	HeLa
AMEL	X	X,X
CSF1PO	11,12	9,10
D13S317	12	12,13.3
D16S539	9,13	9,10
D18S51	17,18	16,16
D19S433	18	13,14
D21S11	28,30.2	27,28
D2S1338	19	17,17
D3S1358	15,16,17	15,18
D5S818	8,9	11,12

D7S820	11	8,12
D8S1179	12,14	12,13
FGA	23	21,21
TH01	7,9.3	7,7
TPOX	11	8,12
vWA	16,19	16,18

4.2.2.4 Mycoplasma PCR

All eukaryotic cell lines used in this study were regularly verified to be negative for mycoplasma contamination using the *Venor®GeM Classic Mycoplasma PCR Detection Kit* (Minerva Biolabs GmbH) according to manufacturer's instructions.

4.2.3 Nucleic acid techniques

4.2.3.1 Analytical digestion of plasmid DNA

The identity of plasmid DNA can be confirmed using specific endonucleases that generate a distinct restriction pattern. In this study, this technique was employed to either confirm the identity of plasmid DNA derived from Maxi preparations or to identify positive bacterial clones carrying newly generated expression vectors. In both cases, the plasmid DNA was digested using restriction endonucleases for 1.5 h at 37 °C, followed by agarose gel electrophoresis to visualize the DNA restriction pattern (**Table 4**).

Table 4: Digestion of plasmid DNA with endonucleases.

Component (Concentration/Amount)	**Volume**
Plasmid DNA (500 ng)	2.0 µl
FD Green Buffer (10x)	2.0 µl
Enzyme I	0.2 µl
Enzyme II	0.2 µl
ddH_2O	15.6 µl
Total	**20 µl**

4.2.3.2 Agarose gel electrophoresis

Plasmid DNA, either intact or digested with restriction enzymes, can be visualized using agarose gel electrophoresis. Here, DNA or RNA fragments are separated according to their size in an electrical field. Ethidium bromide (EtBr) or other intercalating substances are used to visualize the DNA in the gel. For a 1 % agarose gel, 1 g of agarose was dissolved in 100 ml of 1xTAE buffer, EtBr was added, and the solution was poured into the gel chamber. Samples are either ready-to-use (using FD Green Buffer) or mixed with a 6x DNA loading dye and then loaded onto the gel. Electrophoresis was carried out for 45 to 60 min at 120 V. Visualization was performed using the *Gel Documentation System Gel Doc XR* (Bio-Rad).

4.2.3.3 Isolation of total RNA from eukaryotic cells or murine tissue

Total RNA was isolated from HEK293T cells to obtain cDNA of human ANP32A for insertion into the pcDNA3.1 expression vector. Briefly, HEK293T cells (approx. 4 x 10^6 cells) were harvested by centrifugation (1000 x g, 5 min, 4 °C) and the cell pellet was resuspended in 1 ml of Trizol reagent. 200 µl of chloroform were added and the tube was continuously inverted for 15 s. After centrifugation at 12.000 x g for 15 min (RT), the aqueous phase was transferred to a fresh tube, mixed with 500 µl of 2-propanol and incubated for 10 min at RT. The tube was centrifuged (12.000 x g, 10 min, RT) and the pellet fraction (RNA) was washed with 1 ml of 70 % ethanol. The pellet was air-dried for 5 to10 min and dissolved in 100 µl of ddH_2O (RNAse free, pre-warmed to 70 °C) by incubation for 10 min at 55 °C. RNA aliquots of 20 µl were stored at -80 °C. For qRT-PCR or NGS analyses, total RNA was isolated from murine lung tissue using the *innuPrep RNA Mini Kit* (Analytik Jena) according to manufacturer's instructions, with minor modifications. Therefore, approximately 30 mg of extracted lung tissue (stored at -80°C) was used. An additional on-column treatment with DNase (*RNase-Free DNase Set*; Qiagen) was performed to digest genomic DNA. RNA was eluted with 30 µl of RNase-free ddH_2O. The concentration was measured on *NanoDrop1000*, *Ribolock RNA inhibitor* (Life Technologies GmbH; 0.75 µl / 30 µl of eluted RNA) was added and RNAs were stored at -80 °C for subsequent analyses.

4.2.3.4 Polymerase chain reaction (PCR)

Polymerase chain reaction (PCR) is a molecular method to amplify DNA or cDNA sequences using primers, exogenously provided polymerases, and heat cyclers. The primers were designed according to standard guidelines [361]. All primer sequences were generated using the *Clone Manager 9 Professional Edition* software. T_M melting temperatures were calculated using the

online tool *Oligonucleotide Properties Calculator* (http://biotools.nubic.northwestern.edu/OligoCalc.html).

In this study, PCR was used for genotyping (chapter 4.2.8.1), cloning of the ANP32A ORF into eukaryotic expression vectors (pcDNA3.1 or pEGFP; non-tagged, with C-terminal FLAG or GFP tag), and site directed mutagenesis of pcDNA3.1-ANP32A vectors (chapter 4.2.3.5). **Table 5** summarizes the setup of the PCR reaction, including the cycling parameters. The generation of cDNA from isolated RNA is further described in chapter 4.2.3.6.

Table 5: Setup of the PCR reaction (including cycling parameters).

Component	Concentration	Final concentration	Volume
ddH_2O	-	-	32 µl
HF buffer	5x	1x	10 µl
Primer 1 (p5, forward: 5‘ → 3‘)	10 µM	400 nM	2 µl
Primer 2 (p3, reverse: 3‘ → 5‘)	10 µM	400 nM	2 µl
Template DNA (cDNA)	-	-	2 µl
dNTPs	10 mM	200 nM	1 µl
Phusion HF DNA Polymerase	2 U/µl	2 U	1 µl
Total			**50 µl**
PCR cycling	**98 °C, 5 min** **98 °C, 10 sec** **57-62 °C, 30 sec** **72 °C, 50 sec** **72 °C, 10 min** **4 °C, ∞**	**30 cycles**	

4.2.3.5 Site-directed mutagenesis PCR and digestion with DpnI

The site-directed mutagenesis (SDM) approach was used to introduce nucleotide mutations into pcDNA3.1-ANP32A expression vectors leading to amino acid substitutions in the basic nuclear localization signal (NLS; WT, “KRKR”; mutNLS1, “AAKR”; mutNLS2, “AAAA”). Herein, the template DNA was amplified using a primer pair that carries the desired mutation. After the PCR, the parental template DNA was digested with the DpnI enzyme which recognizes methylated

DNA, and the digested sample was transformed into *E. coli* XL1-Blue cells (chapter 4.2.3.11). The setup pf the PCR reaction, including the cycling parameters, is shown in **Table 6**.

Table 6: Setup of the PCR reaction for SDM (including cycling parameters).

Component	Concentration	Final concentration	Volume
ddH_2O	-	-	29 µl
HF buffer	5x	1x	10 µl
Primer 1 (p5, forward: 5‘ → 3‘)	10 µM	400 nM	2 µl
Primer 2 (p3, reverse: 3‘ → 5‘)	10 µM	400 nM	2 µl
Template DNA	10 ng/µl	50 ng	5 µl
dNTPs	10 mM	200 nM	1 µl
Phusion HF DNA Polymerase	2 U/µl	2 U	1 µl
Total			**50 µl**
PCR Cycling	**98 °C, 5 min** **98 °C, 30 sec** **65 °C, 60 sec** **72 °C, 10 min** **72 °C, 5 min** **4 °C, ∞**	**20 cycles**	

4.2.3.6 Reverse transcription PCR (RT-PCR)

Reverse transcriptase (RT) is an enzyme that catalyzes the synthesis of complementary DNA (cDNA) based on an RNA template using either a specific primer for a gene of interest or a random primer mix to generate a pool of cDNAs from all (m)RNAs present in the sample. Here, a reverse transcription reaction was carried out to generate cDNA of the human ANP32A open reading frame (ORF), based on total RNA isolated from HEK293T cells (chapter 4.2.3.3) and ANP32A specific p5 and p3 primers. The quantitative RT-PCR (qRT-PCR) reaction to measure expression levels of pro-inflammatory genes in lung tissue from infected mice is further outlined in chapter 4.2.3.13.

The setup of the ANP32A RT reaction is displayed in **Table 7**. First, cDNA synthesis was performed using the ANP32A-specific p3 primer. Then, a classical PCR reaction was used for

amplification of the ANP32A-ORF with specific restriction sites for endonucleases at each end (BamHI, NotI) (chapter 4.2.3.4).

Table 7: Setup of RT reaction for cDNA synthesis.

Component	**Volume/Amount**
ddH_2O	ad 13 µl
Primer 1 (p3, reverse: 3‘ → 5‘), 10 µM	1 µl
dNTPs, 10 mM	1 µl
RNA	~ 500 ng
Total	**13µl**
PCR Cycling	**65 °C, 5 min**
First Strand Buffer (5x)	4 µl
DTT, 0.1 M	1 µl
Ribolock RNAse Inhibitor	1 µl
Superscript III RT, 200 U/µl	1 µl
Total	**20 µl**
PCR Cycling	**25 °C, 5 min** **55 °C, 60 min** **70 °C, 15 min**

4.2.3.7 Purification of PCR products

The products of PCR reactions, as described in chapter 4.2.3.4, were further purified using the *QIAquick PCR Purification Kit* (Qiagen) according to manufacturer’s instructions to wash out the polymerase, nucleotides and primers. The DNA was eluted in 30 µl of ddH_2O and either stored at -20 °C or directly used for preparative digestion with restriction enzymes (chapter 4.2.3.8).

4.2.3.8 Preparative digestion of PCR products with restriction endonucleases

In order to prepare the purified PCR products (chapter 4.2.2.7) and the destination vector (pcDNA3.1) for ligation, both were digested with specific restriction endonucleases (BamHI, NotI) for 1.5 h at 37 °C. The setup of the reaction is shown in **Table 8**.

Table 8: Setup of preparative digestion of PCR products with restriction endonucleases.

Component	Volume
PCR product or Vector (100 ng/µl)	2 µl (PCR product) or 5 µl (vector)
FD Green Buffer, 10x	2 µl
BamHI	0.2 µl
NotI	0.2 µl
ddH_2O	15.6 µl (PCR product) or 12.6 µl (vector)
Total	**20 µl**

4.2.3.9 Gel extraction of plasmid DNA

PCR products that were digested with restriction enzymes for ligation were loaded onto a 1 % agarose gel. The digested DNA fragments (insert and vector) were visualized using the *Gel documentation system Gel Doc XR* (Bio-Rad), cut out of the gel and extracted from the gel piece using the *QIAquick Gel Extraction Kit* (Qiagen) according to manufacturer's instructions. Elution of DNA was performed in 30 µl of ddH_2O.

4.2.3.10 Ligation of DNA fragments into expression vectors

The gel-extracted PCR product (human ANP32A ORF; chapter 4.2.3.9) was ligated into the pcDNA3.1 expression vector using the *T4 DNA Ligase* (New England Biolabs). The ligation reaction (**Table 9**) was incubated for 2 h at RT.

Table 9: Setup of the T4 ligation reaction.

Component	Volume
Insert DNA (PCR product)	5 µl
Vector DNA (pcDNA3.1)	1 µl
Ligation buffer (10x)	1 µl
T4 DNA Ligase	1 µl
ddH_2O	2 µl
Total	**10 µl**

4.2.3.11 Transformation of chemically-competent *E. coli* bacteria

For the preparation of chemically competent *E. coli* XL1 Blue bacteria, a bacterial culture (OD_{600} 0.6 – 0.8) was centrifuged (6.000 x g, 5 min, 4 °C) and the pelleted cells were resuspended in TSS buffer, aliquoted into pre-cooled Eppendorf tubes (à 200 µl) and stored at -80 °C. The competency of the cells was determined by transformation of a defined amount of pcDNA3.1 vector DNA, plating on ampicillin supplemented LB agar plates and counting of colonies the next day.

$$\text{Competency}\left(\frac{\text{colonies}}{\mu g}\right) = \frac{\text{Number of colonies}}{\text{Amount of DNA transfected } (\mu g)} * \text{Dilution Factor}$$

The heat-shock technique was used to transform chemically competent bacteria with plasmid DNA. Here, an increase in temperature ('heat-shock') causes the cell membrane to become porous, which allows the uptake of the genetic information from the surrounding medium. Briefly, an aliquot of competent cells was thawed on ice and 10 µl of ligated plasmid DNA (chapter 4.2.3.10) were directly added to the cells. After incubation on ice for 30 min, the cells were placed for 70 s at 42 °C in a water bath. Immediately afterwards, the cells were placed on ice for 2 min. 800 µl of pre-warmed LB medium (w/o antibiotics) were added and the cells were incubated at 37 °C (750 rpm) for 60 min. The bacterial cells were harvested by centrifugation (800 x g, 5 min), resuspended in 100 - 200 µl of LB medium and plated on LB agar plates containing ampicillin. The plates were incubated overnight at 37 °C and colony growth was analyzed after approximately 16 h. At least six individual clones were further propagated on plate as well as in liquid LB medium culture for Mini preparation of plasmid DNA (chapter

4.2.1.2). Plasmid DNA was further analyzed by analytical digestion with restriction endonucleases to identify clones that carry the correct insert (i.e., the ANP32A ORF; chapter 4.2.3.1). The original plates were wrapped with parafilm and stored at 4 °C until further usage.

4.2.3.12 Sanger sequencing of plasmid DNA

In order to confirm that the correct insert (ANP32A ORF) without any mutations was ligated into the pcDNA3.1 expression vector, the plasmid DNA isolated from positive clones that carry DNA with the expected restriction pattern was sequenced. Therefore, the sequencing reaction was set up as displayed in **Table 10** and the samples were sent to the external service provider *Seqlab* (www.seqlab.de; Göttingen, Germany) for Sanger sequencing. Commercially available sequencing primers were used that specifically recognize parts of the CMV promoter (CMV, forward: 5' → 3') or the polyadenylation signal (BGH, reverse: 3' → 5'), both of which are located in the backbone of the pcDNA3.1 vector.

Table 10: Setup of Sanger sequencing reaction.

Component	Volume/Amount
Plasmid DNA	1.200 ng
Primer (CMV or BGH, 30 µM)	3.0 µl
ddH_2O	ad 15 µl
Total	**15 µl**

4.2.3.13 Quantitative real-time reverse transcription PCR (qRT-PCR)

In this study, the qRT-PCR technique was employed to determine the expression levels of pro-inflammatory genes (*MCP-1/CCL-2, IL-6, IFN-β1, TNF-α, IL-1β, IRF-7, CXCL10,* and *Mx1*) or viral RNA in lung tissue from infected ANP32B$^{+/+}$ and ANP32B$^{-/-}$ mice. Herein, a pool of cDNAs was generated based on total RNA isolated from murine lung tissue (chapter 4.2.3.3) and a *random nonamer (p9) primer mix* (GeneLink). Then, expression levels of target genes were quantified using specific primer pairs (chapter 4.1.8). The amplification reaction was carried out in 96-well plates using the *SYBR Green reagent* (Roche) and the *LightCycler® 96* system (Roche). As a reference, murine ribosomal protein 9 (mRPS9) expression was quantified using specific primers (chapter 4.1.8). Obtained Ct values were further evaluated manually using the

$2^{-\Delta\Delta Ct}$ *method* [362]. **Tables 11 and 12** summarize the cDNA synthesis and quantitative amplification reaction, respectively.

Table 11: Setup of cDNA synthesis using a random nonamer (p9) primer mix.

Component	**Volume**
ddH_2O	8.5 µl
Primer p9, 10 µM	2.0 µl
dNTPs, 10 mM	1.0 µl
RNA	1.5 µl (500 – 1500 ng)
Total	**13 µl**
PCR Cycling	**65 °C, 5 min**
First Strand Buffer (5x)	4 µl
DTT, 0.1 M	1 µl
Ribolock RNAse Inhibitor (40 U/µl)	1 µl
Superscript III RT (200 U/µl)	1 µl
Total	**20 µl**
PCR Cycling	**25 °C, 5 min** **50 °C, 60 min** **70 °C, 15 min**

Table 12: Setup of quantitative amplification reaction using SYBR Green reagent.

Component / PCR Cycling	**Volume**
ddH_2O	7.4 µl
Primer forward (20 µM)	0.3 µl
Primer reverse (20 µM)	0.3 µl
Fast Start Essential Green Master (2x)	10.0 µl

cDNA template	2.0 µl	
Total	**20 µl**	
PCR Cycling	**95 °C, 5 min**	
	95 °C, 15 sec	**45 cycles**
	60 °C, 10 sec	
	72 °C, 20 sec	
	95 °C, 15 sec	
	67 °C, 15 sec	
	67 °C → 95 °C, 1 sec intervals	

4.2.3.14 Next generation sequencing (NGS)

RNA isolated from the lungs of virus-infected or PBS control-treated ANP32B$^{+/+}$ and ANP32B$^{-/-}$ mice at 3 days post infection was subjected to next generation sequencing (NGS) to determine the gene expression profile (i.e., transcriptome) in these animals. These experiments were carried out by the NGS facility of the Heinrich Pette Institute, Hamburg, Germany. Only high quality RNA (RIN ≥ 7), assessed using the *Agilent RNA 6000 Nano Kit* (Agilent Technologies), was used for NGS analysis. Selective purification of polyadenylated mRNA was performed using the *NEBNext Poly(A) mRNA Magnetic Isolation Module* (New England Biolabs). Then, the *NEXTflex rapid Directional qRNA-Seq Kit* (Bio Scientific) was used to create compatible sequencing libraries for Illumina sequencing. After assessment of library quality (*Agilent DNA 1000 Kit*; Agilent Technologies), sequencing was carried out on a *NextSeq 500* (Illumina) with the *NextSeq 500/550 High Output Kit v2.*5 (75 cycles; Illumina).

High quality FASTQ data were aligned to the annotated human reference genome hg38 using STAR [359]. Gene counts were quantified with the build-in gene quantification function of STAR. DeSeq2 was used to identify differentially expressed genes (DGEs) using significance and log2FoldChange cutoffs (FDR < 0.1; Log2FoldChange ≥ 1 or ≤ -1) [357]. Significantly disregulated genes were evaluated manually according to their associated gene ontology (GO) terms (chapter 4.2.9.5). Genes presented in the Top10 of significantly altered GOs were further visualized using heatmaps which were created with the online tool *ClustVis* (chapter 4.2.9.4) [355].

4.2.3.15 Transfection of eukaryotic cells

Transfection of eukaryotic cells can be performed by different techniques/strategies, including non-chemical (e.g. electroporation) and chemical methods. The chemical compounds used for transfection range from calcium phosphate over liposomes to complex cationic polymers, which bind to the DNA followed by internalization of these complexes via endocytosis. Here, the cationic polymer polyethylenimine (PEI) or the commercially available *Lipofectamine 2000* (Lipo2k; Invitrogen) were used to transfect HEK293T cells with plasmid DNA and/or siRNAs. The following table provides an overview on the usage of either PEI or Lipo2k for the respective transfection experiments performed in this study (**Table 13**). In general, PEI (≤ 4 µg/ml) was used to transfect adherent cells or cells in suspension, while Lipo2k (1 µl per µg of DNA or 10 µl per 200 pmol of siRNA) was exclusively used for transfection in suspension.

Table 13: Usage of PEI and Lipofectamine 2000 (Lipo2k) for transfection of eukaryotic cells.

Compound	Experiment
PEI	vRNP reconstitution assay
	Expression test of ANP32A variants
Lipo2k	Co-immunoprecipitation (CoIP) assays
	siRNA transfection
	Delivery of CRISPR/Cas vectors
	Transfection of plasmid DNA for confocal fluorescence microscopy

For adherent transfection, the DNA to be transfected was mixed with optimized growth medium (OptiMEM) and PEI reagent. The mixture was incubated at RT for 15 min to allow the formation of PEI-DNA complexes. The growth medium was removed from the cells seeded the day before and replaced by DMEM-TF medium. Finally, the transfection mix was applied to the cells in a drop-wise fashion. Since PEI has a toxic effect on the cells, the transfection mix was removed after 6-8 h and replaced with fresh DMEM-TF medium.

For transfection in suspension, cells growing in T75 flasks were harvested using trypsin and the number of cells was counted using a *Neubauer counting chamber*. Subsequently, a cell suspension with a defined amount of cells per ml medium was prepared (in DMEM-TF medium, if not otherwise stated) and seeded into multi-well plates or 10 cm dishes. Plasmid DNA or siRNA were prepared in OptiMEM medium and incubated for 5 min at RT. Also, PEI or Lipo2k were prepared by pipetting the required amount of either compound into OptiMEM medium and

incubation for 5 min at RT. Then, PEI or Lipo2k in OptiMEM were added to the DNA/siRNA mixes followed by incubation for 20 min at RT. Finally, the transfection mixes were applied drop-wise to the cells. The medium on Lipo2k transfected cells was replaced with fresh DMEM-TF medium at 24h post transfection (p.t.), while the medium of PEI transfected cells was replaced at 6-8 h p.t.

The general parameters that were used for the different transfection experiments are summarized in **Table 14**. More detailed information is provided for particular methods in the respective chapters.

Table 14: Detailed parameters of transfection experiments. Transfection was performed in suspension, if not otherwise stated.

Experiment	Format	Amount of cells/ml	Chapter
siRNA transfection	6-well	6.6 x 10^5	4.2.4.1
CRISPR/Cas plasmid transfection	24-well	1.0 x 10^5 (adherent)	4.2.4.2
Expression test (WB)	6- or 12-well	6.6 x 10^5	4.2.4.3
CoIP (WB & SILAC-MS)	10 cm dish	4.5 x 10^5	4.2.4.5
vRNP reconstitution assay	12-well	2.5 x 10^5 (adherent)	4.2.4.6
Transfection for confocal microscopy	Glass bottom dish	2.5 x 10^5	4.2.7.1

4.2.4 Protein biochemical methods

4.2.4.1 Protein knockdown in eukaryotic cells using specific siRNAs

Small-interfering RNAs (siRNAs) can be used to specifically reduce the amount of transcribed mRNA of a particular protein in eukaryotic cells. This technique is based on the cellular RNA interference (RNAi) pathway that involves the RNA-induced silencing complex (RISC). Once activated, the siRNA, which is 20 to 25 bp in length and complementary to the mRNA of the target protein, guides the RISC complex to the mRNA which in turn is cleaved and degraded [363]. In this study, siRNAs targeting transcribed mRNAs of importin-α7 and ANP32A were used to silence their gene expression. Briefly, HEK293T cells were transfected with siRNAs targeting either importin-a7 (200 pmol) or ANP32A (125 pmol). After 24h, cells were re-transfected with

the same siRNAs for another 48h to achieve the highest knockdown efficiency. As a control, *Allstars negative control siRNA* (200 or 125 pmol; Qiagen) was used. Functional studies with siRNA silenced cells were performed 72 h after the first siRNA transfection. Knockdown of the target protein was verified by Western blotting (chapter 4.2.4.4).

4.2.4.2 Generation of eukaryotic knockout cell lines using CRISPR/Cas

Prokaryotes, such as bacteria or archaea, protect themselves from foreign DNA using CRISPR (*clustered regularly interspaced short palindromic repeats*), internal DNA sequences that are derived from a previous bacteriophage infection. Upon infection with a similar bacteriophage, RNAs expressed from the CRISPR loci guide the bacterial enzyme Cas9 (*CRISPR-associated protein 9)* to the foreign DNA which in turn is cleaved and degraded. This powerful technique has been adapted to generate protein knockouts in eukaryotic cells by expressing the Cas9 protein and a targeting guide RNA, often combined in a single expression vector [364].

Here, the CRISPR/Cas9 approach was used to generate human HEK293T cell lines with either importin-α7 or ANP32A knockout. Therefore, an expression vector (1 µg) encoding the Cas9 protein, one to three guide RNAs, and a GFP marker was transfected into HEK293T cells. As a negative control, a CRISPR/Cas9 vector (1 µg) expressing a non-targeting guide RNA was used (Santa Cruz). Transfected cells expressing GFP were sorted in 96-well plates (1 cell per well) on a *FACS Aria-Fusion cell sorting system* (BD Biosciences) to generate clonal cell lines. Protein knockout was verified by Western blotting (chapter 4.2.4.4). Functional studies were conducted in two different knockout cell lines to exclude clonal artefacts.

4.2.4.3 Preparation of total protein lysates from eukaryotic cells

Expression of the ANP32A constructs that were generated in this study was verified by transfection into HEK293T cells, followed by cell lysis and Western blot analysis. In short, 2 µg of expression constructs were transfected into HEK293T cells using PEI reagent, and 24 h p.t. the cells were lysed as described below. SDS-PAGE and Western blotting was performed using antibodies that either detect ANP32A or the introduced FLAG tag on the protein.

Preparation of cell lysates was always carried out on ice and all centrifugation steps were performed at 4 °C to preserve protein structure and function. Transfected or non-transfected cells were detached from the well, resuspended in 1x PBS and transferred to a 1.5 ml reaction tube. Cells were harvested by centrifugation (2.000 x g, 5 min), the cell pellet was resuspended in an appropriate amount of HEPES lysis buffer and the cell suspension was incubated on ice for 15 to 20 min. Cell debris were removed by centrifugation (16.000 x g, 10 min), the supernatant (i.e., whole cell lysate) was transferred to a fresh tube, mixed with 4x Laemmli loading dye and

incubated for 5 min at 95 °C (1.000 rpm). The samples were shortly spun down and either stored at -20 °C (long-term) or directly used for SDS-PAGE and Western blotting (chapter 4.2.4.4).

4.2.4.4 SDS-PAGE and Western blot

SDS polyacrylamide gel electrophoresis (SDS-PAGE) is a frequently used biochemical method to separate proteins according to their molecular weight in the electrical field, followed by Western blot (WB) analysis using protein or tag-specific antibodies. SDS-PAGE and WB were performed according to standard protocols. In brief, SDS gels were prepared as outlined in **Table 15** and either stored at 4 °C or directly used for gel electrophoresis. Therefore, gels were inserted in a *Mini-PROTEAN Tetra Cell* system (Bio-Rad). Cell lysates or tissue homogenates (5 to 15 µl) were loaded onto the gel along with 2 µl of the *Precision PlusProtein™ Dual Core Standard* (Bio-Rad). Electrophoresis was performed at 70 to 125 V for at least 1.5 h. The *Mini Trans-Blot Cell* (Bio-Rad) was used for Western blotting (70 min, 250 mA). Membranes were extensively washed with 1 x PBS-T between the antibody incubation steps as well as prior to detection. After blocking for 1 h with blocking solution (3 % BSA, in PBS-T), the membrane was incubated with primary antibodies for ≥ 16 h at 4 °C. Afterwards, the membrane was incubated for 1 to 1.5 h with secondary antibodies at RT. For detection, the *SuperSignal West Femto Chemiluminescent Substrate* (Thermo Scientific) and the documentation system *Imagequant LAS 4000* (GE Healthcare) were used according to the manufacturer's instructions.

Table 15: Preparation of SDS gels (4x).

Compound	Resolving gel (10 %)	Stacking gel (4 %)
ddH_2O	7.9 ml	6.8 ml
Resolving gel buffer (4x)	5 ml	-
Stacking gel buffer (4x)	-	1.25 ml
SDS (10 %)	200 µl	100 µl
Rotiphorese Gel 30	6.7 ml	1.7 ml
TEMED	8 µl	10 µl
APS (10 %)	200 µl	100 µl
Total	**20 ml**	**10 ml**

4.2.4.5 Co-immunoprecipitation and SILAC mass spectrometry

In eukaryotic cells, protein-protein interactions can be analyzed by precipitating a protein of interest ('bait') from a whole cell lysate using agarose bead coupled protein-specific antibodies or antibodies that recognize an introduced tag on the particular protein (e.g. FLAG tag). Proteins that naturally interact with the 'bait' protein will also be extracted from the lysate and can subsequently be identified via WB or Mass Spectrometry (MS). This technique is called co-immunoprecipitation (CoIP). In this study, CoIP analyses were performed to identify importin-α interacting cellular and viral proteins in influenza infected HEK293T cells using an unbiased, quantitative SILAC-based MS approach. A subset of identified interacting proteins was further validated by WB.

The SILAC (*stable isotope labeling of amino acids in cell culture)* technique in combination with MS can be used to determine the abundance of differentially labelled proteins or peptides that are derived from up to four different cellular (transfection) conditions. Herein, eukaryotic cells are grown in cell culture media containing either regular amino acids (AA) or isotope-labeled arginine and lysine residues. Proteins will incorporate these labeled AA and can be later distinguished from the unlabeled samples in the mass spectrometer due to mass differences. The SILAC cell culture media used in this study are summarized in chapter 4.1.14.

Three populations of HEK293T cells were cultured in the respective SILAC media (R0K0, R6K4, R10K8) and MS was used to check for incorporation of unlabeled or labeled amino acids after five to six passages (approx. 3 weeks). Then, cells were transfected with expression constructs for C-FLAG-tagged importin-α isoforms (α1, α5, and α7) in 10 cm dishes using Lipo2k reagent. As additional controls, an empty vector expressing C-FLAG only as well as constructs encoding importin-β_1 binding domain (IBB) deficient importin-α variants (ΔIBB) were used. An overview of the transfection procedure is displayed in **Table 16**. After identification of importin-α interacting cellular proteins by SILAC-MS, the CoIP procedure as outlined below was repeated to confirm a subset of these interactions by Western blotting. However, for this experiment cells were cultivated in regular growth medium to exclude any artefacts caused by the labeled amino acids present in the SILAC media.

Approximately 24 h post transfection, cells were either Mock infected or infected with IAV A/WSN/33 (H1N1; $PB2_{627K}$; MOI 0.1) for 16 h (i.e., approximately two replication cycles). The infection procedure is further described in chapter 4.2.5.4. After infection, the cells were detached from the dish, resuspended in 3 ml of 1x PBS and transferred to a 15 ml reaction tube. Cells were pelleted by centrifugation (1.000 x g, 5 min), the cell pellet was resuspended in 1 ml of 1x PBS and the cells were pelleted again by centrifugation. Then, the cell pellet was resuspended in 500 µl of HEPES lysis buffer and incubated on ice for 25 min. The samples were

further sonicated in a waterbath for 30 sec (max. amplitude) to ensure efficient cell lysis and shearing of genomic DNA. After centrifugation at 16.000 x g for 10 min, the supernatant (i.e., whole cell lysate) was transferred to a fresh reaction tube. A sample of 50 µl were transferred to a separate tube, mixed with 4x Laemmli loading dye, heated to 95 °C for 5 min and stored at 4 °C (≤ 24 h) or -20 °C (long-term) (*Input samples*). For co-immunoprecipitation, the *EZview Red ANTI-FLAG M2 affinity gel* (Sigma-Aldrich) was used. An appropriate amount of resin (40 µl per sample) was washed twice with 1x TBS buffer (500 µl per sample), and the washed resin was resuspended in HEPES lysis buffer (600 µl per sample). The equilibrated resin was mixed with the remaining 450 µl of cell lysate, and binding of FLAG-tagged proteins to the resin was performed overnight (≥ 16 h) at 4 °C under rotation. After overnight incubation, the resin was washed three times with 1x TBS buffer (500 µl per sample), with centrifugation steps in between (8.200 x g, 1 min).

Two elution techniques were performed to detach the FLAG-tagged importin-α proteins and their co-immunoprecipitated cellular factors from the resin: First, the resin was incubated with an excess of FLAG peptide (prepared in 1x TBS buffer) for 1 h at 4 °C (1150 rpm). After centrifugation (8.200 x g, 1 min), the supernatant was transferred to a new reaction tube, mixed with 4x Laemmli loading dye, boiled for 5 min at 95°C and stored at -80 °C. Subsequently, 80 µl of 1 x Laemmli loading dye was added to the resin, and the sample was incubated for for 10 min at 95 °C. This step was performed to ensure that all proteins are efficiently eluted from the resin. The eluates were separated from the resin by centrifugation (8.200 x g, 1 min), transferred to fresh tubes, boiled for 5 min at 95°C, and stored at -80°C.

For MS analysis, three samples (R0K0, R6K4, and R10K8) were always pooled as indicated in **Table 16**, whereas WB-based detection of importin-α and interacting cellular proteins was performed with individual samples. Three biological replicates were performed, each with a different SILAC medium for a particular pulldown sample (empty vector, expressing FLAG tag only; importin-α-ΔIBB-C-FLAG; importin-α-WT-C-FLAG), but only the data from experiment 1 were available for evaluation at the time point of thesis submission (**Table 16**).

Experiment 1	Empty Vector, R0K0; α-ΔIBB, R6K4; α-WT, R10K8	(**Table 16**)
Experiment 2 :	Empty Vector, R10K8; α-ΔIBB, R0K0; α-WT, R6K4	
Experiment 3:	Empty Vector, R6K4; α-ΔIBB, R10K8; α-WT, R0K0	

Prior to MS analysis, pooled elution samples were loaded on SDS gels and gel electrophoresis was carried out at 70 V for approximately 30 min. Afterwards, gels were stained with Coomassie Blue solution for 30 min and subsequently destained overnight in destaining solution. Gels were

wrapped in plastic foil and delivered to collaboration partners at the university medical campus Hamburg-Eppendorf (Hamburg, Germany) who performed all mass spectrometric analyses, including pre-processing of raw MS data files.

In brief, SDS-PAGE bands were cut into 1 mm³ cubes and further destained by incubating the gel pieces alternating in acetonitrile (ACN) and 50 mM ammonium bicarbonate buffers. After destaining, proteins were reduced in presence of 10 mM DTT at 60 °C for 30 min and alkylated in 20 mM iodoacetamide (IAA) for 30 min in the dark at 37 °C. Trypsin was added at a 1:100 enzyme-to-protein ratio to perform in-gel digestion over night at 37 °C. Peptides were eluted from the gels pieces by incubating them alternating with ACN and 0.1% formic acid (FA). Samples were dried in a vacuum centrifuge and prior to LC-MS/MS analyses they were resuspended in 0.1 % FA and transferred into a full recovery autosampler vial (Waters).

Chromatographic separation was carried out on a UPLC system (*Dionex Ultimate 3000*, Thermo Fisher Scientific) with a two buffer system (buffer A: 0.1% FA in water, buffer B: 0.1% FA in ACN). Attached to the UPLC was a C18 reversed phase (RP) trap (Acclaim PepMap 100, 100 µm x 2 cm, 100 Å pore size, 5 µm particle size) for desalting and purification, followed by a C18 RP analytical column (Acclaim PepMap 100, 75 µm x 50 cm, 100 Å pore size, 2 µm particle size). Peptides were separated using a 60 min gradient with increasing ACN concentration from 2 % - 30 % ACN. The eluted peptides were analyzed on a *Fusion Quadrupole ion trap orbitrap mass spectrometer* (Thermo Fisher Scientific) in data dependent acquisition (DDA).

For DDA, the mass spectrometer was operated in orbitrap – orbitrap mode at top speed, therefore selecting as many precursors (2^+ - 5^+ charged) from a survey scan ($2x10^5$ ions, 120,000 Resolution, 120 ms fill time) within a 3 s cycle time. These precursors were analyzed by MS/MS (HCD at 30 normalized collision energy, $1x10^5$ ions, 15.000 Resolution, 60 ms fill time) in a range of 400 – 1300 m/z. A dynamic precursor exclusion of 20 s was used.

The collected raw files were searched against the reviewed human (release January 2019, 20.399 protein sequences) and the Influenza A virus (strain A/Wilson-Smith/1933 H1N1, (release November 2019, 13 protein sequences) protein database downloaded from Uniprot and processed with the *Andromeda algorithm* included in the *MaxQuant Software* (Max Plank Institute for Biochemistry, Version 1.6.2.10). Flag peptide elution and elution by boiling in sample buffer from the same enrichment were treated as fractions and only different enrichment pulldowns were handled as individual experiments. The SILAC multiplicity option was used (Lys(0) & Arg(0), Lys(4) & Arg(6), Lys(8) & Arg(10)). Trypsin was selected as enzyme used to generate peptides, allowing a maximum of two missed cleavages. A minimal peptide length of six amino acids and maximal peptide mass of 6.000 Da was defined. Oxidation of methionine, acetylation of protein N-termini and the conversion of glutamine to pyro-glutamic acid were set

as variable modifications. The carbamidomethylation of cysteines was selected as fixed modification. The error tolerance for the first precursor search was 20 ppm, for the following main search 4.5 ppm. Fragment spectra were matched with 20 ppm error tolerance. False discovery rate for peptide spectrum matches and proteins was set to 1 %. For Quantification, all identified razor and unique peptides were considered. All peptide intensities measured for the respective pulldown samples were further evaluated manually as described in chapter 4.2.9.2.

Table 16: Summary of CoIP transfection conditions for SILAC MS using one representative combination of SILAC media.

Sample ID	Medium	Construct name	Amount of DNA	Infection?	Combined Eluates for MS [1]
1	R0K0	pcDNA-C-FLAG empty	20.0 µg	No	1-3
2	R6K4	Importin-α1-ΔIBB-C-FLAG	20.0 µg	No	
3	R10K8	Importin-α1-C-FLAG	20.0 µg	No	
4	R0K0	pcDNA-C-FLAG empty	15.0 µg	No	4-6
5	R6K4	Importin-α5-ΔIBB-C-FLAG	15.0 µg	No	
6	R10K8	Importin-α5-C-FLAG	15.0 µg	No	
7	R0K0	pcDNA-C-FLAG empty	15.0 µg	No	7-9
8	R6K4	Importin-α7-ΔIBB-C-FLAG	15.0 µg	No	
9	R10K8	Importin-α7-C-FLAG	15.0 µg	No	
10	R0K0	pcDNA-C-FLAG empty	20.0 µg	Yes	10-12
11	R6K4	Importin-α1-ΔIBB-C-FLAG	20.0 µg	Yes	
12	R10K8	Importin-α1-C-FLAG	20.0 µg	Yes	
13	R0K0	pcDNA-C-FLAG empty	15.0 µg	Yes	13-15
14	R6K4	Importin-α5-ΔIBB-C-FLAG	15.0 µg	Yes	
15	R10K8	Importin-α5-C-FLAG	15.0 µg	Yes	
16	R0K0	pcDNA-C-FLAG empty	15.0 µg	Yes	16-18
17	R6K4	Importin-α7-ΔIBB-C-FLAG	15.0 µg	Yes	
18	R10K8	Importin-α7-C-FLAG	15.0 µg	Yes	

[1] eluted either with FLAG peptide or by boiling at 95°C

4.2.4.6 vRNP reconstitution assay (vRNP-RA)

The genomic information of influenza viruses is packaged into viral ribonucleoprotein particles (vRNPs), each consisting of the trimeric viral polymerase (PB1, PB2, PA) and the nucleoprotein (NP) that encapsidates the viral RNA. These vRNPs can be reconstituted in eukaryotic cells by transfecting plasmids encoding the individual proteins. As a viral RNA template, the pPol-I-NP-Luc plasmid is co-transfected [238]. From this plasmid, a 'vRNA' encoding the firefly luciferase with non-coding sequence elements of the IAV A/WSN/33 nucleoprotein at each end is expressed via the RNA polymerase I (RNAP I) promoter. Only in the presence of the (reconstituted) viral polymerase, firefly mRNA is transcribed and translated into protein. Therefore, the firefly luciferase activity which is measured on a luminometer serves as readout for the activity of the viral polymerase. As a transfection control, a plasmid constitutively expressing a Renilla luciferase (*pRenilla-TK*; Promega) is used.

In this study, the vRNP-RA was used to study IAV A/WSN/33 ($PB2_{627K}$) polymerase activity in cells with reduced or abolished expression of the positive-regulatory host factors importin-α7 and ANP32A. siRNA silenced or CRISPR/Cas9 generated knockout cells were PEI transfected in 12-well plates with expression constructs for the IAV polymerase (PB1, PB2, PA), viral NP, the firefly luciferase and the Renilla luciferase. **Table 17** displays the detailed transfection protocol. Where indicated, overexpression of either importin-α7, in combination with the transport co-receptors CAS and importin-β_1, or ANP32A was performed. After 24h, the cells were lysed using passive lysis buffer (PLB, 5x; Promega) and luciferase activities were measured in the *TriStar LB 94 luminometer* (Berthold Technologies) using the *Dual-Luciferase Reporter Assay System* (Promega) according to manufacturer's instructions.

Table 17: Summary of transfection conditions for the vRNP reconstitution assay.

Experiment / Reference to Figure …	Plasmid DNA	Amount of DNA / well
All vRNP-RA experiments	pcDNA3.1-A/WSN/33-PB1	100 ng
	pcDNA3.1-A/WSN/33-PB2	100 ng
	pcDNA3.1-A/WSN/33-PA	100 ng
	pcDNA3.1-A/WSN/33-NP	500 ng
	pPol-I-NP-Luc	500 ng
	pRenilla-TK	500 ng

Overexpression of importin-α7 (wt, ΔIBB) in ANP32A-silenced or ANP32A knockout HEK293T cells *[Figure 19]*	pcDNA3.1-importin-α7	300 ng
	pcDNA3.1-importin-α7-ΔIBB	300 ng
	pcDNA3.1-importin-β_1	600 ng
	pcDNA3.1-CAS	300 ng
	pcDNA3.1-empty	300 ng
Overexpression of ANP32A wt and mutNLS constructs in HEK293T cells [*Figure 20]*	pcDNA3.1-ANP32A	100 – 900 ng
	pcDNA3.1-ANP32A-mutNLS1	100 – 900 ng
	pcDNA3.1-ANP32A-mutNLS2	100 – 900 ng
	pcDNA3.1-empty	100 – 900 ng
Overexpression of ANP32 (WT) in importin-α7 silenced or importin-α7 knockout HEK293T cells [*Figure 21*]	pcDNA3.1-ANP32A	300 ng
	pcDNA3.1-empty	300 ng

4.2.4.7 Multiplex immunoassay

The luminex technology, which is based on color-coded beads, enables the simultaneous detection of a large number of cytokines and chemokines (C/Cs) in cell culture supernatants and/or tissue homogenates. Here, this technology was employed to detect a set of C/Cs in lung homogenates from PBS or IAV infected mice. The following murine C/Cs are included in a custom-design multiplex array that was purchased from Invitrogen (Assay-ID: *MXNKRYE*): TNF-α, IFN-α, MCP-1 (CCL2), IL-1β, IL-6, IL-10, IL-17A (CTLA-8) and IL-21. Measurement of C/Cs was performed according to manufacturer's instructions on a *Luminex 200* system (BioRad). Data were further evaluated statistically using *GraphPad Prism* software.

4.2.5 Virological techniques

4.2.5.1 Generation of recombinant influenza A viruses using reverse genetics

In the early 2000s, an 8-plasmid system was established to generate recombinant influenza viruses in eukaryotic cells [350]. This system is based on the pHW2000 vector which contains both cellular RNAP I and II promoters from which viral RNAs and viral mRNAs are expressed simultaneously. By transfection of pHW2000 vectors encoding all eight viral RNA segments into cells, new viral particles are produced, released from the cell and can be harvested to generate a new virus stock.

In general, plasmids were first transfected into HEK293T cells to achieve high plasmid expression levels (Lipo2k transfection, 6-well). Subsequently, the supernatant containing newly formed viral particles was used to infected MDCK cells which are suited for high-titer virus production (6-well). MDCKs were extensively washed prior to infection to remove all traces of serum that could potentially interfere with particle adherence to the cells. Then, the supernatant from the first round of MDCK infection was used to infect MDCK cells seeded in T75 flasks. Finally, after 36 to 48h post infection, the MDCK cell culture supernatant was centrifuged to remove cell debris, sterile-filtered (Ø 22 µm), aliquoted into cryo tubes and stored at -80°C. Viral titers were determined by plaque test (PT) on MDCK cells as described below (chapter 4.2.5.5). For the rescue of influenza viruses with a monobasic cleavage site in the hemagglutinin (HA), TPCK-treated trypsin was added during infection of MDCK cells. Of note, A/WSN/33, although possessing a monobasic cleavage site, does not require exogenously provided trypsin as its NA protein is able to bind to and sequester residual plasminogen from serum, leading to efficient HA activation for cell entry. Therefore, 2 % FBS was included in the MDCK infection medium.
In this study, a recombinant A/WSN/33 ($PB2_{627K}$) virus stock was generated using reverse genetics. The detailed HEK293T transfection protocol is summarized in **Table 18**. The other two virus stocks (A/Aichi/2/68-A/WSN/33, 2+6; A/Vietnam/1194/04) were propagated from existing stocks as described in chapter 4.2.5.2.

Table 18: Summary of transfection for IAV A/WSN/33 (H1N1) rescue using reverse genetics.

Plasmid DNA	Amount of DNA / well
pHW2000-A/WSN/33-PB1	1 µg
pHW2000-A/WSN/33-$PB2_{627K}$	1 µg
pHW2000-A/WSN/33-PA	1 µg
pHW2000-A/WSN/33-NP	1 µg
pHW2000-A/WSN/33-M	1 µg
pHW2000-A/WSN/33-NS	1 µg
pHW2000-A/WSN/33-HA	1 µg
pHW2000-A/WSN/33-NA	1 µg

4.2.5.2 Propagation of influenza A virus on MDCK cells

Virus stocks that already existed when this study was initiated were propagated on MDCK cells. Briefly, MDCK cells grown in 6-well plates were washed once with PBS, and 500 µl of inoculation medium supplemented with 1 µl of virus stock were added. After adherence of viral particles to the cells (37 °C, 30 min), the inoculation medium was removed, cells were extensively washed with PBS, 3 ml of infection medium (including 1:1000 diluted TPCK-treated trypsin for H3N2) were added, and the cells were incubated at 37 °C for 48 h. Then, MDCK cells seeded into T75 flasks the day before were infected with 500 µl of virus-containing supernatant from the first infection. Herein, cells were washed with PBS, infected for 30 min at 37 °C, washed again with PBS, and 10 ml of infection medium were added. At 36 to 72 h post infection (p.i.), the supernatant was harvested, centrifuged to remove cell debris, aliquoted in cryo tubes and stored at -80 °C. Viral titers were determined by PT as described below (chapter 4.2.5.5).

4.2.5.3 Hemagglutination assay with chicken erythrocytes

The IAV hemagglutinin is able to bind to and aggregate chicken erythrocytes (CE) that express sialic acids on their cell surface. This process is termed hemagglutination and can be used to estimate the amount of virus in cell culture supernatants as hemagglutination units (HAUs), for example in the process of generating a new virus stock. In brief, a 10 % CE solution was prepared in 0.9 % NaCl buffer. Serial 2-fold dilutions (2^{-1} to 2^{-8}) of virus-containing cell culture supernatants were prepared in PBS in a V-bottom 96-well plate (total of 50 µl well). Then, the 10 % CE solution was diluted to 1 % in 0.9 % NaCl buffer and CEs were added to the 96-well plate (50 µl per well). The plate was incubated for at least 30 min on ice or at 4°C. Without virus present, the CEs will settle at the bottom of each well in the 96-well plate. In contrast, virus particles present will bind to the CEs via their HA and prevent CE aggregation and settlement. The highest virus dilution where hemagglutination still occurs represents the HAU titer.

4.2.5.4 Infection of eukaryotic cells with influenza A viruses

The replicative fitness of influenza viruses was studied under specific cellular conditions by performing growth kinetics over a time course of 72 h. Therefore, HeLa cells or mLF were seeded in Poly-L-Lysin coated 6-well plates, either 16 h (HeLa) or 6 h (mLF) prior to infection. For virus infection, cells were washed once with PBS, and virus stock diluted to the desired MOI (0.1 for HeLa cells, 1.0 for mLF) in inoculation medium (500 µl) was added. The following formula was used to calculate the required amount of virus:

$$\frac{\text{MOI} * \text{Inoculation volume [x µl]} * \text{Number of cells}}{\text{Virus stock titer}} = \text{µl virus stock in x µl inoculation medium}$$

Adherence of viral particles to the cells was performed for 30 min at 37 °C, followed by removal of the inoculation medium and extensive washing of the cells. Finally, 3 ml of infection medium (supplemented with TPCK-treated trypsin, depending on virus strain) were added. 200 µl of cell culture supernatants were collected at 0, 16 (only for mLF), 24, 48 and 72h post infection and stored at -80 °C. Viral titers were determined by PT on MDCK cells as described below.
In addition to viral replication kinetics, the expression of viral nucleoprotein was determined in Mock or H3N2 IAV infected HeLa cells at 24 h post infection. Therefore, seeded HeLa cells were infected at a MOI of 1.0 as described above. After 24 h, cells were washed once with PBS, and lysed using HEPES cell lysis buffer as outlined in chapter 4.2.4.3. Cell lysates were subjected to SDS-PAGE and WB analysis using a primary antibody detecting IAV nucleoprotein.
Finally, for CoIP SILAC-MS experiments (chapter 4.2.4.5), transfected HEK293T cells were infected with A/WSN/33 (H1N1) at a MOI of 0.1 for 16 h. Infection was carried out as described above, but using 4 ml of inoculation medium and 10 ml of infection medium for each dish.

4.2.5.5 Determination of viral titers by plaque test (PT)

In influenza virology, a plaque test (PT) on MDCK cells is commonly used to determine viral titers as plaque-forming units (PFUs) per ml or per gram of organ tissue. Herein, cell culture supernatants or tissue homogenates were serial diluted 10-fold in PBS. MDCK cells, seeded in multi-well plates the day before (1:6 diluted from confluent T75 flasks), were washed once with PBS, and virus dilutions were added. After 30 min incubation at 37 °C, overlay medium was added to the cells, without removing the virus inoculum. **Table 19** summarizes the different PT parameters, based on the well format that was used.

Table 19: Parameters of PT in different multi-well formats.

Well format	MDCK seeding volume per well	Virus inoculation volume per well	Overlay medium per well	4% PFA volume per well
6-well	3.0 ml	333 µl	3.0 ml	1.5 ml
12-well	1.5 ml	150 µl	1.5 ml	1.0 ml
24-well	1.0 ml	100 µl	1.0 ml	0.5 ml

Cells were further incubated for 72 h at 37 °C. Afterwards, cells were washed with PBS, and fixed with 4 % PFA solution for at least 30 min at 4 °C. All virus strains used in this study form large, visible plaques on the MDCK cell layer, allowing counterstaining with crystal violet solution which stains the nuclei of adherent cells. Viral titers were determined using the following formula:

$$\frac{\text{Number of plaques} * \text{Dilution factor} * 1000}{\text{Inoculation volume}} = \text{virus titer in PFU/ml}$$

4.2.6 Histological techniques

All histological techniques were carried out by Gundula Pilnitz-Stolze, an excellent technical assistant and member of the technology platform '*Histology'* at the HPI.

4.2.6.1 Preparation of murine lung tissue for histology

Lung tissue extracted from PBS or virus infected mice was fixed for at least 7 days in 4 % PFA solution at 4 °C. Then, the tissue was briefly stored in 1x PBS to remove the PFA, followed by paraffin treatment. Therefore, the tissue was treated with increasing concentrations of ethanol and xylol for dehydration. The following steps were performed, and paraffin treatment was carried out in the *tissue infiltration system ASP300* (Leica Biosystems) (**Table 20**).

Table 20: Dehydration and paraffin embedding procedure for histology.

Step	Component	Incubation time	Temperature
1	Ethanol, 70%	1 h	RT
2	Ethanol, 80%	1 h	RT
3	Ethanol, 90%	1 h	RT
4	Ethanol, 95%	1 h	RT
5	Ethanol, 100 %	1 h	RT
6	Ethanol, 100 %	1.5 h	RT
7	Xylol I	1 h	RT
8	Xylol II	1 h	RT
9	Paraffin Type 3	1 h	58°C

10	Paraffin Type 3	1 h	58°C
11	Paraffin Type 3	1 h	58°C

Tissue samples were embedded in paraffin using the *embedding center EG1160* (Leica Biosystems) and stored in the dark at RT until further processing. To generate thin sections of the tissue, the paraffin blocks were shortly cooled down to -12 °C, thin sections (Ø 4 µm) were prepared using the *Mikrotom*, and sections were directly transferred to a water bath heated to 42 °C. Subsequently, the FFPE (*formalin-fixed paraffin-embedded*) tissue thin sections were dried on object slides overnight at 37 °C.

Prior to the staining procedures as outlined below, the FFPE sections were deparaffinized and rehydrated using the tissue infiltration system and alternative chemicals replacing ethanol (i.e., *Ottix Shaper*) and xylol (i.e., *Ottix Plus*). The individual steps are summarized in **Table 21**.

Table 21: Deparaffinization and rehydration of FFPE sections prior to staining procedures.

Step	Component	Incubation time
1	Ottix Plus, I	5 min
2	Ottix Plus, II	5 min
3	Ottix Plus, III	5 min
4	Ottix Plus, IV	5 min
5	Ottix Shaper, I	2 min
6	Ottix Shaper, II	2 min
7	Ottix Shaper, III	2 min
8	Ottix Shaper, IV	2 min
9	ddH_2O	2 min
10	ddH_2O	2 min

4.2.6.2 Hematoxylin and eosin (H/E) staining of murine lung tissue

Deparaffinized and rehydrated FFPE tissue thin sections were subjected to staining with hematoxylin and eosin to visualize cellular basophil (acidic; e.g. cell nucleus and rough ER) and eosinophil (basic; e.g. cell cytoplasm and mitochondria) structures, respectively. Sections were stained with a mixture of hematoxylin and eosin, followed by dehydration. All steps performed are displayed in **Table 22**. Finally, FFPE sections were mounted with Eukitt and stored in the dark at RT until microscopic evaluation (chapter 4.2.7.2).

Table 22: H/E staining procedure for murine lung tissue.

Step	Component	Treatment / Incubation time
1	ddH_2O	2 min
2	H/E solution	4 min
3	Tap water	10 s
4	Ethanol (100%), incl. 3% HCl	10 s
5	Tap water	5 min
6	Ottix Shaper, I	10 times, a few seconds each
7	Ottix Shaper, II	10 times, a few seconds each
8	Ottix Shaper, III	10 times, a few seconds each
9	Ottix Shaper, IV	5 min
10	Ottix Plus, I	10 times, a few seconds each
11	Ottix Plus, II	10 times, a few seconds each
12	Ottix Plus, III	10 times, a few seconds each
13	Ottix Plus, IV	10 times, a few seconds each
14	Xylol	10 times, total of ≥ 10 min

4.2.6.3 Immunohistochemical (IHC-P) staining of viral antigen in murine lung tissue

In order to detect virus-infected cells (i.e., viral antigen positive cells) and to evaluate viral tropism, deparaffinized and rehydrated FFPE tissue thin sections were stained for viral antigen (NP) using an immunohistochemical (IHC-P) staining procedure.

First, FFPE sections were treated with *Citrate Plus Puffer* for demasking of viral antigen (**Table 23**). All subsequent steps were carried out at room temperature (RT), and all washing steps were carried out with 1x PBS for 5 min each, if not otherwise stated. Since detection of viral antigen is based on an HRP (*horse radish peroxidase*) coupled secondary antibody (see below), the endogenous peroxidases were inhibited by incubation of the object slides for 15 min in 3 % H_2O_2 solution (prepared in methanol), followed by two washing steps. For blocking of endogenous biotin, biotin receptors, and avidin binding sites, the *Avidin-Biotin Block SP2001* kit (Zytomed) was used according to manufacturer's instructions (15 min for each solution, two washing steps at the end). Potential background staining caused by primary or secondary antibodies was reduced by two blocking steps: First, using the blocking buffer provided with the *ZytoChemPlus (HRP) Broad Spectrum (DAB)* kit, primary antibody background staining was reduced (5 min, two washing steps). Second, unspecific binding of the secondary antibody was reduced by blocking in 10 % donkey serum (in PBS) for 30 min (no washing afterwards). Then, tissue thin sections were incubated with a primary antibody (1:10.000, in DCS buffer) against viral nucleoprotein for 75 min, followed by three washing steps in PBS-T and three washing steps in PBS. Incubation with an anti-rabbit, biotin-conjugated secondary antibody (1:200 in PBS, supplemented with 2 % donkey serum) was performed for 25 min. Slides were washed again with PBS-T and PBS as described above. Finally, incubation with a streptavidin-HRP conjugate was carried out for 15 min, slides were washed twice and detection of viral antigen was performed with the HRP substrate 3,3'-diaminobenzidin (DAB). The reaction was stopped by adding ddH_2O after sufficient staining was observed under the microscope (approximately 3-5 min). For counterstaining, an additional H/E staining was performed as described above (chapter 4.2.6.2). Herein, the staining procedure was matched to the intensity of the DAB staining.

Table 23: Demasking of viral antigen in FFPE sections with Citrate Plus Buffer.

Step	Description
1	Incubation for 16 min in the microwave (850W)
2	Incubation for 5 min in the microwave (450W)
3	Cooling of samples for 20 min
4	Washing of samples with 1 x PBS for 5 min

4.2.7 Microscopy techniques

4.2.7.1 Confocal fluorescence microscopy

The subcellular localization of GFP- or FLAG-tagged ANP32A variants (WT, mutNLS1, mutNLS2) was analyzed by immunostaining and confocal fluorescence microscopy. All reagents were prepared in 1 x D-PBS, and all washing steps were performed with 1 x D-PBS for 2 min each on a shaker. The entire staining procedure was carried out at RT, if not otherwise noted. Briefly, HEK293T cells were transfected in Poly-Lysin-coated glass-bottom dishes (Ibidi GmbH) with the respective expression constructs as outlined in **Table 24** (Lipo2k transfection, in suspension). At 24 h post transfection, cells were washed once and fixed in 4 % PFA solution for 10 min at 37 °C. The nuclei of cells transfected with GFP-tagged ANP32A expression constructs were stained for 1 h with *Hoechst 33342* reagent (1:1000 dilution; final concentration: 20 nM). Cells transfected with FLAG-tagged ANP32A expression constructs were washed twice after PFA fixation, followed by permeabilization with 0.1 % Triton-X-100 (in D-PBS) for 20 min. After two washing steps, the fixed and permeabilized cells were immersed for 1 h in 3 % BSA solution for blocking. Subsequently, cells were stained with a primary antibody recognizing the FLAG tag (dilution 1:500) for 1.5 h. Cells were washed three times and subjected to staining with a secondary, Alexa555-coupled antibody (diluted 1:500) for 1h. Both antibodies were prepared in 3 % BSA solution. Staining of nuclei with *Hoechst 33342* reagent (1:1.000 dilution) was included in this step. The stained cells were washed three times and stored in 1.5 ml of D-PBS/dish at 4°C.

Table 24: Transfection of HEK293T cells for confocal fluorescence microscopy.

Plasmid DNA	Amount of DNA / dish
pcDNA3.1-C-FLAG-empty	3 µg
pcDNA3.1-ANP32A-WT-C-FLAG	3 µg
pcDNA3.1-ANP32A-mutNLS1-C-FLAG	3 µg
pcDNA3.1-ANP32A-mutNLS2-C-FLAG	3 µg
pcDNA3.1-empty	3 µg
pEGFP-ANP32A	3 µg
pEGFP-ANP32A-mutNLS1	3 µg
pEGFP-ANP32A-mutNLS2	3 µg

Images were acquired on a confocal *Nikon Eclipse Ti-E spinning disc* microscope (Nikon, Japan) at 100-fold magnification. Image processing was performed using *Nikon NIS-Elements Advanced Research* (version 4.51; Nikon, Japan) and *Adobe Photoshop CS4 software* (Adobe Systems Incorporated). For quantification purposes, 5x5 images were acquired and nuclear ANP32A levels were determined using ImageJ/Fiji software and a custom-designed plugin for semi-automatic quantification. Two 5x5 images were taken for each transfection condition, and three biological replicates were performed (i.e., quantification and merge of a total of six 5x5 images).

4.2.7.2 Visualization of H/E or IHC-P stained murine lung tissue

Lung sections that were stained with H/E or a primary antibody against viral nucleoprotein (chapter 4.2.6) were imaged on a *Nikon Eclipse 80i upright light* microscope coupled with *Color Camera Nikon DS-Ri2*. Images were captured at 10x magnification and three independent fields were taken from each slide. Images were further processed using Adobe *Photoshop CS* software.

4.2.8 Animal experiments

All animal experiments conducted in this study were in strict accordance with the guidelines of the German animal protection law. All protocols used were approved by the German authorities (Behörde für Stadtentwicklung und Umwelt Hamburg, licensing number: 08/17). Mice used in this study were bred and housed under specific pathogen-free (SPF) conditions at the Heinrich Pette Institute, Leibniz Institute for Experimental Virology, Hamburg, Germany. All mice used for infection experiments were housed in individually ventilated cages (IVC). Infections with the highly pathogenic H5N1 human isolate were carried out in the biosafety level 3 (BSL-3) facility at the Heinrich Pette Institute following standard operation procedures (SOPs). If possible, equal numbers of 10- to 12-week-old female and male mice were used for all infection experiments.

4.2.8.1 Generation, breeding and genotyping of ANP32 knockout mice

Breeding, handling and genotyping of mice used in this study were taken care of by the excellent staff of the technology platform '*small animal models'* at the HPI.

In this study, two different knockout mouse models were used to study the role of ANP32 proteins on influenza pathogenesis. For ANP32A, a classical constitutive knockout model was established [351]. To generate the C57BL/6J ANP32A$^{-/-}$ mouse line and the wild type littermates (ANP32A$^{+/+}$) thereof, sperm was purchased from the EMMA depository (EM:07238) and used for

embryo transfer at the University Medical Center Hamburg-Eppendorf, Hamburg, Germany. Genotyping was performed using genomic DNA extracted from ear stamps, PCR and custom-designed primers. Briefly, genomic DNA was extracted from a single ear stamp by incubation of the stamp in lysis buffer overnight at 55 °C (500 rpm). Then, the tube was mixed, centrifuged (21.000 x g, 10 min, RT) and the supernatant was transferred to a new reaction tube pre-filled with 500 µl of isopropanol. After mixing, the tube was centrifuged again as described, the supernatant was discarded, and the pellet containing genomic DNA was air-dried for 20 min at RT. Subsequently, the pellet was resuspended in 100 µl ddH_2O for 1 h at 37 °C. **Table 25** summarizes the protocol for the PCR reaction. The PCR products were subsequently visualized on a 2 % agarose gel (chapter 4.2.3.2). For $ANP32A^{+/+}$ mice, a 900bp DNA fragment was expected, while for $ANP32A^{-/-}$ mice a 700 bp fragment was expected. Knockout efficiency in the organs of interest (lung, brain) was further confirmed on protein level by Western blotting (chapter 4.2.4.4).

Table 25: Genotyping of ANP32A mice by PCR and agarose gel electrophoresis.

Component	Concentration	Final concentration	Volume
ddH_2O	-	-	10.4 µl
Buffer (Qiagen)	10x	1x	2 µl
Primer 1 (p5, forward: 5‘ → 3‘)	10 µM	200 nM	0.4 µl
Primer 2 (p3, reverse: 3‘ → 5‘)	10 µM	200 nM	0.4 µl
Genomic DNA	-	-	2 µl
dNTPs	10 mM	200 nM	0.4 µl
Taq polymerase (Qiagen)	5 U/µl	2 U	0.4 µl
Total			**16 µl**
PCR cycling	**94 °C, 15 min** **94 °C, 45 sec** **60.5 °C, 60 sec** **72 °C, 40 sec** **72 °C, 10 min**	**40 cycles**	

For ANP32B, a conditional ANP32B knockout mouse model was chosen, since previous reports demonstrated that germline knockout of ANP32B disrupts early development, leading either to death of the offspring *in utero* or significantly decreased viability later in life [365, 366].
C57BL/6J ANP32B$^{-/-}$ mice and the wild type littermates (ANP32B$^{+/+}$) thereof were generated using Cre recombinase as recently described [352]. Herein, the knockout is induced by feeding Tamoxifen-containing nutrients to 6-week old mice for approximately 4 weeks. After tamoxifen-induced expression of the Cre recombinase, the enzyme excises exon 4 of the ANP32B gene, framed by loxP sites at each end, and thereby completely disrupts ANP32B protein expression in all organs assessed, including the lung and the brain ([352]; this study). Genotyping was performed using genomic DNA extracted from ear stamps, PCR and custom-designed primers. Genomic DNA was extracted as described above and the PCR reaction was performed as described, but using *Taq DNA polymerase* (Qiagen) [352]. The PCR products were visualized by 2 % agarose gel electrophoresis (chapter 4.2.3.2). The knockout efficiency in the organs of interest (lung, brain) was further verified on protein level by Western blotting (chapter 4.2.4.4).

4.2.8.2 Narcosis, infection and euthanization of mice

For infection experiments, mice were shortly placed in isoflurane (Forene) narcosis using a vaporizer, followed by intraperitoneal (i.p.) narcosis with a mixture of ketamine (100 mg/ml, 20 µl per mouse) and xylazine (20 mg/ml, 10 µl per mouse), prepared in 0.9 % of sterile sodium chloride solution. The narcosis volume was always matched to the weight of each individual animal according to the following formula: weight [g] x 10 – 50 = µl narcosis volume. The virus inoculum was prepared by appropriate dilution of virus stock in 1 x PBS to the desired infection dose (10^1 or 10^3 PFU/50 µl). Approximately 20 min after administration of narcotics and checking for vital reflexes, 50 µl of virus inoculum or PBS only was administered intranasally and mice were observed for a few minutes to ensure sustained and steady breathing. Mice were monitored daily and scored according to parameters as defined and approved by the German authorities. At the humane endpoint of 25 % loss of original weight or when a respective score (i.e., ≥ 25) was reached, mice were briefly placed in isoflurane narcosis and euthanized by cervical dislocation.

4.2.8.3 Weight loss and survival experiments

Weight loss and survival (WL/S) experiments were carried out over a time period of 14 days. The weight of each individual animal was recorded daily, and mice were euthanized at the primary humane endpoint of 25 % loss of original weight at infection day 0. WL/S curves were generated using *Microsoft Excel* and *GraphPad Prism* software (Graphpad, Inc.).

4.2.8.4 Harvesting of blood and organs

In order to harvest organs at 3 or 6 days post infection, PBS or virus infected mice were briefly placed in isoflurane narcosis, blood was collected retrobulbary in EDTA tubes and animals were euthanized by cervical dislocation. The whole blood was centrifuged for 10 min at 2.000 x g (4°C), the plasma/serum (i.e. supernatant) was aliquoted into fresh tubes and stored at -80 °C until further processing. The abdominal and chest cavities were opened and the lung was removed. Furthermore, the skulls of the mice were opened using surgical scissors and the brain was harvested.

For total RNA isolation, the whole lung was preserved in RNA later reagent (Qiagen) for 24 h at 4 °C. Then, four equal parts (~ 30 mg each) were distributed into tubes pre-filled with metal beads and stored at -80 °C until further processing (e.g. RNA isolation, chapter 4.2.2.3).

For histological examination (chapter 4.2.6), a single lung lobe was stored in 4 % PFA solution (in PBS) at 4 °C.

For determination of virus titers and measurement of cytokines, lung and brain tissue was removed and the weight was recorded. Then, the tissue was directly homogenized in PBS. Therefore, the tissue (one lung lobe or whole brain) was placed in screw cap tubes filled with glass beads, 0.8 ml of PBS were added and the tissue was homogenized using a RETSCH homogenizer (20 Hz, 4 °C, 10 min). The cell suspension was centrifuged for 5 min at 6.000 x g to pellet the larger tissue pieces and the supernatant was aliquoted and stored at -80 °C. Viral titers were determined by PT on MDCK cells as described in chapter 4.2.5.5.

In order to confirm knockout of either ANP32A or ANP32B in murine tissue on protein level, lung and brain were harvested from three animals per genotype ($ANP32A^{+/+}$, $ANP32A^{-/-}$, $ANP32B^{+/+}$, $ANP32B^{-/-}$) and approximately 30 mg of extracted tissue were homogenized in HEPES lysis buffer using a RETCH homogenizer (20 Hz, 2 min; 30 Hz, 1 min). To allow complete cell lysis, the suspension was incubated on ice for 20 min, followed by centrifugation (20 min, 20.000 x g, 4°C) to remove cell debris. Supernatants were mixed with 4 x Laemmli Loading Dye, heated to 95 °C for 5 min and stored at -20 °C for WB analysis (chapter 4.2.4.4).

4.2.8.5 Isolation and culturing of murine lung fibroblasts

Male $ANP32A^{-/-}$ or $ANP32B^{-/-}$ mice and the wild type male littermates thereof were briefly placed in isoflurane narcosis, blood was collected retrobulbary and mice were sacrificed by cervical dislocation. Lungs from two mice of each genotype were removed, washed once with PBS, cut into small parts and mixed together. The tissue was digested with collagenase (in DMEM medium) for 1 h at 37 °C, followed by digestion with DNase (in DMEM medium) for 10 min at room temperature (RT). Then, the tissue was squeezed through a 45 µM mesh filter using

DMEM medium, and the cell suspension was centrifuged at 300 x g for 10 min at 4°C. The pelleted cells were resuspended in mLF growth medium and seeded into 24-well plates, 1 ml per well. Cells were incubated for 72 h at 37 °C. After 72h, cells were trypsinized for a few minutes to separate the fibroblasts from the epithelial cells, which are more resistant to trypsin. Cells were then passaged twice a week by differential trypsination until only fibroblast cells remained. These fibroblast cells were further maintained in culture for approximately 25 passages until they showed fast and contact-independent growth, indicative of spontaneous immortalization. Every 5 to 6 passages, the respective ANP32 knockout was verified on protein level by Western blotting.

4.2.9 *In silico* analyses

4.2.9.1 Visualization of importin-α7 – ANP32A interaction using *Pymol*

The interaction of importin-α7 with ANP32A, as observed in CoIP experiments, was further analyzed using *in silico* modelling and the software *Pymol.* In brief, RosettaDock, a Monte Carlo based multi-scale docking algorithm of the Rosetta modeling suite [367-370], was used to model the available protein structure of ANP32A (PDB *4XOS*; without C-terminal low-complexity region (LCAR)) onto the available protein structure of importin-α7 (PDB *4UAD*; without importin-β_1 binding (IBB) domain). In total, 10.000 iterations were simulated by altering the position of the ANP32A structure by 3 Å translation and 8° rotation and evaluating the new interaction in each step [368]. The docking result with a significantly larger *interface score* (i.e., the energy of the interaction) compared to all other results was selected (-9.339 vs. -6.969). This conformation also showed the second best *total score* (-770.917), which represents more unfavorable docking solutions the larger it gets [368] (https://github.com/hzi-bifo/Importin_a7-ANP32A-interaction).
This *in silico* analysis was performed by collaboration partners (Dr. Thorsten Klingen, Prof. Dr. Alice McHardy) at the Helmholtz Centre for Infection Research in Braunschweig, Germany.

4.2.9.2 Evaluation of pre-processed mass spectrometry data

Pre-processed raw mass spectrometry data were further evaluated manually. Therefore, SILAC ratios were calculated with the peptide intensities measured for each peptide corresponding to a particular cellular or viral protein. Herein, the ratio of peptide intensity *M* or *H* (i.e., precipitated with importin-α-ΔIBB or -WT, medium or heavy labeled amino acids, ‘M’ or ‘H’, respectively) over peptide intensity *L* (i.e., precipitated in the empty vector control, light amino acids, ‘L’) was calculated for each protein (M/L and H/L, respectively). Ratios were then $\log_2$-transformed, and a $\log_2$Fold Change > 1 (i.e., 2-fold enriched with importin-α-ΔIBB or -WT over the empty vector control) was considered statistically significant. In addition, those cellular proteins that were only

precipitated with importin-α-ΔIBB and/or -WT, but not in the empty vector control were also considered 'true' importin-α interaction partners. Protein lists (SILAC log2FoldChange >1; only precipitated with importin-α-ΔIBB; only precipitated with importin-α-WT) were merged for each particular importin-α isoform, duplicates were removed, and data were imported into STRING to generate interacting networks (chapter 4.2.9.3).

4.2.9.3 Visualization of MS-derived interactome data using *STRING* and Cytoscape software

The STRING 11.2 functional protein association networks online tool (www.string-db.org) was used to determine predicted interactions of importin-α isoforms (α1, α5, α7) with co-immunoprecipitated cellular and viral proteins which were identified by SILAC-MS. In order to filter out interactions with less validity, a high confidence score of 0.9 was applied. Data were exported from STRING and further visualized using *Cytoscape* software.

4.2.9.4 Visualization of NGS-derived transcriptomic data using *ClustVis*

Heatmap analysis of transcriptomic data generated in this study was carried out using the online tool *ClustVis* [355]. Therefore, disregulated genes were extracted from the Top10 of significantly altered gene ontologies (GOs) for each respective comparison performed, and a log2FoldChange (Log2FC) cut-off of ≥ 2 (upregulated genes) or ≤ -1 (downregulated genes) was applied. Then, genes presented in all 10 GOs were merged to remove duplicates, and NGS-derived gene expression counts were assigned to each significantly disregulated gene for each individual animal. Finally, genes and gene expression counts were subjected to heatmap analysis using *ClustVis*. The color code represents the standard deviation from the mean of normalized expression values (*z-score*) within each group (n = 3 animals).

4.2.9.5 Gene ontology analyses using the ToppGene Suite

Importin-α interacting cellular proteins identified by SILAC-MS as well as disregulated genes in IAV infected ANP32B mice derived from transcriptome measurements were further subjected to gene ontology analysis using the ToppGene Suite (https://toppgene.cchmc.org/) [360] to identify common biological functions among these cellular factors and genes, respectively. Parameters applied were: FDR correction and cut-off p-value ≤ 0.05 (probability density function).

4.2.9.6 Alignment of nucleic and amino acid sequences

Nucleic and amino acid sequences were aligned using *CloneManager Professional 9* software and either linear or BLOSUM62 scoring matrices, respectively. Nucleic acid sequences were

derived from the National Center of Biotechnology Information (NCBI). Amino acid sequences were also derived from NCBI or directly translated from the nucleotide sequence using *CloneManager Professional 9* software.

4.2.10 Statistical evaluations

All statistical evaluations in this study were carried out with *GraphPad Prism* v5 software, and significant statistical differences were further divided based on *p*-values into 3 groups: **p* < 0.05, ***p* < 0.01, ****p* < 0.001.

Statistical significant differences in viral polymerase activity assays (*n* ≥ 3 biological replicates, each with technical triplicates), quantified immunofluorescence data (chapter 4.2.7.1), or in quantified Western blot data (*n* ≥ 3 biological replicates) were determined using the two-tailed Student's *t*-test, always compared to the respective positive controls set to 100 %.

Significant changes in cytokine and chemokine expression levels (mRNA/qPCR or protein/luminex) in murine lung tissue were analyzed using two-way ANOVA with Bonferroni post-hoc correction (n = 4-7 animals/group).

5. Results

5.1 The importin-α interactome as a platform to study molecular mechanisms of IAV replicative fitness in human cells

In the last decade, substantial evidence has emerged that importin-α isoforms drive IAV interspecies transmission from birds to mammals, along with increased pathogenicity in mammalian hosts [50, 237, 250]. Particularly, importin-α7 was identified as a positive regulator of viral polymerase activity, promoting viral replicative fitness and, in turn, elevated pathogenicity in mammalian cells and small animal models [50, 251, 293]. Although the detailed mechanism underlying importin-α7 function remained unknown, it was hypothesized that it might indirectly control viral replication by regulating the cytoplasmic-nuclear shuttling of specific host cell factors that are required for high-level IAV replication. To address this hypothesis, in this study, an unbiased SILAC mass spectrometry (MS) approach was performed to determine the importin-α7 interactome in human cells.

5.1.1 Establishment of a SILAC-based mass spectrometry approach to identify importin-α interaction partners in human cells

Co-immunoprecipitation coupled with SILAC-MS is a powerful quantitative technique that allows detection of interacting cellular proteins with high sensitivity. Here, this technique was employed to identify cellular interaction partners of importin-α7 in influenza infected human HEK293T cells. **Figures 8** summarizes the experimental setup. After transfection of expression constructs encoding FLAG-tagged importin-α7, cells were either mock-treated or infected with IAV A/WSN/33 (H1N1; $PB2_{627K}$) for 16 h. Then, cells were lysed and importin-α7 along with its interacting cellular proteins was precipitated from cell lysates using an anti-FLAG resin. After SDS-PAGE, Coomassie staining and in-gel proteolytic digestion, co-immunoprecipitated proteins were identified by MS (**Figure 8**).

Several controls were included to improve the robustness and validity of the approach: First, an empty vector expressing only the FLAG tag (‘*DYKDDDDK*’) was used to eliminate any proteins from the interactome that unspecifically interacted with the resin (e.g. keratins). Second, due to the intrinsic property of the shuttling importin-α isoforms that continuously associate and disassociate with their nuclear transport cargos, an importin-α7 variant with a deleted importin-β_1 binding domain (ΔIBB) was used as additional control. In theory, importin-α7-ΔIBB would still bind to the NLS motif presented by a cargo protein, but interaction with the transport co-receptor

importin-β_1 and, in turn, nuclear translocation and dissociation of the complex would be prevented. Therefore, it was expected that importin-α7-ΔIBB would interact more stably with NLS-presenting cellular cargos compared to its intact importin-α7-WT analogue.

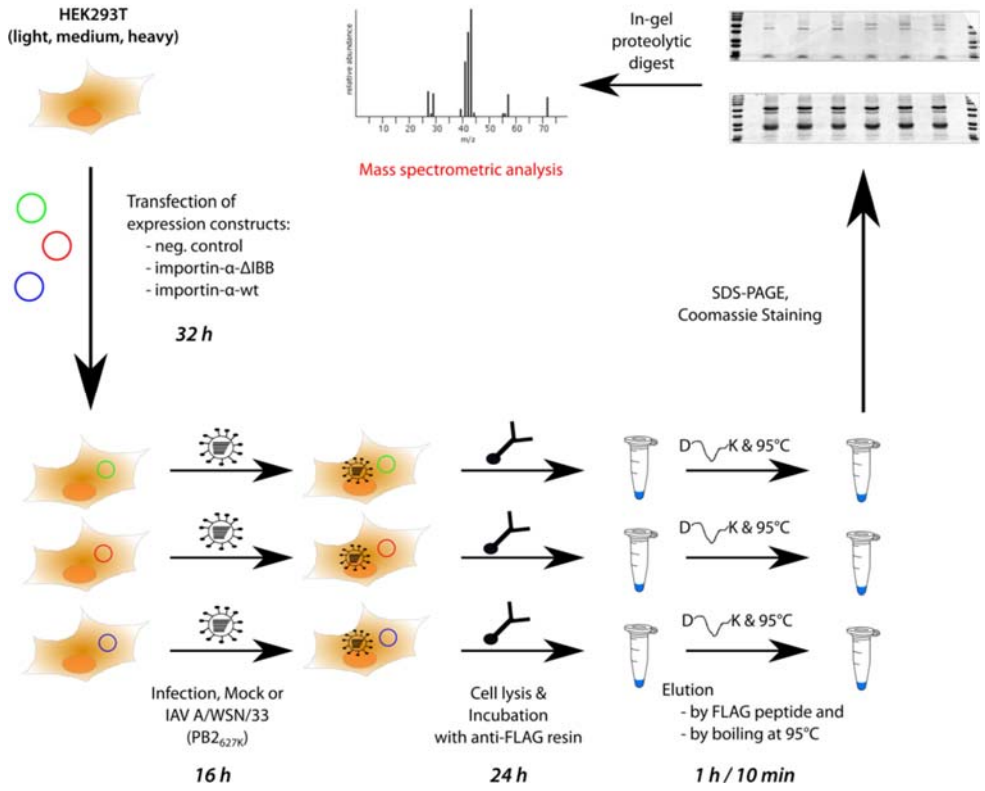

Figure 8: A co-immunoprecipitation coupled with SILAC mass spectrometry approach to determine the importin-α interactome in human cells. FLAG-tagged importin-α isoforms (importin-α1, -α5, -α7; WT or ΔIBB) were expressed in human HEK293T cells, along with an empty vector control expressing only the FLAG tag (neg. control). After 32 h, cells were infected with IAV A/WSN/33 (H1N1; $PB2_{627K}$) for 16h. Mock infection was carried out as control. Then, cells were lysed and cell lysates were incubated with an anti-FLAG resin for 24 h at 4 °C. FLAG-tagged importin-α isoforms as well as their interacting cellular proteins were eluted from the resin, first by incubation with an excess of FLAG peptide followed by boiling of the resin at 95 °C. Eluates for a particular importin-α isoform were pooled (set of 3: neg. control, ΔIBB, WT) and loaded on an SDS gel. After Coomassie staining, proteins were in-gel proteolytically digested and the derived peptides were analyzed by mass spectrometry.

Finally, as additional controls, the importin-α1 and -α5 interactomes were determined as well. Importin-α1 promotes human-type IAV polymerase activity in a nuclear transport-dependent manner, in contrast to importin-α7, while importin-α5 shows a high sequence similarity to importin-α7, but plays no significant role in IAV infections [250, 251] .

For elution of the FLAG-tagged proteins from the resin, two different approaches were chosen: First, proteins were eluted by incubation of the resin with an excess of FLAG peptide that would compete with the FLAG-tagged importins on the resin. Using this rather gentle elution method, the FLAG-recognizing antibodies remain bound to the resin which would allow the detection of immunoprecipitated proteins without inference of light and heavy antibody chains in Western blotting. However, to ensure that all precipitated proteins are efficiently eluted from the resin, another elution step by boiling the same samples at 95 °C was included.
Successful and comparable precipitation of FLAG-tagged proteins as well as productive infection of the cells was verified by Western blotting (**Figure 9**).

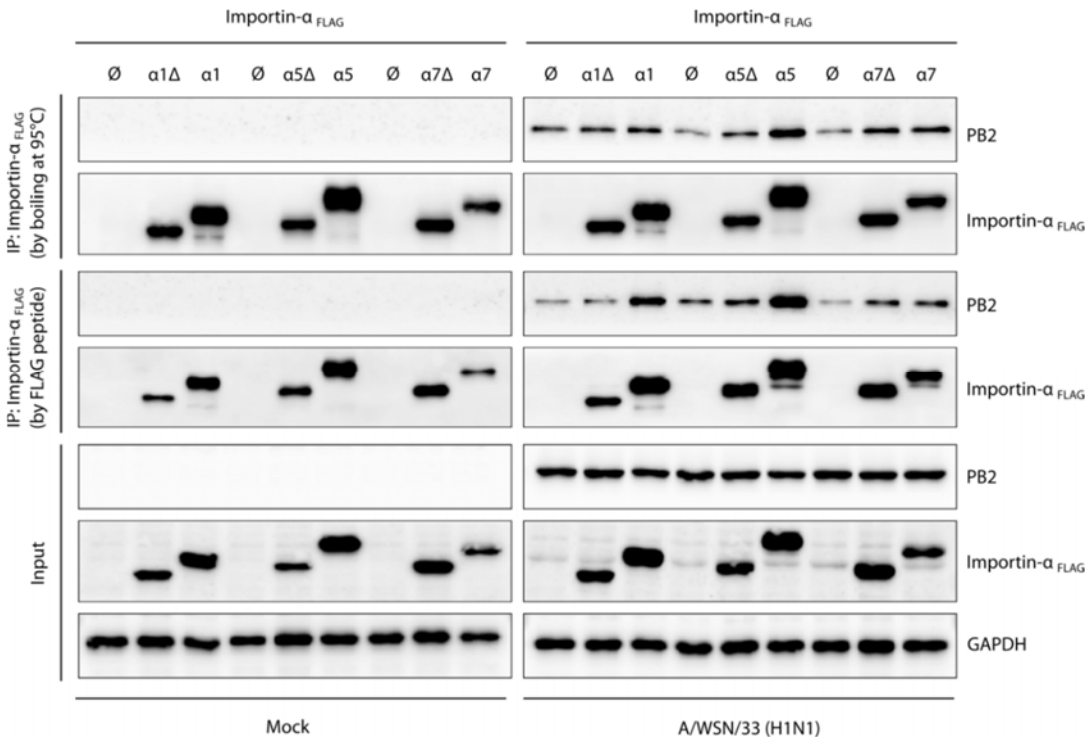

Figure 9: Confirmation of efficient importin-α pulldown in co-immunoprecipitated samples from SILAC-MS experiments. Representative Western blot showing efficient and comparable expression (*input*) as well as precipitation (*IP:* Importin-α_{FLAG}) of all importin-α isoforms (WT, ΔIBB) from cell lysates, for both elution steps performed. Productive infection with IAV A/WSN/33 (H1N1; $PB2_{627K}$) was confirmed by detection of viral PB2 protein. GAPDH was used as a loading control for the input samples. IP samples were free from cell lysate contaminations as no GAPDH expression was observed. PB2 interacted with all importin-α isoforms, although also a slight unspecific interaction was observed in the neg. control (Ø).

All FLAG-tagged importin-α isoforms (ΔIBB or WT) were precipitated from the resin efficiently and to comparable levels (**Figure 9**). Productive infection with IAV A/WSN33 (H1N1; $PB2_{627K}$) was confirmed by detection of the viral PB2 protein. As observed in previous studies, PB2 interacted with all three importin-α isoforms [251]. However, also a slight unspecific interaction with the resin was detected in the empty vector control (Ø) (**Figure 9**).

Taken together, successful co-immunoprecipitation of FLAG-tagged importin-α isoforms from uninfected or influenza infected cells was established. In the next chapter, the MS-based identification of cellular interaction partners of the individual importin-α proteins will be described in more detail.

5.1.2 The importin-α interactome in uninfected or influenza infected human cells

MS analysis was used to determine cellular proteins that were precipitated with the individual importin-α isoforms in either mock or influenza infected cells. Herein, peptides obtained after in-gel proteolytic digestion of pooled co-immunoprecipitated samples (sets of 3: neg. control, unlabeled amino acids, '*L'*; importin-α-ΔIBB, medium labeled amino acids, '*M'*; importin-α-WT, heavy labeled amino acids, '*H'*) were mapped to the *Uniprot* database in order to identify the respective cellular proteins from which these peptides were derived.

In the first analysis step, the obtained raw peptide intensities corresponding to each identified protein were further evaluated manually to identify cellular proteins that were significantly enriched with importin-α-WT (H) over the empty vector control (L). For each importin-α isoform and for each identified protein, the respective peptide intensities were plotted as peptide intensity measured in the empty vector control (L) over the peptide intensity measured in the importin-α-WT (H) condition (log_{10} transformed values) (***Appendix*, Figures 42-44, A and C**). Linear regression was performed, and all cellular proteins significantly enriched with importin-α-WT are shown above the red regression line, indicative of a specific interaction with the importin-α protein. In contrast, all proteins appearing below the regression line were enriched in the empty vector control, indicative of an unspecific interaction with the resin. Precipitated importin-α (*KPNAx*) and importin-β_1 (*KPNB1*) proteins are highlighted, including the respective importin-α bait protein used for immunoprecipitation (***Appendix*, Figures 42-44, A and C**).

Since only one MS dataset was available at the time point of thesis submission, a high-stringency cutoff was applied to accurately filter out unspecific interactions. Therefore, a ratio of the peptide intensity *L* (i.e. found in empty vector control) over the peptide intensity *H* (i.e. precipitated with importin-α-WT) was calculated for each identified protein. Obtained ratios were

log_2-transformed and plotted over the combined L+H peptide intensity. A log_2FoldChange > 1 (i.e., 2-fold enriched with importin-α-WT over the empty vector control) was considered as statistically significant (***Appendix*, Figure 42-44, B and D**). This cutoff is indicated with a red line, and all proteins appearing right from this cutoff line are considered as specific importin-α-WT interacting factors. As before, precipitated importin-α (KPNAx) and importin-β_1 (KPNB1) proteins, including the importin-α bait protein, are highlighted.

It should be noted that those proteins for which peptides only have been found in the importin-α-WT pulldown, but not in the empty vector control, are not reflected in this analysis. Furthermore, cellular proteins significantly enriched with importin-α-ΔIBB are also not included. A complete list of these cellular factors that were significantly enriched with importin-α-WT or -ΔIBB is provided in ***Appendix,* Tables 29-30, 33-34, and 37-38**.

In absolute numbers, 49/79 cellular proteins were precipitated with importin-α1-WT/ΔIBB, 89/87 proteins with importin-α5-WT/ΔIBB, and 49/53 proteins with importin-α7-WT/ΔIBB, in uninfected and influenza infected cells, respectively (***Appendix,* Tables 29-30, 33-34, and 37-38**). Although unexpected, these rather low numbers of identified proteins might be best explained by the high-stringency cutoff as well as the fact that some importin-α isoforms were not included in this study (e.g. importin-α3 and -α4). With the next MS datasets becoming available, the cutoff used here can be further adjusted, which will likely increase the number of statistically significant importin-α interaction partners.

In order to obtain a more detailed overview of importin-α interaction partners in mock or influenza infected cells, interactome networks were created using the online *STRING 10.0 functional protein association tool* and further visualized using *Cytoscape* software. Based on a combined list of proteins precipitated with all three importin-α isoforms (WT or ΔIBB), the output illustrates predicted and experimentally validated interactions of importin-α1, -α5 and -α7 with their co-immunoprecipitated cellular proteins (**Figure 10 and 11**). The importin-α proteins are differentially colored and shown in the center of the interacting network (diamond shapes), while all interacting proteins are depicted as ellipses, forming distinct clusters (numbered with Roman numerals). Cellular proteins without any described interaction are shown at the bottom. The color-code indicates whether a particular protein has been precipitated with one, two, or all three importin-α proteins (**Figure 10 and 11**).

In uninfected cells (Mock), most of the importin-α interacting proteins clustered into 9 distinct groups (**Figure 10**). In general, a tight interaction network comprising at least three cellular proteins was designated as a cluster. As evident in **Figure 10** and described above, significantly higher numbers of cellular proteins were precipitated with importin-α5 (*n* = 89), compared to importin-α1 and -α7 (both *n* = 49). In a total of 121 proteins, 13 proteins precipitated with all

three importin-α isoforms (10.7 %), 42 proteins interacted with two out of three importin-α isoforms (34.7 %), and 66 proteins displayed specificity for one particular importin-α isoform (54.6 %) (**Figure 10**; ***Appendix*, Tables 29, 33 and 37**). Gene ontology (GO) analysis of some of the larger clusters further revealed an association of these proteins with fundamental cellular processes, such as translation (*cluster I*), chromatin remodeling (*cluster IV*), intracellular (virus) transport (*cluster VII*), and mRNA splicing (*cluster VIII*) (***Appendix*, Figure 45**). GO analysis of all identified proteins, including those outside of the identified clusters, do not significantly differ from the GOs for the 9 observed clusters (***Appendix*, Tables 31, 35 and 39**).

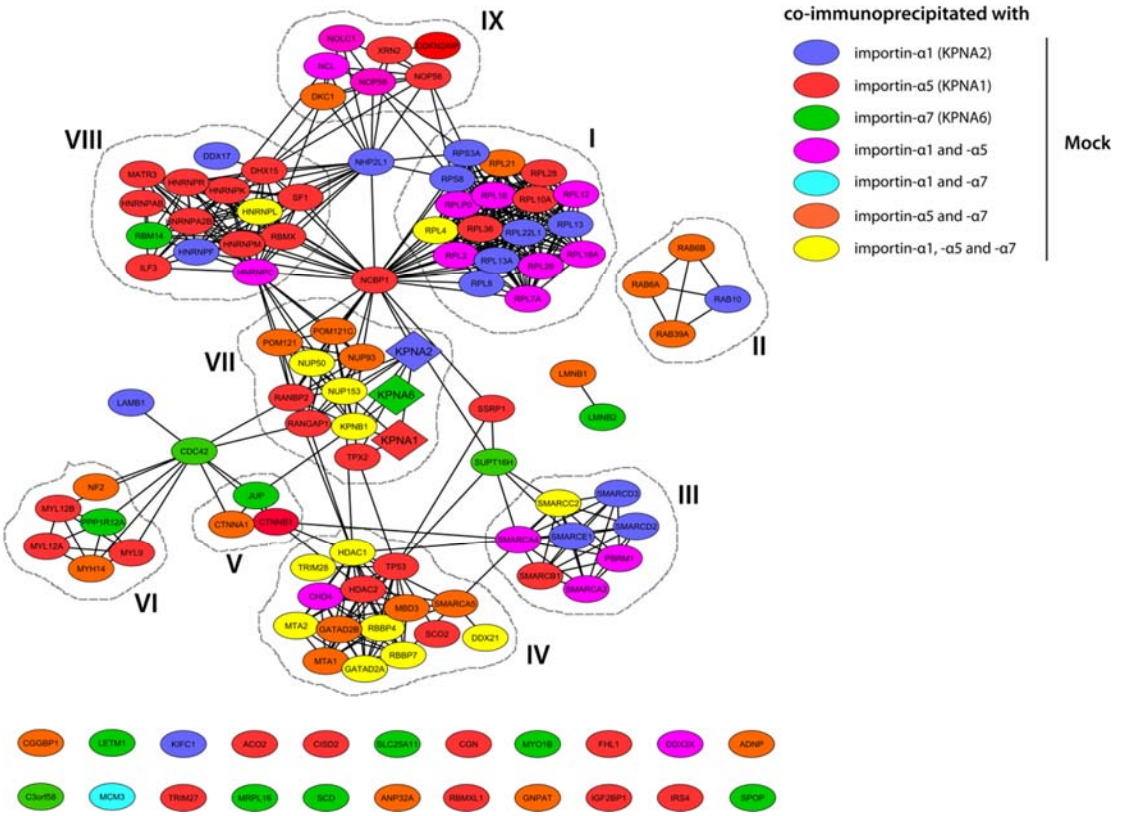

Figure 10: The combined importin-α1, -α5 and -α7 interactome in uninfected HEK293T cells. Shown is an interaction network of all three importin-α isoforms and their co-immunoprecipitated cellular proteins in mock infected cells (created with *STRING 10.0* and *Cytoscape*). Importin-α isoforms are shown in the center of the network (diamond shapes, differentially colored). Co-immunoprecipitated cellular proteins (shown as ellipses) are grouped into 9 distinct clusters (numbered by Roman numerals). Clusters are defined as a tight sub-network comprising at least three individual proteins. The color-code indicates whether precipitation of a particular protein occurred with one, two, or all three importin-α isoforms. Cellular proteins without any described interaction are shown at the bottom.

Major cellular proteins that connected at least three independent clusters were identified as CDC42 (*cell division control protein 42 homolog;* clusters V, VI and VII), NCBP1 (*nuclear cap-binding protein subunit 1*; clusters I, VII, VIII), and NHP2L1 (*H/ACA ribonucleoprotein complex subunit 2-like protein 1*; clusters I, VIII and IX), all of which were precipitated with a specific importin-α isoform (**Figure 10**)**.** Individual clusters were also dominated by specific importins (e.g. cluster VIII by importin-α5, cluster I, III and IX by importin-α1 and -α5, and cluster II, VI and VIII by importin-α5 and -α7), indicating that cargo properties beyond the NLS motif likely influence importin-α binding, as described before (**Figure 10**) [322]. The highest number of cellular proteins precipitated with all three importin-α isoforms was identified in cluster IV (*chromatin remodeling*), which might suggest that these essential proteins have evolved to bind to multiple importins for efficient nuclear translocation, independently of the availability of a particular importin-α isoform (**Figure 10**). Interestingly, no clear cluster was identified that was dominated by importin-α7, which therefore distinguishes it from the other two importin-α isoforms (**Figure 10**).

In influenza infected cells (H1N1), a similar pattern of clusters was identified, suggesting that viral infection does not alter the overall cargo binding specificity of the importin-α isoforms (**Figure 11**). Also, the binding preferences of the cargo proteins for the different importin-α isoforms were not significantly altered: Out of 138 proteins, 20 proteins precipitated with all three importin-α isoforms (31.2 %), 43 proteins interacted with two out of three importin-α isoforms (34.7 %), and 75 proteins displayed specificity for one particular importin-α isoform (54.1 %) (**Figure 11**; ***Appendix*, Tables 30, 34 and 38**).

Regarding total numbers of identified proteins, no major differences were observed for importin-α5 and -α7 between uninfected and infected cells (n = 87 vs. 89 and n = 53 vs. 49, respectively). On the other hand, in infected cells, a significantly higher number of proteins was precipitated with importin-α1 (n = 79 vs. 49) (***Appendix,* Tables 29-30, 33-34, and 37-38**). This is potentially interesting and might not only be a result of differential importin-α1 pulldown efficiency in the two different conditions.

In comparison to uninfected cells, two additional small clusters of proteins were observed in infected cells, and GO analyses revealed that these are either linked to DNA repair (*cluster X*) or cell architecture (*cluster XI*) (**Figure 11**; ***Appendix*, Figure 46 and Tables 32, 36 and 40**). Particularly for cluster X, these findings might indicate that influenza infection triggers importin-α mediated nuclear translocation of cellular proteins that are required to counteract virus-induced DNA damage, a phenomenon that only recently has been described [371]. Although potentially intriguing, this hypothesis would require further investigation. Moreover, in influenza infected cells, a distinct cluster entirely representing importin-α7 interaction partners was identified

(*cluster II*; Rab protein signal transduction), which might have a functional, yet unknown role during influenza infection (**Figure 11; *Appendix*, Figure 46**). NCBP1, the major node protein connecting clusters I, VII, and VIII in uninfected cells, was also present in the importin-α interactome in influenza infected cells. However, its binding specificity shifted from importin-α5 to importin-α1 during viral infection (**Figure 10 and 11**). Analysis of the pending MS datasets coupled with Western blotting will be important to clarify whether this observation is reproducible and thus might have biological relevance.

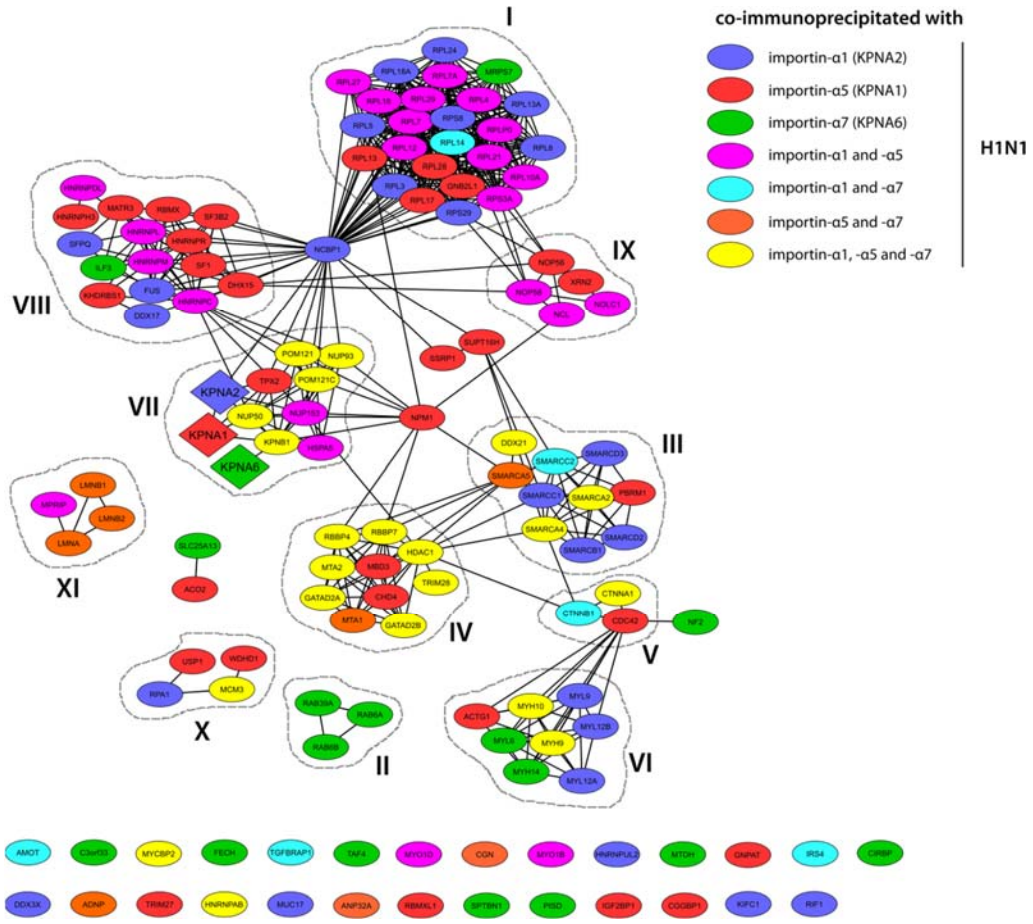

Figure 11: The combined importin-α1, -α5 and -α7 interactome in influenza infected HEK293T cells. Shown is an interaction network of all three importin-α isoforms and their co-immunoprecipitated cellular proteins in influenza infected cells (created with *STRING 10.0* and *Cytoscape*). Importin-α isoforms are shown in the center of the network (diamond shapes, differentially colored). Co-immunoprecipitated cellular proteins (shown as ellipses) are grouped into 11 distinct clusters (numbered by Roman numerals). Clusters are defined as a tight sub-network comprising at least three individual proteins. The color-code indicates whether precipitation of a particular protein occurred with one, two, or all three importin-α isoforms. Cellular proteins without any described interaction are shown at the bottom.

5.1.3 Importin-α7 interacting cellular factors and their role in influenza infection

In line with the initial hypothesis that importin-α7 regulates viral replication indirectly by controlling the cellular localization of an unknown host factor, cellular proteins that were precipitated with importin-α7 during viral infection were of particular interest for subsequent functional studies. STRING analysis was used to visualize the importin-α7 interactome in uninfected (Mock) as well as in influenza infected cells (H1N1) (**Figure 12**).

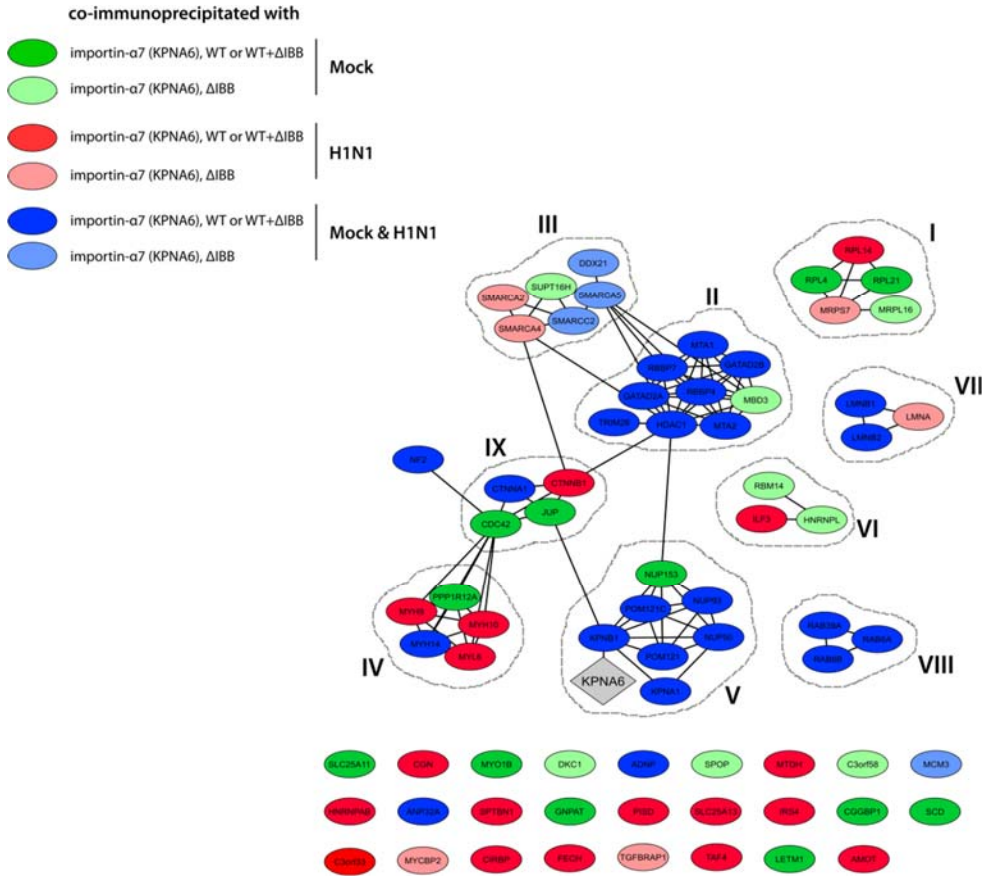

Figure 12: The combined importin-α7 interactome in uninfected and influenza infected HEK293T cells. Shown is an interaction network of importin-α7 (WT, ΔIBB) and its co-immunoprecipitated cellular proteins in mock as well as influenza (H1N1) infected cells (created with *STRING 10.0* and *Cytoscape*). Co-immunoprecipitated cellular proteins (shown as ellipses) are grouped into 9 distinct clusters (numbered by Roman numerals). Importin-α7 is shown in cluster V (diamond shape). Clusters are defined as a tight sub-network comprising at least three individual proteins. The color-code indicates whether precipitation of a particular protein occurred in mock or influenza infected cells, or both, and either with importin-α7-WT or -ΔIBB, or both. Cellular proteins without any described interaction are shown at the bottom.

GO analysis of importin-α7 interacting cellular proteins revealed a strong association with chromatin remodeling (i.e. gene expression) and intracellular transport processes, both in mock and influenza infected cells (***Appendix*, Tables 39-40).**

In order to identify promising candidates that might contribute to importin-α7 function during influenza infection, the following interacting proteins were excluded from subsequent analyses: i) cellular proteins only precipitated in mock infected cells (11/53; 20.7 %); ii) cellular proteins that also precipitated with importin-α1 as well as -α5, suggesting a low specificity for importin-α7; and iii) cellular proteins that have not been yet associated with a role during influenza infection. Cellular factors that were only precipitated with one other importin-α isoform in addition to importin-α7 were not excluded from the candidate list. This was justified by the fact that, to this end, no *in vitro* binding assays using purified proteins have been performed that would allow quantitative evaluation of importin-α – cargo binding affinities.

Applying the above mentioned criteria, the list of potential candidates was narrowed down to 13 importin-α7 interacting cellular proteins. **Table 26** provides an overview of these cellular proteins and their proposed or experimentally-validated function during influenza infection.

Table 26: Importin-α7 interacting cellular proteins and their role during influenza infection. Shown are the cellular proteins that were precipitated with importin-α7 (WT, ΔIBB) in influenza infected cells and their described positive- or negative-regulatory function (proposed or experimentally validated) during influenza infection (n.d., not determined). Exclusion criteria were applied as described in the main text. Precipitation with a second importin-α isoform in addition to importin-α7 is indicated as well.

Gene name/ Protein name	Also precipitated with importin-	Regulatory function during influenza infection	Reference
ANP32A Acidic leucine rich nuclear phosphoprotein 32 family member A	α5	Positive	[252, 303, 305, 306]
CIRBP Cold-inducible RNA-binding protein	-	Negative n.d.	[372] [218]
CTNNB1 Catenin beta-1	α1	Positive	[218]
ILF3 Interleukin enhancer-binding factor 3	-	Negative	[241, 373-376]
KPNA1 Importin subunit alpha 5	-	Positive	[50, 251, 289, 377]

LMNA Prelamin-A/C; Lamin-A/C	α5	n.d.	[378, 379]
LMNB1 Lamin B1	α5	n.d.	[380]
LMNB2 Lamin-B2	α5	n.d.	[378]
RAB6A Ras-related protein Rab-6A	-	n.d.	[381]
RAB6B Ras-related protein Rab-6B	-	Positive	[382]
SLC25A13 Calcium-binding mitochondrial carrier protein Aralar2	-	n.d.	[383]
TAF4 Transcription initiation factor TFIID subunit 4	-	Negative	[384]
TGFBRAP1 Transforming growth factor-beta receptor-associated protein 1	α1	n.d.	[382]

Among the importin-α7 interacting cellular proteins presented in **Table 26**, particularly ANP32A (*acidic leucine rich phosphoprotein family member 32A*) was an interesting candidate for further investigation. In 2016, ANP32A was discovered as a novel host factor that mediates adaptation of restricted avian-type ($PB2_{627E}$) IAV polymerases in mammalian cells. Herein, a 33 amino acid insertion in the avian ANP32A protein that is lacking in the human homologue was shown to be critical for overcoming this restriction [252]. Furthermore, it was proposed that human ANP32A could also act as a co-factor for the mammalian-adapted ($PB2_{627K}$) IAV polymerase in human cells, supporting high-level virus replication [252]. Strikingly, like importin-α7, ANP32A also promotes $PB2_{627K}$ viral polymerase activity in a species-dependent manner [50, 251]. Thus, these findings warranted to further investigate whether a functional relationship might exist between these two positive-regulatory host factors.

First, the importin-α7 pulldown experiment was repeated to confirm its interaction with ANP32A in mock and influenza infected cells by Western blotting. For this experiment, the cells were cultivated in regular growth medium to exclude any artefacts caused by the SILAC media that were used for the MS analysis. As demonstrated in **Figure 13**, ANP32A was precipitated with both importin-α7-WT and -ΔIBB, independently of viral infection. Also, viral NP was precipitated

with both importin-α7-WT and -ΔIBB to similar levels, whereas viral PB2 showed a strong binding preference for the importin-α7-ΔIBB protein (**Figure 13**).

As an additional control, cellular NCBP1 protein was included. In MS analyses, NCBP1 was only precipitated with importin-α1 and -α5 in infected and uninfected cells, respectively, but not with importin-α7 in either condition. NCBP1, a nuclear cap binding protein involved in the export of cellular mRNAs, has also been described to play a role during influenza infection [385]. Interestingly, in contrast to the SILAC-MS data, NCBP1 was also precipitated with importin-α7-ΔIBB and, to lesser extent, importin-α7-WT (**Figure 13**). This finding highlights the limitations of MS-based CoIP experiments, particularly in the context of transient interactions, and further it demonstrates the importance of using independent techniques, such as Western blotting, to confirm the observed interactions. In the next chapters, the interaction of importin-α7 with ANP32A will be further characterized in the context of nuclear transport and the regulation of $PB2_{627K}$ IAV polymerase activity in human cells.

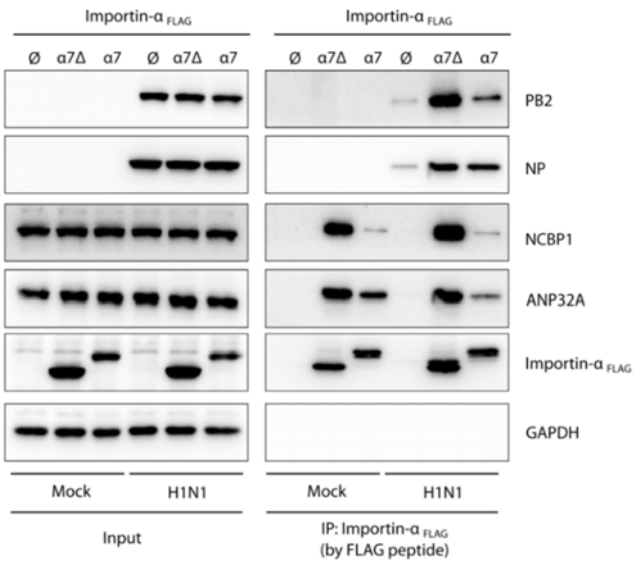

Figure 13: Confirmation of the importin-α7 – ANP32A interaction by Western blotting. FLAG-tagged importin-α7 (WT, ΔIBB) was expressed in human HEK293T cells along with an empty vector control (Ø). Cells were infected with IAV A/WSN/33 (H1N1; $PB2_{627K}$) for 16 h, followed by cell lysis and precipitation of FLAG-tagged importin-α7 using an anti-FLAG resin. FLAG-tagged importin-α7 as well as co-immunoprecipitated cellular proteins were eluted from the resin using an excess of FLAG peptide. Western blotting was performed to detect cellular ANP32A and, as a control, NCBP1 in the input and elution (IP) samples. Viral NP and PB2 proteins were detected to confirm productive infection of the cells. GAPDH was used as loading control for the input samples. Shown is a representative Western blot of three independent experiments.

5.2 Interplay of importin-α7 and ANP32A in promoting human-type IAV replicative fitness in human cells

Since ANP32A interacted with importin-α7 in uninfected as well as influenza infected cells (**Figure 13**) and fulfills its major function in the nucleus [296], it was hypothesized that ANP32A might be a cargo protein of the importin-α7 regulated nuclear import pathway. This hypothesis was further addressed using biochemical analyses coupled with fluorescence microscopy.

5.2.1 Nuclear transport of ANP32A occurs via the importin-α pathway

The C-terminal part of ANP32A comprises a basic, monopartite NLS motif (Lys-Arg-Lys-Arg; '*KRKR*'), based on prediction analyses (**Figure 14, A**). To adress the question whether ANP32A gains access to the nucleus via the classical importin-α/importin-β_1 pathway, expression vectors were generated for either wild type (WT) ANP32A or ANP32A variants with alanine mutations in the NLS motif (mutNLS1, '*AAKR*'; mutNLS2, '*AAAA*') (**Figure 14, B**). To study the localization of these constructs in the presence of endogenous ANP32A, C-terminal FLAG- or GFP tags were introduced onto the expressed proteins.

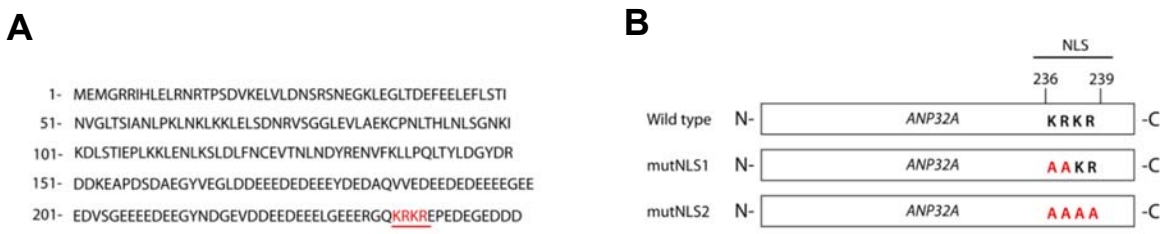

Figure 14: The C-terminus of ANP32A comprises a bona fide NLS motif. A, Prediction analyses revealed a classical, basic, monopartite NLS motif in the C-terminal part of human ANP32A (amino acids 236-239; '*KRKR*'). **B,** To study importin-α dependent nuclear translocation of ANP32A, expression constructs were generated for either wild type (WT) ANP32A or ANP32A variants with mutations in the NLS motif (mutNLS1, '*AAKR*'; mutNLS2, '*AAAA'*). For subsequent analyses in cells expressing endogenous ANP32A, these constructs were designed to express either non-tagged ANP32A, or C-terminal GFP- or FLAG-tagged ANP32A.

First, subcellular localization of the different ANP32A variants (WT; mutNLS1; mutNLS2) was investigated in HEK293T cells using fluorescence microscopy. In order to exclude any tag-specific artefacts, localization of both GFP- and FLAG-tagged ANP32A proteins was analyzed. As expected, and in line with previous reports, WT ANP32A was strictly localized to the nucleus,

independent of the introduced tag on the protein (**Figure 15, A and B**) [386]. In contrast, mutNLS1 and mutNLS1 ANP32A proteins (GFP- or FLAG-tagged) accumulated in the cytoplasm of the cell (**Figure 15, A and B**). Quantification of cellular ANP32A localization revealed significantly reduced nuclear levels of both mutated ANP32A variants, compared to WT ANP32A. Herein, mutation of the NLS motif in the GFP-tagged constructs reduced nuclear localization of ANP32A by almost 50 %, while mutations in the FLAG-tagged constructs decreased nuclear localization by 35 % (**Figure 15, C**).

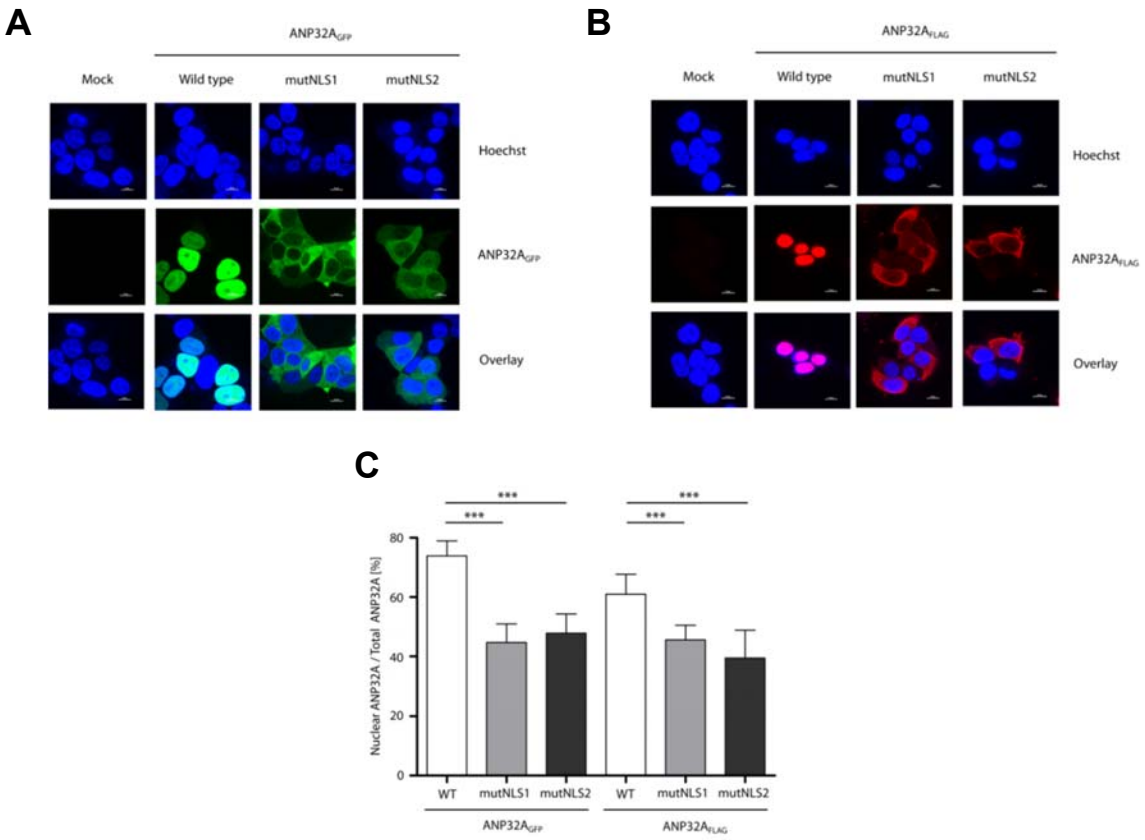

Figure 15: Localization of GFP- or FLAG-tagged WT and mutNLS ANP32A variants in HEK293T cells. A and B, WT or mutNLS ANP32A expression constructs (GFP- or FLAG-tagged) were expressed for 24 h in HEK293T cells. An empty vector was used as negative control (Mock). Cells were fixed in 4 % PFA solution and nuclei of cells expressing GFP-tagged ANP32A variants were stained with Hoechst dye. Cells expressing FLAG-tagged ANP32A proteins were subjected to immunostaining with a primary anti-FLAG antibody, followed by staining with a secondary Alexa555 antibody. Images were acquired on a confocal spinning disc microscope at 100x magnification. Scale bars represent 10 µm. **C,** Quantification of nuclear ANP32A was performed in three biological replicates, each with two acquired fluorescent images, using a custom-designed quantification macro for the ImageJ software. Statistical differences were determined using the two-tailed Student's *t*-test (*** $p < 0.001$).

These results suggest that alternative import pathways might be involved in nuclear translocation of ANP32A (either by simple diffusion or using other import adapter proteins), and that the larger GFP tag seems to hamper these processes to higher degree compared to the smaller FLAG tag. It also has to be noted, that the quantification of the fluorescent images is not 100 % accurate. More importantly, it does not entirely reflect the visual evaluation. This is mainly due to the fact only a fraction of the cells (< 30 %) on each acquired image expressed the tagged ANP32A variants, which significantly deteriorated the signal-to-noise ratio. Furthermore, applying different thresholds throughout the quantification process placed a small bias on these analyses. Nevertheless, these data clearly show that ANP32A predominantly gains access to the nucleus via the importin-α mediated nuclear import pathway.

In order to evaluate whether cytoplasmic accumulation of the mutNLS ANP32A proteins (**Figure 15**) was a result of disrupted binding to importin-α, co-immunoprecipitation with FLAG-tagged ANP32A variants was performed. FLAG-tagged WT and mutNLS ANP32A constructs were expressed in HEK293T cells, precipitated from cell lysates, and interaction with importin-α5 and -α7 was analyzed by Western blotting using an antibody recognizing both isoforms (**Figure 16**).

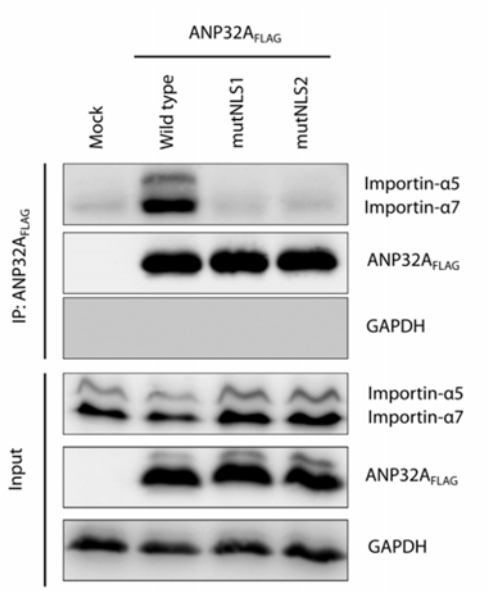

Figure 16: Mutation of the NLS motif in ANP32A disrupts its binding to importin-α5 and -α7. FLAG-tagged WT and mutNLS ANP32A constructs were expressed in HEK293T cells followed by precipitation from cell lysates using an anti-FLAG resin. After elution using an excess of FLAG peptide, co-immunoprecipitation of cellular importin-α5 and -α7 isoforms was analyzed by Western blotting. Shown is a representative Western blot of three independent experiments. The importin-α5/α7 antibody recognizes both isoforms.

WT ANP32A interacted with both importin-α5 and -α7, confirming the SILAC-MS data (**Figure 16**). Interestingly, mutation of either two (mutNLS1) or all four (mutNLS2) basic amino acids in the NLS motif of ANP32A completely disrupted its binding to either importin-α protein (**Figure 16**).

As a final approach to characterize the importin-α7 - ANP32A interaction, available structural information on importin-α7 (PDB file *4UAD*) and ANP32A (PDB file *4XOS*) were used to model their interaction according to an *in silico* docking algorithm (*Rosetta*). Although the C-terminal region of ANP32A, which comprises the NLS motif, has not been crystallized yet, within the generated model, the C-terminal end of the available crystal structure of ANP32A was oriented towards the major NLS binding site of importin-α7 (**Figure 17;** residues predicted to be involved in NLS binding are highlighted in red; [44]). This model further supports the co-immunoprecipitation data (**Figure 16**), showing that binding of ANP32A to importin-α5 and -α7 is mediated via its NLS motif.

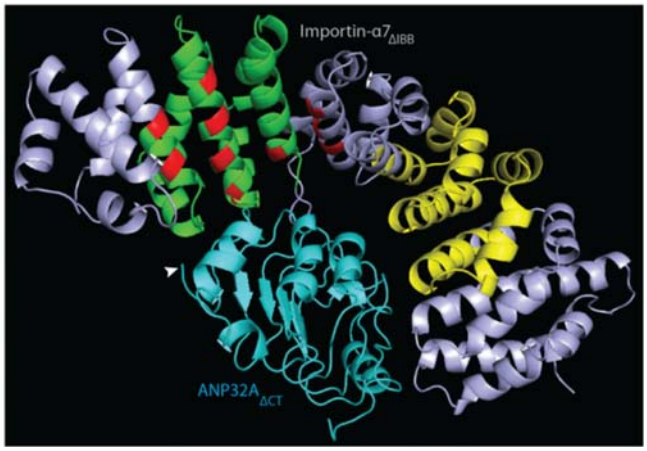

Figure 17: Modelling of the interaction of ANP32A with importin-α7 *in silico*. The crystal structure of ANP32A (without C-terminal low-complexity acid region (LCAR), ANP32A$_{\Delta CT}$; PDB *4XOS*) was modeled onto the crystal structure of importin-α7 (without importin-β$_1$ binding (IBB) domain, importin-α7$_{\Delta IBB}$; PDB *4UAD*) using the *Rosetta* docking algorithm. Shown is the most accurate docking complex, based on the calculated total and interface scores. The major and minor NLS binding sites of importin-α7 are colored (green and yellow, respectively), and residues in the major NLS binding site predicted to be involved in cargo binding are indicated in red (adapted from [44]).

Collectively, these findings clearly demonstrate that the interaction of ANP32A with importin-α7 (and -α5) via the NLS motif is crucial for its nuclear translocation. Based on these results, further analyses were carried out to investigate whether these two proteins might act in concert in promoting viral replication in human cells.

5.2.2 Importin-α7 promotes $PB2_{627K}$ IAV polymerase activity independently of ANP32A

In order to study whether ANP32A might contribute to importin-α7 function, a combined gain- and loss-of-function approach was performed. For this purpose, an importin-α7 overexpressing viral polymerase activity assay was used that had been established in the laboratory [348]. Previously, the establishment of this urgently required *in vitro* system was hampered mainly by the complexity of the nuclear import machinery. Importantly, this machinery not only consists of an importin-α adapter protein, but also the nuclear transport co-receptors, importin-β_1 and CAS, Ran proteins that provide the energy for the transport process, as well as components of the nuclear pore (**Figure 18, A**).

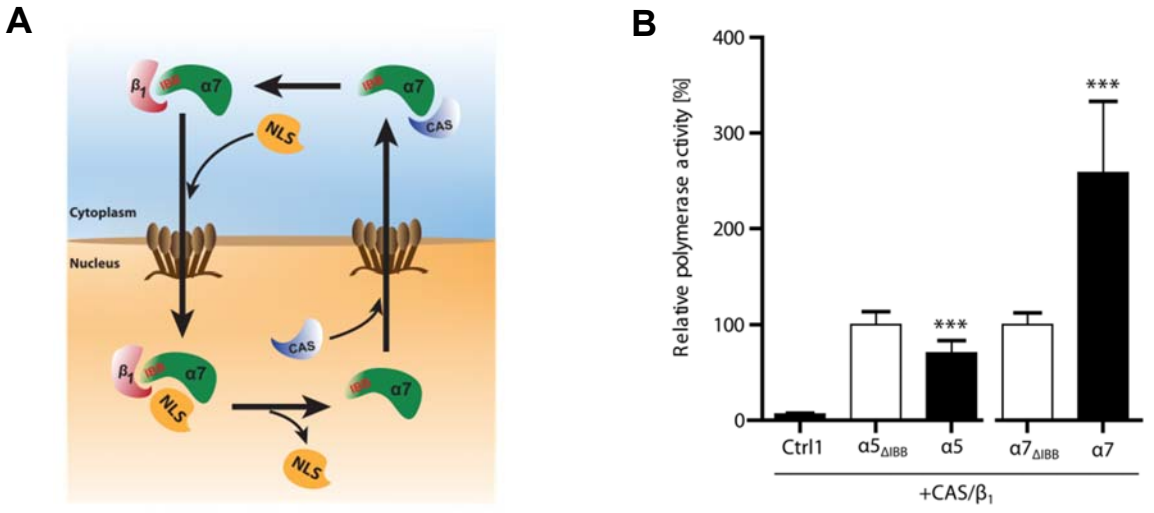

Figure 18: Importin-α7 promotes IAV polymerase activity in the context of a balanced and functional nuclear transport machinery. A, Schematic overview of the importin-α mediated classical nuclear import pathway (shown representative for importin-α7), including the transport co-receptors, importin-β_1 for nuclear import and the importin-α recycling factor CAS. Abbreviations used are: α7, importin-α7; β_1, importin-β_1; NLS, cargo protein presenting a NLS motif; CAS, cellular apoptosis susceptibility protein. **B**, Viral polymerase activity assay in importin-α overexpressing HEK293T cells. HEK293T cells were transfected with expression constructs for IAV A/WSN/33 (H1N1) vRNP (PB1, PB2, PA, NP; negative control without PB2 (Ctrl1)), firefly luciferase, Renilla luciferase (transfection control), importin-β_1, CAS, and importin-α5 or -α7 (WT or ΔIBB). Luciferase activities were measured 24 h post transfection, and firefly activities were normalized to the Renilla transfection control. The positive controls (importin-α-ΔIBB) were set to 100 %. Statistical significance was calculated in relation to the positive controls using the two-tailed student's *t*-test (***p < 0.001). *n* = 3 independent experiments. (adapted from [348]).

At first, using a minireplicon system, viral polymerase activity was measured in cells overexpressing only importin-α7 but no additional components of the nuclear transport machinery. Surprisingly, a significant reduction in viral polymerase activity was observed, which at first sight did not match the proposed positive-regulatory function of the importin-α7 isoform [251, 348]. The next step therefore aimed to identify the minimal set of components that needed to be co-overexpressed along with importin-α7 to maintain the balance of the nuclear transport machinery. Finally, in a step-wise process, importin-β_1 (i.e. the co-receptor for nuclear import) and CAS (i.e. the importin-α recycling factor) were identified as essential components that, when co-expressed, promoted an importin-α7-dependent increase in viral polymerase activity (**Figure 18, B**). As a further assay improvement to study nuclear transport-dependent effects, the import-deficient importin-α7-ΔIBB construct was included to replace the empty vector control. Strikingly, compared to importin-α7-ΔIBB, importin-α7-WT increased viral replicative fitness by almost 150 %. Of note, despite the high sequence similarity to importin-α7 (~ 80 %), overexpressed importin-α5-WT only slightly decreased viral polymerase activity compared to its ΔIBB counterpart, highlighting the distinct and unique role of importin-α7 during influenza infection.

In order to evaluate whether ANP32A is required for importin-α7 function, the newly established importin-α7 gain-of-function assay was complemented with an ANP32A loss-of-function approach. Therefore, the positive-regulatory effect of overexpressed importin-α7 on viral polymerase activity was analyzed in either ANP32A-silenced or ANP32A knockout (KO) HEK293T cells (**Figure 19**). Carrying out both approaches was important to improve the validity of the obtained results. First, siRNA silencing leads to residual levels of ANP32A protein that might still be sufficient to promote importin-α7 function. Second, complete knockout of ANP32A using the CRISPR/Cas technology could induce off target effects or interfere with essential ANP32A-regulated cellular processes, thereby affecting cell viability and thus causing artificial results. siRNA-induced silencing or CRISPR/Cas-mediated KO of ANP32A was confirmed by Western blotting (**Figure 19, A and B, lower panels**). Control-silenced cells or cells treated with a non-targeting CRISPR/Cas vector were used as control. Importantly, compared to the importin-α7-ΔIBB control, importin-α7-WT consistently induced high-level virus polymerase activity in both control-treated cells as well as in cells with reduced or depleted ANP32A expression levels (**Figure 19, A and B, upper panels**).

In summary, these results strongly suggest that importin-α7 promotes replicative fitness of the $PB2_{627K}$ adapted IAV polymerase independently of ANP32A. Thus, future studies are required to decipher the exact mode-of-action underlying importin-α7 function during influenza infection.

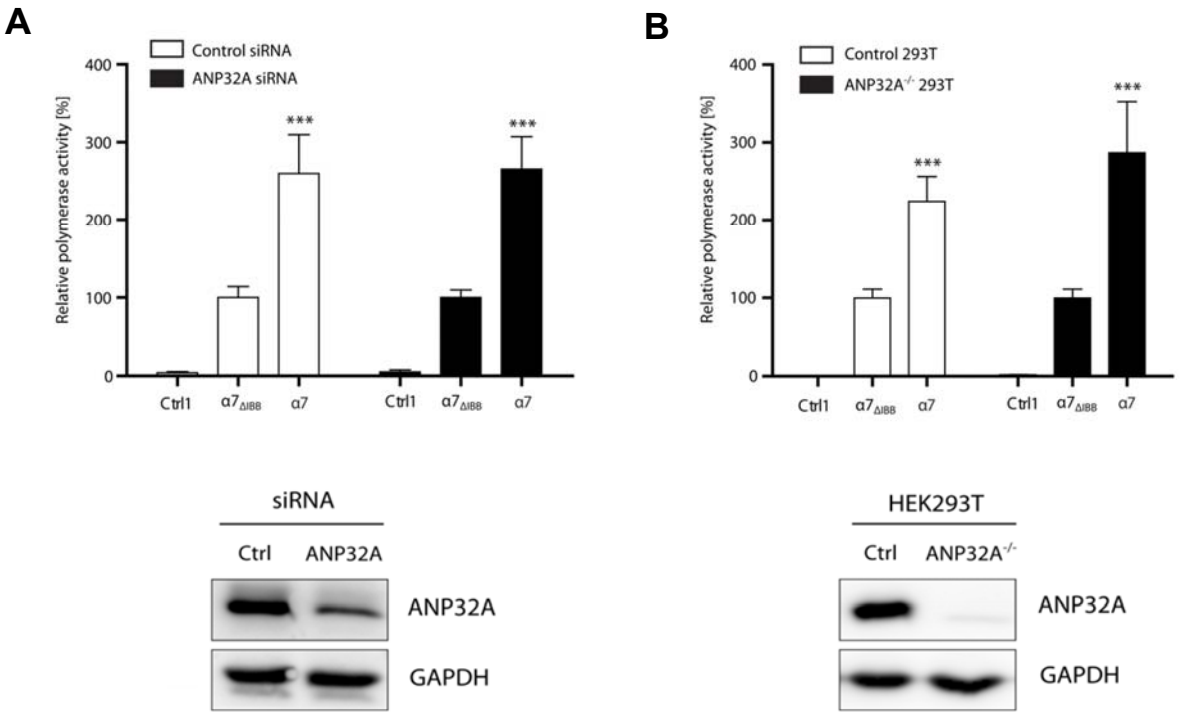

Figure 19: Importin-α7 promotes IAV polymerase activity independently of ANP32A. A and B, Viral polymerase activity assay in importin-α7 overexpressing HEK293T cells after silencing or knockout of ANP32A. ANP32A-silenced HEK293T cells **(A)** or HEK293T cells with a deleted ANP32A gene **(B)** were transfected with expression constructs for IAV A/WSN/33 (H1N1) vRNP (PB1, PB2, PA, NP; negative control without PB2 (Ctrl1)), firefly luciferase, Renilla luciferase (transfection control), importin-β_1, CAS, and importin-α7 (WT or ΔIBB). Control-silenced cells **(A)** or cells treated with a non-targeting CRISPR/Cas construct **(B)** were used as controls. Luciferase activities were measured 24 h post transfection, and firefly activities were normalized to the Renilla transfection control. The positive controls (importin-α7-ΔIBB) were set to 100 %. Statistical significance was calculated in relation to the positive controls using the two-tailed student's *t*-test (***p < 0.001). *n* = 3 independent experiments. Silencing or knockout of ANP32A was confirmed by Western blotting using an ANP32A-specific antibody (lower panels). GAPDH was used as loading control. siRNA-mediated silencing reduced the ANP32A protein expression levels by approximately 50 % (**A**, lower panel).

5.2.3 ANP32A promotes IAV replicative fitness independently of importin-α7

Although importin-α7 was shown to potentiate high-level IAV polymerase activity independently of ANP32A, it was further hypothesized that ANP32A acts as a co-factor of the viral polymerase inside the nucleus where viral replication takes place, and thus requires the importin-α machinery, particularly importin-α7, for nuclear translocation. This hypothesis is supported by the fact that WT ANP32A was almost exclusively localized to the nucleus (**Figure 15**).

Furthermore, a major function of ANP32A involves the regulation of cellular gene expression as part of the INHAT complex [296], a process that also occurs within the host cell's nucleus.
In order to provide molecular evidence for a nuclear ANP32A mode-of-function during influenza infection, an ANP32A gain-of-function system was established which is based on overexpressed WT and mutNLS ANP32A proteins (**Figure 14**). These ANP32A proteins with mutations in the NLS motif were almost exclusively localized to the cytoplasm, caused by disrupted binding to importin-α5 and -α7 (**Figure 15 and 17**).
Surprisingly, these cytoplasm-restricted mutNLS ANP32A proteins induced high-level viral polymerase activity comparably to WT ANP32A and in a concentration-dependent manner (**Figure 20**, upper panel). Western blotting confirmed similar expression levels of both WT and mutNLS constructs (**Figure 20**, lower panel).

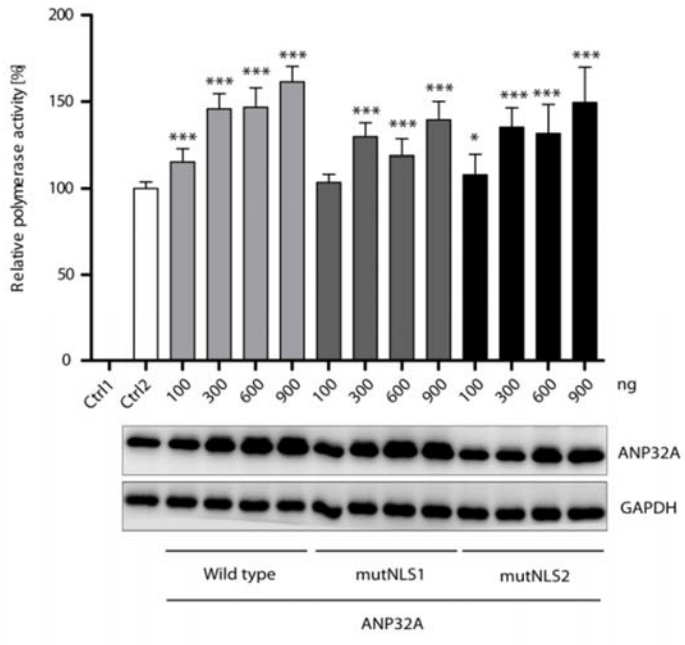

Figure 20: ANP32A variants with mutations in the NLS motif retain their ability to promote high-level viral polymerase activity in human cells. Viral polymerase activity assay in ANP32A (WT, mutNLS) overexpressing HEK293T cells. HEK293T cells were transfected with expression constructs for IAV A/WSN/33 (H1N1) vRNP (PB1, PB2, PA, NP; negative control without PB2 (Ctrl1)), firefly luciferase, Renilla luciferase (transfection control), and either WT or mutNLS ANP32A (100-900 ng). An empty expression vector was used as background control (Ctrl2). Luciferase activities were measured 24 h post transfection, and firefly activities were normalized to the Renilla transfection control. The positive control (empty vector; Ctrl2) was set to 100 %. Statistical significance was calculated in relation to the positive control using the two-tailed student's *t*-test (*p < 0.05; ***p < 0.001). *n* = 3 independent experiments.

These findings suggest that ANP32A fulfills its function, at least in part, in the cytoplasm of the cell. However, as discussed above, it is possible that alternative, importin-α-independent nuclear import pathways contribute to nuclear localization of ANP32A.

In a final experiment, it should be addressed whether the presence of importin-α7 itself is critical for ANP32A function, even though a direct interaction between the two proteins via the NLS motif does not seem to play a role in this process (**Figure 20**). Therefore, the effect of WT ANP32A overexpression on viral polymerase activity was investigated in HEK293T cells with reduced or depleted importin-α7 expression levels (**Figure 21**).

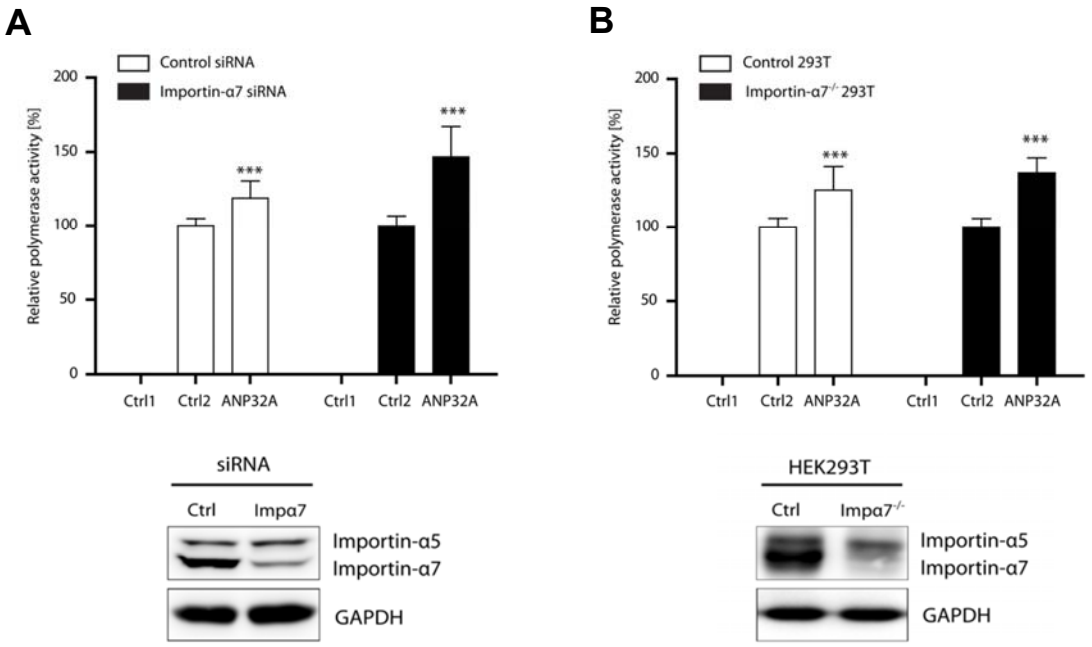

Figure 21: ANP32A promotes viral polymerase activity in human cells independently of importin-α7. A and B, Viral polymerase activity assay in ANP32A overexpressing HEK293T cells after silencing or knockout of importin-α7. Importin-α-silenced HEK293T cells **(A)** or HEK293T cells with a deleted importin-α7 gene **(B)** were transfected with expression constructs for IAV A/WSN/33 (H1N1) vRNP (PB1, PB2, PA, NP; negative control without PB2 (Ctrl1)), firefly luciferase, Renilla luciferase (transfection control), and WT ANP32A. Control-silenced cells **(A)** or cells treated with a non-targeting CRISPR/Cas construct **(B)** were used control. Luciferase activities were measured 24 h post transfection, and firefly activities were normalized to the Renilla transfection control. The positive control (empty vector; Ctrl2) was set to 100 %. Statistical significance was calculated in relation to the positive controls using the two-tailed student's *t*-test (***p < 0.001). *n* = 3 independent experiments. Silencing (**A**) or knockout (**B**) of importin-α7 was confirmed by Western blotting using an antibody recognizing both importin-α5 and -α7 (lower panels). GAPDH was used as loading control. siRNA-mediated silencing reduced the importin-α7 protein expression levels by approximately 70 % (**A**, lower panel).

In analogy to **Figure 19**, a dual approach was conducted using cells either treated with importin-α7-specific siRNA or with a CRISPR/Cas-induced importin-α7 knockout (**Figure 21**). As expected, overexpressed WT ANP32A significantly increased viral polymerase activity in control-silenced cells or cells treated with a non-targeting CRISPR/Cas control vector. Importantly, this effect was also retained in cells with reduced or depleted importin-α7 protein expression (**Figure 21**). Silencing or knockout of importin-α7 was confirmed by Western blotting (**Figure 21, lower panels**).Collectively, the findings presented here suggest that ANP32A acts independently of importin-α7 on viral replication. Moreover, ANP32A might unfold a rather unexpected, cytoplasmic function during influenza infection, albeit this theory requires further investigation.

5.3 Role of ANP32 proteins on $PB2_{627K}$ IAV replication and pathogenicity in mammals

ANP32 proteins, particularly ANP32A, have been recently shown to drive IAV avian-mammalian adaptation as well as high-level human-type IAV replication in cell culture settings [252, 305]. However, it is still unknown whether these cellular proteins are also required for efficient human-type IAV replication and pathogenicity in mammalian hosts. This question was now addressed in the present study using ANP32A and ANP32B knockout mice. In addition to weight loss and survival experiments, key parameters of viral pathogenesis were investigated, including viral replication in the lung and brain as well as virus-induced cytokine responses.

5.3.1 Phylogenetic analysis of human and murine ANP32 proteins

In higher eukaryotes, the ANP32 protein family comprises three main family members: ANP32A, ANP32B and ANP32E [296]. Since knockout mice are used in this study, amino acid (AA) sequences of the human and murine ANP32A and ANP32B homologues (hANP32A/B and mANP32A/B, respectively) were aligned in order to estimate how conserved these proteins are across mammalian species. hANP32A and mANP32A share 88 % AA sequence similarity, while hANP32B and mANP32B share 81 % AA sequence similarity (**Table 27**). These relatively high AA sequence similarities suggest that the mouse model is suited to study the role of ANP32 proteins on IAV pathogenesis, and to translate the obtained findings to humans.

Table 27: Amino acid sequence similarity [%] of human and murine ANP32A and ANP32B proteins.

	hANP32A	**mANP32A**	**hANP32B**	**mANP32B**
hANP32A	100	88	70	63
mANP32A	88	100	68	61
hANP32B	69	68	100	81
mANP32B	63	61	81	100

5.3.2 ANP32B, but not ANP32A promotes IAV pathogenicity in mice

5.3.2.1 Confirmation of ANP32 knockout in the murine lung and brain

In order to confirm the ANP32 knockout on protein level, lung and brain were harvested from ANP32A and ANP32B knockout mice ($ANP32A^{-/-}$ and $ANP32B^{-/-}$, respectively) as well as their

wild type (WT) littermates (ANP32A$^{+/+}$ and ANP32B$^{+/+}$, respectively). Organs were homogenized in cell lysis buffer, and organ lysates were subjected to Western blotting to detect ANP32 expression. ANP32A expression was completely absent in the lung and brain of three different ANP32A$^{-/-}$ mice assessed (**Figure 22, A**). Likewise, the tamoxifen-induced knockout of ANP32B could be confirmed in three different ANP32B$^{-/-}$ mice (**Figure 22, B**)

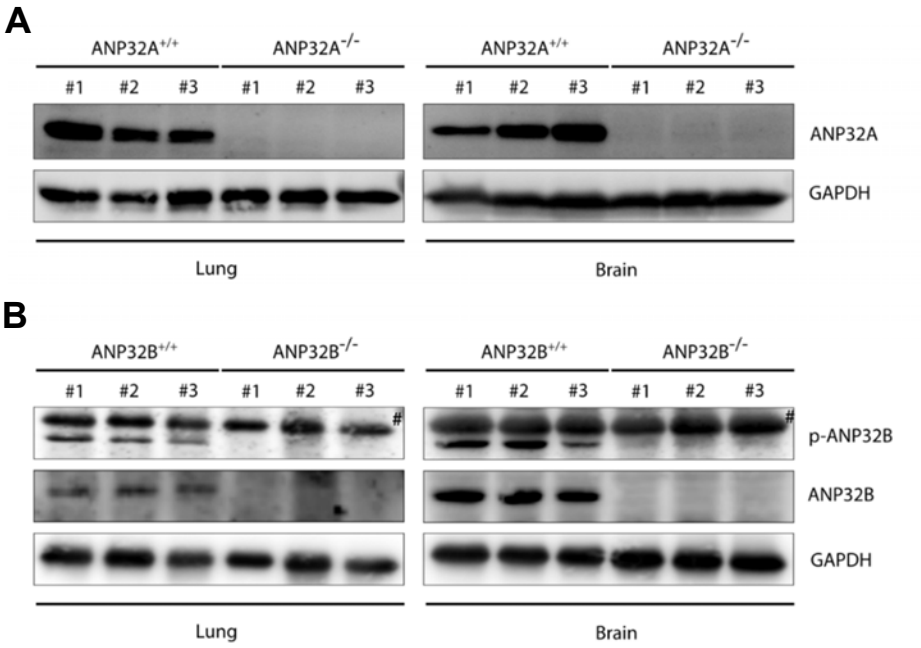

Figure 22: Confirmation of ANP32 protein knockout in the lung and brain of ANP32A$^{-/-}$ and ANP32B$^{-/-}$ mice. A and B, Lung and brain homogenates were prepared from ANP32A$^{-/-}$ (**A**) or ANP32B$^{-/-}$ (**B**) mice as well as their corresponding wild type littermates (ANP32A$^{+/+}$ and ANP32B$^{+/+}$, respectively). ANP32 protein expression was analyzed by Western blotting using protein-specific antibodies. GAPDH was used as a loading control. *n* = 3 animals per genotype. #, unspecific band.

5.3.2.2 IAV pathogenesis in ANP32A$^{+/+}$ and ANP32A$^{-/-}$ mice

Mice lacking the ANP32A gene (ANP32A$^{-/-}$) were infected with human IAV isolates (seasonal H3N2, human-type H5N1 HPAIV) to study the role of ANP32A on viral pathogenesis. Infection of ANP32A$^{-/-}$ mice with these viruses did not result in any differences in weight loss or survival, compared to the ANP32A$^{+/+}$ littermates (**Figure 23**). Using a high virus dose, both H3N2 and H5N1 caused 100 % lethality in ANP32A$^{+/+}$ and ANP32A$^{-/-}$ mice (**Figure 23, A-D**). Absence of ANP32A upon low-dose H5N1 infection did also not affect viral pathogenesis (**Figure 23, E and F**). These findings suggest that murine ANP32A is dispensable for high IAV pathogenicity in mice.

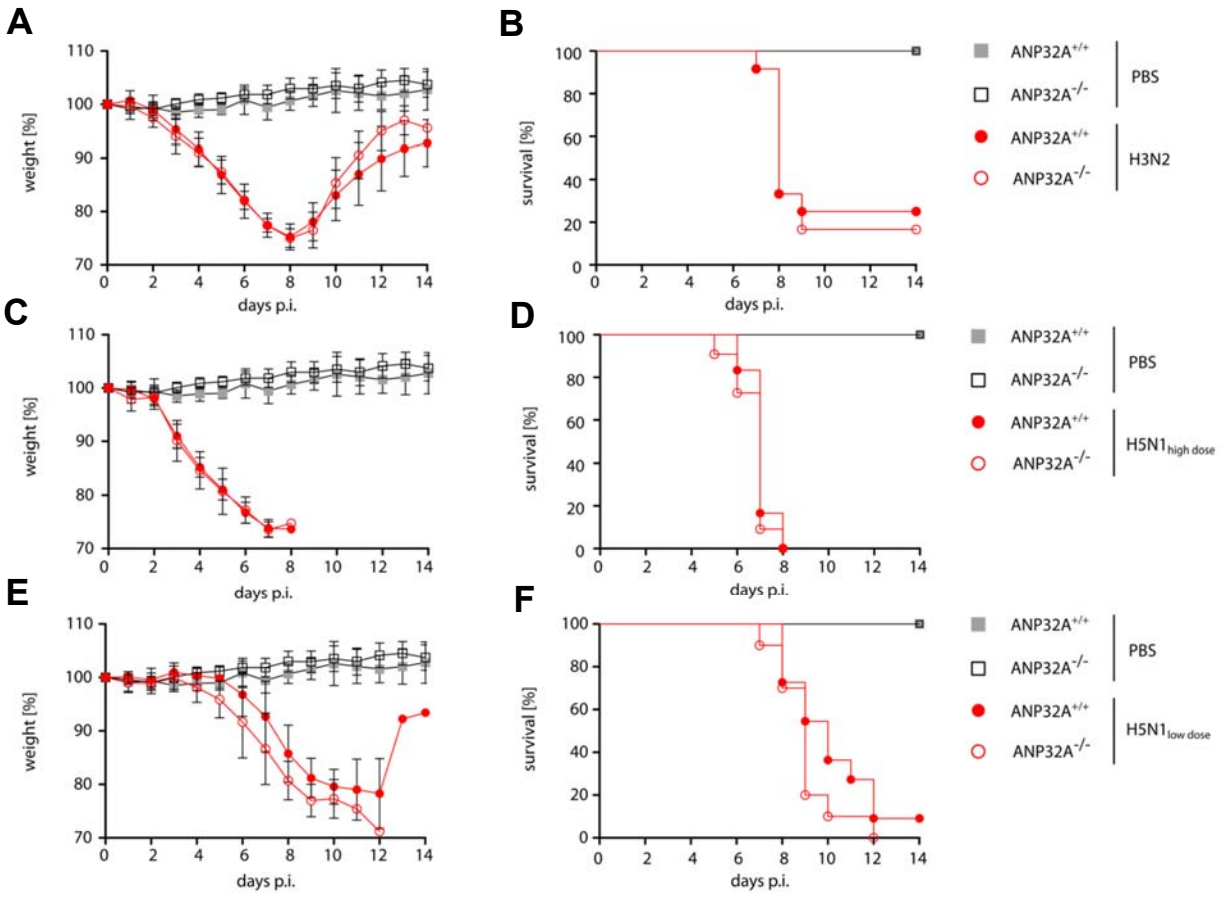

Figure 23: Influenza A virus pathogenesis is not affected in ANP32A$^{-/-}$ mice. ANP32A$^{-/-}$ (red circles) as well as their corresponding wild type littermates (ANP32A$^{+/+}$) were either control treated with PBS (grey and black squares) or infected with a seasonal H3N2 subtype (**A and B**; 10^3 pfu) or a highly pathogenic H5N1 human isolate (**C and D;** high dose, 10^3 pfu; **E and F,** low dose**,** 10^1 pfu). Weight loss (**A, C, E**) and survival (**B, D, F**) were monitored for 14 days post infection (days p.i.). Weight loss data are presented as means ± SD (PBS: *n* = 6-7, virus-infected groups: *n* = 10-12).

5.3.2.3 IAV pathogenesis in ANP32B$^{+/+}$ and ANP32B$^{-/-}$ mice

ANP32B-deficient mice (ANP32B$^{-/-}$) infected with seasonal H3N2 influenza showed reduced weight loss and improved survival compared to their ANP32B$^{+/+}$ littermates (**Figure 24, A and B**). While 80 % of the ANP32B$^{-/-}$ mice survived, 100 % death was observed in ANP32B$^{+/+}$ mice challenged with H3N2 IAV (**Figure 24, A and B**). High-dose infection with a human-type H5N1 HPAIV isolate resulted in 100 % lethality in both ANP32B$^{+/+}$ and ANP32B$^{-/-}$ mice, however weight loss and death were delayed in ANP32B$^{-/-}$ mice (**Figure 24, C and D**). In contrast, survival rates in ANP32B$^{-/-}$ mice challenged with low-dose H5N1 infection increased from 10 % to 80 %

(**Figure 24, E and F).** Taken together, in contrast to ANP32A, ANP32B promotes H3N2 and H5N1 IAV pathogenicity in mice.

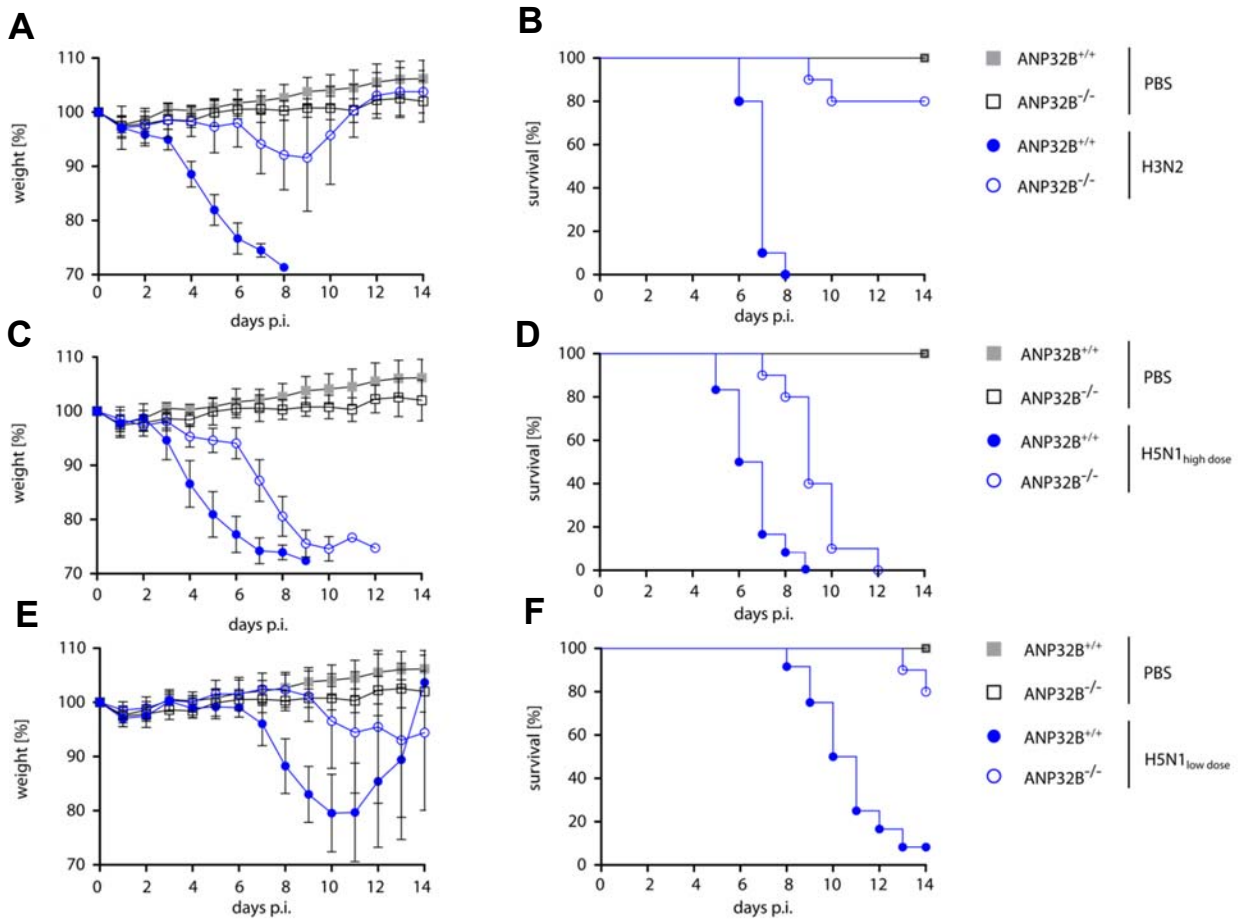

Figure 24: Improved survival in ANP32B$^{-/-}$ mice challenged with human influenza isolates. ANP32B$^{-/-}$ (blue circles) as well as their corresponding wild type littermates (ANP32B$^{+/+}$) were either control treated with PBS (grey and black squares) or infected with a seasonal H3N2 subtype (**A and B**; 10^3 pfu) or a highly pathogenic H5N1 human isolate (**C and D;** high dose, 10^3 pfu; **E and F,** low dose**,** 10^1 pfu). Weight loss (**A, C, E**) and survival (**B, D, F**) were monitored for 14 days post infection (days p.i.). Weight loss data are presented as means ± SD (PBS: *n* = 6-7, virus-infected groups: *n* = 10-12).

5.3.3 ANP32B is required for IAV replication in mice and in murine cells

5.3.3.1 Viral replication in the lung and brain of ANP32A$^{+/+}$ and ANP32A$^{-/-}$ mice

Based on the proposed positive-regulatory function of ANP32A, the absence of ANP32A might have an impact on viral replication in the lung and brain of H3N2 and H5N1 infected mice, even without affecting overall viral pathogenesis. However, no significant differences in viral titers in

the lung or brain were observed in ANP32A$^{-/-}$ mice compared to their ANP32A$^{+/+}$ littermates (***Appendix*, Figure 47**). Thus, ANP32A is not required for viral replication and pathogenicity in mice.

5.3.3.2 Viral replication in the lung and brain of ANP32B$^{+/+}$ and ANP32B$^{-/-}$ mice

In the lungs of H3N2 infected ANP32B$^{-/-}$ mice, virus replication was decreased 10-fold at 3 and 6 days post infection (d p.i.), compared to the ANP32B$^{+/+}$ littermates (**Figure 25, A**). In line with the respiratory tropism of H3N2, no virus replication was observed in the brains of infected mice (**Figure 25, A**). ANP32B$^{+/+}$ mice infected with H5N1 presented high virus titers in the lung (3 and 6 d p.i.) as well as the in the brain at 6 d p.i. (**Figure 25, B**). In ANP32B$^{-/-}$ mice, however, 10-fold reduced H5N1 virus replication was observed in the lung at both 3 and 6 d p.i. (**Figure 25, B**). Surprisingly, systemic H5N1 virus replication was, except for one animal, not detectable in the brains of ANP32B$^{-/-}$ mice at 6 d p.i., suggesting that either virus dissemination from the lung is blocked or that the absence of ANP32B in the brain impairs viral replication on site (**Figure 25, B**). Conclusively, ANP32B is required for efficient virus replication in the murine lung.

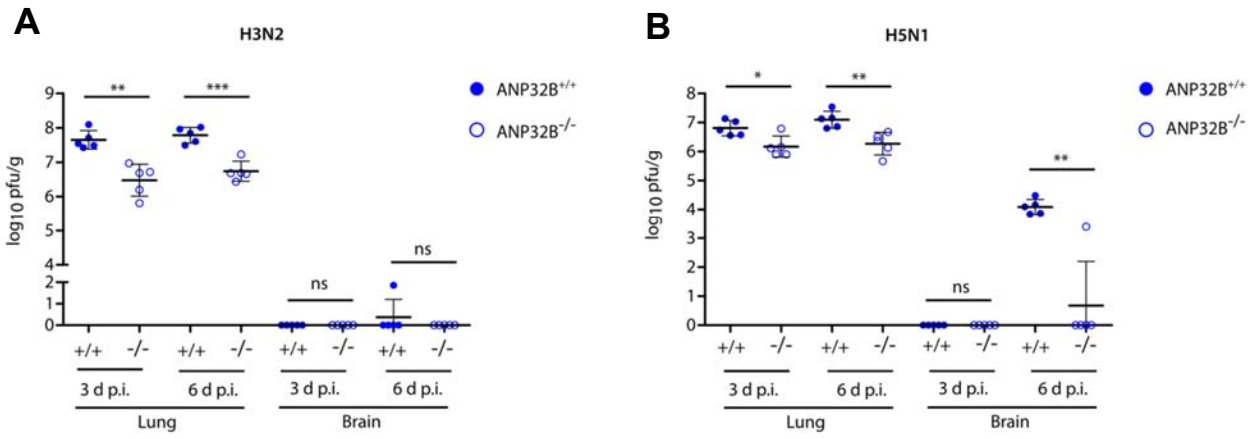

Figure 25: ANP32B deficiency impairs influenza A virus replication in mice. A and B, ANP32B$^{+/+}$ and ANP32B$^{-/-}$ mice were either control treated with PBS or infected with 10^3 pfu of a seasonal H3N2 subtype **(A)** or a highly pathogenic H5N1 human isolate **(B).** Viral titers were determined 3 and 6 days p.i. in lung and brain of infected animals. No virus was detected in PBS infected mice (*n* = 5). Presented are individual organ titers for each animal as well as the means ± SD for each group (*n* = 5-6). Statistically significant differences were calculated using the two-tailed Student's *t*-test (*p < 0.05, **p < 0.01, ***p < 0.001).

5.3.3.3 Viral replication and cell tropism in the lung of infected ANP32A$^{-/-}$ and ANP32B$^{-/-}$ mice

Next, the viral cell tropism was evaluated in the lung of IAV infected ANP32A$^{-/-}$ and ANP32B$^{-/-}$ mice as well as their wild type littermates. Lungs harvested from virus infected ANP32A$^{+/+}$ and ANP32A$^{-/-}$ mice at 3 d p.i. showed similar infiltration with immune cells as well as comparable amounts of viral antigen in both bronchial and alveolar tissue (***Appendix*, Figure 48**). These data further confirm that absence of ANP32A does not affect viral replication or cell tropism in the murine lung. On the other hand, histological examination of lung tissue derived from virus infected ANP32B$^{+/+}$ and ANP32B$^{-/-}$ mice revealed reduced H3N2 and H5N1 virus antigen in the lungs of ANP32B$^{-/-}$ mice at 3 d p.i., both in bronchial and alveolar epithelium (**Figure 26**). At 6 d p.i., however, no clear differences in lung infiltration (H/E) or viral antigen staining (IHC) were observed between ANP32B$^{+/+}$ and ANP32B$^{-/-}$ mice (**Figure 26**). These findings suggest that ANP32B deficiency delays viral replication particularly during the early stages of infection, in line with the delayed weight loss observed in the ANP32B$^{-/-}$ mice (**Figure 24**).

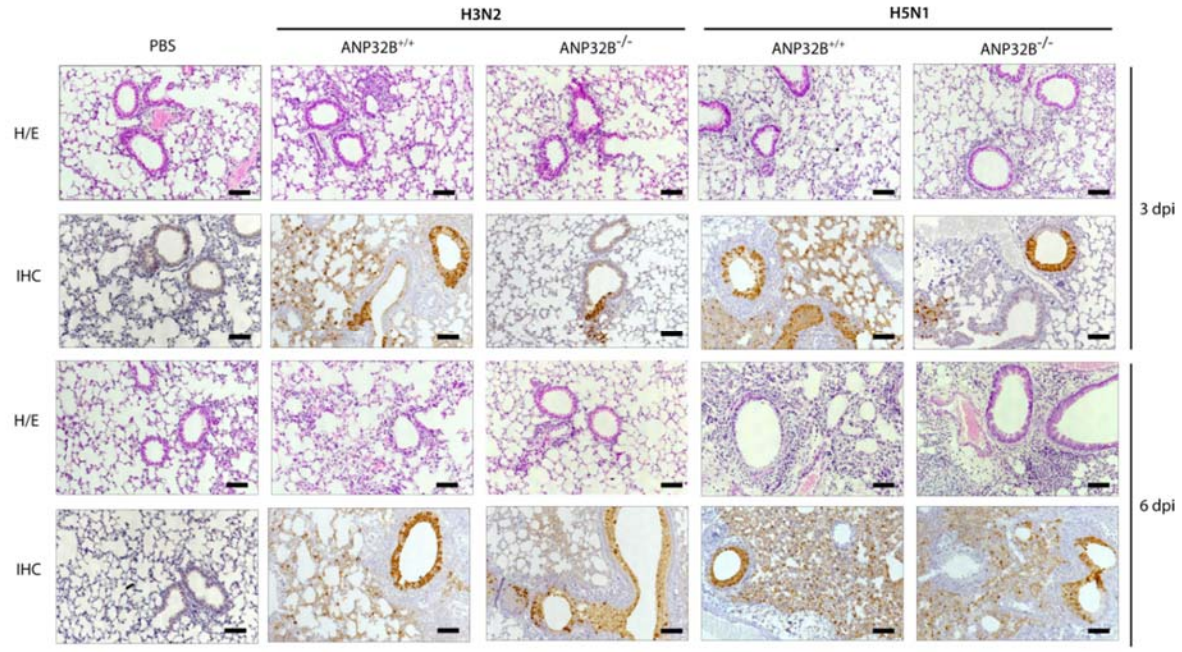

Figure 26: ANP32B deficiency impairs influenza A virus replication in bronchial and alveolar murine lung tissue at 3 days post infection. ANP32B$^{+/+}$ and ANP32B$^{-/-}$ mice were either control treated with PBS or infected with 10^3 pfu of a seasonal H3N2 subtype or a highly pathogenic H5N1 human isolate. At 3 and 6 d p.i., lungs from infected animals were removed and immunohistochemically (IHC) stained for viral NP antigen. Additionally, hematoxylin and eosin (H/E) staining was performed. Shown are representative images for each group (*n* = 5). Scale bar represents 10 µm. Original magnification, 10x.

5.3.3.4 Viral replication in murine cells lacking the ANP32A or ANP32B genes

In order to further study molecular mechanisms of ANP32 function during influenza infection *in vitro*, murine lung fibroblast (mLF) cell lines were generated from ANP32A$^{-/-}$ and ANP32B$^{-/-}$ mice as well as their wild type littermates (ANP32A$^{+/+}$ and ANP32B$^{+/+}$, respectively). Knockout of ANP32A and ANP32B in these cell lines was verified by Western blotting (**Figure 27**).

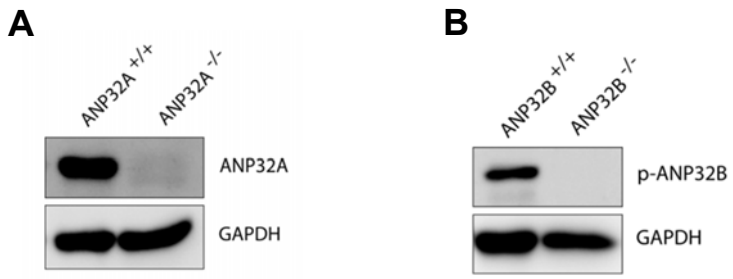

Figure 27: Establishment of murine lung fibroblast cell lines deficient for ANP32 proteins. A and B, Cells were isolated from ANP32A$^{-/-}$ and ANP32B$^{-/-}$ mice as well as their wild type littermates (ANP32A$^{+/+}$ and ANP32B$^{+/+}$, respectively) and spontaneously immortalized by serial passaging. Knockout of the target proteins (**A**, ANP32A; **B**, ANP32B) was verified by Western blotting using protein-specific antibodies. GAPDH was used as a loading control.

For human ANP32A and ANP32B, positive-regulatory functions have been described using cell culture experiments [252]. Since murine ANP32A was not required for high-level virus replication and pathogenicity *in vivo* (**Figure 23; *Appendix*, Figures 47 and 48**), it was hypothesized that knockout of ANP32A only presents a phenotype in *in vitro* cell culture settings. However, mLF cells lacking ANP32A (ANP32A$^{-/-}$) supported H3N2 virus replication comparably to mLFs expressing the ANP32A protein (ANP32A$^{+/+}$) (***Appendix*, Figure 49**).

In sharp contrast, significantly reduced H3N2 and H5N1 replicative capacity was observed in mLFs deficient for ANP32B (**Figure 28**). Remarkably, H5N1 virus replication was barely detectable in ANP32B$^{-/-}$ mLF cells (**Figure 28, B**). Conclusively, in contrast to ANP32A, murine ANP32B acts as positive host cell factor for IAV replication *in vitro* and *in vivo*.

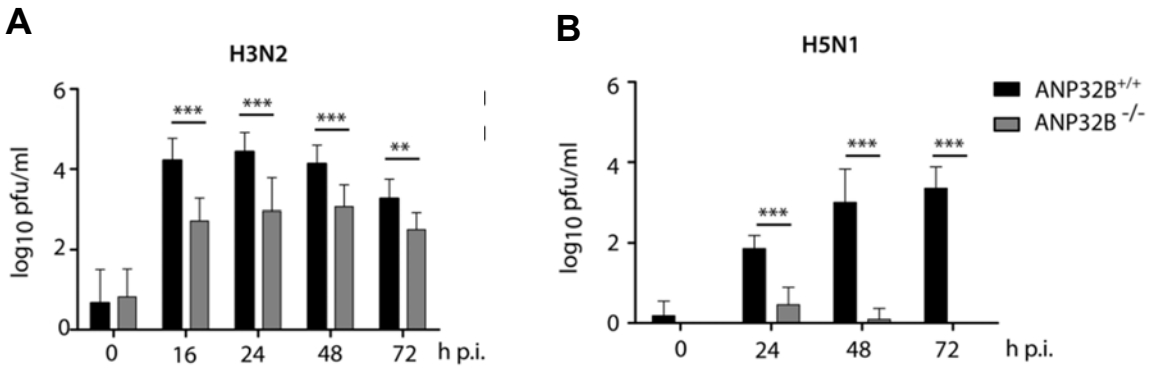

Figure 28: H3N2 and H5N1 virus replication is severely reduced in murine lung fibroblast cells derived from ANP32B$^{-/-}$ mice. A and B, Murine lung fibroblasts derived from ANP32B$^{+/+}$ or ANP32B$^{-/-}$ mice were infected with H3N2 **(A)** or H5N1 **(B)** human-type influenza viruses over a time period of 72 h. Viral titers were determined by plaque test on MDCK cells at the indicated time points. Statistically significant differences were determined using the two-tailed Student's *t*-test (**p < 0.01; ***p < 0.001). *n* = 3 independent experiments.

5.3.4 ANP32B contributes to IAV replicative fitness in human cells

In recent studies, siRNA or CRISPR/Cas-based approaches have been used to evaluate the role of ANP32 proteins on $PB2_{627K}$-adapted IAV replication in human cells, leading to controversial results to some degree [252, 304-306]. In order to address this issue and to further investigate whether the ANP32B mode-of-action is restricted to murine cells or can be extrapolated to human cells, H3N2 and H5N1 virus replication was assessed in human HeLa cells lacking the ANP32B gene (**Figure 29**).

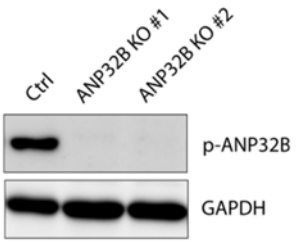

Figure 29: Generation of human HeLa cells with a deleted ANP32B gene. Human HeLa cells deficient for ANP32B were generated using the CRISPR/Cas technology and kindly provided by collaboration partners at the Heinrich Pette Institute. Knockout of ANP32B was verified in two individual clones (ANP32B KO #1 and #2, respectively) by Western blotting, in comparison to control cells (Ctrl). GAPDH was used as a loading control.

Two individual ANP32B knockout (KO) HeLa cell lines (ANP32B KO #1 and #2, respectively) were used to exclude clonal artefacts. Western blotting confirmed the knockout of ANP32B in these cells, compared to the control treated cells (Ctrl) (**Figure 29**).As demonstrated in **Figure 30**, H3N2 as well as H5N1 replication was significantly reduced in both ANP32B KO cell lines, compared to the Ctrl cells. However, the effects observed in human cells were not as prominent as in murine cells (**Figure 28**), suggesting species-specific differences in ANP32B function.

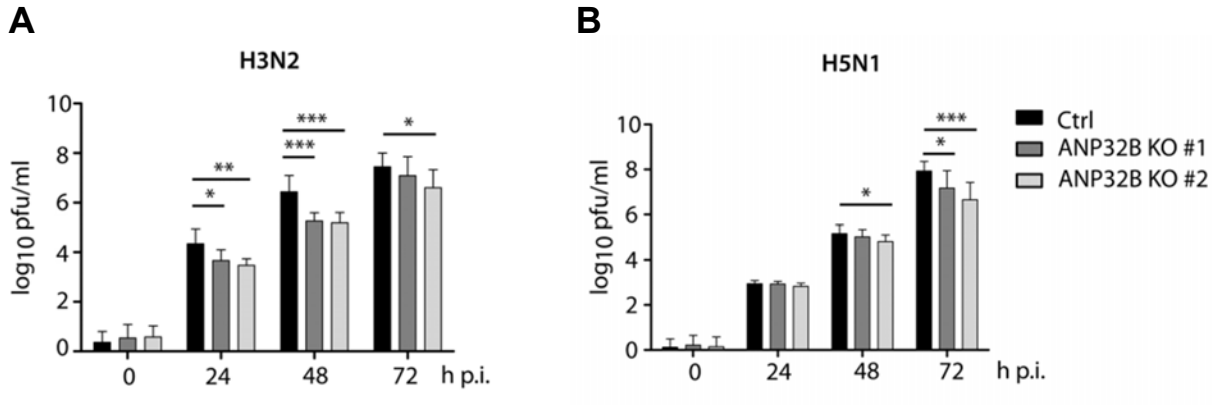

Figure 30: H3N2 and H5N1 IAV replication is reduced in human HeLa cells lacking ANP32B. A and B, Human HeLa cells with a deleted ANP32B gene were generated using the CRISPR/Cas technology and infected with H3N2 **(A)** or H5N1 **(B)** human-type IAV over a time course of 72 h. Viral titers were determined by plaque test on MDCK cells at the indicated time points. Two different knockout cell lines were used to exclude clonal artefacts (ANP32B KO #1 and ANP32B KO #2, respectively). Cells treated with a CRISPR/Cas construct expressing a non-targeting guide RNA were used as control (Ctrl). Statistically significant differences were determined using the two-tailed Student's *t*-test (*p < 0.05; **p < 0.01; ***p < 0.001). *n* = 3 independent experiments.

Furthermore, it was suggested that the reduced viral titers in human cells lacking the ANP32B gene (**Figure 30**) might be due to a direct effect of ANP32B on viral replication, as proposed before [307]. To address this question, ANP32B knockout HeLa cells were infected with H3N2 IAV and expression of viral nucleoprotein (NP) was analyzed at 24 h p.i. by Western blotting. Importantly, viral NP expression was reduced by ~50 % in both ANP32B knockout cell lines tested, compared to the Ctrl cells (***Appendix*, Figure 50)**. These results further indicate that ANP32B acts as a co-factor for the viral polymerase and thereby promotes virus replication.

5.3.5 Pro-inflammatory immune response is reduced in ANP32B-deficient mice

The pathogenesis of influenza viruses in the mouse model, but also in humans is based on additive effects of active viral replication as well as a strong immune reaction towards the virus infection, both of which cause destruction of lung epithelium, progression to ARDS and ultimately high lethality. Therefore, as a key parameter of viral pathogenesis, the immune response was investigated in the lungs of H3N2 and H5N1 IAV infected mice.

In ANP32A$^{-/-}$ mice, no major differences in the expression of pro-inflammatory cytokines/chemokines (C/C) could be observed compared to ANP32B$^{+/+}$ mice (***Appendix*, Figure 51**), in line with similar viral replication kinetics and disease outcome in these mice (**Figure 23; *Appendix*, Figure 47**). Infection of these mice with both H3N2 and H5N1 caused a strong upregulation of IFN-α, TNF-α, MCP-1, IL-1β and IL-6 expression, leading to a "cytokine storm" that largely contributes to the high virulence of these viruses in mice (***Appendix*, Figure 51**). Other cytokines, in part with anti-inflammatory functions, such as IL-10, also did not show altered expression in ANP32A$^{+/+}$ versus ANP32A$^{-/-}$ mice (***Appendix***, **Figure 51**). This further confirms that ANP32A is not involved in the regulation of virus-induced cytokine responses in the murine lung.

In ANP32B$^{+/+}$ mice, similar C/C responses were detected compared to ANP32A$^{+/+}$ and ANP32A$^{-/-}$ mice, with high expression levels of all pro-inflammatory C/C assessed (IFN-α, TNF-α, MCP-1, IL-1β and IL-6) (**Figure 31, A-E**). In sharp contrast, H3N2 and H5N1 infection induced pro-inflammatory C/C responses were significantly reduced in ANP32B$^{-/-}$ mice, particularly 3 d p.i (**Figure 31, A-E**). This is in line with the delayed weight loss of ANP32B$^{-/-}$ mice during the early phases of infection (**Figure 24**). Remarkably, at 3 d p.i., IFN-α levels were below detection limits in ANP32B$^{-/-}$ mice upon H3N2 and H5N1 infection, compared to their ANP32B$^{+/+}$ littermates (**Figure 31, A**). Interestingly, H5N1 and, to lesser extent, H3N2 infected ANP32B$^{-/-}$ mice mounted a higher IL-10 cytokine response at 6 d p.i., suggesting a general switch towards an anti-inflammatory state (**Figure 31, F**). IL-17A and IL-21 induction was similar in H3N2 and H5N1 infected ANP32B$^{+/+}$ or ANP32B$^{-/-}$ mice (**Figure 31, G and H**). It is important to note that most prominently IFN-α induction was dependent on the presence of ANP32B, highlighting its pivotal role in regulating antiviral immunity in the murine lung.

In summary, the absence of ANP32B could be correlated to a significant reduction of pro-inflammatory C/C responses in the virus infected murine lung, which likely contributed to the increased survival of ANP32B$^{-/-}$ mice upon otherwise lethal influenza challenge (**Figure 24**).

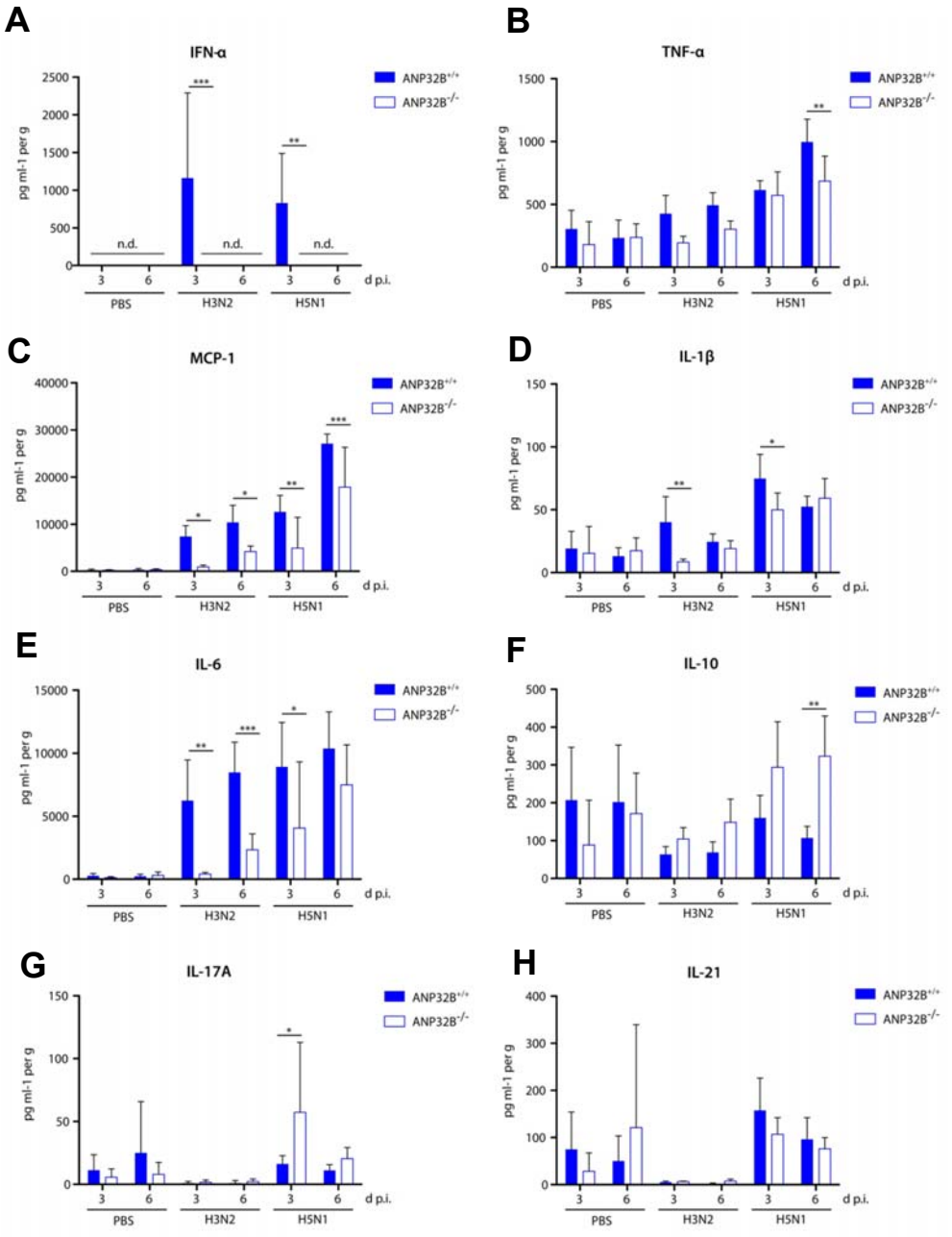

Figure 31: Reduced cytokine and chemokine response in IAV infected ANP32B$^{-/-}$ mice. A-H, ANP32B$^{+/+}$ and ANP32B$^{-/-}$ mice were either control treated with PBS or infected with 10^3 pfu of a seasonal H3N2 subtype or a highly pathogenic H5N1 human isolate. At 3 and 6 d p.i., cytokine and chemokine expression levels were determined in lung homogenates using a multiplex immunoassay. Interferon-α (**A**, IFN-α), tumor necrosis factor α (**B**, TNF-α), monocyte chemotactic protein 1 (**C**, MCP-1), interleukin 1β (**D**, IL-1β), interleukin 6 (**E**, IL-6), interleukin 10 (**F**, IL-10), interleukin 17A (**G**, IL-17A), and interleukin 21 (**H**, IL-21). Presented are the concentrations measured for each cytokine/chemokine as mean ± SD for each group (*n* = 5-7). Statistical significance was calculated using two-way ANOVA with Bonferroni post-test (* $p < 0.05$, ** $p < 0.01$, *** $p < 0.001$; n.d., not detected).

5.3.6 Transcriptome in infected ANP32B$^{-/-}$ mice reveals global changes in pro-inflammatory gene expression

Based on the significant reduction in pro-inflammatory cytokine expression in ANP32B deficient mice (**Figure 31**), potential involved cellular pathways were further elucidated on a global level using genome-wide transcriptome analyses. Therefore, total RNA was isolated from the lungs of H3N2 or H5N1 IAV infected ANP32B$^{+/+}$ and ANP32B$^{-/-}$ mice at 3 d p.i. and subjected to next generation sequencing. First, the differential gene expression was analyzed in virus infected ANP32B$^{+/+}$ mice compared to the PBS treated control mice. MA plot analyses revealed a large number of upregulated genes upon influenza infection, while only a few genes were found to be downregulated (***Appendix*, Figure 52 and Tables 41-44**). As expected, pro-inflammatory genes (e.g. Ifnb1, Ccl2, Cxcl10) associated with a response to viral infection were most prominently upregulated in H3N2 and H5N1 infected mice, as evident from gene ontology (GO) analyses (**Figure 32**). Herein, particularly established target genes of the antiviral transcription factor NF-κB, such as Mx1 and Irf7, were significantly upregulated in infected ANP32B$^{+/+}$ mice (**Figure 32**; ***Appendix*, Tables 41-44**). Disregulated genes presented in the Top10 of altered GOs were further visualized using heat map analyses. As shown in **Figure 33**, the H3N2 and H5N1 infected mice are clearly differentiated from the PBS treated control mice. Taken together, these data highlight the important contribution of high pro-inflammatory C/C responses ('cytokine storm') to lethal influenza disease outcome in mice.

Next, the transcriptomic profile was evaluated in the lungs of infected ANP32B$^{-/-}$ compared to ANP32B$^{+/+}$ mice. Interestingly, a major shift towards a downregulated gene expression profile was observed in influenza infected ANP32B$^{-/-}$ mice, as demonstrated by MA plot analyses (***Appendix*, Figure 53 and Tables 45-48**). Compared to H3N2 infected ANP32B$^{-/-}$ mice, a higher proportion of significantly downregulated genes was identified in H5N1 IAV infected mice (521 vs. 320 genes, respectively). Furthermore, while certain genes were repressed during both virus infections (e.g. Irf7 or Ifnb1), expression of others was more prominently reduced upon H5N1 infection (e.g. IL-1β, IL-6, Ccl2). These data suggest that common as well as different ANP32B-regulated pathways might exist that influence the disease outcome in a virus subtype-specific manner. Of note, only a small number of significantly upregulated genes that were linked to cilia movement and assembly were found in H5N1 infected ANP32B$^{-/-}$ mice, while no significantly upregulated genes were identified upon H3N2 IAV infection (***Appendix*, Tables 45-48**).

GO analyses further revealed that a majority of the downregulated genes in the ANP32B$^{-/-}$ mice was associated with the host immune response to viral infection (e.g. Ccl2, IL-6, or IL-1β) (**Figure 34**). Heat map visualization of these downregulated genes in the infected ANP32B$^{-/-}$

mice revealed a distinct transcriptional profile, characterized by a global reduction of antiviral gene expression, that clearly distinguishes the ANP32B$^{-/-}$ mice from their ANP32B$^{+/+}$ littermates during influenza infection (**Figure 35**).

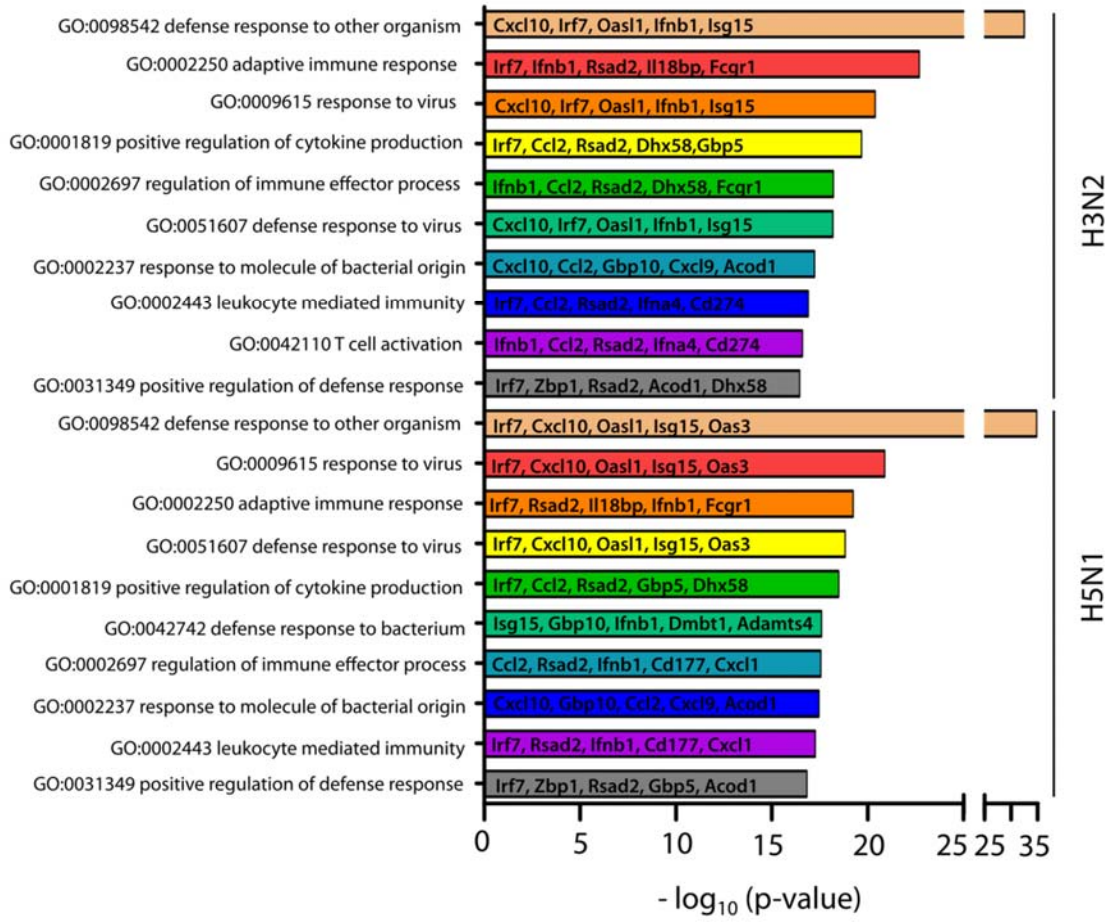

Figure 32: Gene ontology analysis of disregulated genes in ANP32B$^{+/+}$ mice during influenza infection. ANP32B$^{+/+}$ and ANP32B$^{-/-}$ mice were either control treated with PBS or infected with 10^3 pfu of a seasonal H3N2 subtype or a highly pathogenic H5N1 human isolate. At 3 d p.i., lungs were removed, total RNA was isolated and subjected to next generation sequencing (*n = 3* animals per group). Shown are the enriched Top10 gene ontologies (GOs) upon influenza A virus infection in ANP32B$^{+/+}$ mice compared to PBS treated control mice, sorted by *p*-value. Top5 of upregulated genes are shown for each respective GO.

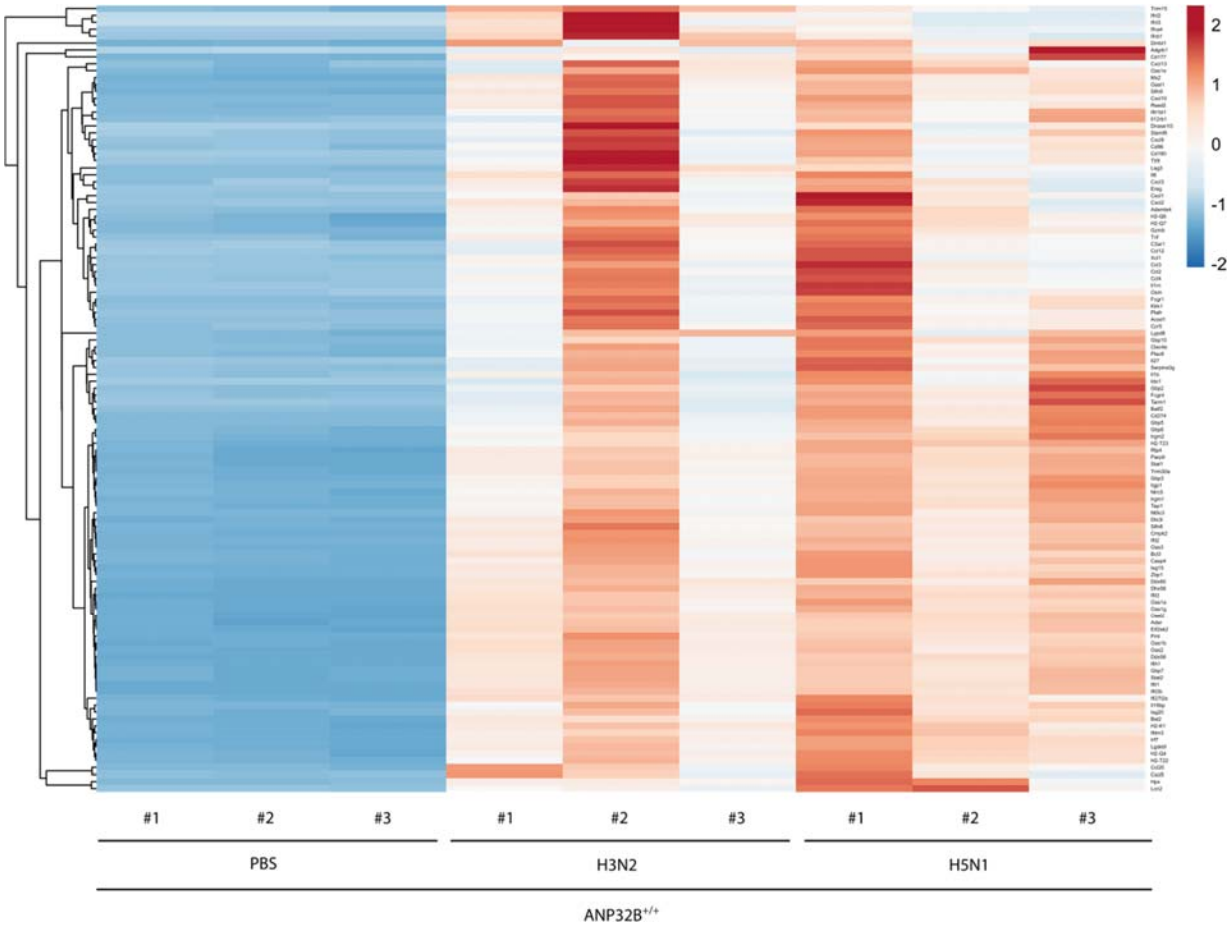

Figure 33: Global expression profile of inflammatory genes in ANP32B$^{+/+}$ mice during influenza infection. ANP32B$^{+/+}$ and ANP32B$^{-/-}$ mice were either control treated with PBS or infected with 10^3 pfu of a seasonal H3N2 subtype or a highly pathogenic H5N1 human isolate. At 3 d p.i., lungs were removed, total RNA was isolated and subjected to next generation sequencing (*n = 3* animals per group). Shown is a heat map analysis of significantly upregulated genes during influenza A virus infection in ANP32B$^{+/+}$ mice, based on GOs (**Figure 32**). Color-code represents standard deviation from the mean of normalized expression values (*z-score*) within each group (*n* = 3 animals per group; cut-off: log2FoldChange ≥ 2).

It should be noted that some variability between the three different H3N2 IAV infected ANP32B$^{+/+}$ mice was observed regarding their individual transcriptional profiles (**Figure 35, left panel**). Particularly, ANP32B$^{+/+}$ mouse #2 showed a higher cytokine response compared to mice #1 and #3 of the same group. In order to identify parameters of correlation, qRT-PCR was used to determine the amount of viral nucleoprotein (NP) RNA in the lungs of these infected mice. As shown in **Figure 36**, ANP32B$^{+/+}$ mouse #2 showed higher than average NP RNA expression values. Thus, the transcriptomic profile (**Figure 35, left panel**) reflects biological variability and needs to be evaluated in the context of viral infection efficiency.

The reduced expression of pro-inflammatory C/C (MCP-1, TNF-α, IL-6, IFN-β1, IL-1β, CXCL10), antiviral transcription factors (IRF7) and effector proteins (Mx1) in H3N2 and H5N1 infected ANP32B$^{-/-}$ mice at 3 d p.i. could be also confirmed by qRT-PCR (**Figure 37**). Most prominently, expression of IFN-β1 (H3N2), IL-1β (H5N1), MCP-1 and IL-6 (both viral subtypes) was downregulated in ANP32B$^{-/-}$ mice, compared to ANP32B$^{+/+}$ mice (**Figure 37**).

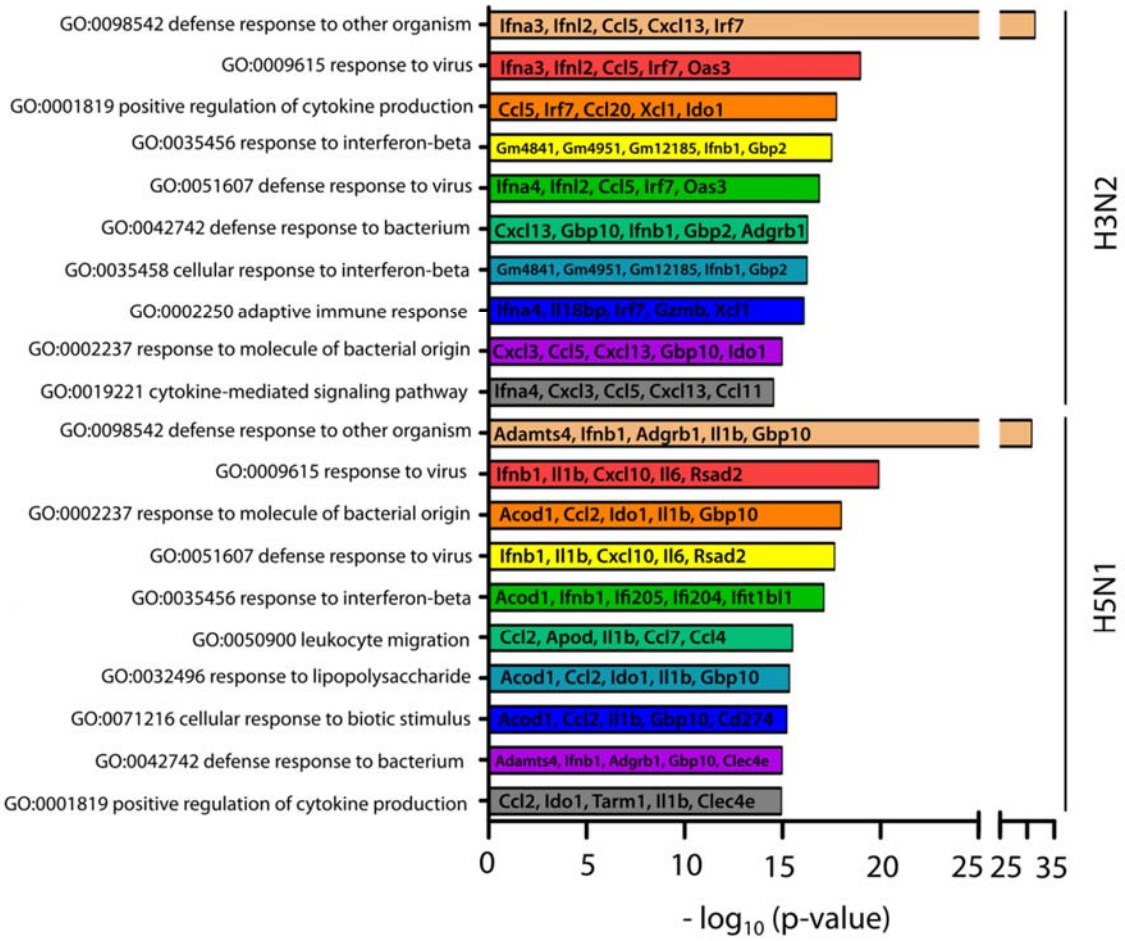

Figure 34: Gene ontology analysis of disregulated genes in ANP32B$^{+/+}$ vs. ANP32B$^{-/-}$ mice during influenza infection. ANP32B$^{+/+}$ and ANP32B$^{-/-}$ mice were either control treated with PBS or infected with 10^3 pfu of a seasonal H3N2 subtype or a highly pathogenic H5N1 human isolate. At 3 d p.i., lungs were removed, total RNA was isolated and subjected to next generation sequencing (*n = 3* animals per group). Shown are the enriched Top10 gene ontologies (GOs) upon influenza A virus infection in ANP32B$^{+/+}$ mice compared to ANP32B$^{-/-}$ mice, sorted by *p*-value. Top5 of upregulated genes are shown for each respective GO.

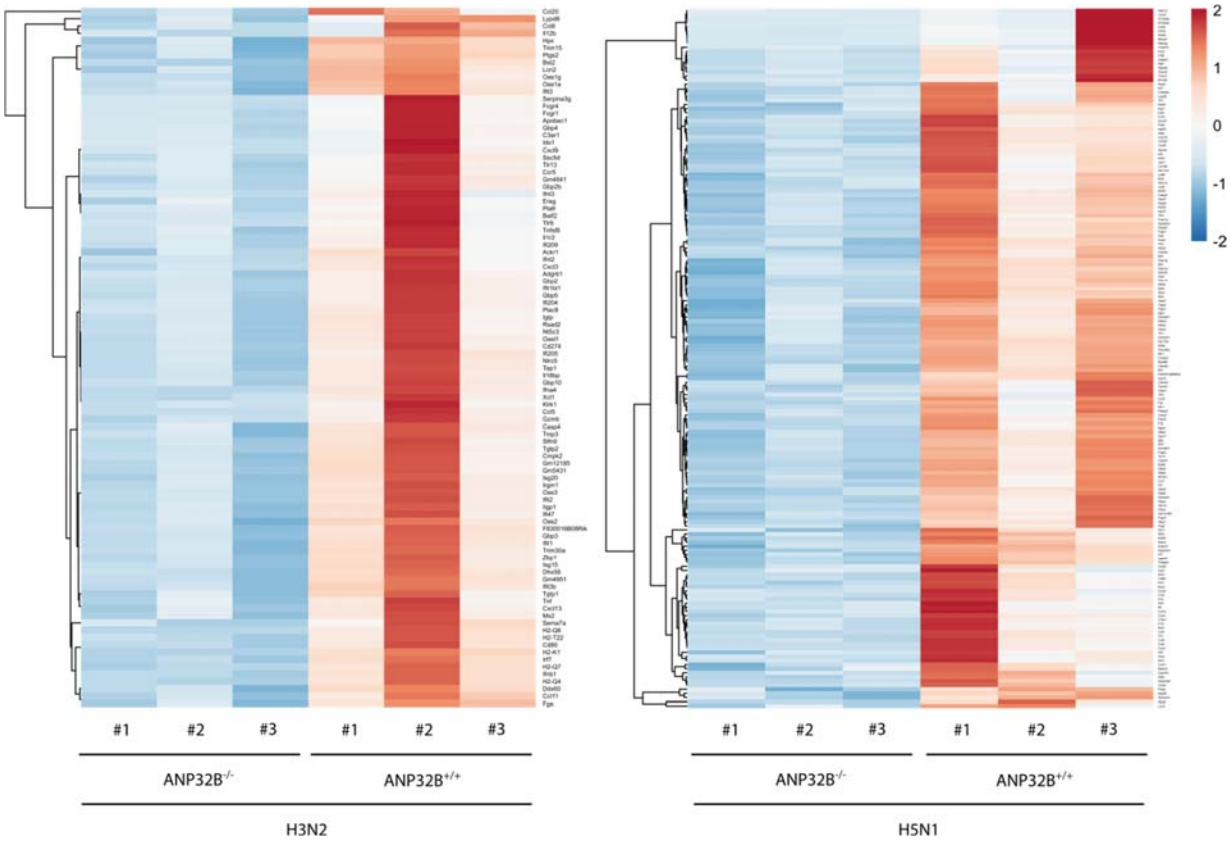

Figure 35: Global expression profile of inflammatory genes in ANP32B$^{+/+}$ vs. ANP32B$^{-/-}$ mice during influenza infection. ANP32B$^{+/+}$ and ANP32B$^{-/-}$ mice were either control treated with PBS or infected with 10^3 pfu of a seasonal H3N2 subtype or a highly pathogenic H5N1 human isolate. At 3 d p.i., lungs were removed, total RNA was isolated and subjected to next generation sequencing (*n = 3* animals per group). Shown is a heat map analysis of significantly downregulated genes during influenza A virus infection in ANP32B$^{+/+}$ versus ANP32B$^{-/-}$ mice, based on GOs (**Figure 34**). Color-code represents standard deviation from the mean of normalized expression values (*z-score*) within each group (*n* = 3 animals per group; cut-off: log2FoldChange ≤ -1).

In summary, the transcriptional landscape of the IAV infected murine lung strongly suggests that ANP32B plays a crucial role in the regulation of pro-inflammatory gene expression that ultimately dictates influenza disease outcome in mice.

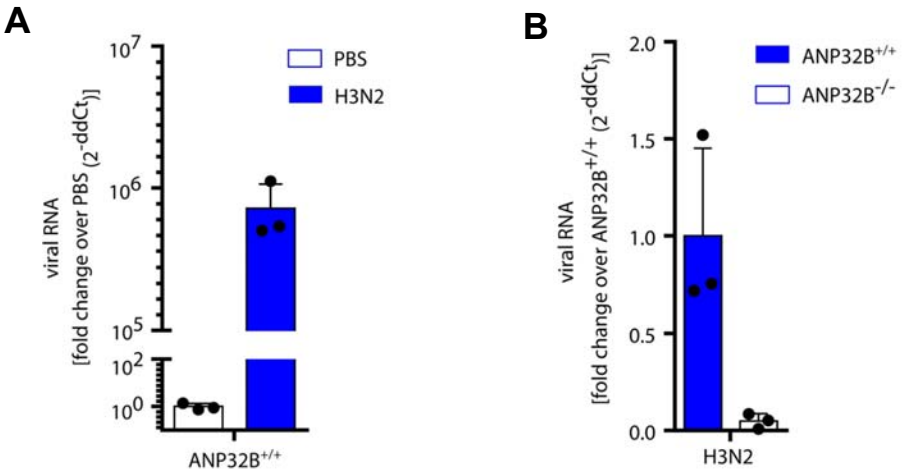

Figure 36: Viral replication in infected ANP32B$^{+/+}$ and ANP32B$^{-/-}$ mice. A and B, Lungs were harvested from PBS control treated or H3N2 (10^3 pfu) infected ANP32B$^{+/+}$ and ANP32B$^{-/-}$ mice at 3 d p.i. Total RNA was isolated and expression levels of viral nucleoprotein (NP) RNA in infected ANP32B$^{+/+}$ mice was determined by qRT-PCR, compared to PBS control treated mice **(A)** or infected ANP32B$^{-/-}$ mice **(B)**. Raw NP expression values were normalized to murine ribosomal protein 9. Shown are the relative NP mRNA expression values as fold change over PBS **(A)** or ANP32B$^{+/+}$ **(B)**. *n* = 3 animals per group.

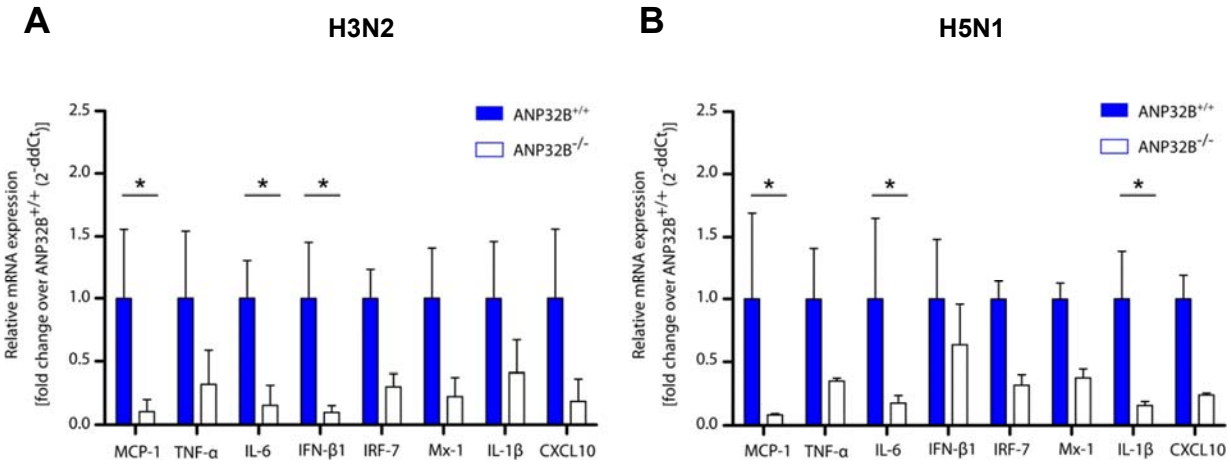

Figure 37: Virus-induced cytokine responses are reduced in ANP32B$^{-/-}$ mice. A and B, ANP32B$^{+/+}$ and ANP32B$^{-/-}$ mice were infected with 10^3 pfu of a H3N2 subtype (**A**) or a highly pathogenic H5N1 human isolate (**B**). At 3 d p.i., lungs were removed and total RNA was isolated. mRNA expression levels of a series of pro-inflammatory cytokines/chemokines (MCP-1, TNF-α, IL-6, IFN-β1, CXCL10, IL-1β), antiviral transcription factors (IRF-7) and effector proteins (Mx1) were measured by qRT-PCR. Raw expression values were normalized to murine ribosomal protein 9. Shown are the relative mRNA expression values as fold change over ANP32B$^{+/+}$. Statistically significant differences were calculated using two-way ANOVA with Bonferroni post-test (* $p < 0.05$). *n* = 3 animals per group.

6. Discussion

6.1 The role of importin-α-mediated nuclear transport in human health and disease

In higher eukaryotes, membranes are used to create distinct sub-structures or compartments within the cell. An essential compartment is the nucleus which harbors the genome of the cell and is separated from the cytoplasm by a double-membraned envelope in which transport channels, termed nuclear pore complexes (NPCs), are embedded. While small molecules (< 40-50 kDa) can pass these gateways by passive diffusion, albeit with exceptions, larger proteins and protein complexes are actively shuttled into the nucleus using transport receptors [309, 340]. Accessory factors, such as Ran proteins, bind to and hydrolyze GTP at either side of the NPCs which serves as energy source for the transport process [342]. In addition to the bi-directional transport of proteins across the nuclear membrane, the nuclear export of cellular RNAs also occurs via the NPCs. Here, a subset of mRNAs, miRNAs, and tRNAs uses specific export receptors in a similar manner to protein transport, whereas bulk mRNA export is mediated independently of Ran proteins via the NXF1 (TAP)-NXT1 (p15) pathway [387].

Importin-α isoforms, also termed karyopherins, constitute the largest family of nuclear import receptors [314, 315]. Nuclear import is initiated when a cytoplasmic cargo protein presents a nuclear localization signal (NLS), which subsequently is recognized and bound by a member of the importin-α family [44]. Post-translational modifications or association with inhibitory factors are often used as an elegant mode to regulate nuclear transport [388]. One well-characterized example is the NF-κB signaling pathway, a key player in cell proliferation and antiviral immunity. Herein, only upon stimulation, the inhibitor of NF-κB, IκBα, is phosphorylated and degraded which exposes the NLS motif on NF-κB and allows recognition by importin-α, particularly by importin-α3 and -α4 [389, 390]. Once importin-α is bound to a cargo protein, it recruits the transport co-receptor importin-β_1 and the hetero-trimeric complex translocates through the NPC into the nucleus. Both, dissociation of the complex as well as recycling of importin-α and importin-β_1 to the cytoplasm involves the action of Ran proteins [44, 314].

Nuclear trafficking needs to be tightly controlled in order to maintain cellular homeostasis. Accordingly, disturbed nuclear transport can lead to a variety of human diseases, including tumorigenesis, neuropathological and developmental disorders, and susceptibility to viral or bacterial infections [310-313, 391]. In the next chapter, the role of importin-α isoforms in human health and disease will be further discussed in light of their respective cargo binding specificities, a hallmark of importin-α function.

6.1.1 Diverse cargo binding specificities are a hallmark of importin-α function

A long-standing dogma in nuclear transport states that the presence and accessibility of a NLS motif on a cargo protein is both necessary and sufficient for importin-α-mediated nuclear import [392-394]. However, this dogma was recently challenged by studies showing that other parameters beyond the NLS amino acid sequence, such as the three-dimensional context of the cargo protein, can also influence importin-α binding specificity [322, 323]. To maintain cellular homeostasis particularly in stress conditions, a rapid and tightly regulated response is required. In viral infections, for example, antiviral transcription factors, such as NF-κB and STAT proteins, need to get prioritized access to the nucleus in order to mount an appropriate cellular response in a timely fashion. Herein, based on reduced autoinhibition by the internal importin-β_1 binding (IBB) domain compared to the other importin-α isoforms (e.g. importin-α1), importin-α3 has been proposed to provide a 'fast-track' to the nucleus [48]. In support of this concept, importin-α3 was recently shown to promote NF-κB nuclear entry upon influenza infection, which likely represents the first line of cellular defense and thus needs to proceed with highest priority [291].

Despite the highly conserved structure, accumulating evidence suggests that each of the importin-α isoforms recognizes and transports a very distinct set of cargo proteins into the nucleus [395]. However, although many studies have reported specific cargos for individual importin-α proteins as well as other nuclear transport receptors (NTRs; e.g. importin-4 or transportin-1) [395-397], a detailed cargo landscape for all importin-α isoforms is still missing, especially under stress conditions such as viral infection. For instance, no interactome was described yet for human importin-α7, which has been shown before to be a major driver of high-level IAV replicative fitness and pathogenicity in mammals, albeit the underlying molecular mechanisms are still largely unknown [50, 251]. Thus, in the present study, a SILAC-based mass spectrometry (MS) approach was performed to identify importin-α7 interacting cellular proteins in IAV (H1N1) infected human cells.

6.1.2 Comprehensive analysis of importin-α7 interacting cellular factors in influenza infected human cells

As described above, transient importin-α – cargo interactions complicate attempts to determine a comprehensive interactome of human importin-α isoforms using pulldown experiments. To address this issue, in this study, importin-α variants with deleted IBB domains were included in the CoIP experiments. This was based on the hypothesis that importin-α-ΔIBB could still interact with its cargo proteins, but recruitment of importin-β_1 and, in turn, nuclear transport and dissociation of the complex would be prevented. In line, many studies aiming to characterize

importin-α – cargo binding events (e.g. with the influenza PB2 protein) have used importin-α-ΔIBB constructs to enhance and stabilize the respective interaction, particularly in crystallographic studies [48, 327, 398, 399]. Indeed, compared to importin-α7-WT, Western blotting could confirm increased interaction of importin-α7-ΔIBB with a subset of assessed cellular (ANP32A, NCBP1) and viral (PB2) proteins. Based on these findings, it was rather unexpected that MS analysis of importin-α7 interacting factors revealed no major differences in terms of absolute numbers of proteins precipitated with either importin-α7-WT or -ΔIBB, independently of viral infection. Interestingly, while some proteins interacted with both importin-α7 variants, others displayed a distinct binding affinity for either WT or ΔIBB importin-α7. These results might indicate that certain cargos with a generally reduced affinity for importin-α7 bind more efficiently to importin-α7 lacking the autoinhibitory IBB domain, whereas other cargos preferentially interact with full-length importin-α7 that is able to bind to importin-β_1, thereby exposing the NLS binding grooves for cargo recognition. If correct, this hypothesis would further support the current concept that importin-α – cargo binding is not only determined by the NLS motif, but also by other intrinsic features of the cargo protein, such as 3D-structure, as well as the ability of importin-α to associate with its transport co-receptor importin-β_1. However, it should be noted that the findings presented here are based on a single MS experiment. Therefore, evaluation of the pending MS datasets will be crucial for a more thorough understanding of the diverse characteristics of cellular cargo proteins that ultimately determine their binding specificity and affinity for individual importin-α isoforms in human cells.

Based on the primary aim of this study to identify cellular proteins specifically interacting with importin-α7, also importin-α1 and -α5 interacting networks were determined by SILAC-MS. Both of these importin-α isoforms were chosen as controls due to their differential functions during influenza infection: Importin-α1, like importin-α7, was shown to be a positive regulator of human-type ($PB2_{E627K}$ or $PB2_{D701N}$/NP_{N319K}) IAV polymerase activity and replication in human cells [50, 251]. However, while the molecular mechanism underlying the exact importin-α7 mode-of-function remained unknown, importin-α1 was proposed to promote nuclear import of viral NP and PB2, particularly in the context of the $PB2_{D701N}$/NP_{N319K} host-adaptive signatures [250]. In contrast to importin-α1 and -α7, importin-α5 was demonstrated to play no major role during IAV infection, even despite sharing high sequence similarity (> 80 %) with importin-α7 [50, 251]. Taken together, these data suggest that the importin-α7 specific interactome in human cells might comprise a single or a subset of host cell proteins that contribute to importin-α7 function during IAV infection.

Compared to importin-α7, almost twice the number of cellular proteins was precipitated with importin-α1/-α5. Moreover, in contrast to importin-α7, these proteins showed a strong binding

affinity for full-length importin-α1 and -α5, compared to the respective ΔIBB controls. Although subtle differences in the pulldown efficiency of the different importin-α isoforms cannot be excluded, it is likely that importin-α7 is more selective regarding its nuclear transport cargos.

Based on GO analyses, cellular factors enriched with importin-α7 are involved in chromatin organization, chromatin remodeling and RNA processing as part of large intracellular machineries (e.g. NuRD complex), matching the results described for interaction partners of the murine importin-α7 homologue [396]. Furthermore, cellular proteins with an established role in nuclear transport were also abundant in the importin-α7 interactome. Overall, no significant differences were revealed by GO analysis of importin-α1/-α5 interacting cellular proteins, although compared to importin-α7 ribosomal proteins were significantly enriched with these importin-α isoforms. Of note, cellular proteins specifically precipitated with importin-α5 and, to less extend, with importin-α1 were associated with the cellular splicing machinery. These findings indicate that all importin-α isoforms assessed in this study share both common as well as differential subsets of nuclear import cargos, adding another layer of complexity to the diverse functions of individual members of the importin-α family in cellular homeostasis.

Interestingly, in the study by Hügel *and colleagues,* 807 cellular proteins were identified as binding partners of murine importin-α7, which is almost 20-fold the number of proteins found in this study [396]. These contradictive findings may have multiple causes: First, although almost identical on the amino acid level (> 99%), single amino acid substitutions in murine compared to human importin-α7 might have an effect on cargo binding specificities. However, it is more likely that the observed differences are due to the different cellular systems (mouse ovary vs. HEK239T lysate) and pulldown techniques (*in vitro* vs. *in vivo*) used by Hügel *et al.,* compared to this study. Moreover, the SILAC-MS approach performed in this work was based on pooled eluates from both empty vector control and importin-α7 pulldowns, which might be more suited to accurately filter out unspecific interactions. Finally, as described before in the *Results* chapter, some ‘true’ positive hits might have been unintentionally removed from the importin-α7 interactome due to the high-confidence cut-off applied. With the additional MS datasets becoming available, this cut-off can be further adjusted, which will likely increase the number of specific importin-α7 interacting cellular proteins. Nevertheless, Hügel *and colleagues* described a conserved set of 20 importin-α7 binding partners, either derived from mouse ovary or a murine fibroblast cell line, and 50 % (10/20; e.g. LMNB1, SMARCC2 or RBBP4) of these proteins were also precipitated with importin-α7 in this study [396]. Considering that some of the murine importin-α7 interacting proteins might be specifically expressed in mouse ovaries, this significant overlap further confirms the validity of the importin-α7 interactions described here.

Of note, in another study conducted by Mackmull *et al*., approximately 800 cellular proteins were found to interact with importin-α1, which is also 10-fold higher compared to the number of importin-α1 interacting cellular factors found in this work. However, since the authors used a proximity-labeling approach, the number of validated importin-α1 import cargos might be overestimated [397].

6.1.3 Dual role of importin-α7 interacting cellular factors during influenza infection

Based on the initial hypothesis that importin-α7 promotes human-type ($PB2_{627K}$) IAV polymerase activity and replication indirectly by regulating the cellular localization of other host cell proteins, importin-α7 binding partners were systematically screened for any proposed or experimentally-validated function during influenza infection. Beforehand, stringent criteria were applied to narrow down the list of potential candidates. First, cellular proteins that were only found in the importin-α7 interactome in uninfected cells were excluded as these are unlikely to contribute to importin-α7 function in the context of viral infection. Second, only those proteins were retained that were implicated before to be involved in any step of the influenza replication cycle, based on literature research. Finally, cellular factors that were precipitated with all three importin-α isoforms, suggesting non-selective importin-α binding, were also removed from the candidate list. In contrast, those proteins with a specificity for importin-α7 and only one other isoform (i.e. importin-α1 or -α5) were maintained. The rationale thereof was based on the fact that the observed interactions between specific cargo proteins and the individual importin-α isoforms need to be verified in the pending MS datasets, as well as using independent techniques, such as Western blotting. However, it has to be acknowledged that none of these techniques provide sufficient quantitative power to accurately measure exact importin-α – cargo binding affinities, for example as dissociation (K_d) values. To do so, this would require the use of purified proteins *in vitro*, which in turn would raise the question of whether the obtained K_d values reflect the binding events that occur within the cell where multiple cargo proteins compete with each other for importin-α binding. Nevertheless, this type of measurements was beyond the scope (and, in part, technical feasibility) of this study. In any case, the contribution of the selected host cell factors to importin-α7 function had to be confirmed using functional assays.

Applying the abovementioned criteria, the list of potential candidates was reduced to 13 cellular proteins, of which 7 were only precipitated with importin-α7, but not with importin-α1 or -α5, indicating a high specificity for importin-α7 mediated nuclear import. Albeit the exact function of the majority of these host cell factors during influenza infection is still unknown, recent literature

revealed that some of these proteins promote viral replication (ANP32A, CTNNB1, KPNA1/Importin-α5, and RAB6B), while others (CIRBP, ILF3, TAF4) have a negative-regulatory function and restrict viral replication. For example, both CTNNB1 (*catenin beta-1*) and RAB6B (*Ras-related protein Rab-6b*) were identified in genome-wide RNAi screens as essential host cell proteins for efficient viral genome replication and viral progeny production, respectively [218, 382]. On the other hand, ILF3 (*interleukin enhancer-binding factor 3*), also known as NF90, and TAF4 (*transcription initiation factor TFIID subunit 4*) were both shown to interfere with viral replication by promoting cellular immune responses, either by direct stimulation of ISG expression or by disabling antagonistic viral factors, such as the viral NS1 protein [373, 374, 384]. Certainly, it would be interesting to investigate whether subcellular localization of these antiviral host factors is altered in the absence of importin-α7 and whether this has a functional consequence for influenza virus replication and cellular immune activation. However, several studies using either cell culture or small animal models showed that importin-α7 deficiency is directly linked to decreased viral replicative fitness and, only as a secondary effect, reduced expression of pro-inflammatory cytokines, specifically in the lungs of influenza infected mice [50, 251, 292, 293]. Based on the proposed concept that importin-α7 indirectly promotes human-type IAV replication and pathogenicity via its role in nuclear transport, these data strongly hint to the involvement of a positive-regulatory rather than antiviral host cell factor that contributes to importin-α7 function. Herein, ANP32A presented a particularly interesting candidate, even though it was precipitated with both importin-α7 and -α5 in MS analyses.

In 2015, a Japanese research group identified ANP32A (alias pp32) and ANP32B (alias APRIL) as cellular factors that support viral cRNA-to-vRNA replication, albeit using a cell-free *in vitro* system [307]. In a pivotal study conducted by Long and colleagues, ANP32A was then identified as a key factor that drives avian-mammalian adaptation of $PB2_{627E}$ containing IAV polymerases in a species-dependent manner [252]. The authors of this study could show that the avian ANP32A (avANP32A) protein possesses a 33 amino acid insertion which is lacking in mammalian ANP32A proteins. Co-expression of avANP32A could rescue the otherwise highly restricted avian-type influenza polymerase in human cells – a phenomenon that since its first description in the early 1990s only remained poorly understood [236, 252]. Importantly, Long *et al*. could further demonstrate that the activity of the mammalian-adapted ($PB2_{627K}$) IAV polymerase is significantly reduced in ANP32A siRNA silenced human cells [252]. Similar results were obtained after silencing of ANP32B, a closely related family member of ANP32A [252, 296]. Conversely, another study showed that overexpression of ANP32A in human A549 cells increased the rate of viral RNA synthesis [400]. Collectively, these data indicate that human ANP32A promotes replicative fitness of $PB2_{627K}$-adapted IAV polymerases in human cells and

thus might also be involved in the proposed indirect function of importin-α7 during influenza infection.

In the following chapter, the investigated reciprocal interplay of importin-α7 and ANP32A in promoting human-type IAV polymerase activity will be discussed in more detail. Furthermore, alternative hypotheses regarding the molecular mechanisms underlying the importin-α7 mode-of-action will be presented in light of current literature as well as evidence from other independent studies in our laboratory.

6.2 The importin-α7 interactome as platform to study molecular mechanisms of IAV replication and pathogenesis

In recent years, genome-wide RNAi screening studies as well as studies aiming to determine cellular binding partners of the IAV polymerase complex have substantially contributed to the identification of host cell factors that are required throughout the viral replication cycle and might therefore pose novel targets for therapeutic intervention [218, 241, 374, 382, 383, 401]. However, the exact mode-of-function of the majority of these cellular proteins in IAV interspecies transmission and pathogenicity in mammals remains largely unknown to this day. One particular family of host factors, the importin-α isoforms, which are the major constituents of the nuclear import machinery in the cell, has been extensively studied in the last decade, revealing diverse functions during influenza infection: While importin-α3 was shown to act as an inhibitor of avian-type viral replication and pathogenicity, likely by promoting the nuclear import of activated NF-κB [291], importin-α7 was identified as a positive regulator of human-type IAV viral polymerase activity, replicative fitness and pathogenicity in mammalian cells as well as small animal models [50, 251, 292, 293]. Notably, importin-α1 was required by both avian- and human-adapted influenza viruses for efficient viral replication [50]. Therefore, a switch from importin-α3 to importin-α7 dependency is a hallmark of IAV avian-mammalian adaptation. According to current concept, sufficient diversity between avian and mammalian importin-α isoforms constitutes the driving force for this switch, by posing a selective pressure for viral adaptation during interspecies transmission from birds to mammals [50, 238]. Importantly, the exact mode-of-action by which importin-α7 promotes viral polymerase activity in mammalian cells is currently unknown, albeit a molecular mechanism beyond the nuclear transport of vRNP subunits has been proposed [251]. The present study therefore aimed to provide further mechanistical insights into importin-α7 function during influenza infection.

6.2.1 ANP32A uses the classical importin-α/importin-β_1 pathway for nuclear import

Previously, it was suggested that importin-α7 could either act directly on viral transcription and replication, or indirectly by promoting the nuclear import of other host cell factors that function as co-factors of the viral polymerase within the nucleus [237]. In order to address the latter hypothesis, an unbiased, SILAC-based MS approach was conducted in this study to determine the importin-α7 specific interactome in human cells. These experiments were performed in IAV infected cells, as importin-α7 – cargo interactions might be altered in the presence of actively replicating virus. After applying certain exclusion criteria (chapter 6.1.3), 13 candidate proteins were obtained, one of which was ANP32A, a novel cellular factor that, in line with the above mentioned concept of protein diversity between avian and mammalian species, promotes IAV host adaptation and replicative fitness in mammals in a species-dependent manner [252]. However, as for importin-α7, the molecular mechanism underlying ANP32A function is also currently unknown.

Western blotting was used to confirm the interaction of importin-α7 with ANP32A in influenza infected cells. Herein, two interesting observations were made: First, ANP32A interacted with both importin-α7-WT and -ΔIBB, while only an interaction with full-length importin-α7 was detected in MS. Second, the interaction of importin-α7-WT with ANP32A was slightly reduced in influenza infected compared to mock infected cells, whereas this was not the case for the ΔIBB variant. Confirmation of these interactions was performed in cells cultivated in regular growth media; however, it is unlikely that the incorporated labeled amino acids affect the function of the protein. Whether the reduced binding of importin-α7-WT to ANP32A upon influenza infection has a functional consequence remains unknown and requires further investigations.

The decision to further investigate a functional relationship between importin-α7 and ANP32A was based on two key aspects: First, several reports showed that ANP32A has a predominant nuclear function due to its established role in chromatin remodeling and transcriptional regulation, in line with the strict nuclear localization shown by others and also demonstrated in this study [296, 402]. Second, ANP32A has been shown to promote IAV vRNA synthesis from the cRNA intermediate, a process that occurs in the nucleus of the host cell [307]. Therefore, it was hypothesized that ANP32A might require importin-α7 mediated nuclear translocation to act on viral replication within the nucleus. As a prerequisite thereof, it was first explored whether ANP32A uses the classical importin-α/importin-β_1 pathway to gain access to the nucleus. Using expression vectors for NLS-deficient ANP32A variants, fluorescence microscopy and co-immunoprecipitation analyses, it could be shown that ANP32A is indeed imported into the

nucleus in an NLS- and importin-α5/-α7-dependent fashion, consistent with previous reports [302]. However, as already discussed above, at this stage it was not possible to clearly distinguish between importin-α5 or -α7 mediated nuclear transport of ANP32A. Early experiments using siRNAs to knockdown either importin-α protein, or both, did not show any differences regarding the subcellular localization of ANP32A (*data not shown*), probably because of residual protein levels. Thus, importin-α5 and -α7 specific knockout cell lines might be more suited to investigate whether ANP32A preferentially uses a particular importin-α isoform for nuclear import. However, the establishment of these cell lines proved to be challenging and was only successful for importin-α7 at the end of this study, likely due to detrimental effects of the respective knockouts on essential cellular processes, such as nuclear transport and gene expression. This is in line with the distinct cargo binding specificities determined in this study, particularly for importin-α5 (e.g. *host cell splicing factors*).

Nevertheless, it also has to be noted that ANP32A proteins with mutations in the NLS motif still showed some nuclear localization, albeit significantly less compared to the WT protein. These data suggest that alternative, less abundant nuclear import pathways are activated when the interaction of ANP32A with importin-α is disrupted. Furthermore, it could also be imagined that, due to its rather small size (~ 28 kDa), ANP32A translocates through NPCs simply by passive diffusion. In any case, it is important to highlight that even if ANP32A is able to get access to the nucleus in an importin-α-independent manner, it is also possible that ANP32A (re-)associates with importin-α7 within the nucleus, either via the NLS motif or via alterative, yet unknown interaction sites, and both proteins act in concert on viral replication. Indeed, *in silico* modelling of the available crystal structures of ANP32A and importin-α7 revealed several potential binding sites, in addition to the C-terminal part of ANP32A that comprises the NLS motif and was oriented towards the major NLS binding groove in importin-α7.

Collectively, these findings indicate that ANP32A preferentially uses the classical importin-α/importin-β pathway for nuclear import. However, this process might be uncoupled from a putative reciprocal interplay of importin-α7 and ANP32A in promoting viral replicative fitness inside the nucleus.

6.2.2 Importin-α7 and ANP32A promote high-level IAV replicative fitness by functionally-independent and spatially-separated mechanisms

Next, it was assessed whether ANP32A might contribute to importin-α7-induced modulation of human-type ($PB2_{627K}$) polymerase activity in human cells, which has been shown before to drive IAV adaptation from birds to mammals [238]. In order to study the interplay of these two host

factors, a combined gain- and loss-of-function approach was designed. This approach was based on measuring viral polymerase activity in cells overexpressing either importin-α7 or ANP32A. Simultaneously, expression of the respective counterpart was silenced or completely abolished using siRNA or CRISPR/Cas technologies, respectively. That way, an elegant system was established to study the reciprocal interplay between importin-α7 and ANP32A with respect to promoting high-level viral polymerase activity in human cells.

First, as it was the main subject of this study, a complex importin-α7 overexpressing vRNP reconstitution assay was established [348]. Surprisingly, overexpression of importin-α7 alone dramatically decreased viral polymerase activity, likely due to creating an unbalance in the nuclear transport machinery which ultimately disturbs cellular homeostasis and thereby reduces viral replication. To address this issue, a minimal set of components of the nuclear transport machinery was co-expressed, which significantly enhanced the ability of overexpressed importin-α7 to unfold its positive-regulatory function on viral replication and transcription. These components included both the nuclear import co-receptor importin-β_1 as well as the recycling factor CAS which, in conjunction with RanGTP, shuttles importin-α back to the cytoplasm [44]. Moreover, the assay was further improved by including importin-α7-ΔIBB as a novel background control, replacing the empty vector used before. The fact that the IBB domain was critical for the importin-α7-induced increase in viral polymerase activity strongly suggested that it acts on viral replication within the nucleus, in agreement with previous reports [251], and/or that nuclear transport of a cellular or viral cargo protein is somehow involved in this process.

In the next step, the successfully established importin-α7 overexpressing polymerase activity assay was conducted in the absence of ANP32A. As described before, two approaches were followed in which expression of ANP32A was either reduced by siRNA or completely abolished using the CRISPR/Cas technology. The rationale thereof was to exclude any artificial effects of the respective treatment that could falsify the results. Importantly, it could be shown that depletion of ANP32A expression levels did not alter the importin-α7 mediated increase in viral polymerase activity. Thus, it was concluded that ANP32A does not contribute to importin-α7 function. Future studies should therefore concentrate on other importin-α7 interacting cellular proteins, independently of whether they promote or restrict viral replication, and also include host cell factors with a yet unknown function during influenza infection. Finally, it should be considered that importin-α7 unfolds its positive-regulatory function entirely independent of nuclear import of host or viral factors. For example, importin-α proteins have been implicated to promote nuclear export of cellular mRNAs, which involves their interplay with importin-β_1 as well as the cap-binding complex (CBC; composed of NCBP1/CBP80 and NCBP2/CBP20) of the host

cell [327]. An intriguing, yet still unproved hypothesis which suggests a role of this particular importin-α function in influenza infection will be further discussed in chapter 6.2.3.

All experiments conducted to this point were based on the currently accepted view that ANP32A acts as co-factor of the viral polymerase within the nucleus where viral genome replication and transcription take place [252, 302, 307]. This would imply that ANP32A needs to get access to the nucleus which requires an intact NLS motif in order to interact with the importin-α machinery, as demonstrated in this study. To address the question whether the proposed positive-regulatory function of ANP32A depends on the nuclear transport machinery of the cell, two key experiments were performed, both of which were based on an ANP32A gain-of-function vRNP reconstitution assay: First, to investigate the role of nuclear localization on ANP32A function, the ANP32A NLS mutants, which were shown to accumulate in the cytoplasm, were evaluated for their ability to increase viral polymerase activity. Second, cells with reduced or depleted levels of importin-α7 were used to analyze whether importin-α7 contributes to the ANP32A mode-of-action, either indirectly by promoting nuclear entry of ANP32A or directly by forming a regulatory complex together with ANP32A that stimulates viral replication.

As a prerequisite of these experiments, it could be demonstrated that overexpressed WT ANP32A increases viral polymerase activity, albeit the effect was not as pronounced as observed in the importin-α7 gain-of-function system. Although further studies would be required, these findings might already indicate that importin-α7 is superior over ANP32A in promoting human-type ($PB2_{627K}$) IAV replicative fitness and, in turn, pathogenicity in mammals. Most importantly, neither mutation of the NLS motif in ANP32A nor depletion of importin-α7 expression levels did alter the positive-regulatory effect of ANP32A on viral polymerase activity. Therefore, ANP32A seems to act independently of importin-α7 on IAV replication. Surprisingly, however, the data presented here suggest that regulation of viral polymerase activity by ANP32A occurs, at least in part, via a known or novel cytoplasmic function of ANP32A [296], albeit this requires further experimental evidence.

Figure 38 summarizes the key findings from this study regarding the mechanistical interplay of importin-α7 and ANP32A during IAV infection.

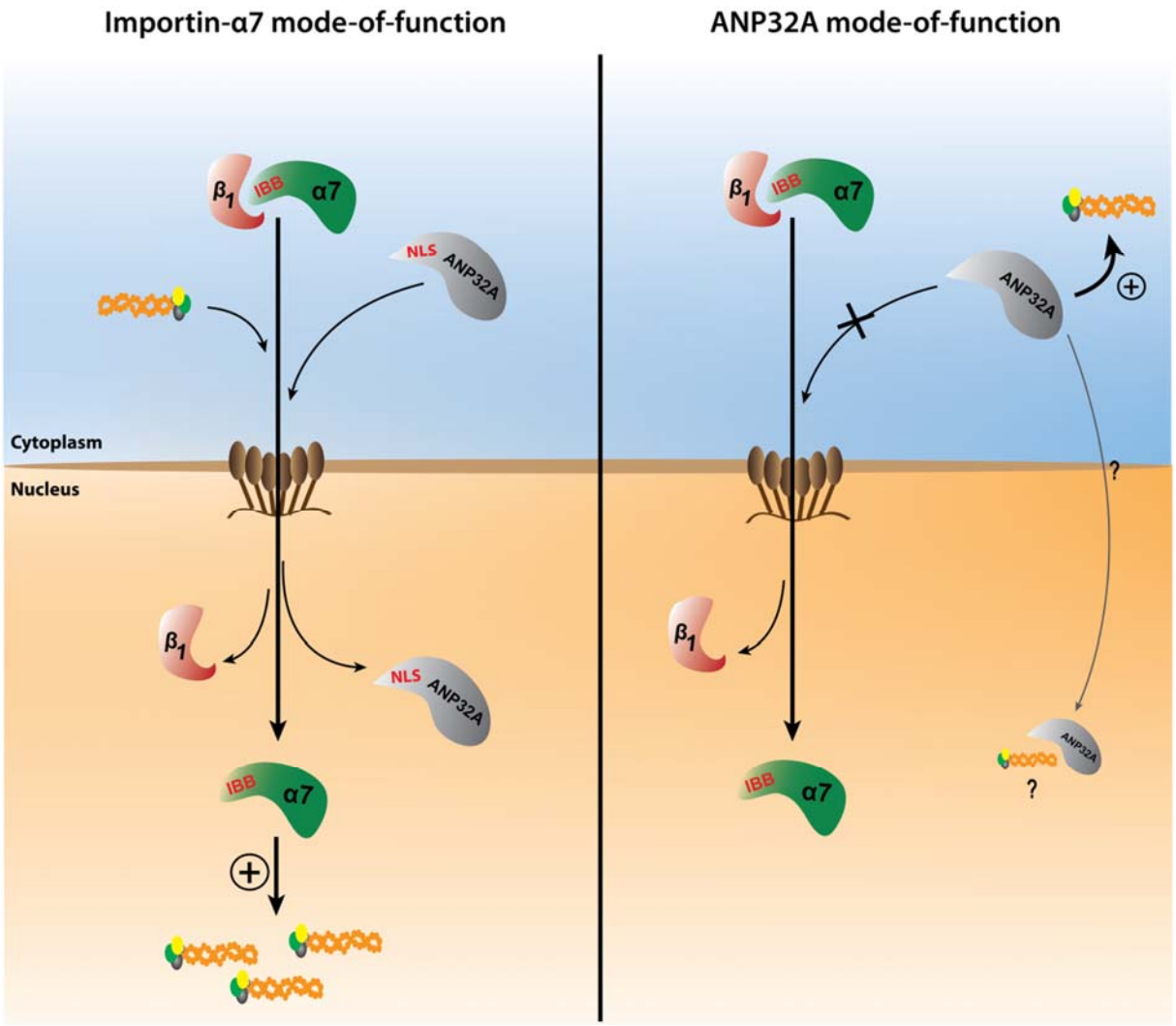

Figure 38: Importin-α7 and ANP32A promote human-type IAV replicative fitness by functionally-independent and spatially-separated mechanisms. Left panel, Importin-α7 (and -α5) mediates nuclear import of ANP32A via its C-terminal NLS motif. However, inside the nucleus, importin-α7 promotes viral polymerase activity independently of ANP32A. Herein, the importin-β_1 binding (IBB) domain was identified as a structural component critical for importin-α7 function. **Right panel,** Mutations in the NLS motif restrict ANP32A localization to the cytoplasm but have no major impact on the ANP32A-mediated increase in viral polymerase activity. Although nuclear entry of ANP32A might occur via alternative import pathways (or passive diffusion), it does not seem to require importin-α7 to unfold is function in either cellular compartment.

The distinct and unique positive-regulatory role of importin-α7 during influenza infection with various subtypes, including both seasonal and HPAIV strains, has been confirmed in several mammalian cell lines and small animal models [50, 251, 292, 293]. Furthermore, a recent

publication from our laboratory as well as independent reports demonstrated the high abundance of the importin-α7 isoform in the human nasal mucosa as well as throughout the upper and lower human (and murine) respiratory tract, which provides a strong cellular basis to promote IAV replication and pathogenicity in mammals [291, 403]. In contrast, the expression levels of ANP32A in the human respiratory airway are still unknown, and thus its potential impact on IAV replication remains to be determined.

Finally, there is accumulating evidence that specifically importin-α7 is also required for replication of other human-pathogenic viruses beyond influenza, including Zika, Ebola and Coronavirus ([330, 333]; and *unpublished data*). In light of the currently ongoing SARS-CoV-2 pandemic and the ever-present possibility of new zoonotic outbreaks [404-406], it will be fundamentally important to also study the role of importin-α7 and its interacting cellular partners in these viral infections. In the future, these studies might aid the development of broad novel antiviral treatment strategies against zoonotic viruses that continue to pose a major health threat to the human population.

6.2.3 The molecular mechanism underlying importin-α7 function during IAV infection – Current theories and concepts

The present study aimed to provide mechanistical insights into the molecular function of importin-α7 during influenza infection by determining its interactome in human cells. The rationale thereof was based on the hypothesis that importin-α7 indirectly regulates viral replication through controlling the subcellular localization of other host cell factors. Using a combined gain- and loss-of-function approach, it could be demonstrated that ANP32A, an importin-α7 interacting cellular factor in influenza infected cells, does not contribute to the positive-regulatory effect of importin-α7 on viral polymerase activity. In order to obtain a more detailed and comprehensive understanding of the diverse importin-α7 – cargo interactions during influenza infection, the established importin-α7 overexpression system could now be used to systematically screen a wider panel of host factors, either with positive, negative or yet unknown modes-of-action during influenza infection, for their potential contribution to importin-α7 function (**Figure 39**, concept I: *Nuclear transport*).

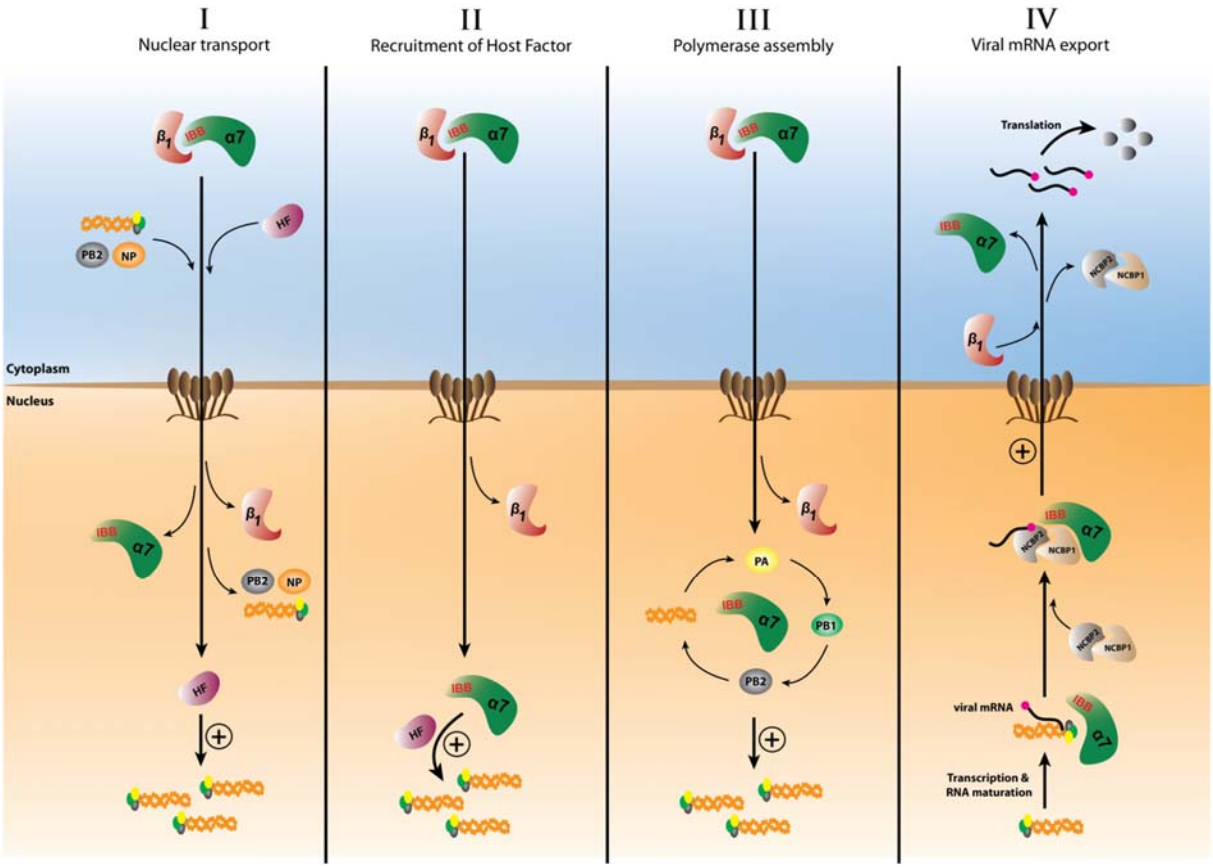

Figure 39: The molecular mechanism underlying importin-α7 function during influenza infection – Current theories and concepts. Shown are four different theories on how importin-α7 might promote high-level replicative fitness of human-type ($PB2_{627K}$) IAV in human cells. Abbreviations used are: α7, importin-α7; β_1, importin-β_1; HF, host factor. NCBP1/NCBP2, nuclear cap binding protein 1 and 2, respectively. *Concept I*: Importin-α7 promotes nuclear import of a yet unknown host factor which in turn contributes to viral replication. *Concept II*: Inside the nucleus, importin-α7 recruits a yet unknown, positive-regulatory host factor to the viral polymerase complex. *Concept III*: Importin-α7 assists in viral polymerase assembly in a chaperone-like manner. *Concept IV*: Importin-α7 forms a scaffold between the transcribing viral polymerase and the cellular cap-binding complex (NCBP1, NCBP2). After nuclear export, recruitment of importin-β_1 triggers the release of the viral mRNAs into the cytoplasm for translation.

In recent years, substantial body of evidence has emerged that importin-α isoforms are involved in a large variety of cellular processes beyond nuclear transport, including regulation of gene expression, mRNA export, cellular stress response, and nuclear envelope formation. Interestingly, even a receptor-like function on the cell surface has been described [318]. Without a doubt, the progress in cell biology and imaging techniques will likely further increase the portfolio of different importin-α associated functions in the near future.

Based on these key findings, it was also suggested that importin-α7 could act on viral genome replication and transcription by other means independent of nuclear transport, for example i) by promoting polymerase assembly in a chaperone-like manner (**Figure 39**, concept III: *Polymerase assembly*) or ii) by regulating the nuclear-cytoplasmic trafficking of viral mRNAs (**Figure 39**, concept IV: *Viral mRNA export*). Furthermore, importin-α7 might act as a scaffold protein that actively recruits other host cell factors to the viral polymerase (**Figure 39**, concept II: *Recruitment of host factor*) [237, 318, 327, 407].

As already described above, the concept that importin-α7 might bridge the transcribing IAV polymerase, for example by interaction with PB2 or NP, with the cellular cap-binding complex and thereby promotes export of viral mRNAs, is intriguing. Importantly, there is some evidence from the literature as well as from another independent study in our laboratory supporting this theory. First of all, in a pivotal publication by Dias *et al.*, the authors established the structural basis for importin-α/importin-β_1-mediated nuclear export of cellular mRNAs [327]. Herein, they showed that inside the nucleus importin-α interacts with the larger subunit NCBP1 (CBP80) of the CBC complex, which itself binds to newly synthesized, capped mRNAs via the smaller NCBP2 (CBP20) subunit. After translocation of this macromolecular ribonucleoprotein complex through the NPC into the cytoplasm, importin-α recruits importin-β_1 via its IBB domain, which in turn binds to NCBP2 and displaces the mRNA from the complex [327]. Thus, both importin-α and importin-β_1 are essential components in this process [327, 408]. In another study, RNA immunoprecipitation experiments revealed an interaction of viral mRNAs with the CBC, from which the authors concluded that viral mRNAs exploit the same pathways used by cellular mRNAs for nuclear export [385].

Importin-α7 was shown to strongly interact with human-type ($PB2_{627K}$) influenza vRNPs, likely via the NLS motifs present in PB2 and NP, although other yet unknown interaction sites might exist [251]. However, it is currently unknown whether importin-α7 stays attached or re-associates with the viral polymerase after nuclear import. If true, this would further strengthen the concept that importin-α7 creates a scaffold that brings together the actively transcribing IAV polymerase and the CBC for nuclear export of viral mRNAs (**Figure 39**, concept IV: *Viral mRNA export*).

Indeed, experimental evidence exists that supports this concept. First, as shown in this study, importin-α7-ΔIBB and, to less extend, importin-α7-WT interacted with NCBP1 in infected cells. Similarly, the viral PB2 protein also bound more strongly to importin-α7 lacking the IBB domain. These data suggest that both, NCBP1 and viral PB2, form a stable complex with importin-α7-ΔIBB that can no longer be dissociated by binding to importin-β_1 in the cytoplasm. Final molecular evidence for the presented hypothesis was obtained in a separate study. Here, it was shown that overexpression of an importin-α7 variant with a single isoleucine-to-methionine

amino acid substitution at position 162 (I162M) could even further increase viral polymerase activity compared to the WT importin-α7 protein (*unpublished data*). Importantly, co-immunoprecipitation experiments also revealed a stronger interaction of this importin-α7 mutant with cellular NCBP1, albeit this has yet to be confirmed during influenza infection.

Collectively, these findings highlight the importance of future studies to determine whether the interplay between the viral polymerase, importin-α7 and the CBC is functionally conserved to enhance the synthesis of viral proteins and thereby promote high-level influenza virus replication in human cells.

Figure 39 illustrates the current concepts and theories that might provide further insights into the molecular mechanism underlying importin-α7 function during IAV infection in mammals.

6.3 Species-dependent ability of ANP32 proteins to promote IAV replication and pathogenesis in mammals

Influenza A virus cross-species transmission from birds to mammals continues to pose a major threat to human health. In light of the next influenza pandemic which can strike at any time and may claim up to 80 million lives worldwide, according to predictions by WHO, it is fundamentally important to decipher the dynamic and complex virus-host interactions that drive IAV interspecies transmission, as well as to identify novel targets for therapeutic interventions.

One particular group of host factors, members of the ANP32 protein family (ANP32A, ANP32B), was recently identified to promote animal-to-man transmission of IAV [252]. Moreover, mammalian, including human ANP32 proteins were shown to be important for efficient human-type influenza virus replication in human cells [252]. However, these factors were initially studied in cell culture only and thus their contribution to IAV replication and pathogenicity in mammals remains unknown. In the present study, this important question was addressed using an *in vivo* influenza infection model and mice lacking either the ANP32A or ANP32B gene. The obtained results will be discussed in the following chapter with respect to the species-dependent differences in ANP32 function during influenza infection.

6.3.1 Differential role of ANP32A and ANP32B during influenza infection in mammalian hosts

Since their initial discovery, ANP32 proteins have become a major focus in influenza research. However, their role in human-type ($PB2_{627K}$) IAV replication and pathogenicity remained unknown to this day, mainly due to the lack of appropriate animal models. Here, first evidence was now obtained regarding the *in vivo* relevance of these factors during influenza infection by

using ANP32A or ANP32B knockout mice. Importantly, absence of ANP32A did not affect high-titer IAV replication, virus-induced cytokine responses or pathogenicity of both seasonal (H3N2) and highly pathogenic avian (H5N1) IAV in mice. These results strongly suggest that ANP32A, although it might play a role in cross-species transmission, is not required for efficient replication of IAV carrying adaptive mutations in mammals. At first sight, these observations seem to be contradictive to the initial studies using human cell lines. There, the authors demonstrated that reduction of ANP32A expression levels by siRNA significantly decreased viral polymerase activity and the production of virus progeny [252]. However, these findings were challenged by recent reports showing that IAV with the mammalian-adaptive $PB2_{627K}$ signature replicate efficiently in human cells deficient for ANP32A [304-306]. Interestingly, Liang *et al.* further provided evidence that the presence of ANP32A might correlate with the ability of an avian-type ($PB2_{627E}$) IAV polymerase to acquire the adaptive $PB2_{627K}$ signature, a phenotype that is often observed after human infection with HPAIV, such as H5N1 and H7N9 [127, 179, 304]. Particularly, it was shown that knockout of ANP32A in mice forced an avian-type H7N9 influenza virus to switch from $PB2_{E627K}$ to $PB2_{D701N}$ host adaptation [304]. These findings are further collaborated by another study in which the authors investigated the role ANP32A on intraspecies adaptation of influenza viruses within their avian reservoir. Using a mathematical approach to model the evolution of avian-type IAV in dependency of ANP32A, Domingues *and colleagues* proposed that differential ANP32A splicing and expression patterns within different bird species pose a selection pressure that drives influenza adaptation in avian hosts [301]. These results, together with the fact that AIV replication was highly restricted in avian cells lacking ANP32A, suggest that targeting ANP32A expression particularly in domestic poultry might present a viable approach to inhibit IAV replication in this intermediate host and thus prevent viral spread to the human population [303]. Nevertheless, further studies also involving infection experiments with live poultry are required to support this concept.

In the study by Staller *et al.,* the authors also investigated the ability of ANP32A proteins from different mammalian species to promote $PB2_{627K}$ IAV polymerase activity in human cells. Interestingly, it was demonstrated that a critical aspartate residue at position 130 was linked to species-dependent differences in ANP32A function. In contrast to human ANP32A, the murine ANP32A homologue contains an alanine at this position which renders it inactive in promoting high-level virus polymerase activity in human cells [305]. These data might explain why ANP32A deficiency did not influence viral replication or pathogenicity in mice, as shown in the present study. Future studies, including the use of primary human lung epithelial cells, are therefore urgently required to decipher the exact contribution of ANP32A to influenza disease outcome in humans.

While murine ANP32A was dispensable for seasonal or HPAIV replication and pathogenicity, this study could show for the first time that mice lacking the ANP32B gene are protected from otherwise lethal H3N2 and H5N1 influenza infection. Both, reduced viral replication and significantly diminished pro-inflammatory immune responses were herein identified as correlates of protection. Importantly, knockout of ANP32B in human HeLa cells also impaired viral replication, albeit not as prominently as observed in murine cells lacking ANP32B. Although cell type-specific effects cannot be excluded, this observation is likely based on the fact that human ANP32A, which like murine and human ANP32B contains the potent aspartate residue at position 130, is still expressed in the ANP32B-deficient HeLa cells. Nevertheless, knockout of human ANP32B still significantly reduced viral replication even in the presence of ANP32A, in contrast to what has been observed in ANP32A knockout cells [304-306]. Hence, these findings suggest that the viral polymerase has evolved to co-opt ANP32B preferentially over ANP32A for viral replication in human cells. Thus, further in-depth studies using primary cells are required in the future to dissect the individual contribution of ANP32A and ANP32B to influenza pathogenesis in humans.

It has been suggested by others that ANP32 proteins directly promote IAV replication by acting as co-factors for the viral polymerase, particularly in the process of vRNA synthesis from the cRNA intermediate, and thereby contribute to viral pathogenesis in mammalian hosts [299, 302, 307, 383]. In line, knockout of ANP32B in either murine or human cell culture significantly decreased viral replication, favoring the concept of a direct function. This is further supported by the finding that ANP32B deficiency reduces viral NP expression in human cells. Although several theories on ANP32 function are currently discussed [94], the exact molecular mechanism underlying the direct ANP32B (and ANP32A?) mode-of-action remains to be determined.

Although H3N2 and H5N1 viral replication was 10-fold reduced in mice lacking the ANP32B gene, compared to the wild type ANP32B$^{+/+}$ littermates, both viral subtypes still replicated to high titers which would be expected to result in lethal outcome. However, ANP32B$^{-/-}$ mice showed significantly increased survival from 10 to 80 %, particularly after high-dose or low dose-dose challenge with H3N2 or H5N1 IAV, respectively. Therefore, in the next step, the virus-induced immune response was analyzed as another key parameter of viral pathogenesis. Surprisingly, using various methods to determine the expression levels of pro-inflammatory cytokines and chemokines (IFN-α, TNF-α, IL-6, MCP-1, IL-1β, IFN-β1, CXCL10), antiviral transcription factors (IRF-7) and effector proteins (Mx-1), including genome-wide transcriptome analysis, it could be shown that survival of ANP32B$^{-/-}$ mice correlated with a global reprogramming of immune activation upon influenza infection. In particular, a shift towards an adequate, more beneficial

immune response was observed that ultimately enhanced survival of the mice even in the presence of high-titer virus replication. Of note, increased expression of the anti-inflammatory cytokine IL-10 might be involved in this process [409]. Furthermore, it should be highlighted that expression of most of the pro-inflammatory genes assessed is regulated by NF-κB, a major player in antiviral immunity [410, 411].

Altogether, these data suggest that ANP32B deficiency protects mice from lethal influenza infection by reducing viral replication and dampening the host immune response (**Figure 40**). Herein, ANP32B itself might possess an immune-regulatory function, which could be linked to regulation of NF-κB activity upon viral infection. This novel finding as well as its implications for antiviral drug design by targeting host factors will be further discussed in the next chapter.

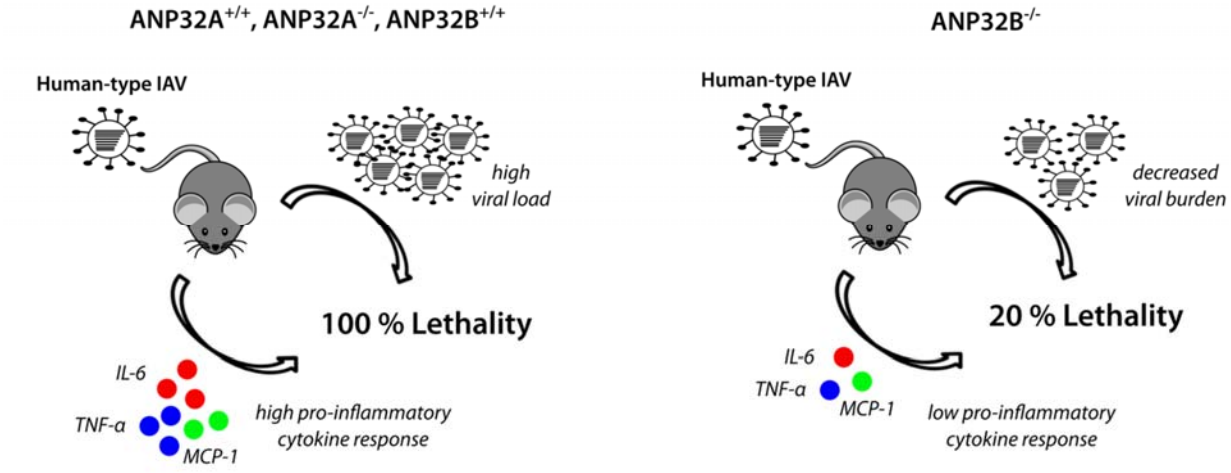

Figure 40: Molecular mechanisms of IAV pathogenesis in ANP32B deficient mice. Left panel, ANP32A wild type (ANP32A$^{+/+}$) or knockout (ANP32A$^{-/-}$) mice as well as mice expressing the ANP32B gene (ANP32B$^{+/+}$) succumb to influenza A virus infection due to high virus load and pro-inflammatory cytokine responses ('cytokine storm'). **Right panel,** In contrast, survival of ANP32B$^{-/-}$ mice upon human-type (PB2$_{627K}$) influenza A virus infection correlates with decreased viral burden and global suppression of pro-inflammatory cytokines responses.

6.3.2 Is ANP32B as a novel key regulator of inflammation and immunity in mice?

In humans, ANP32B shares approximately 80 % amino acid sequence similarity with its closely related family member ANP32A, yet both proteins are associated with diverse functions in the cell. Due to the high degree of conservation between human and murine ANP32 proteins (>80 %), it is likely that both ANP32A and ANP32B also fulfill distinct functions in mice.

Based on studies using human cell lines or knockout mouse models, particularly ANP32B was identified as a master regulator in the cell that is involved in various cellular processes, including: i) inhibition of gene expression by binding to histones (H3-H4) and/or transcription factors (e.g. Kruppel-like factor 5, KLF5) [412, 413], ii) negative regulation of apoptosis by inhibiting caspase-3 activation [414, 415], iii) export of cellular as well as viral mRNAs with adenosine-rich elements [416-419], iv) activation of dendritic cells by promoting CD83 expression [419, 420], and v) regulation of cell proliferation and tumorigenesis by modulating AKT activity [421]. In a recent study by Chemnitz *et al*., using a conditional ANP32B knockout mouse line the authors further demonstrated that ANP32B is involved in enhancing adaptive immune responses in an experimental model of autoimmune encephalomyelitis, albeit the molecular mechanism is still unknown [352]. On the other hand, using the same mouse model in this study, it could be shown that ANP32B deficiency leads to a significant decrease in (innate) immune activation upon influenza challenge. Collectively, these observations imply that ANP32B differentially modulates key innate and adaptive immunity pathways in dependency of the respective stimulus applied.

In the case of influenza infection, the immunopathology that, in addition to active viral replication, largely contributes to the development of ARDS and lethal disease outcome is severely reduced in mice lacking the ANP32B gene. Future studies should therefore attempt to unravel the molecular mechanisms underlying ANP32B-mediated modulation of cellular immunity in the context of viral infection and/or other human diseases. In particular, the role of NF-κB activation in this process needs to be further investigated. As shown by Yang *and colleagues*, PI3K (*phosphatidylinositol 3-kinase*) – induced phosphorylation of the AKT kinase, a known activator of NF-κB, is strongly downregulated in the absence of ANP32B [422-424]. Furthermore, it is known that the PI3K-pathway itself is activated during several stages of the influenza replication cycle [425]. Thus, the cross-talk between ANP32B, AKT and NF-kB might be an important axis during influenza infection that could present a novel therapeutic target to prevent virus-induced immunopathology and death in humans.

6.4 Conclusion

This study aimed to provide mechanistic insights into the molecular function of two major families of host cell factors that promote human-type IAV polymerase activity, replicative fitness and pathogenicity in mammals: Importin-α isoforms, particularly importin-α7, and ANP32 proteins. An unbiased, SILAC-based MS approach was successfully established to investigate the interplay between importin-α7 and ANP32A during IAV infection in human cells. Herein, it was shown that both proteins act independently of each other on viral replication. Furthermore, it could be demonstrated that ANP32B, in contrast to ANP32A, promotes high-titer IAV replication and pathogenicity in mice.

Future studies are urgently required to decipher the detailed mechanisms by which human importin-α7 and ANP32B promote human-type IAV replication and pathogenesis. Ultimately, these findings might support the development of novel treatment strategies against severe influenza in humans.

7. Literature

1. Hause, B.M., et al., *Characterization of a novel influenza virus in cattle and Swine: proposal for a new genus in the Orthomyxoviridae family.* mBio, 2014. **5**(2): p. e00031-14.
2. Presti, R.M., et al., *Quaranfil, Johnston Atoll, and Lake Chad viruses are novel members of the family Orthomyxoviridae.* J Virol, 2009. **83**(22): p. 11599-606.
3. Tong, S., et al., *A distinct lineage of influenza A virus from bats.* Proc Natl Acad Sci U S A, 2012. **109**(11): p. 4269-74.
4. Tong, S., et al., *New world bats harbor diverse influenza A viruses.* PLoS Pathog, 2013. **9**(10): p. e1003657.
5. Webster, R.G., et al., *Evolution and ecology of influenza A viruses.* Microbiol Rev, 1992. **56**(1): p. 152-79.
6. Bouvier, N.M. and P. Palese, *The biology of influenza viruses.* Vaccine, 2008. **26 Suppl 4**: p. D49-53.
7. Noda, T., *Native morphology of influenza virions.* Front Microbiol, 2011. **2**: p. 269.
8. Noda, T. and Y. Kawaoka, *Structure of influenza virus ribonucleoprotein complexes and their packaging into virions.* Rev Med Virol, 2010. **20**(6): p. 380-91.
9. Hutchinson, E.C., et al., *Conserved and host-specific features of influenza virion architecture.* Nat Commun, 2014. **5**: p. 4816.
10. Shaw, M.L., et al., *Cellular proteins in influenza virus particles.* PLoS Pathog, 2008. **4**(6): p. e1000085.
11. Arranz, R., et al., *The structure of native influenza virion ribonucleoproteins.* Science, 2012. **338**(6114): p. 1634-7.
12. Moeller, A., et al., *Organization of the influenza virus replication machinery.* Science, 2012. **338**(6114): p. 1631-4.
13. Pflug, A., et al., *Structure of influenza A polymerase bound to the viral RNA promoter.* Nature, 2014. **516**(7531): p. 355-60.
14. Naffakh, N., et al., *Host restriction of avian influenza viruses at the level of the ribonucleoproteins.* Annu Rev Microbiol, 2008. **62**: p. 403-24.
15. Flick, R. and G. Hobom, *Interaction of influenza virus polymerase with viral RNA in the 'corkscrew' conformation.* J Gen Virol, 1999. **80 (Pt 10)**: p. 2565-72.
16. Horimoto, T. and Y. Kawaoka, *Influenza: lessons from past pandemics, warnings from current incidents.* Nat Rev Microbiol, 2005. **3**(8): p. 591-600.
17. Chen, W., et al., *A novel influenza A virus mitochondrial protein that induces cell death.* Nat Med, 2001. **7**(12): p. 1306-12.
18. Conenello, G.M., et al., *A single mutation in the PB1-F2 of H5N1 (HK/97) and 1918 influenza A viruses contributes to increased virulence.* PLoS Pathog, 2007. **3**(10): p. 1414-21.
19. Yamayoshi, S., et al., *Identification of a Novel Viral Protein Expressed from the PB2 Segment of Influenza A Virus.* J Virol, 2016. **90**(1): p. 444-56.
20. Wise, H.M., et al., *A complicated message: Identification of a novel PB1-related protein translated from influenza A virus segment 2 mRNA.* J Virol, 2009. **83**(16): p. 8021-31.

21. Jagger, B.W., et al., *An overlapping protein-coding region in influenza A virus segment 3 modulates the host response.* Science, 2012. **337**(6091): p. 199-204.
22. Bavagnoli, L., et al., *The novel influenza A virus protein PA-X and its naturally deleted variant show different enzymatic properties in comparison to the viral endonuclease PA.* Nucleic Acids Res, 2015. **43**(19): p. 9405-17.
23. Muramoto, Y., et al., *Identification of novel influenza A virus proteins translated from PA mRNA.* J Virol, 2013. **87**(5): p. 2455-62.
24. Wise, H.M., et al., *Identification of a novel splice variant form of the influenza A virus M2 ion channel with an antigenically distinct ectodomain.* PLoS Pathog, 2012. **8**(11): p. e1002998.
25. Dias, A., et al., *The cap-snatching endonuclease of influenza virus polymerase resides in the PA subunit.* Nature, 2009. **458**(7240): p. 914-8.
26. Selman, M., et al., *Adaptive mutation in influenza A virus non-structural gene is linked to host switching and induces a novel protein by alternative splicing.* Emerg Microbes Infect, 2012. **1**(11): p. e42.
27. Neumann, G., T. Noda, and Y. Kawaoka, *Emergence and pandemic potential of swine-origin H1N1 influenza virus.* Nature, 2009. **459**(7249): p. 931-9.
28. Weis, W., et al., *Structure of the influenza virus haemagglutinin complexed with its receptor, sialic acid.* Nature, 1988. **333**(6172): p. 426-31.
29. Couceiro, J.N., J.C. Paulson, and L.G. Baum, *Influenza virus strains selectively recognize sialyloligosaccharides on human respiratory epithelium; the role of the host cell in selection of hemagglutinin receptor specificity.* Virus Res, 1993. **29**(2): p. 155-65.
30. Matrosovich, M.N., et al., *Human and avian influenza viruses target different cell types in cultures of human airway epithelium.* Proc Natl Acad Sci U S A, 2004. **101**(13): p. 4620-4.
31. van Riel, D., et al., *Human and avian influenza viruses target different cells in the lower respiratory tract of humans and other mammals.* Am J Pathol, 2007. **171**(4): p. 1215-23.
32. Tumpey, T.M., et al., *A two-amino acid change in the hemagglutinin of the 1918 influenza virus abolishes transmission.* Science, 2007. **315**(5812): p. 655-9.
33. Klenk, H.D., et al., *Activation of influenza A viruses by trypsin treatment.* Virology, 1975. **68**(2): p. 426-39.
34. Lazarowitz, S.G. and P.W. Choppin, *Enhancement of the infectivity of influenza A and B viruses by proteolytic cleavage of the hemagglutinin polypeptide.* Virology, 1975. **68**(2): p. 440-54.
35. Chen, C. and X. Zhuang, *Epsin 1 is a cargo-specific adaptor for the clathrin-mediated endocytosis of the influenza virus.* Proc Natl Acad Sci U S A, 2008. **105**(33): p. 11790-5.
36. Rust, M.J., et al., *Assembly of endocytic machinery around individual influenza viruses during viral entry.* Nat Struct Mol Biol, 2004. **11**(6): p. 567-73.
37. de Vries, E., et al., *Dissection of the influenza A virus endocytic routes reveals macropinocytosis as an alternative entry pathway.* PLoS Pathog, 2011. **7**(3): p. e1001329.
38. Sieczkarski, S.B. and G.R. Whittaker, *Influenza virus can enter and infect cells in the absence of clathrin-mediated endocytosis.* J Virol, 2002. **76**(20): p. 10455-64.
39. Lakadamyali, M., M.J. Rust, and X. Zhuang, *Endocytosis of influenza viruses.* Microbes Infect, 2004. **6**(10): p. 929-36.

40. Helenius, A., *Unpacking the incoming influenza virus.* Cell, 1992. **69**(4): p. 577-8.
41. Hay, A.J., et al., *The molecular basis of the specific anti-influenza action of amantadine.* EMBO J, 1985. **4**(11): p. 3021-4.
42. Martin, K. and A. Helenius, *Nuclear transport of influenza virus ribonucleoproteins: the viral matrix protein (M1) promotes export and inhibits import.* Cell, 1991. **67**(1): p. 117-30.
43. Bui, M., G. Whittaker, and A. Helenius, *Effect of M1 protein and low pH on nuclear transport of influenza virus ribonucleoproteins.* J Virol, 1996. **70**(12): p. 8391-401.
44. Stewart, M., *Molecular mechanism of the nuclear protein import cycle.* Nat Rev Mol Cell Biol, 2007. **8**(3): p. 195-208.
45. Cros, J.F., A. Garcia-Sastre, and P. Palese, *An unconventional NLS is critical for the nuclear import of the influenza A virus nucleoprotein and ribonucleoprotein.* Traffic, 2005. **6**(3): p. 205-13.
46. O'Neill, R.E., et al., *Nuclear import of influenza virus RNA can be mediated by viral nucleoprotein and transport factors required for protein import.* J Biol Chem, 1995. **270**(39): p. 22701-4.
47. Tarendeau, F., et al., *Structure and nuclear import function of the C-terminal domain of influenza virus polymerase PB2 subunit.* Nat Struct Mol Biol, 2007. **14**(3): p. 229-33.
48. Pumroy, R.A., et al., *Molecular determinants for nuclear import of influenza A PB2 by importin alpha isoforms 3 and 7.* Structure, 2015. **23**(2): p. 374-84.
49. Hutchinson, E.C. and E. Fodor, *Nuclear import of the influenza A virus transcriptional machinery.* Vaccine, 2012. **30**(51): p. 7353-8.
50. Gabriel, G., et al., *Differential use of importin-alpha isoforms governs cell tropism and host adaptation of influenza virus.* Nat Commun, 2011. **2**: p. 156.
51. Reich, S., D. Guilligay, and S. Cusack, *An in vitro fluorescence based study of initiation of RNA synthesis by influenza B polymerase.* Nucleic Acids Res, 2017. **45**(6): p. 3353-3368.
52. Fodor, E., *The RNA polymerase of influenza a virus: mechanisms of viral transcription and replication.* Acta Virol, 2013. **57**(2): p. 113-22.
53. Portela, A. and P. Digard, *The influenza virus nucleoprotein: a multifunctional RNA-binding protein pivotal to virus replication.* J Gen Virol, 2002. **83**(Pt 4): p. 723-34.
54. Engelhardt, O.G., M. Smith, and E. Fodor, *Association of the influenza A virus RNA-dependent RNA polymerase with cellular RNA polymerase II.* J Virol, 2005. **79**(9): p. 5812-8.
55. Martinez-Alonso, M., N. Hengrung, and E. Fodor, *RNA-Free and Ribonucleoprotein-Associated Influenza Virus Polymerases Directly Bind the Serine-5-Phosphorylated Carboxyl-Terminal Domain of Host RNA Polymerase II.* J Virol, 2016. **90**(13): p. 6014-6021.
56. Lukarska, M., et al., *Structural basis of an essential interaction between influenza polymerase and Pol II CTD.* Nature, 2017. **541**(7635): p. 117-121.
57. Guilligay, D., et al., *The structural basis for cap binding by influenza virus polymerase subunit PB2.* Nat Struct Mol Biol, 2008. **15**(5): p. 500-6.
58. Reich, S., et al., *Structural insight into cap-snatching and RNA synthesis by influenza polymerase.* Nature, 2014. **516**(7531): p. 361-6.
59. Robertson, J.S., M. Schubert, and R.A. Lazzarini, *Polyadenylation sites for influenza virus mRNA.* J Virol, 1981. **38**(1): p. 157-63.

60. Poon, L.L., et al., *Direct evidence that the poly(A) tail of influenza A virus mRNA is synthesized by reiterative copying of a U track in the virion RNA template.* J Virol, 1999. **73**(4): p. 3473-6.
61. Dou, D., et al., *Influenza A Virus Cell Entry, Replication, Virion Assembly and Movement.* Front Immunol, 2018. **9**: p. 1581.
62. Inglis, S.C. and C.M. Brown, *Spliced and unspliced RNAs encoded by virion RNA segment 7 of influenza virus.* Nucleic Acids Res, 1981. **9**(12): p. 2727-40.
63. Lamb, R.A., et al., *Mapping of the two overlapping genes for polypeptides NS1 and NS2 on RNA segment 8 of influenza virus genome.* Proc Natl Acad Sci U S A, 1980. **77**(4): p. 1857-61.
64. Lamb, R.A. and C.J. Lai, *Sequence of interrupted and uninterrupted mRNAs and cloned DNA coding for the two overlapping nonstructural proteins of influenza virus.* Cell, 1980. **21**(2): p. 475-85.
65. Lamb, R.A., C.J. Lai, and P.W. Choppin, *Sequences of mRNAs derived from genome RNA segment 7 of influenza virus: colinear and interrupted mRNAs code for overlapping proteins.* Proc Natl Acad Sci U S A, 1981. **78**(7): p. 4170-4.
66. Ayllon, J. and A. Garcia-Sastre, *The NS1 protein: a multitasking virulence factor.* Curr Top Microbiol Immunol, 2015. **386**: p. 73-107.
67. Pflug, A., et al., *Structural insights into RNA synthesis by the influenza virus transcription-replication machine.* Virus Res, 2017. **234**: p. 103-117.
68. Newcomb, L.L., et al., *Interaction of the influenza a virus nucleocapsid protein with the viral RNA polymerase potentiates unprimed viral RNA replication.* J Virol, 2009. **83**(1): p. 29-36.
69. York, A., et al., *Isolation and characterization of the positive-sense replicative intermediate of a negative-strand RNA virus.* Proc Natl Acad Sci U S A, 2013. **110**(45): p. E4238-45.
70. Resa-Infante, P., et al., *The influenza virus RNA synthesis machine: advances in its structure and function.* RNA Biol, 2011. **8**(2): p. 207-15.
71. Neumann, G., M.T. Hughes, and Y. Kawaoka, *Influenza A virus NS2 protein mediates vRNP nuclear export through NES-independent interaction with hCRM1.* EMBO J, 2000. **19**(24): p. 6751-8.
72. Shimizu, T., et al., *Crucial role of the influenza virus NS2 (NEP) C-terminal domain in M1 binding and nuclear export of vRNP.* FEBS Lett, 2011. **585**(1): p. 41-6.
73. Akarsu, H., et al., *Crystal structure of the M1 protein-binding domain of the influenza A virus nuclear export protein (NEP/NS2).* EMBO J, 2003. **22**(18): p. 4646-55.
74. Amorim, M.J., et al., *A Rab11- and microtubule-dependent mechanism for cytoplasmic transport of influenza A virus viral RNA.* J Virol, 2011. **85**(9): p. 4143-56.
75. Daniels, R., et al., *N-linked glycans direct the cotranslational folding pathway of influenza hemagglutinin.* Mol Cell, 2003. **11**(1): p. 79-90.
76. Bos, T.J., A.R. Davis, and D.P. Nayak, *NH2-terminal hydrophobic region of influenza virus neuraminidase provides the signal function in translocation.* Proc Natl Acad Sci U S A, 1984. **81**(8): p. 2327-31.
77. Dou, D., et al., *Type II transmembrane domain hydrophobicity dictates the cotranslational dependence for inversion.* Mol Biol Cell, 2014. **25**(21): p. 3363-74.

78. Hull, J.D., R. Gilmore, and R.A. Lamb, *Integration of a small integral membrane protein, M2, of influenza virus into the endoplasmic reticulum: analysis of the internal signal-anchor domain of a protein with an ectoplasmic NH2 terminus.* J Cell Biol, 1988. **106**(5): p. 1489-98.
79. Wang, N., et al., *The cotranslational maturation program for the type II membrane glycoprotein influenza neuraminidase.* J Biol Chem, 2008. **283**(49): p. 33826-37.
80. Hebert, D.N., et al., *The number and location of glycans on influenza hemagglutinin determine folding and association with calnexin and calreticulin.* J Cell Biol, 1997. **139**(3): p. 613-23.
81. Saito, T., G. Taylor, and R.G. Webster, *Steps in maturation of influenza A virus neuraminidase.* J Virol, 1995. **69**(8): p. 5011-7.
82. Tatu, U., C. Hammond, and A. Helenius, *Folding and oligomerization of influenza hemagglutinin in the ER and the intermediate compartment.* EMBO J, 1995. **14**(7): p. 1340-8.
83. Stieneke-Grober, A., et al., *Influenza virus hemagglutinin with multibasic cleavage site is activated by furin, a subtilisin-like endoprotease.* EMBO J, 1992. **11**(7): p. 2407-14.
84. Bottcher, E., et al., *Proteolytic activation of influenza viruses by serine proteases TMPRSS2 and HAT from human airway epithelium.* J Virol, 2006. **80**(19): p. 9896-8.
85. Bottcher-Friebertshauser, E., et al., *The hemagglutinin: a determinant of pathogenicity.* Curr Top Microbiol Immunol, 2014. **385**: p. 3-34.
86. Gottschalk, A., *Neuraminidase: the specific enzyme of influenza virus and Vibrio cholerae.* Biochim Biophys Acta, 1957. **23**(3): p. 645-6.
87. Palese, P., et al., *Characterization of temperature sensitive influenza virus mutants defective in neuraminidase.* Virology, 1974. **61**(2): p. 397-410.
88. McAuley, J.L., et al., *Influenza Virus Neuraminidase Structure and Functions.* Front Microbiol, 2019. **10**: p. 39.
89. Stallknecht, D.E. and S.M. Shane, *Host range of avian influenza virus in free-living birds.* Vet Res Commun, 1988. **12**(2-3): p. 125-41.
90. Wahlgren, J., *Influenza A viruses: an ecology review.* Infect Ecol Epidemiol, 2011. **1**.
91. Kida, H., R. Yanagawa, and Y. Matsuoka, *Duck influenza lacking evidence of disease signs and immune response.* Infect Immun, 1980. **30**(2): p. 547-53.
92. Hinshaw, V.S., et al., *Replication of avian influenza A viruses in mammals.* Infect Immun, 1981. **34**(2): p. 354-61.
93. Parrish, C.R., P.R. Murcia, and E.C. Holmes, *Influenza virus reservoirs and intermediate hosts: dogs, horses, and new possibilities for influenza virus exposure of humans.* J Virol, 2015. **89**(6): p. 2990-4.
94. Long, J.S., et al., *Host and viral determinants of influenza A virus species specificity.* Nat Rev Microbiol, 2019. **17**(2): p. 67-81.
95. Drake, J.W., *Rates of spontaneous mutation among RNA viruses.* Proc Natl Acad Sci U S A, 1993. **90**(9): p. 4171-5.
96. Steinhauer, D.A. and J.J. Holland, *Rapid evolution of RNA viruses.* Annu Rev Microbiol, 1987. **41**: p. 409-33.
97. Holland, J., et al., *Rapid evolution of RNA genomes.* Science, 1982. **215**(4540): p. 1577-85.

98. Boni, M.F., *Vaccination and antigenic drift in influenza.* Vaccine, 2008. **26 Suppl 3**: p. C8-14.
99. *https://www.who.int/en/news-room/fact-sheets/detail/influenza-(seasonal), accessed on 03.02.2020*.
100. Beare, A.S. and R.G. Webster, *Replication of avian influenza viruses in humans.* Arch Virol, 1991. **119**(1-2): p. 37-42.
101. Ma, W., R.E. Kahn, and J.A. Richt, *The pig as a mixing vessel for influenza viruses: Human and veterinary implications.* J Mol Genet Med, 2008. **3**(1): p. 158-66.
102. Saunders-Hastings, P.R. and D. Krewski, *Reviewing the History of Pandemic Influenza: Understanding Patterns of Emergence and Transmission.* Pathogens, 2016. **5**(4).
103. Alexander, D.J., *A review of avian influenza in different bird species.* Vet Microbiol, 2000. **74**(1-2): p. 3-13.
104. Horimoto, T., et al., *Proprotein-processing endoproteases PC6 and furin both activate hemagglutinin of virulent avian influenza viruses.* J Virol, 1994. **68**(9): p. 6074-8.
105. Alexander, D.J., G. Parsons, and R.J. Manvell, *Experimental assessment of the pathogenicity of eight avian influenza A viruses of H5 subtype for chickens, turkeys, ducks and quail.* Avian Pathol, 1986. **15**(4): p. 647-62.
106. Mo, I.P., et al., *Comparative pathology of chickens experimentally inoculated with avian influenza viruses of low and high pathogenicity.* Avian Dis, 1997. **41**(1): p. 125-36.
107. Banks, J., et al., *Changes in the haemagglutinin and the neuraminidase genes prior to the emergence of highly pathogenic H7N1 avian influenza viruses in Italy.* Arch Virol, 2001. **146**(5): p. 963-73.
108. Khatchikian, D., M. Orlich, and R. Rott, *Increased viral pathogenicity after insertion of a 28S ribosomal RNA sequence into the haemagglutinin gene of an influenza virus.* Nature, 1989. **340**(6229): p. 156-7.
109. Maurer-Stroh, S., et al., *The highly pathogenic H7N3 avian influenza strain from July 2012 in Mexico acquired an extended cleavage site through recombination with host 28S rRNA.* Virol J, 2013. **10**: p. 139.
110. Orlich, M., H. Gottwald, and R. Rott, *Nonhomologous recombination between the hemagglutinin gene and the nucleoprotein gene of an influenza virus.* Virology, 1994. **204**(1): p. 462-5.
111. Pasick, J., et al., *Intersegmental recombination between the haemagglutinin and matrix genes was responsible for the emergence of a highly pathogenic H7N3 avian influenza virus in British Columbia.* J Gen Virol, 2005. **86**(Pt 3): p. 727-31.
112. Suarez, D.L., et al., *Recombination resulting in virulence shift in avian influenza outbreak, Chile.* Emerg Infect Dis, 2004. **10**(4): p. 693-9.
113. Garcia, M., et al., *Heterogeneity in the haemagglutinin gene and emergence of the highly pathogenic phenotype among recent H5N2 avian influenza viruses from Mexico.* J Gen Virol, 1996. **77 (Pt 7)**: p. 1493-504.
114. Horimoto, T., et al., *Origin and molecular changes associated with emergence of a highly pathogenic H5N2 influenza virus in Mexico.* Virology, 1995. **213**(1): p. 223-30.
115. Perdue, M.L., et al., *Virulence-associated sequence duplication at the hemagglutinin cleavage site of avian influenza viruses.* Virus Res, 1997. **49**(2): p. 173-86.
116. Subbarao, K., et al., *Characterization of an avian influenza A (H5N1) virus isolated from a child with a fatal respiratory illness.* Science, 1998. **279**(5349): p. 393-6.

117. Claas, E.C., et al., *Human influenza A H5N1 virus related to a highly pathogenic avian influenza virus.* Lancet, 1998. **351**(9101): p. 472-7.
118. *https://www.who.int/influenza/human_animal_interface/2019_11_25_tableH5N1.pdf?ua=1, accessed on 03.02.2020*.
119. Yuen, K.Y., et al., *Clinical features and rapid viral diagnosis of human disease associated with avian influenza A H5N1 virus.* Lancet, 1998. **351**(9101): p. 467-71.
120. Peiris, J.S., et al., *Re-emergence of fatal human influenza A subtype H5N1 disease.* Lancet, 2004. **363**(9409): p. 617-9.
121. To, K.F., et al., *Pathology of fatal human infection associated with avian influenza A H5N1 virus.* J Med Virol, 2001. **63**(3): p. 242-6.
122. Peiris, J.S., M.D. de Jong, and Y. Guan, *Avian influenza virus (H5N1): a threat to human health.* Clin Microbiol Rev, 2007. **20**(2): p. 243-67.
123. Murray, C.J., et al., *Estimation of potential global pandemic influenza mortality on the basis of vital registry data from the 1918-20 pandemic: a quantitative analysis.* Lancet, 2006. **368**(9554): p. 2211-8.
124. *https://www.who.int/news-room/detail/11-03-2019-who-launches-new-global-influenza-strategy, accessed on 03.02.2020*.
125. Herfst, S., et al., *Airborne transmission of influenza A/H5N1 virus between ferrets.* Science, 2012. **336**(6088): p. 1534-41.
126. Imai, M., et al., *Experimental adaptation of an influenza H5 HA confers respiratory droplet transmission to a reassortant H5 HA/H1N1 virus in ferrets.* Nature, 2012. **486**(7403): p. 420-8.
127. Gao, R., et al., *Human infection with a novel avian-origin influenza A (H7N9) virus.* N Engl J Med, 2013. **368**(20): p. 1888-97.
128. Yu, H., et al., *Human infection with avian influenza A H7N9 virus: an assessment of clinical severity.* Lancet, 2013. **382**(9887): p. 138-45.
129. *https://www.who.int/csr/don/05-september-2018-ah7n9-china/en/, accessed on 03.02.2020*.
130. Ke, C., et al., *Human Infection with Highly Pathogenic Avian Influenza A(H7N9) Virus, China.* Emerg Infect Dis, 2017. **23**(8): p. 1332-1340.
131. Yu, D., et al., *The re-emergence of highly pathogenic avian influenza H7N9 viruses in humans in mainland China, 2019.* Euro Surveill, 2019. **24**(21).
132. Imai, M., et al., *A Highly Pathogenic Avian H7N9 Influenza Virus Isolated from A Human Is Lethal in Some Ferrets Infected via Respiratory Droplets.* Cell Host Microbe, 2017. **22**(5): p. 615-626 e8.
133. Pu, Z., et al., *Potential Pandemic of H7N9 Avian Influenza A Virus in Human.* Front Cell Infect Microbiol, 2018. **8**: p. 414.
134. Lipsitch, M. and C. Viboud, *Influenza seasonality: lifting the fog.* Proc Natl Acad Sci U S A, 2009. **106**(10): p. 3645-6.
135. Lowen, A.C., et al., *Influenza virus transmission is dependent on relative humidity and temperature.* PLoS Pathog, 2007. **3**(10): p. 1470-6.
136. Shaman, J. and M. Kohn, *Absolute humidity modulates influenza survival, transmission, and seasonality.* Proc Natl Acad Sci U S A, 2009. **106**(9): p. 3243-8.
137. Cauchemez, S., et al., *Estimating the impact of school closure on influenza transmission from Sentinel data.* Nature, 2008. **452**(7188): p. 750-4.

138. Dowell, S.F., *Seasonal variation in host susceptibility and cycles of certain infectious diseases.* Emerg Infect Dis, 2001. **7**(3): p. 369-74.
139. Cannell, J.J., et al., *Epidemic influenza and vitamin D.* Epidemiol Infect, 2006. **134**(6): p. 1129-40.
140. Hirve, S., et al., *Influenza Seasonality in the Tropics and Subtropics - When to Vaccinate?* PLoS One, 2016. **11**(4): p. e0153003.
141. Moura, F.E., *Influenza in the tropics.* Curr Opin Infect Dis, 2010. **23**(5): p. 415-20.
142. *https://www.who.int/news-room/fact-sheets/detail/influenza-(seasonal), accessed on 03.02.2020*.
143. Putri, W., et al., *Economic burden of seasonal influenza in the United States.* Vaccine, 2018. **36**(27): p. 3960-3966.
144. Neumann, G. and Y. Kawaoka, *Transmission of influenza A viruses.* Virology, 2015. **479-480**: p. 234-46.
145. Taubenberger, J.K., *The origin and virulence of the 1918 "Spanish" influenza virus.* Proc Am Philos Soc, 2006. **150**(1): p. 86-112.
146. McAuley, J.L., et al., *Host Immunological Factors Enhancing Mortality of Young Adults during the 1918 Influenza Pandemic.* Front Immunol, 2015. **6**: p. 419.
147. Morens, D.M., J.K. Taubenberger, and A.S. Fauci, *Predominant role of bacterial pneumonia as a cause of death in pandemic influenza: implications for pandemic influenza preparedness.* J Infect Dis, 2008. **198**(7): p. 962-70.
148. Kobasa, D., et al., *Aberrant innate immune response in lethal infection of macaques with the 1918 influenza virus.* Nature, 2007. **445**(7125): p. 319-23.
149. Reid, A.H., et al., *Origin and evolution of the 1918 "Spanish" influenza virus hemagglutinin gene.* Proc Natl Acad Sci U S A, 1999. **96**(4): p. 1651-6.
150. Geiss, G.K., et al., *Cellular transcriptional profiling in influenza A virus-infected lung epithelial cells: the role of the nonstructural NS1 protein in the evasion of the host innate defense and its potential contribution to pandemic influenza.* Proc Natl Acad Sci U S A, 2002. **99**(16): p. 10736-41.
151. Kobasa, D., et al., *Enhanced virulence of influenza A viruses with the haemagglutinin of the 1918 pandemic virus.* Nature, 2004. **431**(7009): p. 703-7.
152. McAuley, J.L., et al., *Expression of the 1918 influenza A virus PB1-F2 enhances the pathogenesis of viral and secondary bacterial pneumonia.* Cell Host Microbe, 2007. **2**(4): p. 240-9.
153. Tumpey, T.M., et al., *Characterization of the reconstructed 1918 Spanish influenza pandemic virus.* Science, 2005. **310**(5745): p. 77-80.
154. Tumpey, T.M., et al., *Existing antivirals are effective against influenza viruses with genes from the 1918 pandemic virus.* Proc Natl Acad Sci U S A, 2002. **99**(21): p. 13849-54.
155. Tumpey, T.M., et al., *Pathogenicity and immunogenicity of influenza viruses with genes from the 1918 pandemic virus.* Proc Natl Acad Sci U S A, 2004. **101**(9): p. 3166-71.
156. Van Hoeven, N., et al., *Human HA and polymerase subunit PB2 proteins confer transmission of an avian influenza virus through the air.* Proc Natl Acad Sci U S A, 2009. **106**(9): p. 3366-71.
157. Watanabe, T., et al., *Viral RNA polymerase complex promotes optimal growth of 1918 virus in the lower respiratory tract of ferrets.* Proc Natl Acad Sci U S A, 2009. **106**(2): p. 588-92.

158. Kawaoka, Y., S. Krauss, and R.G. Webster, *Avian-to-human transmission of the PB1 gene of influenza A viruses in the 1957 and 1968 pandemics.* J Virol, 1989. **63**(11): p. 4603-8.
159. Scholtissek, C., et al., *On the origin of the human influenza virus subtypes H2N2 and H3N2.* Virology, 1978. **87**(1): p. 13-20.
160. Jackson, C., *History lessons: the Asian flu pandemic.* Br J Gen Pract, 2009. **59**(565): p. 622-3.
161. Cockburn, W.C., P.J. Delon, and W. Ferreira, *Origin and progress of the 1968-69 Hong Kong influenza epidemic.* Bull World Health Organ, 1969. **41**(3): p. 345-8.
162. Viboud, C., et al., *Multinational impact of the 1968 Hong Kong influenza pandemic: evidence for a smoldering pandemic.* J Infect Dis, 2005. **192**(2): p. 233-48.
163. Girard, M.P., et al., *The 2009 A (H1N1) influenza virus pandemic: A review.* Vaccine, 2010. **28**(31): p. 4895-902.
164. *https://www.who.int/immunization/newsroom/newsstory_seasonal_influenza_vaccination_pregnancy/en/, accessed on 03.02.2020*.
165. Novel Swine-Origin Influenza, A.V.I.T., et al., *Emergence of a novel swine-origin influenza A (H1N1) virus in humans.* N Engl J Med, 2009. **360**(25): p. 2605-15.
166. Moghadami, M., *A Narrative Review of Influenza: A Seasonal and Pandemic Disease.* Iran J Med Sci, 2017. **42**(1): p. 2-13.
167. Lessler, J., et al., *Incubation periods of acute respiratory viral infections: a systematic review.* Lancet Infect Dis, 2009. **9**(5): p. 291-300.
168. Cate, T.R., *Clinical manifestations and consequences of influenza.* Am J Med, 1987. **82**(6A): p. 15-9.
169. Taubenberger, J.K. and D.M. Morens, *The pathology of influenza virus infections.* Annu Rev Pathol, 2008. **3**: p. 499-522.
170. Mosby, L.G., S.A. Rasmussen, and D.J. Jamieson, *2009 pandemic influenza A (H1N1) in pregnancy: a systematic review of the literature.* Am J Obstet Gynecol, 2011. **205**(1): p. 10-8.
171. Kunisaki, K.M. and E.N. Janoff, *Influenza in immunosuppressed populations: a review of infection frequency, morbidity, mortality, and vaccine responses.* Lancet Infect Dis, 2009. **9**(8): p. 493-504.
172. Ruuskanen, O., et al., *Viral pneumonia.* Lancet, 2011. **377**(9773): p. 1264-75.
173. McElhaney, J.E., et al., *T-Cell Immunity to Influenza in Older Adults: A Pathophysiological Framework for Development of More Effective Vaccines.* Front Immunol, 2016. **7**: p. 41.
174. Fox, T.G. and J.C. Christenson, *Influenza and parainfluenza viral infections in children.* Pediatr Rev, 2014. **35**(6): p. 217-27; quiz 228.
175. Gern, J.E., *Viral respiratory infection and the link to asthma.* Pediatr Infect Dis J, 2004. **23**(1 Suppl): p. S78-86.
176. Guilbert, T.W. and L.C. Denlinger, *Role of infection in the development and exacerbation of asthma.* Expert Rev Respir Med, 2010. **4**(1): p. 71-83.
177. Likos, A.M., et al., *Influenza viremia and the potential for blood-borne transmission.* Transfusion, 2007. **47**(6): p. 1080-8.
178. Beigel, J.H., et al., *Avian influenza A (H5N1) infection in humans.* N Engl J Med, 2005. **353**(13): p. 1374-85.

179. de Jong, M.D., et al., *Fatal outcome of human influenza A (H5N1) is associated with high viral load and hypercytokinemia.* Nat Med, 2006. **12**(10): p. 1203-7.
180. Liu, Q., Y.H. Zhou, and Z.Q. Yang, *The cytokine storm of severe influenza and development of immunomodulatory therapy.* Cell Mol Immunol, 2016. **13**(1): p. 3-10.
181. Wang, G.F., W. Li, and K. Li, *Acute encephalopathy and encephalitis caused by influenza virus infection.* Curr Opin Neurol, 2010. **23**(3): p. 305-11.
182. Tsai, J.P. and A.J. Baker, *Influenza-associated neurological complications.* Neurocrit Care, 2013. **18**(1): p. 118-30.
183. Rezkalla, S.H. and R.A. Kloner, *Influenza-related viral myocarditis.* WMJ, 2010. **109**(4): p. 209-13.
184. Middleton, P.J., R.M. Alexander, and M.T. Szymanski, *Severe myositis during recovery from influenza.* Lancet, 1970. **2**(7672): p. 533-5.
185. Belser, J.A., et al., *The eyes have it: influenza virus infection beyond the respiratory tract.* Lancet Infect Dis, 2018. **18**(7): p. e220-e227.
186. Peltola, V., T. Heikkinen, and O. Ruuskanen, *Clinical courses of croup caused by influenza and parainfluenza viruses.* Pediatr Infect Dis J, 2002. **21**(1): p. 76-8.
187. Halpin, T.J., et al., *Reye's syndrome and medication use.* JAMA, 1982. **248**(6): p. 687-91.
188. Davis, L.E. and M. Kornfeld, *Influenza A virus and Reye's syndrome in adults.* J Neurol Neurosurg Psychiatry, 1980. **43**(6): p. 516-21.
189. Chertow, D.S. and M.J. Memoli, *Bacterial coinfection in influenza: a grand rounds review.* JAMA, 2013. **309**(3): p. 275-82.
190. Florescu, D.F. and A.C. Kalil, *The complex link between influenza and severe sepsis.* Virulence, 2014. **5**(1): p. 137-42.
191. Metersky, M.L., et al., *Epidemiology, microbiology, and treatment considerations for bacterial pneumonia complicating influenza.* Int J Infect Dis, 2012. **16**(5): p. e321-31.
192. Eccles, R., *Understanding the symptoms of the common cold and influenza.* Lancet Infect Dis, 2005. **5**(11): p. 718-25.
193. Perez Rubio, A. and J.M. Eiros, *Cell culture-derived flu vaccine: Present and future.* Hum Vaccin Immunother, 2018. **14**(8): p. 1874-1882.
194. Pandey, A., et al., *Egg-independent vaccine strategies for highly pathogenic H5N1 influenza viruses.* Hum Vaccin, 2010. **6**(2): p. 178-88.
195. Zost, S.J., et al., *Contemporary H3N2 influenza viruses have a glycosylation site that alters binding of antibodies elicited by egg-adapted vaccine strains.* Proc Natl Acad Sci U S A, 2017. **114**(47): p. 12578-12583.
196. Robertson, J.S., et al., *Structural changes in the haemagglutinin which accompany egg adaptation of an influenza A(H1N1) virus.* Virology, 1987. **160**(1): p. 31-7.
197. Palache, A.M., R. Brands, and G.J. van Scharrenburg, *Immunogenicity and reactogenicity of influenza subunit vaccines produced in MDCK cells or fertilized chicken eggs.* J Infect Dis, 1997. **176 Suppl 1**: p. S20-3.
198. Halperin, S.A., A.C. Nestruck, and B.J. Eastwood, *Safety and immunogenicity of a new influenza vaccine grown in mammalian cell culture.* Vaccine, 1998. **16**(13): p. 1331-5.
199. Reisinger, K.S., et al., *Subunit influenza vaccines produced from cell culture or in embryonated chicken eggs: comparison of safety, reactogenicity, and immunogenicity.* J Infect Dis, 2009. **200**(6): p. 849-57.

200. Mameli, C., et al., *Influenza Vaccination: Effectiveness, Indications, and Limits in the Pediatric Population.* Front Pediatr, 2019. **7**: p. 317.
201. Kissling, E., et al., *Effectiveness of influenza vaccine against influenza A in Europe in seasons of different A(H1N1)pdm09 and the same A(H3N2) vaccine components (2016-17 and 2017-18).* Vaccine X, 2019. **3**: p. 100042.
202. *https://www.ecdc.europa.eu/en/seasonal-influenza/season-2017-18, accessed on 04.02.2020*.
203. *https://www.g-ba.de/presse/pressemitteilungen/740/, accessed on 04.02.2020*.
204. Webster, R.G. and E.A. Govorkova, *Continuing challenges in influenza.* Ann N Y Acad Sci, 2014. **1323**: p. 115-39.
205. Moscona, A., *Oseltamivir resistance--disabling our influenza defenses.* N Engl J Med, 2005. **353**(25): p. 2633-6.
206. Wester, A. and A.K. Shetty, *Peramivir injection in the treatment of acute influenza: a review of the literature.* Infect Drug Resist, 2016. **9**: p. 201-14.
207. Bright, R.A., et al., *Adamantane resistance among influenza A viruses isolated early during the 2005-2006 influenza season in the United States.* JAMA, 2006. **295**(8): p. 891-4.
208. Poland, G.A., R.M. Jacobson, and I.G. Ovsyannikova, *Influenza virus resistance to antiviral agents: a plea for rational use.* Clin Infect Dis, 2009. **48**(9): p. 1254-6.
209. Memoli, M.J., et al., *Rapid selection of oseltamivir- and peramivir-resistant pandemic H1N1 virus during therapy in 2 immunocompromised hosts.* Clin Infect Dis, 2010. **50**(9): p. 1252-5.
210. Furuta, Y., T. Komeno, and T. Nakamura, *Favipiravir (T-705), a broad spectrum inhibitor of viral RNA polymerase.* Proc Jpn Acad Ser B Phys Biol Sci, 2017. **93**(7): p. 449-463.
211. Goldhill, D.H., et al., *The mechanism of resistance to favipiravir in influenza.* Proc Natl Acad Sci U S A, 2018. **115**(45): p. 11613-11618.
212. Noshi, T., et al., *In vitro characterization of baloxavir acid, a first-in-class cap-dependent endonuclease inhibitor of the influenza virus polymerase PA subunit.* Antiviral Res, 2018. **160**: p. 109-117.
213. Hayden, F.G., et al., *Baloxavir Marboxil for Uncomplicated Influenza in Adults and Adolescents.* N Engl J Med, 2018. **379**(10): p. 913-923.
214. Gubareva, L.V., et al., *Assessing baloxavir susceptibility of influenza viruses circulating in the United States during the 2016/17 and 2017/18 seasons.* Euro Surveill, 2019. **24**(3).
215. Omoto, S., et al., *Characterization of influenza virus variants induced by treatment with the endonuclease inhibitor baloxavir marboxil.* Sci Rep, 2018. **8**(1): p. 9633.
216. Takashita, E., et al., *Detection of influenza A(H3N2) viruses exhibiting reduced susceptibility to the novel cap-dependent endonuclease inhibitor baloxavir in Japan, December 2018.* Euro Surveill, 2019. **24**(3).
217. Yip, T.F., et al., *Advancements in Host-Based Interventions for Influenza Treatment.* Front Immunol, 2018. **9**: p. 1547.
218. Watanabe, T., et al., *Influenza virus-host interactome screen as a platform for antiviral drug development.* Cell Host Microbe, 2014. **16**(6): p. 795-805.
219. Darwish, I., S. Mubareka, and W.C. Liles, *Immunomodulatory therapy for severe influenza.* Expert Rev Anti Infect Ther, 2011. **9**(7): p. 807-22.

220. Chen, G.W., et al., *Genomic signatures of human versus avian influenza A viruses.* Emerg Infect Dis, 2006. **12**(9): p. 1353-60.
221. Schrauwen, E.J., et al., *Determinants of virulence of influenza A virus.* Eur J Clin Microbiol Infect Dis, 2014. **33**(4): p. 479-90.
222. Rott, R., *The pathogenic determinant of influenza virus.* Vet Microbiol, 1992. **33**(1-4): p. 303-10.
223. Rogers, G.N., et al., *Single amino acid substitutions in influenza haemagglutinin change receptor binding specificity.* Nature, 1983. **304**(5921): p. 76-8.
224. Rogers, G.N. and J.C. Paulson, *Receptor determinants of human and animal influenza virus isolates: differences in receptor specificity of the H3 hemagglutinin based on species of origin.* Virology, 1983. **127**(2): p. 361-73.
225. Matrosovich, M., et al., *Early alterations of the receptor-binding properties of H1, H2, and H3 avian influenza virus hemagglutinins after their introduction into mammals.* J Virol, 2000. **74**(18): p. 8502-12.
226. Shi, Y., et al., *Enabling the 'host jump': structural determinants of receptor-binding specificity in influenza A viruses.* Nat Rev Microbiol, 2014. **12**(12): p. 822-31.
227. Deom, C.M., A.J. Caton, and I.T. Schulze, *Host cell-mediated selection of a mutant influenza A virus that has lost a complex oligosaccharide from the tip of the hemagglutinin.* Proc Natl Acad Sci U S A, 1986. **83**(11): p. 3771-5.
228. Mir-Shekari, S.Y., et al., *The glycosylation of the influenza A virus hemagglutinin by mammalian cells. A site-specific study.* J Biol Chem, 1997. **272**(7): p. 4027-36.
229. Rudneva, I.A., et al., *Restoration of virulence of escape mutants of H5 and H9 influenza viruses by their readaptation to mice.* J Gen Virol, 2005. **86**(Pt 10): p. 2831-8.
230. Stegmann, T., *Membrane fusion mechanisms: the influenza hemagglutinin paradigm and its implications for intracellular fusion.* Traffic, 2000. **1**(8): p. 598-604.
231. Tashiro, M., et al., *Synergistic role of staphylococcal proteases in the induction of influenza virus pathogenicity.* Virology, 1987. **157**(2): p. 421-30.
232. Tashiro, M., et al., *Role of Staphylococcus protease in the development of influenza pneumonia.* Nature, 1987. **325**(6104): p. 536-7.
233. Bottcher-Friebertshauser, E., H.D. Klenk, and W. Garten, *Activation of influenza viruses by proteases from host cells and bacteria in the human airway epithelium.* Pathog Dis, 2013. **69**(2): p. 87-100.
234. Sun, X., J.A. Belser, and T.M. Tumpey, *A novel eight amino acid insertion contributes to the hemagglutinin cleavability and the virulence of a highly pathogenic avian influenza A (H7N3) virus in mice.* Virology, 2016. **488**: p. 120-8.
235. Gabriel, G. and E. Fodor, *Molecular determinants of pathogenicity in the polymerase complex.* Curr Top Microbiol Immunol, 2014. **385**: p. 35-60.
236. Subbarao, E.K., W. London, and B.R. Murphy, *A single amino acid in the PB2 gene of influenza A virus is a determinant of host range.* J Virol, 1993. **67**(4): p. 1761-4.
237. Resa-Infante, P. and G. Gabriel, *The nuclear import machinery is a determinant of influenza virus host adaptation.* Bioessays, 2013. **35**(1): p. 23-7.
238. Gabriel, G., et al., *The viral polymerase mediates adaptation of an avian influenza virus to a mammalian host.* Proc Natl Acad Sci U S A, 2005. **102**(51): p. 18590-5.
239. Steel, J., et al., *Transmission of influenza virus in a mammalian host is increased by PB2 amino acids 627K or 627E/701N.* PLoS Pathog, 2009. **5**(1): p. e1000252.

240. Hatta, M., et al., *Molecular basis for high virulence of Hong Kong H5N1 influenza A viruses.* Science, 2001. **293**(5536): p. 1840-2.
241. Bortz, E., et al., *Host- and strain-specific regulation of influenza virus polymerase activity by interacting cellular proteins.* mBio, 2011. **2**(4).
242. Shinya, K., et al., *PB2 amino acid at position 627 affects replicative efficiency, but not cell tropism, of Hong Kong H5N1 influenza A viruses in mice.* Virology, 2004. **320**(2): p. 258-66.
243. Zhou, B., et al., *Asparagine substitution at PB2 residue 701 enhances the replication, pathogenicity, and transmission of the 2009 pandemic H1N1 influenza A virus.* PLoS One, 2013. **8**(6): p. e67616.
244. Bogs, J., et al., *Reversion of PB2-627E to -627K during replication of an H5N1 Clade 2.2 virus in mammalian hosts depends on the origin of the nucleoprotein.* J Virol, 2011. **85**(20): p. 10691-8.
245. Salomon, R., et al., *The polymerase complex genes contribute to the high virulence of the human H5N1 influenza virus isolate A/Vietnam/1203/04.* J Exp Med, 2006. **203**(3): p. 689-97.
246. Taubenberger, J.K., et al., *Characterization of the 1918 influenza virus polymerase genes.* Nature, 2005. **437**(7060): p. 889-93.
247. Gao, Y., et al., *Identification of amino acids in HA and PB2 critical for the transmission of H5N1 avian influenza viruses in a mammalian host.* PLoS Pathog, 2009. **5**(12): p. e1000709.
248. Richard, M., et al., *Limited airborne transmission of H7N9 influenza A virus between ferrets.* Nature, 2013. **501**(7468): p. 560-3.
249. Mehle, A. and J.A. Doudna, *Adaptive strategies of the influenza virus polymerase for replication in humans.* Proc Natl Acad Sci U S A, 2009. **106**(50): p. 21312-6.
250. Gabriel, G., A. Herwig, and H.D. Klenk, *Interaction of polymerase subunit PB2 and NP with importin alpha1 is a determinant of host range of influenza A virus.* PLoS Pathog, 2008. **4**(2): p. e11.
251. Hudjetz, B. and G. Gabriel, *Human-like PB2 627K influenza virus polymerase activity is regulated by importin-alpha1 and -alpha7.* PLoS Pathog, 2012. **8**(1): p. e1002488.
252. Long, J.S., et al., *Species difference in ANP32A underlies influenza A virus polymerase host restriction.* Nature, 2016. **529**(7584): p. 101-4.
253. Manz, B., M. Schwemmle, and L. Brunotte, *Adaptation of avian influenza A virus polymerase in mammals to overcome the host species barrier.* J Virol, 2013. **87**(13): p. 7200-9.
254. Baz, M., et al., *Synergistic PA and HA mutations confer mouse adaptation of a contemporary A/H3N2 influenza virus.* Sci Rep, 2019. **9**(1): p. 16616.
255. Nguyen, H.T., A.M. Fry, and L.V. Gubareva, *Neuraminidase inhibitor resistance in influenza viruses and laboratory testing methods.* Antivir Ther, 2012. **17**(1 Pt B): p. 159-73.
256. Hai, R., et al., *Influenza A(H7N9) virus gains neuraminidase inhibitor resistance without loss of in vivo virulence or transmissibility.* Nat Commun, 2013. **4**: p. 2854.
257. Kamal, R.P., J.M. Katz, and I.A. York, *Molecular determinants of influenza virus pathogenesis in mice.* Curr Top Microbiol Immunol, 2014. **385**: p. 243-74.

258. Uhlendorff, J., et al., *Functional significance of the hemadsorption activity of influenza virus neuraminidase and its alteration in pandemic viruses.* Arch Virol, 2009. **154**(6): p. 945-57.
259. Benton, D.J., et al., *Role of Neuraminidase in Influenza A(H7N9) Virus Receptor Binding.* J Virol, 2017. **91**(11).
260. Wagner, R., M. Matrosovich, and H.D. Klenk, *Functional balance between haemagglutinin and neuraminidase in influenza virus infections.* Rev Med Virol, 2002. **12**(3): p. 159-66.
261. Xu, R., et al., *Functional balance of the hemagglutinin and neuraminidase activities accompanies the emergence of the 2009 H1N1 influenza pandemic.* J Virol, 2012. **86**(17): p. 9221-32.
262. Yen, H.L., et al., *Hemagglutinin-neuraminidase balance confers respiratory-droplet transmissibility of the pandemic H1N1 influenza virus in ferrets.* Proc Natl Acad Sci U S A, 2011. **108**(34): p. 14264-9.
263. Gen, F., et al., *Attenuation of an influenza A virus due to alteration of its hemagglutinin-neuraminidase functional balance in mice.* Arch Virol, 2013. **158**(5): p. 1003-11.
264. Munier, S., et al., *A genetically engineered waterfowl influenza virus with a deletion in the stalk of the neuraminidase has increased virulence for chickens.* J Virol, 2010. **84**(2): p. 940-52.
265. Matsuoka, Y., et al., *Neuraminidase stalk length and additional glycosylation of the hemagglutinin influence the virulence of influenza H5N1 viruses for mice.* J Virol, 2009. **83**(9): p. 4704-8.
266. Blumenkrantz, D., et al., *The short stalk length of highly pathogenic avian influenza H5N1 virus neuraminidase limits transmission of pandemic H1N1 virus in ferrets.* J Virol, 2013. **87**(19): p. 10539-51.
267. Hale, B.G., et al., *The multifunctional NS1 protein of influenza A viruses.* J Gen Virol, 2008. **89**(Pt 10): p. 2359-76.
268. Min, J.Y., et al., *A site on the influenza A virus NS1 protein mediates both inhibition of PKR activation and temporal regulation of viral RNA synthesis.* Virology, 2007. **363**(1): p. 236-43.
269. Guo, Z., et al., *NS1 protein of influenza A virus inhibits the function of intracytoplasmic pathogen sensor, RIG-I.* Am J Respir Cell Mol Biol, 2007. **36**(3): p. 263-9.
270. Nemeroff, M.E., et al., *Influenza virus NS1 protein interacts with the cellular 30 kDa subunit of CPSF and inhibits 3'end formation of cellular pre-mRNAs.* Mol Cell, 1998. **1**(7): p. 991-1000.
271. Krug, R.M., *Functions of the influenza A virus NS1 protein in antiviral defense.* Curr Opin Virol, 2015. **12**: p. 1-6.
272. Hale, B.G., et al., *Inefficient control of host gene expression by the 2009 pandemic H1N1 influenza A virus NS1 protein.* J Virol, 2010. **84**(14): p. 6909-22.
273. Ayllon, J., et al., *A single amino acid substitution in the novel H7N9 influenza A virus NS1 protein increases CPSF30 binding and virulence.* J Virol, 2014. **88**(20): p. 12146-51.
274. Twu, K.Y., et al., *The H5N1 influenza virus NS genes selected after 1998 enhance virus replication in mammalian cells.* J Virol, 2007. **81**(15): p. 8112-21.
275. Seo, S.H., E. Hoffmann, and R.G. Webster, *Lethal H5N1 influenza viruses escape host anti-viral cytokine responses.* Nat Med, 2002. **8**(9): p. 950-4.

276. Zanin, M., et al., *Molecular basis of mammalian transmissibility of avian H1N1 influenza viruses and their pandemic potential.* Proc Natl Acad Sci U S A, 2017. **114**(42): p. 11217-11222.
277. Watanabe, T., M. Imai, and Y. Kawaoka, *NS1 is the fluid for "flu-transmission".* Proc Natl Acad Sci U S A, 2017. **114**(42): p. 11012-11014.
278. Varga, Z.T., et al., *The influenza virus protein PB1-F2 inhibits the induction of type I interferon at the level of the MAVS adaptor protein.* PLoS Pathog, 2011. **7**(6): p. e1002067.
279. Hayashi, T., L.A. MacDonald, and T. Takimoto, *Influenza A Virus Protein PA-X Contributes to Viral Growth and Suppression of the Host Antiviral and Immune Responses.* J Virol, 2015. **89**(12): p. 6442-52.
280. Gaucherand, L., et al., *The Influenza A Virus Endoribonuclease PA-X Usurps Host mRNA Processing Machinery to Limit Host Gene Expression.* Cell Rep, 2019. **27**(3): p. 776-792 e7.
281. Shi, M., et al., *Evolutionary conservation of the PA-X open reading frame in segment 3 of influenza A virus.* J Virol, 2012. **86**(22): p. 12411-3.
282. Oishi, K., S. Yamayoshi, and Y. Kawaoka, *Identification of Amino Acid Residues in Influenza A Virus PA-X That Contribute to Enhanced Shutoff Activity.* Front Microbiol, 2019. **10**: p. 432.
283. Hale, B.G., R.A. Albrecht, and A. Garcia-Sastre, *Innate immune evasion strategies of influenza viruses.* Future Microbiol, 2010. **5**(1): p. 23-41.
284. Hung, M.C. and W. Link, *Protein localization in disease and therapy.* J Cell Sci, 2011. **124**(Pt 20): p. 3381-92.
285. Cho, I., M.R. Jackson, and J. Swift, *Roles of Cross-Membrane Transport and Signaling in the Maintenance of Cellular Homeostasis.* Cell Mol Bioeng, 2016. **9**: p. 234-246.
286. Deng, T., et al., *Role of ran binding protein 5 in nuclear import and assembly of the influenza virus RNA polymerase complex.* J Virol, 2006. **80**(24): p. 11911-9.
287. Naito, T., et al., *Involvement of Hsp90 in assembly and nuclear import of influenza virus RNA polymerase subunits.* J Virol, 2007. **81**(3): p. 1339-49.
288. Resa-Infante, P., et al., *The host-dependent interaction of alpha-importins with influenza PB2 polymerase subunit is required for virus RNA replication.* PLoS One, 2008. **3**(12): p. e3904.
289. Boivin, S. and D.J. Hart, *Interaction of the influenza A virus polymerase PB2 C-terminal region with importin alpha isoforms provides insights into host adaptation and polymerase assembly.* J Biol Chem, 2011. **286**(12): p. 10439-48.
290. Tarendeau, F., et al., *Host determinant residue lysine 627 lies on the surface of a discrete, folded domain of influenza virus polymerase PB2 subunit.* PLoS Pathog, 2008. **4**(8): p. e1000136.
291. Thiele, S., et al., *Cellular importin-α3 expression dynamics in the lung regulate antiviral response pathways against influenza.* Cell Reports (*accepted*), 2020.
292. Resa-Infante, P., et al., *Importin-alpha7 is required for enhanced influenza A virus replication in the alveolar epithelium and severe lung damage in mice.* J Virol, 2014. **88**(14): p. 8166-79.
293. Bertram, S., et al., *H7N9 Influenza A Virus Exhibits Importin-alpha7-Mediated Replication in the Mammalian Respiratory Tract.* Am J Pathol, 2017. **187**(4): p. 831-840.

294. Resa-Infante, P., et al., *Targeting Importin-alpha7 as a Therapeutic Approach against Pandemic Influenza Viruses.* J Virol, 2015. **89**(17): p. 9010-20.
295. Resa-Infante, P., et al., *Alternative interaction sites in the influenza A virus nucleoprotein mediate viral escape from the importin-alpha7 mediated nuclear import pathway.* FEBS J, 2019. **286**(17): p. 3374-3388.
296. Reilly, P.T., et al., *Cracking the ANP32 whips: important functions, unequal requirement, and hints at disease implications.* Bioessays, 2014. **36**(11): p. 1062-71.
297. Mehle, A. and J.A. Doudna, *An inhibitory activity in human cells restricts the function of an avian-like influenza virus polymerase.* Cell Host Microbe, 2008. **4**(2): p. 111-22.
298. Mistry, B., et al., *Elucidating the Interactions between Influenza Virus Polymerase and Host Factor ANP32A.* J Virol, 2020. **94**(3).
299. Baker, S.F., M.P. Ledwith, and A. Mehle, *Differential Splicing of ANP32A in Birds Alters Its Ability to Stimulate RNA Synthesis by Restricted Influenza Polymerase.* Cell Rep, 2018. **24**(10): p. 2581-2588 e4.
300. Bi, Z., et al., *Insights into species-specific regulation of ANP32A on the mammalian-restricted influenza virus polymerase activity.* Emerg Microbes Infect, 2019. **8**(1): p. 1465-1478.
301. Domingues, P., et al., *Profiling host ANP32A splicing landscapes to predict influenza A virus polymerase adaptation.* Nat Commun, 2019. **10**(1): p. 3396.
302. Domingues, P. and B.G. Hale, *Functional Insights into ANP32A-Dependent Influenza A Virus Polymerase Host Restriction.* Cell Rep, 2017. **20**(11): p. 2538-2546.
303. Long, J.S., et al., *Species specific differences in use of ANP32 proteins by influenza A virus.* Elife, 2019. **8**.
304. Liang, L., et al., *Low Polymerase Activity Attributed to PA Drives the Acquisition of the PB2 E627K Mutation of H7N9 Avian Influenza Virus in Mammals.* mBio, 2019. **10**(3).
305. Staller, E., et al., *ANP32 Proteins Are Essential for Influenza Virus Replication in Human Cells.* J Virol, 2019. **93**(17).
306. Zhang, H., et al., *Fundamental Contribution and Host Range Determination of ANP32A and ANP32B in Influenza A Virus Polymerase Activity.* J Virol, 2019. **93**(13).
307. Sugiyama, K., et al., *pp32 and APRIL are host cell-derived regulators of influenza virus RNA synthesis from cRNA.* Elife, 2015. **4**.
308. Gorlich, D. and I.W. Mattaj, *Nucleocytoplasmic transport.* Science, 1996. **271**(5255): p. 1513-8.
309. Terry, L.J., E.B. Shows, and S.R. Wente, *Crossing the nuclear envelope: hierarchical regulation of nucleocytoplasmic transport.* Science, 2007. **318**(5855): p. 1412-6.
310. Greber, U.F. and M. Fornerod, *Nuclear import in viral infections.* Curr Top Microbiol Immunol, 2005. **285**: p. 109-38.
311. Hill, R., et al., *Targeting nucleocytoplasmic transport in cancer therapy.* Oncotarget, 2014. **5**(1): p. 11-28.
312. Kim, H.J. and J.P. Taylor, *Lost in Transportation: Nucleocytoplasmic Transport Defects in ALS and Other Neurodegenerative Diseases.* Neuron, 2017. **96**(2): p. 285-297.
313. McLane, L.M. and A.H. Corbett, *Nuclear localization signals and human disease.* IUBMB Life, 2009. **61**(7): p. 697-706.
314. Goldfarb, D.S., et al., *Importin alpha: a multipurpose nuclear-transport receptor.* Trends Cell Biol, 2004. **14**(9): p. 505-14.

315. Kelley, J.B., et al., *Karyopherin alpha7 (KPNA7), a divergent member of the importin alpha family of nuclear import receptors.* BMC Cell Biol, 2010. **11**: p. 63.
316. Kohler, M., et al., *Cloning of two novel human importin-alpha subunits and analysis of the expression pattern of the importin-alpha protein family.* FEBS Lett, 1997. **417**(1): p. 104-8.
317. Kohler, M., et al., *Differential expression of classical nuclear transport factors during cellular proliferation and differentiation.* Cell Physiol Biochem, 2002. **12**(5-6): p. 335-44.
318. Miyamoto, Y., K. Yamada, and Y. Yoneda, *Importin alpha: a key molecule in nuclear transport and non-transport functions.* J Biochem, 2016. **160**(2): p. 69-75.
319. Lange, A., et al., *Classical nuclear localization signals: definition, function, and interaction with importin alpha.* J Biol Chem, 2007. **282**(8): p. 5101-5.
320. Conti, E., et al., *Crystallographic analysis of the recognition of a nuclear localization signal by the nuclear import factor karyopherin alpha.* Cell, 1998. **94**(2): p. 193-204.
321. Fontes, M.R., T. Teh, and B. Kobe, *Structural basis of recognition of monopartite and bipartite nuclear localization sequences by mammalian importin-alpha.* J Mol Biol, 2000. **297**(5): p. 1183-94.
322. Friedrich, B., et al., *Nuclear localization signal and protein context both mediate importin alpha specificity of nuclear import substrates.* Mol Cell Biol, 2006. **26**(23): p. 8697-709.
323. Sankhala, R.S., et al., *Three-dimensional context rather than NLS amino acid sequence determines importin alpha subtype specificity for RCC1.* Nat Commun, 2017. **8**(1): p. 979.
324. Kutay, U., et al., *Export of importin alpha from the nucleus is mediated by a specific nuclear transport factor.* Cell, 1997. **90**(6): p. 1061-71.
325. Dankof, A., et al., *KPNA2 protein expression in invasive breast carcinoma and matched peritumoral ductal carcinoma in situ.* Virchows Arch, 2007. **451**(5): p. 877-81.
326. Wang, C.I., et al., *Importin subunit alpha-2 is identified as a potential biomarker for non-small cell lung cancer by integration of the cancer cell secretome and tissue transcriptome.* Int J Cancer, 2011. **128**(10): p. 2364-72.
327. Dias, S.M., et al., *The molecular basis for the regulation of the cap-binding complex by the importins.* Nat Struct Mol Biol, 2009. **16**(9): p. 930-7.
328. Yasuda, Y., et al., *Nuclear retention of importin alpha coordinates cell fate through changes in gene expression.* EMBO J, 2012. **31**(1): p. 83-94.
329. Frieman, M., et al., *Severe acute respiratory syndrome coronavirus ORF6 antagonizes STAT1 function by sequestering nuclear import factors on the rough endoplasmic reticulum/Golgi membrane.* J Virol, 2007. **81**(18): p. 9812-24.
330. Gabriel, G., et al., *Importin-alpha7 Is Involved in the Formation of Ebola Virus Inclusion Bodies but Is Not Essential for Pathogenicity in Mice.* J Infect Dis, 2015. **212 Suppl 2**: p. S316-21.
331. Gustin, K.E., *Inhibition of nucleo-cytoplasmic trafficking by RNA viruses: targeting the nuclear pore complex.* Virus Res, 2003. **95**(1-2): p. 35-44.
332. Pryor, M.J., et al., *Nuclear localization of dengue virus nonstructural protein 5 through its importin alpha/beta-recognized nuclear localization sequences is integral to viral infection.* Traffic, 2007. **8**(7): p. 795-807.
333. Yang, L., et al., *Karyopherin Alpha 6 Is Required for Replication of Porcine Reproductive and Respiratory Syndrome Virus and Zika Virus.* J Virol, 2018. **92**(9).

334. Neufeldt, C.J., et al., *Hepatitis C virus-induced cytoplasmic organelles use the nuclear transport machinery to establish an environment conducive to virus replication.* PLoS Pathog, 2013. **9**(10): p. e1003744.
335. Canton, J., et al., *MERS-CoV 4b protein interferes with the NF-kappaB-dependent innate immune response during infection.* PLoS Pathog, 2018. **14**(1): p. e1006838.
336. Fraser, J.E., et al., *Investigating dengue virus nonstructural protein 5 (NS5) nuclear import.* Methods Mol Biol, 2014. **1138**: p. 301-28.
337. Basler, C.F. and G.K. Amarasinghe, *Evasion of interferon responses by Ebola and Marburg viruses.* J Interferon Cytokine Res, 2009. **29**(9): p. 511-20.
338. Rout, M.P. and J.D. Aitchison, *Pore relations: nuclear pore complexes and nucleocytoplasmic exchange.* Essays Biochem, 2000. **36**: p. 75-88.
339. Suntharalingam, M. and S.R. Wente, *Peering through the pore: nuclear pore complex structure, assembly, and function.* Dev Cell, 2003. **4**(6): p. 775-89.
340. Pemberton, L.F. and B.M. Paschal, *Mechanisms of receptor-mediated nuclear import and nuclear export.* Traffic, 2005. **6**(3): p. 187-98.
341. Cook, A., et al., *Structural biology of nucleocytoplasmic transport.* Annu Rev Biochem, 2007. **76**: p. 647-71.
342. Fried, H. and U. Kutay, *Nucleocytoplasmic transport: taking an inventory.* Cell Mol Life Sci, 2003. **60**(8): p. 1659-88.
343. Fagotto, F., U. Gluck, and B.M. Gumbiner, *Nuclear localization signal-independent and importin/karyopherin-independent nuclear import of beta-catenin.* Curr Biol, 1998. **8**(4): p. 181-90.
344. Rexach, M. and G. Blobel, *Protein import into nuclei: association and dissociation reactions involving transport substrate, transport factors, and nucleoporins.* Cell, 1995. **83**(5): p. 683-92.
345. Lee, S.J., et al., *Structural basis for nuclear import complex dissociation by RanGTP.* Nature, 2005. **435**(7042): p. 693-6.
346. Matsuura, Y. and M. Stewart, *Nup50/Npap60 function in nuclear protein import complex disassembly and importin recycling.* EMBO J, 2005. **24**(21): p. 3681-9.
347. *https://www.who.int/news-room/feature-stories/ten-threats-to-global-health-in-2019, accessed on 03.02.2020*.
348. Beck, S., *Role of importin-α7 SNPs on influenza virus replication, Master Thesis*. 2016, University of Würzburg.
349. Wang, P., P. Palese, and R.E. O'Neill, *The NPI-1/NPI-3 (karyopherin alpha) binding site on the influenza a virus nucleoprotein NP is a nonconventional nuclear localization signal.* J Virol, 1997. **71**(3): p. 1850-6.
350. Hoffmann, E., et al., *A DNA transfection system for generation of influenza A virus from eight plasmids.* Proc Natl Acad Sci U S A, 2000. **97**(11): p. 6108-13.
351. Reilly, P.T., et al., *Generation and characterization of the Anp32e-deficient mouse.* PLoS One, 2010. **5**(10): p. e13597.
352. Chemnitz, J., et al., *The acidic protein rich in leucines Anp32b is an immunomodulator of inflammation in mice.* Sci Rep, 2019. **9**(1): p. 4853.
353. Neumann, G., et al., *An improved reverse genetics system for influenza A virus generation and its implications for vaccine production.* Proc Natl Acad Sci U S A, 2005. **102**(46): p. 16825-9.

354. Tarnow, C., et al., *TMPRSS2 is a host factor that is essential for pneumotropism and pathogenicity of H7N9 influenza A virus in mice.* J Virol, 2014. **88**(9): p. 4744-51.
355. Metsalu, T. and J. Vilo, *ClustVis: a web tool for visualizing clustering of multivariate data using Principal Component Analysis and heatmap.* Nucleic Acids Res, 2015. **43**(W1): p. W566-70.
356. Shannon, P., et al., *Cytoscape: a software environment for integrated models of biomolecular interaction networks.* Genome Res, 2003. **13**(11): p. 2498-504.
357. Love, M.I., W. Huber, and S. Anders, *Moderated estimation of fold change and dispersion for RNA-seq data with DESeq2.* Genome Biol, 2014. **15**(12): p. 550.
358. Szklarczyk, D., et al., *STRING v11: protein-protein association networks with increased coverage, supporting functional discovery in genome-wide experimental datasets.* Nucleic Acids Res, 2019. **47**(D1): p. D607-D613.
359. Dobin, A., et al., *STAR: ultrafast universal RNA-seq aligner.* Bioinformatics, 2013. **29**(1): p. 15-21.
360. Chen, J., et al., *ToppGene Suite for gene list enrichment analysis and candidate gene prioritization.* Nucleic Acids Res, 2009. **37**(Web Server issue): p. W305-11.
361. Lottspeich, F. and H. Zorbas, *Bioanalytik*. 1998: Spektrum Akadamischer Verlag.
362. Livak, K.J. and T.D. Schmittgen, *Analysis of relative gene expression data using real-time quantitative PCR and the 2(-Delta Delta C(T)) Method.* Methods, 2001. **25**(4): p. 402-8.
363. Dana, H., et al., *Molecular Mechanisms and Biological Functions of siRNA.* Int J Biomed Sci, 2017. **13**(2): p. 48-57.
364. Jiang, F. and J.A. Doudna, *CRISPR-Cas9 Structures and Mechanisms.* Annu Rev Biophys, 2017. **46**: p. 505-529.
365. Leo, V.I., R.M. Bunte, and P.T. Reilly, *BALB/c-congenic ANP32B-deficient mice reveal a modifying locus that determines viability.* Exp Anim, 2016. **65**(1): p. 53-62.
366. Reilly, P.T., et al., *Acidic nuclear phosphoprotein 32kDa (ANP32)B-deficient mouse reveals a hierarchy of ANP32 importance in mammalian development.* Proc Natl Acad Sci U S A, 2011. **108**(25): p. 10243-8.
367. Gray, J.J., et al., *Protein-protein docking with simultaneous optimization of rigid-body displacement and side-chain conformations.* J Mol Biol, 2003. **331**(1): p. 281-99.
368. Chaudhury, S., et al., *Benchmarking and analysis of protein docking performance in Rosetta v3.2.* PLoS One, 2011. **6**(8): p. e22477.
369. Wang, C., P. Bradley, and D. Baker, *Protein-protein docking with backbone flexibility.* J Mol Biol, 2007. **373**(2): p. 503-19.
370. Wang, C., O. Schueler-Furman, and D. Baker, *Improved side-chain modeling for protein-protein docking.* Protein Sci, 2005. **14**(5): p. 1328-39.
371. Chambers, B.S., et al., *DNA mismatch repair is required for the host innate response and controls cellular fate after influenza virus infection.* Nat Microbiol, 2019. **4**(11): p. 1964-1977.
372. Liao, Y., et al., *The role of cold-inducible RNA binding protein in cell stress response.* Int J Cancer, 2017. **141**(11): p. 2164-2173.
373. Li, T., et al., *NF90 is a novel influenza A virus NS1-interacting protein that antagonizes the inhibitory role of NS1 on PKR phosphorylation.* FEBS Lett, 2016. **590**(16): p. 2797-810.

374. Shapira, S.D., et al., *A physical and regulatory map of host-influenza interactions reveals pathways in H1N1 infection.* Cell, 2009. **139**(7): p. 1255-67.
375. Wang, P., et al., *Nuclear factor 90 negatively regulates influenza virus replication by interacting with viral nucleoprotein.* J Virol, 2009. **83**(16): p. 7850-61.
376. Wen, X., et al., *NF90 exerts antiviral activity through regulation of PKR phosphorylation and stress granules in infected cells.* J Immunol, 2014. **192**(8): p. 3753-64.
377. Boulo, S., et al., *Human importin alpha and RNA do not compete for binding to influenza A virus nucleoprotein.* Virology, 2011. **409**(1): p. 84-90.
378. Li, Y., et al., *Proteome Response of Chicken Embryo Fibroblast Cells to Recombinant H5N1 Avian Influenza Viruses with Different Neuraminidase Stalk Lengths.* Sci Rep, 2017. **7**: p. 40698.
379. Xin, L., et al., *Infection susceptibility and immune senescence with advancing age replicated in accelerated aging Lmna(Dhe) mice.* Aging Cell, 2015. **14**(6): p. 1122-6.
380. Cilloniz, C., et al., *Molecular signatures associated with Mx1-mediated resistance to highly pathogenic influenza virus infection: mechanisms of survival.* J Virol, 2012. **86**(5): p. 2437-46.
381. Chen, A., R.J. AbuJarour, and R.K. Draper, *Evidence that the transport of ricin to the cytoplasm is independent of both Rab6A and COPI.* J Cell Sci, 2003. **116**(Pt 17): p. 3503-10.
382. Karlas, A., et al., *Genome-wide RNAi screen identifies human host factors crucial for influenza virus replication.* Nature, 2010. **463**(7282): p. 818-22.
383. Bradel-Tretheway, B.G., et al., *Comprehensive proteomic analysis of influenza virus polymerase complex reveals a novel association with mitochondrial proteins and RNA polymerase accessory factors.* J Virol, 2011. **85**(17): p. 8569-81.
384. Miller, M.S., et al., *Senataxin suppresses the antiviral transcriptional response and controls viral biogenesis.* Nat Immunol, 2015. **16**(5): p. 485-94.
385. Bier, K., A. York, and E. Fodor, *Cellular cap-binding proteins associate with influenza virus mRNAs.* J Gen Virol, 2011. **92**(Pt 7): p. 1627-1634.
386. Kadota, S. and K. Nagata, *pp32, an INHAT component, is a transcription machinery recruiter for maximal induction of IFN-stimulated genes.* J Cell Sci, 2011. **124**(Pt 6): p. 892-9.
387. Natalizio, B.J. and S.R. Wente, *Postage for the messenger: designating routes for nuclear mRNA export.* Trends Cell Biol, 2013. **23**(8): p. 365-73.
388. Ziegler, E.C. and S. Ghosh, *Regulating inducible transcription through controlled localization.* Sci STKE, 2005. **2005**(284): p. re6.
389. Fagerlund, R., et al., *NF-{kappa}B is transported into the nucleus by importin {alpha}3 and importin {alpha}4.* J Biol Chem, 2005. **280**(16): p. 15942-51.
390. Gilmore, T.D., *Introduction to NF-kappaB: players, pathways, perspectives.* Oncogene, 2006. **25**(51): p. 6680-4.
391. Mor, A., M.A. White, and B.M. Fontoura, *Nuclear trafficking in health and disease.* Curr Opin Cell Biol, 2014. **28**: p. 28-35.
392. Kalderon, D., et al., *A short amino acid sequence able to specify nuclear location.* Cell, 1984. **39**(3 Pt 2): p. 499-509.

393. Lanford, R.E., P. Kanda, and R.C. Kennedy, *Induction of nuclear transport with a synthetic peptide homologous to the SV40 T antigen transport signal.* Cell, 1986. **46**(4): p. 575-82.
394. Robbins, J., et al., *Two interdependent basic domains in nucleoplasmin nuclear targeting sequence: identification of a class of bipartite nuclear targeting sequence.* Cell, 1991. **64**(3): p. 615-23.
395. Pumroy, R.A. and G. Cingolani, *Diversification of importin-alpha isoforms in cellular trafficking and disease states.* Biochem J, 2015. **466**(1): p. 13-28.
396. Hugel, S., et al., *Identification of importin alpha 7 specific transport cargoes using a proteomic screening approach.* Mol Cell Proteomics, 2014. **13**(5): p. 1286-98.
397. Mackmull, M.T., et al., *Landscape of nuclear transport receptor cargo specificity.* Mol Syst Biol, 2017. **13**(12): p. 962.
398. Wu, W., et al., *Synergy of two low-affinity NLSs determines the high avidity of influenza A virus nucleoprotein NP for human importin alpha isoforms.* Sci Rep, 2017. **7**(1): p. 11381.
399. Smith, K.M., et al., *Structural basis for importin alpha 3 specificity of W proteins in Hendra and Nipah viruses.* Nat Commun, 2018. **9**(1): p. 3703.
400. Wei, X., et al., *The interaction of cellular protein ANP32A with influenza A virus polymerase component PB2 promotes vRNA synthesis.* Arch Virol, 2019. **164**(3): p. 787-798.
401. Konig, R., et al., *Human host factors required for influenza virus replication.* Nature, 2010. **463**(7282): p. 813-7.
402. Pan, W., et al., *PHAPI/pp32 suppresses tumorigenesis by stimulating apoptosis.* J Biol Chem, 2009. **284**(11): p. 6946-54.
403. Ninpan, K., et al., *Expression of importin-alpha isoforms in human nasal mucosa: implication for adaptation of avian influenza A viruses to human host.* Virol J, 2016. **13**: p. 90.
404. Jernigan, D.B. and C.C.-R. Team, *Update: Public Health Response to the Coronavirus Disease 2019 Outbreak - United States, February 24, 2020.* MMWR Morb Mortal Wkly Rep, 2020. **69**(8): p. 216-219.
405. Jones, K.E., et al., *Global trends in emerging infectious diseases.* Nature, 2008. **451**(7181): p. 990-3.
406. *http://www.emro.who.int/about-who/rc61/zoonotic-diseases.html, accessed on 12.03.2020.*
407. Jakel, S., et al., *Importins fulfil a dual function as nuclear import receptors and cytoplasmic chaperones for exposed basic domains.* EMBO J, 2002. **21**(3): p. 377-86.
408. Dias, S.M., R.A. Cerione, and K.F. Wilson, *Unloading RNAs in the cytoplasm: an "importin" task.* Nucleus, 2010. **1**(2): p. 139-43.
409. Couper, K.N., D.G. Blount, and E.M. Riley, *IL-10: the master regulator of immunity to infection.* J Immunol, 2008. **180**(9): p. 5771-7.
410. Pahl, H.L., *Activators and target genes of Rel/NF-kappaB transcription factors.* Oncogene, 1999. **18**(49): p. 6853-66.
411. Liu, T., et al., *NF-kappaB signaling in inflammation.* Signal Transduct Target Ther, 2017. **2**.

412. Munemasa, Y., et al., *Promoter region-specific histone incorporation by the novel histone chaperone ANP32B and DNA-binding factor KLF5.* Mol Cell Biol, 2008. **28**(3): p. 1171-81.
413. Tochio, N., et al., *Solution structure of histone chaperone ANP32B: interaction with core histones H3-H4 through its acidic concave domain.* J Mol Biol, 2010. **401**(1): p. 97-114.
414. Ohno, Y., et al., *Downregulation of ANP32B exerts anti-apoptotic effects in hepatocellular carcinoma.* PLoS One, 2017. **12**(5): p. e0177343.
415. Shen, S.M., et al., *Downregulation of ANP32B, a novel substrate of caspase-3, enhances caspase-3 activation and apoptosis induction in myeloid leukemic cells.* Carcinogenesis, 2010. **31**(3): p. 419-26.
416. Bauer, A., et al., *ANP32B is a nuclear target of henipavirus M proteins.* PLoS One, 2014. **9**(5): p. e97233.
417. Bodem, J., et al., *Foamy virus nuclear RNA export is distinct from that of other retroviruses.* J Virol, 2011. **85**(5): p. 2333-41.
418. Brennan, C.M., I.E. Gallouzi, and J.A. Steitz, *Protein ligands to HuR modulate its interaction with target mRNAs in vivo.* J Cell Biol, 2000. **151**(1): p. 1-14.
419. Fries, B., et al., *Analysis of nucleocytoplasmic trafficking of the HuR ligand APRIL and its influence on CD83 expression.* J Biol Chem, 2007. **282**(7): p. 4504-15.
420. Ehlers, C., et al., *Post-transcriptional regulation of CD83 expression by AUF1 proteins.* Nucleic Acids Res, 2013. **41**(1): p. 206-19.
421. Yang, S., et al., *ANP32B deficiency impairs proliferation and suppresses tumor progression by regulating AKT phosphorylation.* Cell Death Dis, 2016. **7**: p. e2082.
422. Dan, H.C., et al., *Akt-dependent regulation of NF-{kappa}B is controlled by mTOR and Raptor in association with IKK.* Genes Dev, 2008. **22**(11): p. 1490-500.
423. Bai, D., L. Ueno, and P.K. Vogt, *Akt-mediated regulation of NFkappaB and the essentialness of NFkappaB for the oncogenicity of PI3K and Akt.* Int J Cancer, 2009. **125**(12): p. 2863-70.
424. Manning, B.D. and A. Toker, *AKT/PKB Signaling: Navigating the Network.* Cell, 2017. **169**(3): p. 381-405.
425. Ayllon, J., A. Garcia-Sastre, and B.G. Hale, *Influenza A viruses and PI3K: are there time, place and manner restrictions?* Virulence, 2012. **3**(4): p. 411-4.
426. *https://www.conceptdraw.com/How-To-Guide/hazard-pictograms, accessed on 22.03.2020*.

8. Appendix

8.1 List of hazardous substances according to GHS classification

All hazardous substances that were used in this study are listed in **Table 28**, including H and P statements as well as the associated hazard pictograms (**Figure 41**).

Table 28: List of hazardous substances according to GHS classification.

Chemical, Reagent or Kit	H Statement	P Statement	Harzard Pictogram
2-mercaptoethanol	H301 + H331, H310, H315, H317, H318, H361fd, H373, H410	P201, P262, P280, P301 + P310 + P330, P302 + P352 + P310, P305 + P351 + P338 + P310	05, 06, 08, 09
2-propanol (isopropanol)	H225, H319, H336	P210, P280, P305 + P351 + P338, P337 + P313	02, 07
3,3'-diaminobenzidin (DAB)	H302, H319, H341, H350	P201, P280, P301 + P312 + P330, P305 + P351 + P338, P308 + P313, P337 + P313	07, 08
Ammoniumperoxodisulfate (APS)	H272, H302, H315, H317, H319, H334, H335	P210, P280, P301 + P012 + P030, P302+P352, P305 + P351 + P338	02, 07, 08
Ampicillin sodium-salt	H317, H334	P261, P280, P342 + P311	08
Citrate Plus Buffer (10x)	H315, H319, H335	P280, P302 + P352, P304 + P340, P305 + P351 + P338	07, 08
Crystal violet	H226, H319, H351, H411	P273, P281, P305 + P351 + P338	02, 07, 08, 09
Diethylpyrocarbonate (DEPC)	H226	P210, P370 + P378	02
Dithiothreitol (DTT)	H302, H412	P264, P270, P273, P301 + P312 + P330, P501	07
Dual-Luciferase® Reporter Assay System	H225	P241, P243, P280, P303 + P361 + P353, P370 + P378, P403 + P235	02
Eosin-Y solution	H225, H290, H319	P210, P280, P305 + P351 + P338, P337 + P313, P403 + P235	02, 05

Ethanol (denatured), for disinfection	H225, H319	P210, P233, P305 + P351 + P338	02, 07
Ethanol (pure)	H225, H319	P210, P233, P305 + P351 + P338	02, 07
Ethidium bromide solution (10 mg/ml)	H331, H341	P261, P281, P311	06, 08
Eukitt	H226, H304, H312 + H332, H315, H319, H335, H373	P210-P260-P280-P301 + P310-P305 + P351 + P338-P370 + P378	02, 07, 08
Forene/Isofluorane (100%)	H336	P261, P271, P303 + P340, P312, P403 + P233, P405, P501	07, 08
Formaldehyde (20 or 37%)	H226, H301 + H311 + H331, H314, H317, H335, H341, H350, H370	P201, P210, P260, P280, P301 + P310 + P330, P303 + P361 + P353, P304 + P340 + P310, P305 + P351 + P338 + P310, P308 + P311, P370 + P378, P403 + P233	02, 05, 06, 08
Glacial acetic acid	H226, H314	P210 + P233 + P240 + P241 + P242 + P243 + P264 + P280	02
Halt™ Protease & Phosphatase Inhibitor Cocktail (100x), including EDTA	H317	P280	07
Hematoxylin	H302	P301 + P312 + P330	07
Hydrochloric acid (37 %)	H290, H314, H335	P280, P303 + P361 + P353, P304 + P340, P305 + P351 + P338, P310	05, 07
Hydrogen peroxide	H302, H318, H412	P280, P301 + P312 + P330, P305 + P351 + P338 + P310	05, 07
Igepal (NP 40)	H302, H315, H318, H410	P280, P301 + P312 + P330, P305 + P351 + P338 + P310	05, 07, 09
innuprep RNA Mini Kit	H302, H314, H412	P101, P102, P103, P260, P303 + P361 + P353, P305 + P351 + P338, P310, P405, P501	05, 07
Ketamine (100 mg/ml)	H302, H332	P261, P264, P301 + P312, P304 + P340, P330	07

Mayer's hemalum solution	H302, H319, H373	P260 + P264 + P270 + P280	08
Methanol	H225, H301, H311, H331, H370	P210.3, P270, P280.7, P303 + P361 + P353, P304 + P340, P308 + P311	02, 06, 08
Multiplex mouse immunoassay, custom-designed (IL-1b, IL6, TNF-a, IL-10, IFN-a, MCP-1, IL-17A, IL21)	-	P273, P280, P302 + P352, Ü305 + P351 + P338, P313	07
NucleoBond Xtra Maxi	H226, H315, H319, H334	P210, P261, P280, P342 + P311	02, 07, 08
Ottix Plus	H224, H319, H336, H411	P210, P233, P273, P280, P370 + P378, P403 + P235	02, 07, 09
Ottix Shaper	H225	P210, P233, P241, P242, P370 + P378, P501	02
Paraformaldehyde	H228, H302 + H332, H315, H317, H318, H335, H351	P210, P261, P280, P301 + P312 + P330, P305 + P351 + P338 + P310, P370 + P378	02, 05, 07, 08
Passive Lysis Buffer (5x)	H360	P201, P202, P280, P308 + P313, P405, P501	08
Penicillin-Streptomycin (P/S)	H302, H317, H361	P280, P302 + P352, P308 + P313	07, 08
Phenylmethanesulfonyl fluoride (PMSF)	H301, H314	P280, P301 + P310 + P330, P303 + P361 + P353, P304 + P340 + P310, P305 + P351 + P338	05, 06
Polyethylenimine (PEI)	H302, H317, H319, H411	P273, P280, P305 + P351 + P338	07, 09
Potassium dihydrogene phosphate	H315, H319	P264, P280, P305 + P351 + P338, P321, P332 + P313, P337 + P313	07
Proteinase K	H315, H319, H334, H335	P261, P284, P305 + P351 + P338, P342 + P311, P405, P501	07, 08
Pursept-A Xpress, for disinfection	H225, H319	P210, P271, P305 + P351 + P338, P337 + P313, P403 + P233	02, 07

QIAprep Spin Miniprep Kit	H225, H290, H315, H317, H319, H334, H336	P210, P261, P280, P284, P304 + P340, P342 + P311	02, 05, 07, 08
QIAquick Gel Extraction Kit	H302, H318, H412	P280, P305 + P351 + P338 + P310	05, 07
QIAquick PCR Purification Kit	H225, H315, H319, H336	P210, P280	02, 07
RNAlater RNA Stabilization Reagent	H302, H402	P301 + P312, P330, P270, P264, P273	07
RNase-Free DNase Set	H317, H334	P261, P280, P284, P304 + P340, P342 + P311	08
Rotiphorese Gel 30 (Acrylamide)	H302, H315, H317, H319, H340, H350, H361f, H372	P201 P280.7 P301+P312.0 P302+P352.1 P305+P351+P338 P308+P313 i	07, 08
Sodium azide	H300 + H310 + H330, H373, H410	P262, P273, P280, P301 + P310 + P330, P302 + P352 + P310, P304 + P340 + P310	06, 08, 09
Sodium dodecylsulfate (SDS)	H315, H318, H335	P261, P280, P302 + P352, P304 + P340 + P312, P305 + P351 + P338 + P310	05, 07
Sodium hydroxide (NaOH)	H290, H314	P233, P280, P303 + P361 + P353, P305 + P351 + P338, P310	05
Sodium pyruvate solution (Na-pyruvate; 100 mM)	H317, H319	P280, P302 + P352, P305 + P351 + P338	07
Sterilium, for hand disinfection	H226, H319, H336	P102, P210, P305 + P351 + P338, P337 + P313, P301 + P310, P501	02, 07
Superscript™ III Reverse Transcriptase Kit	H302, H412	P264, P270, P273, P301 + P312 + P330, P501	07
Tetramethylethylenediamine (TEMED)	H225, H302 + H332, H314	P210, P280, P301 + P330 + P331, P303 + P361 + P353, P304 + P340 + P312, P305 + P351 + P338	02, 05, 07
Triton X-100	H318	P280, P305 + P351 + P338, P313	05

Trizol Reagent	H301, H311, H331, H314, H335, H341, H373, H412	P201, P261, P264, P280, P273, P301 + P310, P302 + P352, P303 + P361 + P353, P304 + P340, P305 + P351 + P338, P403 + P233, P501	05, 06, 08
Trypsin from bovine pancreas, TPCK-treated (TPCK trypsin)	H315, H319, H334, H335	P261, P280, P284, P304 + P340, P337 + P313, P342 + P311	07, 08
Virkon S, for disinfection (BSL-3 work)	H302, H314, H318, H334, H317, H410	P260, P280, P285, P270, P301 + P330 + P331, P303 + P361 + P353, P304 + P340, P305 + P351 + P338, P405, P501	05, 07, 08, 09
Xylazine (20 mg/ml)	H301	P264, P301 + P310, P330	06
Xylol	H226, H304, H312 + H332, H315, H319, H373	P210, P301 + P330 + P331, P302 + P352, P305 + P351 + P338, P314,	02, 07, 08
ZytoChemPlus (HRP) Broad Spectrum (DAB) Kit	H341, H350	P201, P281, P308+P313	08

Figure 41: Hazard pictograms. Shown are the 9 hazard pictograms, accompanying Table 28 (adapted from [426]).

8.2 Supplemental information accompanying chapter 5.1

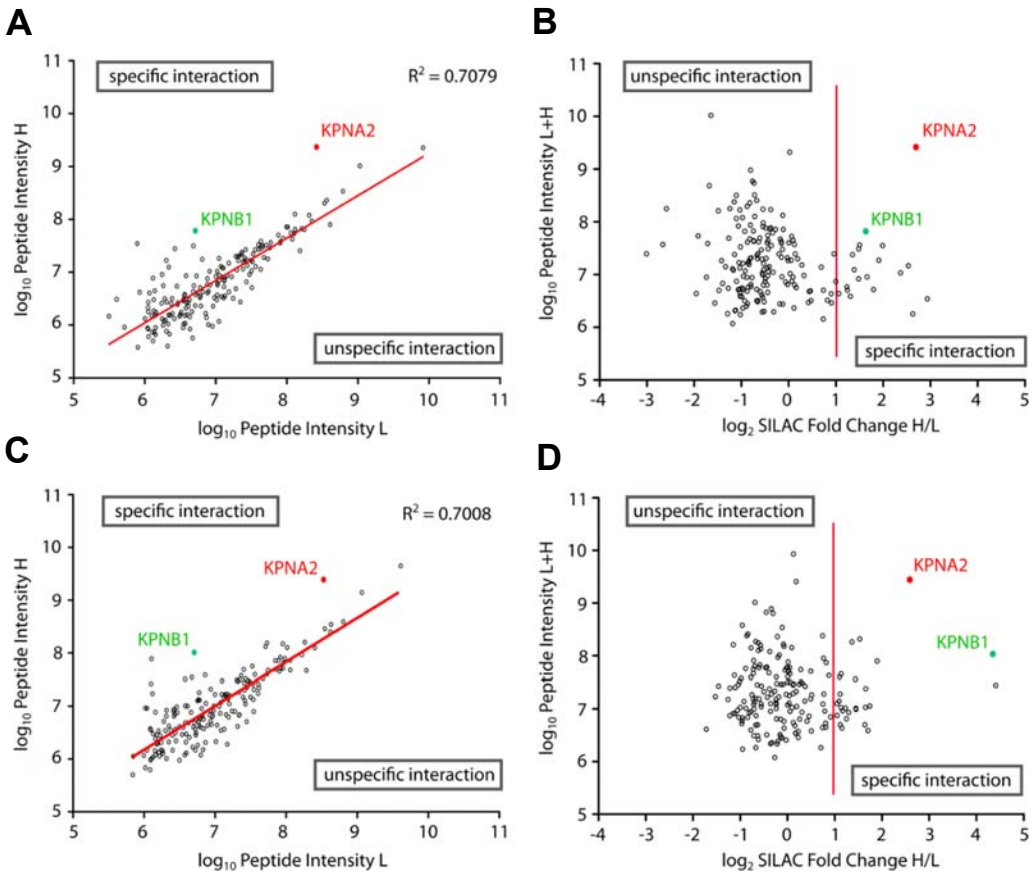

Figure 42: Identification of importin-α1 interaction partners in influenza infected cells using a SILAC-based mass spectrometry approach. A-D, Shown are the cellular proteins that were precipitated both with importin-α1-WT (heavy labeled amino acids; 'H') as well as in the empty vector control (light labeled amino acids; 'L'), in either uninfected **(A and B)** or influenza infected **(C and D)** cells. Identified importin-α (KPNAx) and importin-β_1 (KPNB1) proteins, including the importin-α1-WT bait protein, are highlighted according to their gene names. **A and C,** The measured peptide intensities in the empty vector control (L) were plotted over the respective peptide intensity measured in the importin-α1-WT condition for each identified protein. Linear regression was performed, and cellular proteins significantly enriched with importin-α1-WT are presented above the regression line (red). **B and D,** To filter out unspecific interactions, the ratio of peptide intensity L over peptide intensity H was calculated for each identified protein, $\log_2$-transformed, and plotted over the combined L+H peptide intensity. A $\log_2$Fold Change > 1 (i.e., 2-fold enriched with importin-α1-WT over the empty vector control) was considered statistically significant. This cutoff is indicated with a red line and all proteins appearing right from this cutoff line are considered as specific importin-α1-WT interacting factors.

Table 29: Cellular proteins specifically precipitated with importin-α1 in uninfected cells (Mock). Cellular proteins are listed that were precipitated with importin-α1-WT, -ΔIBB, or both. Criteria for inclusion were: i) significantly enriched over the empty vector control (log2FoldChange >1), or ii) not precipitated in the empty vector control. Shown are the gene name, the Protein ID, the importin-α1 variant (WT and/or ΔIBB) the protein was precipitated with, the number of identified unique peptides, and the log2Fold Change over the empty vector control (n.a., not applicable, i.e. protein was not found in empty vector control). Proteins were sorted alphabetically according to their gene names.

Gene name	Protein ID(s)	Precipitated with	# unique peptides	Log2FoldChange
CHD4	Q14839	ΔIBB	1	1,26867
DDX17	Q92841	WT	1	n.a.
DDX21	Q9NR30	WT	12	1,50376
DDX3X;DDX3Y	O00571;O15523	WT	1	n.a.
GATAD2A	Q86YP4	WT	1	1,05977
GATAD2A	Q86YP4	ΔIBB	1	1,51384
HDAC1	Q13547	ΔIBB	1	n.a.
HNRNPC	P07910	WT	5	1,34908
HNRNPF	P52597	WT	2	1,79527
HNRNPL	P14866	WT	3	1,24056
KIFC1	Q9BW19	WT	3	n.a.
KPNA2	P52292	WT	21	2,69368
KPNA2	P52292	ΔIBB	21	1,45702
KPNB1	Q14974	WT	11	1,62980
LAMB1	P07942	WT	1	n.a.
MCM3	P25205	ΔIBB	1	n.a.
MTA2	O94776	WT	3	n.a.
MTA2	O94776	ΔIBB	3	n.a.
NCL	P19338	WT	6	2,36780
NHP2L1	P55769	WT	1	n.a.

NOLC1	Q14978	WT	3	1,48290
NOP58	Q9Y2X3	WT	1	n.a.
NUP153	P49790	WT	4	n.a.
NUP50	Q9UKX7	WT	10	1,98758
PBRM1	Q86U86	WT	5	1,90697
PBRM1	Q86U86	ΔIBB	5	1,30194
RAB10	P61026	WT	2	n.a.
RBBP4;RBBP7	Q09028;Q16576	WT	3	2,62674
RBBP4;RBBP7	Q09028;Q16576	ΔIBB	3	3,19413
RPL12	P30050	WT	1	n.a.
RPL13	P26373	WT	2	n.a.
RPL13A;RPL13AP3	P40429;Q6NVV1	WT	2	1,38714
RPL18	Q07020	WT	1	n.a.
RPL18A	Q02543	WT	1	n.a.
RPL22L1	Q6P5R6	ΔIBB	1	n.a.
RPL29	P47914	WT	1	n.a.
RPL3	P39023	WT	1	1,30854
RPL4	P36578	WT	1	n.a.
RPL7A	P62424	WT	4	n.a.
RPL8	P62917	WT	3	1,65892
RPLP0;RPLP0P6	P05388;Q8NHW5	WT	3	2,93454
RPS3A	P61247	WT	1	n.a.
RPS8	P62241	WT	3	2,53244
SMARCA4;SMARCA2	P51532;P51531	WT	5	n.a.
SMARCC2	Q8TAQ2	WT	10	1,48176
SMARCC2	Q8TAQ2	ΔIBB	10	1,07540
SMARCD2;SMARCD3	Q92925;Q6STE5	WT	2	n.a.

SMARCE1	Q969G3	WT	2	1,23088
TRIM28	Q13263	ΔIBB	2	n.a.

Table 30: Cellular proteins specifically precipitated with importin-α1 in influenza (A/WSN/33, $PB2_{627K}$) infected cells (H1N1). Cellular proteins are listed that were precipitated with importin-α1-WT, -ΔIBB, or both. Criteria for inclusion were: i) significantly enriched over the empty vector control (log2FoldChange >1), or ii) not precipitated in the empty vector control. Shown are the gene name, the Protein ID, the importin-α1 variant (WT and/or ΔIBB) the protein was precipitated with, the number of identified unique peptides, and the log2Fold Change over the empty vector control (n.a., not applicable, i.e. protein was not found in empty vector control). Proteins were sorted alphabetically according to their gene names.

Gene name	Protein ID(s)	Precipitated with	# unique peptides	Log2FoldChange
AMOT	Q4VCS5	WT	4	1,64959
CTNNA1	P35221	WT	1	n.a.
CTNNB1	P35222	WT	1	n.a.
DDX17	Q92841	WT	2	n.a.
DDX21	Q9NR30	WT	14	1,10225
DDX3X;DDX3Y	O00571;O15523	WT	1	n.a.
FUS	P35637	WT	2	1,11580
GATAD2A	Q86YP4	ΔIBB	1	n.a.
GATAD2B	Q8WXI9	ΔIBB	1	n.a.
HDAC1	Q13547	ΔIBB	1	n.a.
HNRNPAB	Q99729	WT	1	1,15257
HNRNPC	P07910	WT	8	1,13501
HNRNPDL	O14979	WT	1	n.a.
HNRNPL	P14866	WT	4	1,22299
HNRNPM	P52272	WT	1	n.a.

HNRNPUL2	Q1KMD3	WT	1	n.a.
HSPA5	P11021	WT	2	n.a.
IRS4	O14654	WT	2	n.a.
KIFC1	Q9BW19	WT	9	n.a.
KIFC1	Q9BW19	ΔIBB	9	n.a.
KPNA2	P52292	WT	24	2,58967
KPNA2	P52292	ΔIBB	24	1,64630
KPNB1	Q14974	WT	12	4,34834
MCM3	P25205	ΔIBB	1	n.a.
MPRIP	Q6WCQ1	WT	1	n.a.
MTA2	O94776	WT	7	n.a.
MTA2	O94776	ΔIBB	7	n.a.
MUC17	Q685J3	WT	1	1,45191
MYCBP2	O75592	ΔIBB	1	n.a.
MYH10	P35580	WT	31	1,36826
MYH9	P35579	WT	46	1,53230
MYL12A;MYL12B;MYL9	P19105;O14950;P24844	WT	2	n.a.
MYO1B	O43795	WT	2	n.a.
MYO1D	O94832	WT	3	1,63754
NCBP1	Q09161	WT	1	n.a.
NCL	P19338	WT	7	4,41105
NOLC1	Q14978	WT	3	1,65700
NOLC1	Q14978	ΔIBB	3	1,12148
NOP58	Q9Y2X3	WT	3	n.a.
NOP58	Q9Y2X3	ΔIBB	3	n.a.
NUP153	P49790	WT	6	n.a.
NUP50	Q9UKX7	WT	13	1,89871

NUP93	Q8N1F7	WT	1	n.a.
POM121C;POM121	A8CG34;Q96HA1	WT	1	n.a.
RBBP4;RBBP7	Q09028;Q16576	WT	2	n.a.
RBBP4;RBBP7	Q09028;Q16576	ΔIBB	2	n.a.
RIF1	Q5UIP0	WT	1	n.a.
RPA1	P27694	WT	3	n.a.
RPL10A	P62906	WT	2	1,24750
RPL12	P30050	WT	2	n.a.
RPL13A;RPL13AP3	P40429;Q6NVV1	WT	2	1,04970
RPL14	P50914	WT	3	1,11222
RPL18	Q07020	WT	3	1,17005
RPL18A	Q02543	WT	2	n.a.
RPL21	P46778	WT	1	n.a.
RPL24	P83731	WT	3	1,74338
RPL27	P61353	WT	3	n.a.
RPL29	P47914	WT	1	n.a.
RPL3	P39023	WT	1	1,70598
RPL4	P36578	WT	1	n.a.
RPL5	P46777	WT	2	n.a.
RPL7	P18124	WT	1	n.a.
RPL7A	P62424	WT	3	n.a.
RPL8	P62917	WT	3	1,09478
RPLP0;RPLP0P6	P05388;Q8NHW5	WT	2	1,04810
RPS29	P62273	WT	1	n.a.
RPS3A	P61247	WT	2	n.a.
RPS8	P62241	WT	5	1,13514
SFPQ	P23246	WT	1	n.a.

SMARCA4;SMARCA2	P51532;P51531	WT	5	1,44594
SMARCB1	Q12824	WT	2	1,29696
SMARCC1	Q92922	WT	1	n.a.
SMARCC2	Q8TAQ2	WT	10	1,43755
SMARCC2	Q8TAQ2	ΔIBB	10	1,25302
SMARCD2;SMARCD3	Q92925;Q6STE5	WT	1	n.a.
TGFBRAP1	Q8WUH2	ΔIBB	1	n.a.
TRIM28	Q13263	ΔIBB	4	1,03605

Table 31: Gene Ontology (GO) enrichment analysis of importin-α1 (WT, ΔIBB) interaction partners in uninfected cells (Mock). Shown are the Top10 enriched GO terms for *Molecular Function*, *Biological Process* and *Cellular Component*, each sorted by their respective *p* values.

Molecular function

ID	Name	*p* value
GO:0003723	RNA binding	7,70E-18
GO:0003735	structural constituent of ribosome	2,55E-17
GO:0031492	nucleosomal DNA binding	9,86E-12
GO:0005198	structural molecule activity	1,64E-10
GO:0031491	nucleosome binding	6,04E-10
GO:0019843	rRNA binding	8,62E-09
GO:0031490	chromatin DNA binding	2,41E-08
GO:0003682	chromatin binding	2,38E-07
GO:0042623	ATPase activity, coupled	3,65E-06
GO:0035326	cis-regulatory region binding	4,47E-06

Biological process		
ID	**Name**	***p* value**
GO:0019083	viral transcription	1,72E-21
GO:0019080	viral gene expression	6,11E-21
GO:0072599	establishment of protein localization to endoplasmic reticulum	2,13E-17
GO:0006614	SRP-dependent cotranslational protein targeting to membrane	1,61E-16
GO:0006613	cotranslational protein targeting to membrane	2,68E-16
GO:0070972	protein localization to endoplasmic reticulum	3,05E-16
GO:0000184	nuclear-transcribed mRNA catabolic process, nonsense-mediated decay	9,87E-16
GO:0045047	protein targeting to ER	9,87E-16
GO:0043044	ATP-dependent chromatin remodeling	1,57E-15
GO:0072594	establishment of protein localization to organelle	2,50E-15
Cellular component		
ID	**Name**	***p* value**
GO:0022626	cytosolic ribosome	8,49E-23
GO:0022625	cytosolic large ribosomal subunit	9,71E-22
GO:0044391	ribosomal subunit	3,53E-19
GO:0070603	SWI/SNF superfamily-type complex	2,41E-18
GO:1904949	ATPase complex	3,12E-18
GO:0015934	large ribosomal subunit	1,78E-17
GO:1990904	ribonucleoprotein complex	5,16E-17
GO:0005840	ribosome	9,67E-17
GO:0016581	NuRD complex	9,15E-10
GO:0090545	CHD-type complex	9,15E-10

Table 32: Gene Ontology (GO) enrichment analysis of importin-α1 (WT, ΔIBB) interaction partners in influenza (A/WSN/33, $PB2_{627K}$) infected cells. Shown are the Top10 enriched GO terms for *Molecular Function*, *Biological Process* and *Cellular Component*, each sorted by their respective *p* values.

Molecular function

ID	Name	*p* value
GO:0003735	structural constituent of ribosome	1,48E-22
GO:0003723	RNA binding	1,48E-21
GO:0005198	structural molecule activity	1,20E-17
GO:0031492	nucleosomal DNA binding	1,90E-11
GO:0019843	rRNA binding	3,30E-10
GO:0031491	nucleosome binding	1,84E-09
GO:0003682	chromatin binding	6,12E-08
GO:0031490	chromatin DNA binding	1,07E-07
GO:0042623	ATPase activity, coupled	3,60E-07
GO:0035326	cis-regulatory region binding	8,18E-07

Biological process

ID	Name	*p* value
GO:0019083	viral transcription	1,35E-35
GO:0019080	viral gene expression	1,11E-34
GO:0000184	nuclear-transcribed mRNA catabolic process, nonsense-mediated decay	1,68E-26
GO:0045047	protein targeting to ER	1,68E-26
GO:0072599	establishment of protein localization to endoplasmic reticulum	3,53E-26
GO:0006614	SRP-dependent cotranslational protein targeting to membrane	6,68E-26
GO:0006613	cotranslational protein targeting to membrane	1,50E-25
GO:0070972	protein localization to endoplasmic reticulum	2,14E-24
GO:0006413	translational initiation	2,50E-23
GO:0072594	establishment of protein localization to organelle	2,05E-22

Cellular component		
ID	**Name**	***p* value**
GO:0044391	ribosomal subunit	2,39E-24
GO:0015934	large ribosomal subunit	1,20E-22
GO:0005840	ribosome	4,97E-21
GO:1990904	ribonucleoprotein complex	1,01E-20
GO:1904949	ATPase complex	1,44E-16
GO:0070603	SWI/SNF superfamily-type complex	3,00E-15
GO:0005925	focal adhesion	5,77E-14
GO:0030055	cell-substrate junction	9,19E-14
GO:0005844	polysome	1,67E-11
GO:0005912	adherens junction	2,10E-11

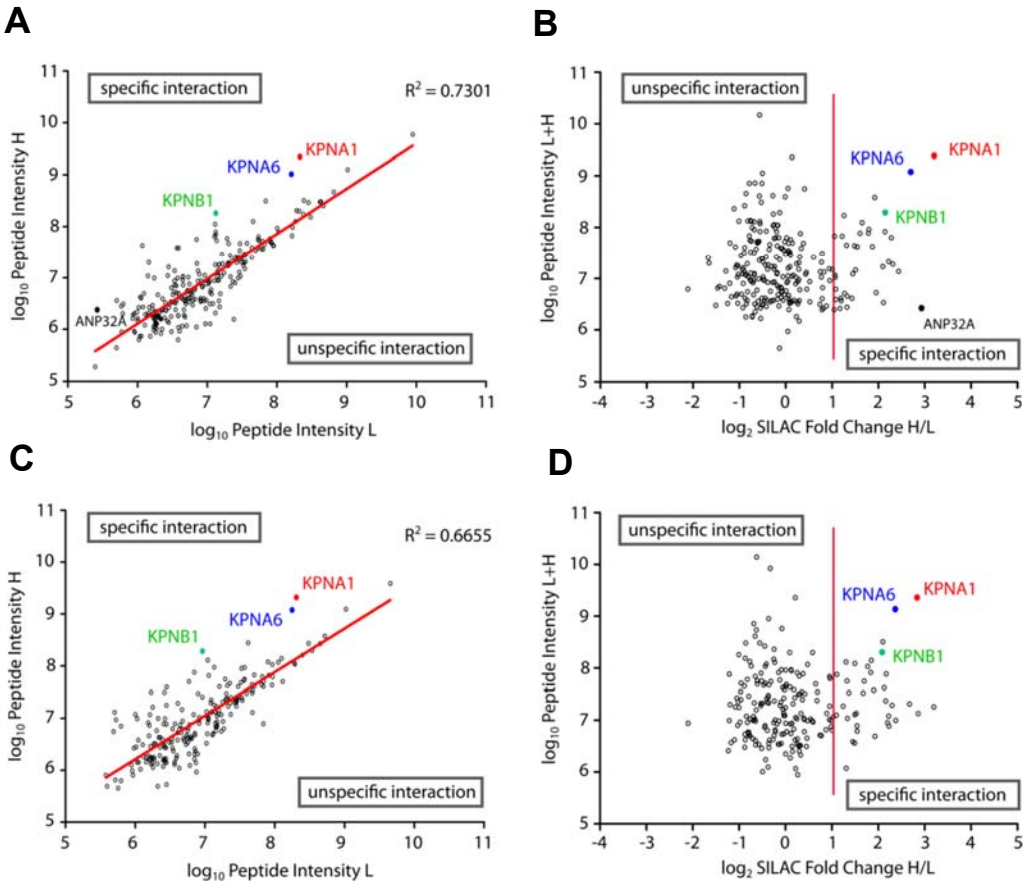

Figure 43: Identification of importin-α5 interaction partners in influenza infected cells using a SILAC-based mass spectrometry approach. A-D, Shown are the cellular proteins that were precipitated both with importin-α5-WT (heavy labeled amino acids; 'H') as well as in the empty vector control (light labeled amino acids; 'L'), in either uninfected **(A and B)** or influenza infected **(C and D)** cells. Identified importin-α (KPNAx) and importin-β_1 (KPNB1) proteins, including the importin-α5-WT bait protein, as well as ANP32A are highlighted according to their gene names. **A and C,** The measured peptide intensities in the empty vector control (L) were plotted over the respective peptide intensity measured in the importin-α5-WT condition for each identified protein. Linear regression was performed, and cellular proteins significantly enriched with importin-α5-WT are presented above the regression line (red). **B and D,** To filter out unspecific interactions, the ratio of peptide intensity L over peptide intensity H was calculated for each identified protein, $\log_2$-transformed, and plotted over the combined L+H peptide intensity. A $\log_2$Fold Change > 1 (i.e., 2-fold enriched with importin-α5-WT over the empty vector control) was considered statistically significant. This cutoff is indicated with a red line and all proteins appearing right from this cutoff line are considered as specific importin-α5-WT interacting factors.

Table 33: Cellular proteins specifically precipitated with importin-α5 in uninfected cells (Mock). Cellular proteins are listed that were precipitated with importin-α5-WT, -ΔIBB, or both. Criteria for inclusion were: i) significantly enriched over the empty vector control (log2FoldChange >1), or ii) not precipitated in the empty vector control. Shown is the gene name, the Protein ID, the importin-α5 variant (WT and/or ΔIBB) the protein was precipitated with, the number of identified unique peptides, and the log2Fold Change over the empty vector control (n.a., not applicable, i.e. protein was not found in empty vector control). Proteins were sorted alphabetically according to their gene names.

Gene name	Protein ID(s)	Precipitated with	# unique peptides	Log2FoldChange
ACO2	Q99798	WT	1	2,43619
ACO2	Q99798	ΔIBB	1	1,55189
ADNP	Q9H2P0	WT	9	2,21915
ADNP	Q9H2P0	ΔIBB	9	1,50360
ANP32A	P39687	WT	3	2,93051
CDKN2AIP	Q9NXV6	WT	2	n.a.
CGGBP1	Q9UFW8	WT	1	n.a.
CGN	Q9P2M7	WT	5	1,06849
CHD4	Q14839	WT	12	1,87058
CISD2	Q8N5K1	ΔIBB	1	n.a.
CTNNB1	P35222	WT	1	n.a.
DDX21	Q9NR30	WT	28	1,92117
DDX3X;DDX3Y	O00571;O15523	WT	2	n.a.
DHX15	O43143	WT	2	n.a.
DKC1	O60832	WT	3	1,19724
FHL1	Q13642	WT	1	n.a.
GATAD2A	Q86YP4	WT	12	2,27992
GATAD2A	Q86YP4	ΔIBB	12	1,16234
GATAD2B	Q8WXI9	WT	4	2,30926
GATAD2B	Q8WXI9	ΔIBB	4	1,11430

GNPAT	O15228	WT	1	n.a.
HDAC1	Q13547	WT	5	2,09373
HDAC1	Q13547	ΔIBB	5	1,45312
HDAC2	Q92769	WT	1	n.a.
HNRNPA2B1	P22626	WT	6	1,31272
HNRNPAB	Q99729	WT	1	1,26951
HNRNPC	P07910	WT	10	1,78522
HNRNPK	P61978	WT	8	1,05367
HNRNPL	P14866	WT	9	2,14405
HNRNPM	P52272	WT	5	1,95351
HNRNPR	O43390	WT	4	n.a.
IGF2BP1	Q9NZI8	WT	3	n.a.
ILF3	Q12906	WT	1	1,32152
IRS4	O14654	WT	1	n.a.
KPNA1	P52294	WT	21	3,20077
KPNA1	P52294	ΔIBB	21	1,43510
KPNA6	O60684	WT	9	2,69566
KPNB1	Q14974	WT	20	2,14685
LMNB1	P20700	WT	23	1,25960
MATR3	P43243	WT	2	n.a.
MBD3	O95983	WT	2	n.a.
MTA1	Q13330	WT	2	n.a.
MTA2	O94776	WT	15	1,79589
MYH14	Q7Z406	WT	3	n.a.
MYL12A;MYL12B;MYL9	P19105;O14950;P24844	WT	1	n.a.
NCBP1	Q09161	WT	2	n.a.
NCL	P19338	WT	4	n.a.

NF2	P35240	WT	1	n.a.
NOLC1	Q14978	WT	3	1,50538
NOP56	O00567	WT	1	1,04712
NOP58	Q9Y2X3	WT	8	n.a.
NOP58	Q9Y2X3	ΔIBB	8	n.a.
NUP153	P49790	WT	10	1,54478
NUP50	Q9UKX7	WT	14	1,64897
NUP93	Q8N1F7	WT	1	n.a.
PBRM1	Q86U86	WT	3	n.a.
POM121C;POM121	A8CG34;Q96HA1	WT	1	n.a.
RAB6B;RAB6A;RAB39A	Q9NRW1;P20340;Q14964	WT	1	n.a.
RANBP2	P49792	WT	3	n.a.
RANGAP1	P46060	WT	2	n.a.
RBBP4;RBBP7	Q09028;Q16576	WT	4	n.a.
RBBP4;RBBP7	Q09028;Q16576	ΔIBB	4	n.a.
RBMXL1;RBMX	Q96E39;P38159	WT	2	2,10933
RPL10A	P62906	WT	2	1,08236
RPL12	P30050	WT	2	n.a.
RPL18	Q07020	WT	4	1,05887
RPL18A	Q02543	WT	2	n.a.
RPL21	P46778	WT	1	n.a.
RPL28	P46779	WT	2	1,19024
RPL29	P47914	WT	1	n.a.
RPL3	P39023	WT	1	1,07998
RPL36	Q9Y3U8	WT	1	n.a.
RPL4	P36578	WT	3	1,42820
RPL7A	P62424	WT	6	n.a.

RPLP0;RPLP0P6	P05388;Q8NHW5	WT	4	1,00403
SCO2	O43819	WT	1	n.a.
SF1	Q15637	WT	3	1,17178
SMARCA4;SMARCA2	P51532;P51531	WT	3	n.a.
SMARCA5	O60264	WT	24	1,60284
SMARCA5	O60264	ΔIBB	24	1,27166
SMARCB1	Q12824	WT	1	1,32809
SMARCC2	Q8TAQ2	WT	3	n.a.
SSRP1	Q08945	WT	2	n.a.
TP53	P04637	WT	1	n.a.
TPX2	Q9ULW0	WT	6	1,44604
TPX2	Q9ULW0	ΔIBB	6	1,50970
TRIM27	P14373	WT	4	n.a.
TRIM27	P14373	ΔIBB	4	n.a.
TRIM28	Q13263	WT	8	1,48403
XRN2	Q9H0D6	WT	11	1,21891

Table 34: Cellular proteins specifically precipitated with importin-α5 in influenza (A/WSN/33, $PB2_{627K}$) infected cells (H1N1). Cellular proteins are listed that were precipitated with importin-α5-WT, -ΔIBB, or both. Criteria for inclusion were: i) significantly enriched over the empty vector control (log2FoldChange >1), or ii) not precipitated in the empty vector control. Shown is the gene name, the Protein ID, the importin-α5 variant (WT and/or ΔIBB) the protein was precipitated with, the number of identified unique peptides, and the log2Fold Change over the empty vector control (n.a., not applicable; i.e. protein was not found in empty vector control). Proteins were sorted alphabetically according to their gene names.

Gene name	Protein ID(s)	Precipitated with	# unique peptides	Log2FoldChange
ACO2	Q99798	WT	1	2,16031
ACO2	Q99798	ΔIBB	1	1,24835
ACTG1	P63261	WT	1	1,32388
ADNP	Q9H2P0	WT	6	n.a.
ANP32A	P39687	WT	3	n.a.
CDC42	P60953	WT	1	n.a.
CGGBP1	Q9UFW8	WT	3	n.a.
CGN	Q9P2M7	WT	3	1,44923
CHD4	Q14839	WT	9	1,67229
CTNNA1	P35221	WT	1	n.a.
DDX21	Q9NR30	WT	31	2,09677
DHX15	O43143	WT	2	n.a.
GATAD2A	Q86YP4	WT	10	1,69644
GATAD2A	Q86YP4	ΔIBB	10	1,13350
GATAD2B	Q8WXI9	WT	3	2,23113
GNB2L1	P63244	WT	2	n.a.
GNPAT	O15228	WT	2	n.a.
HDAC1	Q13547	WT	5	1,52557
HNRNPAB	Q99729	WT	2	1,54092

HNRNPC	P07910	WT	11	1,49431
HNRNPDL	O14979	WT	2	n.a.
HNRNPH3	P31942	WT	1	n.a.
HNRNPL	P14866	WT	10	2,17012
HNRNPM	P52272	WT	5	2,85896
HNRNPR	O43390	WT	4	1,54587
HSPA5	P11021	WT	1	n.a.
IGF2BP1	Q9NZI8	WT	2	1,30947
KHDRBS1	Q07666	WT	2	n.a.
KPNA1	P52294	WT	18	2,83697
KPNA1	P52294	ΔIBB	18	1,87916
KPNA6	O60684	WT	8	2,36527
KPNA6	O60684	ΔIBB	8	1,25912
KPNB1	Q14974	WT	18	2,08243
LMNA	P02545	WT	2	n.a.
LMNB1	P20700	WT	21	1,30334
LMNB2	Q03252	WT	5	1,09862
MATR3	P43243	WT	4	1,02545
MBD3	O95983	WT	2	n.a.
MCM3	P25205	ΔIBB	1	n.a.
MPRIP	Q6WCQ1	WT	1	n.a.
MTA1	Q13330	WT	2	n.a.
MTA2	O94776	WT	13	1,83701
MYCBP2	O75592	ΔIBB	1	n.a.
MYH10	P35580	WT	11	2,67338
MYH9	P35579	WT	15	1,90295
MYO1B	O43795	WT	1	n.a.

MYO1D	O94832	WT	2	1,49168
NCAP	P15682	WT	4	n.a.
NCL	P19338	WT	4	n.a.
NOLC1	Q14978	WT	3	2,29728
NOLC1	Q14978	ΔIBB	3	1,05228
NOP56	O00567	WT	5	1,33571
NOP58	Q9Y2X3	WT	12	2,12740
NOP58	Q9Y2X3	ΔIBB	12	1,31284
NPM1	P06748	WT	4	1,24190
NUP153	P49790	WT	7	3,19823
NUP50	Q9UKX7	WT	15	1,85096
NUP93	Q8N1F7	WT	1	n.a.
PBRM1	Q86U86	WT	2	n.a.
POM121C;POM121	A8CG34;Q96HA1	WT	2	n.a.
RBBP4;RBBP7	Q09028;Q16576	WT	6	n.a.
RBBP4;RBBP7	Q09028;Q16576	ΔIBB	6	n.a.
RBMXL1;RBMX	Q96E39;P38159	WT	3	1,92611
RPL10A	P62906	WT	2	n.a.
RPL12	P30050	WT	3	n.a.
RPL13	P26373	WT	3	2,22442
RPL17	P18621	WT	1	1,00029
RPL18	Q07020	WT	3	2,20043
RPL21	P46778	WT	2	n.a.
RPL27	P61353	WT	2	n.a.
RPL28	P46779	WT	2	n.a.
RPL29	P47914	WT	1	n.a.
RPL4	P36578	WT	3	n.a.

RPL7	P18124	WT	2	n.a.
RPL7A	P62424	WT	3	1,49308
RPLP0;RPLP0P6	P05388;Q8NHW5	WT	2	n.a.
RPS3A	P61247	WT	3	n.a.
SF1	Q15637	WT	1	n.a.
SF3B2	Q13435	WT	2	n.a.
SMARCA4;SMARCA2	P51532;P51531	WT	1	n.a.
SMARCA5	O60264	WT	23	1,76960
SSRP1	Q08945	WT	3	2,37793
SUPT16H	Q9Y5B9	WT	7	n.a.
SUPT16H	Q9Y5B9	ΔIBB	7	n.a.
TPX2	Q9ULW0	WT	1	n.a.
TRIM27	P14373	WT	3	n.a.
TRIM27	P14373	ΔIBB	3	n.a.
TRIM28	Q13263	WT	7	1,36854
USP1	O94782	WT	1	n.a.
WDHD1	O75717	WT	5	n.a.
XRN2	Q9H0D6	WT	10	1,10568

Table 35: Gene Ontology (GO) enrichment analysis of importin-α5 (WT, ΔIBB) interaction partners in uninfected cells (Mock). Shown are the Top10 enriched GO terms for *Molecular Function*, *Biological Process* and *Cellular Component*, each sorted by their respective *p* values.

Molecular function

ID	Name	*p* value
GO:0003723	RNA binding	1,06E-22
GO:0031491	nucleosome binding	1,01E-13
GO:0031492	nucleosomal DNA binding	1,11E-12
GO:0003682	chromatin binding	7,47E-11
GO:0035326	cis-regulatory region binding	7,29E-09
GO:0003735	structural constituent of ribosome	1,07E-08
GO:0031490	chromatin DNA binding	1,58E-08
GO:0008139	nuclear localization sequence binding	2,18E-08
GO:0005198	structural molecule activity	3,12E-07
GO:0005048	signal sequence binding	2,25E-06

Biological process

ID	Name	*p* value
GO:0019083	viral transcription	1,08E-23
GO:0019080	viral gene expression	5,48E-23
GO:0016032	viral process	1,00E-18
GO:0044403	symbiotic process	7,24E-18
GO:0044419	interspecies interaction between organisms	3,46E-17
GO:0043044	ATP-dependent chromatin remodeling	4,06E-17
GO:0072594	establishment of protein localization to organelle	7,18E-16
GO:0033365	protein localization to organelle	3,00E-14
GO:0016071	mRNA metabolic process	8,58E-14
GO:0006401	RNA catabolic process	1,42E-12

Cellular component

ID	Name	*p* value
GO:0070603	SWI/SNF superfamily-type complex	6,25E-20
GO:0016581	NuRD complex	1,06E-17
GO:0090545	CHD-type complex	1,06E-17
GO:1904949	ATPase complex	2,12E-17
GO:0090568	nuclear transcriptional repressor complex	4,11E-16
GO:0022625	cytosolic large ribosomal subunit	1,01E-15
GO:1990904	ribonucleoprotein complex	2,09E-15
GO:0022626	cytosolic ribosome	6,19E-13
GO:0015934	large ribosomal subunit	7,69E-12
GO:0017053	transcriptional repressor complex	1,27E-10

Table 36: Gene Ontology (GO) enrichment analysis of importin-α5 (WT, ΔIBB) interaction partners in influenza (A/WSN/33, $PB2_{627K}$) infected cells. Shown are the Top10 enriched GO terms for *Molecular Function*, *Biological Process* and *Cellular Component*, each sorted by their respective *p* values.

Molecular function

ID	Name	*p* value
GO:0003723	RNA binding	7,12E-23
GO:0003735	structural constituent of ribosome	1,44E-11
GO:0031491	nucleosome binding	1,05E-10
GO:0005198	structural molecule activity	2,17E-10
GO:0003682	chromatin binding	2,77E-09
GO:0008139	nuclear localization sequence binding	1,57E-08
GO:0019843	rRNA binding	2,82E-08
GO:0042623	ATPase activity, coupled	7,39E-08
GO:0031492	nucleosomal DNA binding	1,07E-07

GO:0005048	signal sequence binding	1,62E-06

Biological process

ID	Name	*p* value
GO:0019083	viral transcription	3,29E-24
GO:0019080	viral gene expression	1,68E-23
GO:0072594	establishment of protein localization to organelle	1,29E-17
GO:0016071	mRNA metabolic process	1,64E-16
GO:0016032	viral process	4,41E-16
GO:0045047	protein targeting to ER	2,17E-15
GO:0044403	symbiotic process	2,61E-15
GO:0072599	establishment of protein localization to endoplasmic reticulum	3,61E-15
GO:0044419	interspecies interaction between organisms	1,06E-14
GO:0006614	SRP-dependent cotranslational protein targeting to membrane	1,25E-14

Cellular component

ID	Name	*p* value
GO:0022625	cytosolic large ribosomal subunit	7,02E-18
GO:1990904	ribonucleoprotein complex	3,41E-17
GO:0016581	NuRD complex	2,52E-15
GO:0090545	CHD-type complex	2,52E-15
GO:0015934	large ribosomal subunit	2,99E-15
GO:0070603	SWI/SNF superfamily-type complex	8,25E-15
GO:0022626	cytosolic ribosome	8,75E-15
GO:1904949	ATPase complex	2,09E-14
GO:0090568	nuclear transcriptional repressor complex	3,45E-14
GO:0044391	ribosomal subunit	4,77E-13

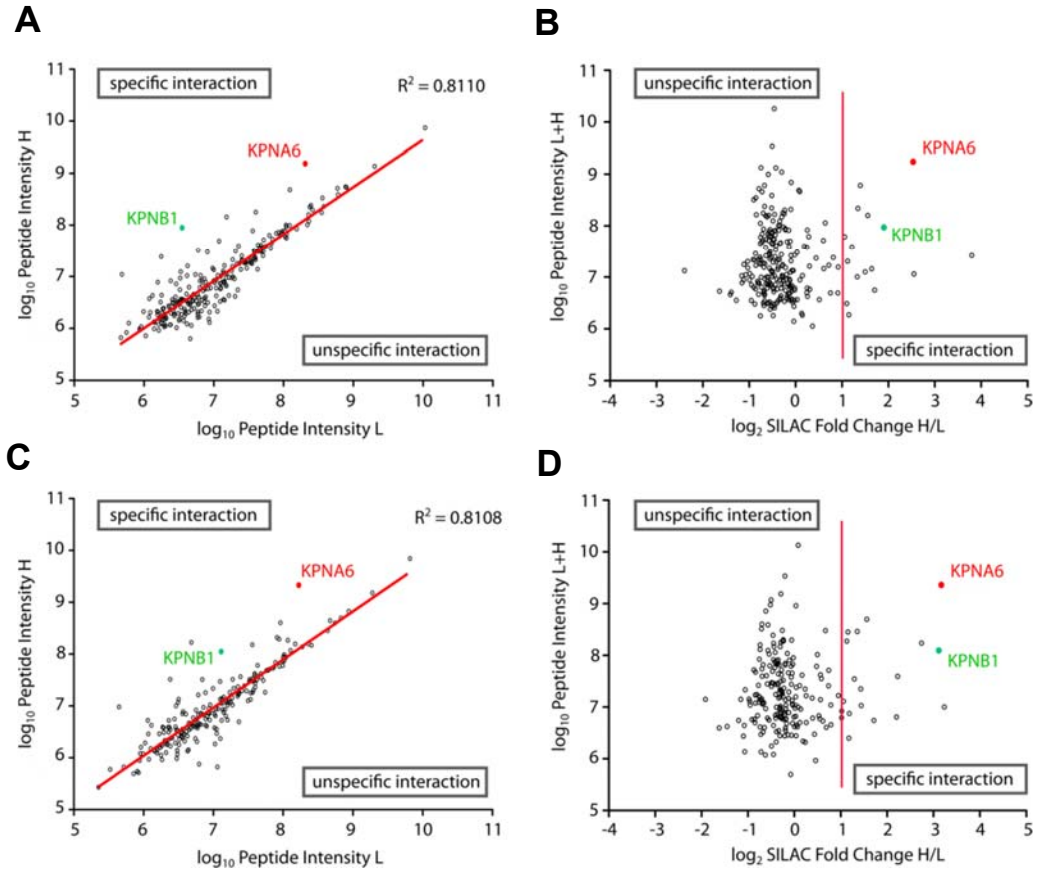

Figure 44: Identification of importin-α7 interaction partners in influenza infected cells using a SILAC-based mass spectrometry approach. A-D, Shown are the cellular proteins that were precipitated both with importin-α7-WT (heavy labeled amino acids; 'H') as well as in the empty vector control (light labeled amino acids; 'L'), in either uninfected **(A and B)** or influenza infected **(C and D)** cells. Identified importin-α (KPNAx) and importin-β_1 (KPNB1) proteins, including the importin-α7-WT bait protein, are highlighted according to their gene names. **A and C,** The measured peptide intensities in the empty vector control (L) were plotted over the respective peptide intensity measured in the importin-α7-WT condition for each identified protein. Linear regression was performed, and cellular proteins significantly enriched with importin-α7-WT are presented above the regression line (red). **B and D,** To filter out unspecific interactions, the ratio of peptide intensity L over peptide intensity H was calculated for each identified protein, $\log_2$-transformed, and plotted over the combined L+H peptide intensity. A $\log_2$Fold Change > 1 (i.e., 2-fold enriched with importin-α7-WT over the empty vector control) was considered statistically significant. This cutoff is indicated with a red line and all proteins appearing right from this cutoff line are considered as specific importin-α7-WT interacting factors.

Table 37: Cellular proteins specifically precipitated with importin-α7 in uninfected cells (Mock). Cellular proteins are listed that were precipitated with importin-α7-WT, -ΔIBB, or both. Criteria for inclusion were: i) significantly enriched over the empty vector control (log2FoldChange >1), or ii) not precipitated in the empty vector control. Shown is the gene name, the Protein ID, the importin-α7 variant (WT and/or ΔIBB) the protein was precipitated with, the number of identified unique peptides, and the log2Fold Change over the empty vector control (n.a., not applicable, i.e. protein was not found in empty vector control). Proteins were sorted alphabetically according to their gene names.

Gene name	Protein ID(s)	Precipitated with	# unique peptides	Log2FoldChange
ADNP	Q9H2P0	WT	6	1,12042
ADNP	Q9H2P0	ΔIBB	6	1,56540
ANP32A	P39687	WT	1	n.a.
C3orf58	Q8NDZ4	ΔIBB	2	n.a.
CDC42	P60953	WT	1	n.a.
CGGBP1	Q9UFW8	WT	3	n.a.
CTNNA1	P35221	WT	4	1,32726
DDX21	Q9NR30	ΔIBB	22	1,84097
DKC1	O60832	ΔIBB	1	n.a.
GATAD2A	Q86YP4	WT	4	1,63715
GATAD2A	Q86YP4	ΔIBB	4	1,88749
GATAD2B	Q8WXI9	WT	3	1,14613
GATAD2B	Q8WXI9	ΔIBB	3	1,54705
GNPAT	O15228	WT	1	n.a.
HDAC1	Q13547	WT	4	n.a.
HDAC1	Q13547	ΔIBB	4	n.a.
HNRNPL	P14866	ΔIBB	10	1,21058
JUP	P14923	WT	4	1,70573
KPNA1	P52294	WT	3	n.a.
KPNA6	O60684	WT	29	2,53346

KPNA6	O60684	ΔIBB	29	2,68563
KPNB1	Q14974	WT	12	1,90362
LETM1	O95202	WT	1	n.a.
LMNB1	P20700	WT	41	1,39336
LMNB1	P20700	ΔIBB	41	1,41684
LMNB2	Q03252	WT	30	1,34352
LMNB2	Q03252	ΔIBB	30	1,62910
MBD3	O95983	ΔIBB	1	n.a.
MCM3	P25205	ΔIBB	1	n.a.
MRPL16	Q9NX20	ΔIBB	2	n.a.
MTA1	Q13330	WT	1	n.a.
MTA1	Q13330	ΔIBB	1	n.a.
MTA2	O94776	WT	14	1,21524
MTA2	O94776	ΔIBB	14	1,57701
MYH14	Q7Z406	WT	2	n.a.
MYO1B	O43795	WT	3	1,49803
NF2	P35240	WT	2	n.a.
NUP153	P49790	WT	7	3,79618
NUP50	Q9UKX7	WT	14	1,55655
NUP50	Q9UKX7	ΔIBB	14	1,20977
NUP93	Q8N1F7	WT	1	1,10344
POM121C;POM121	A8CG34;Q96HA1	WT	1	n.a.
PPP1R12A	O14974	WT	2	n.a.
RAB6B;RAB6A;RAB39A	Q9NRW1;P20340;Q14964	WT	1	n.a.
RBBP4;RBBP7	Q09028;Q16576	WT	4	2,55014
RBBP4;RBBP7	Q09028;Q16576	ΔIBB	4	2,84489
RBM14	Q96PK6	ΔIBB	1	n.a.

RPL21	P46778	WT	1	n.a.
RPL4	P36578	WT	1	n.a.
SCD	O00767	WT	1	n.a.
SLC25A11	Q02978	WT	2	n.a.
SLC25A11	Q02978	ΔIBB	2	n.a.
SMARCA5	O60264	ΔIBB	16	1,57942
SMARCC2	Q8TAQ2	ΔIBB	4	1,20477
SPOP	O43791	ΔIBB	1	n.a.
SUPT16H	Q9Y5B9	ΔIBB	1	n.a.
TRIM28	Q13263	WT	9	1,05617
TRIM28	Q13263	ΔIBB	9	1,23603

Table 38: Cellular proteins specifically precipitated with importin-α7 in influenza (A/WSN/33, $PB2_{627K}$) infected cells (H1N1). Cellular proteins are listed that were precipitated with importin-α7-WT, -ΔIBB, or both. Criteria for inclusion were: i) significantly enriched over the empty vector control (log2FoldChange >1), or ii) not precipitated in the empty vector control. Shown is the gene name, the Protein ID, the importin-α7 variant (WT and/or ΔIBB) the protein was precipitated with, the number of identified unique peptides, and the log2Fold Change over the empty vector control (n.a., not applicable, i.e. protein was not found in empty vector control). Proteins were sorted alphabetically according to their gene names.

Gene name	Protein ID(s)	Precipitated with	# unique peptides	Log2FoldChange
ADNP	Q9H2P0	WT	5	1,05998
ADNP	Q9H2P0	ΔIBB	5	1,30702
AMOT	Q4VCS5	WT	12	2,22808
ANP32A	P39687	WT	1	n.a.
C3orf33	Q6P1S2	WT	1	n.a.
CGN	Q9P2M7	WT	3	1,71374

CIRBP	Q14011	WT	2	n.a.
CTNNA1	P35221	WT	2	n.a.
CTNNB1	P35222	WT	1	n.a.
DDX21	Q9NR30	ΔIBB	17	1,54656
FECH	P22830	WT	3	1,18534
GATAD2A	Q86YP4	WT	4	1,44138
GATAD2A	Q86YP4	ΔIBB	4	1,63394
GATAD2B	Q8WXI9	WT	1	n.a.
GATAD2B	Q8WXI9	ΔIBB	1	n.a.
HDAC1	Q13547	WT	2	n.a.
HDAC1	Q13547	ΔIBB	2	n.a.
HNRNPAB	Q99729	WT	1	1,01977
ILF3	Q12906	WT	1	1,17492
IRS4	O14654	WT	1	n.a.
KPNA1	P52294	WT	3	n.a.
KPNA6	O60684	WT	28	3,16549
KPNA6	O60684	ΔIBB	28	2,86200
KPNB1	Q14974	WT	14	3,11348
LMNA	P02545	ΔIBB	5	1,40299
LMNB1	P20700	WT	33	1,56301
LMNB1	P20700	ΔIBB	33	1,57396
LMNB2	Q03252	WT	23	1,12882
LMNB2	Q03252	ΔIBB	23	1,27804
MCM3	P25205	ΔIBB	1	n.a.
MRPS7	Q9Y2R9	ΔIBB	1	n.a.
MTA1	Q13330	WT	1	n.a.
MTA2	O94776	ΔIBB	8	1,14091

MTDH	Q86UE4	WT	1	n.a.
MYCBP2	O75592	ΔIBB	1	n.a.
MYH10	P35580	WT	34	1,15350
MYH14	Q7Z406	WT	2	n.a.
MYH9	P35579	WT	42	1,35797
MYL6	P60660	WT	4	1,43260
NF2	P35240	WT	1	n.a.
NUP50	Q9UKX7	WT	15	2,74362
NUP50	Q9UKX7	ΔIBB	15	1,98236
NUP93	Q8N1F7	WT	1	n.a.
PISD	Q9UG56	WT	1	n.a.
POM121C;POM121	A8CG34;Q96HA1	WT	1	n.a.
RAB6B;RAB6A;RAB39A	Q9NRW1;P20340;Q14964	WT	1	n.a.
RBBP4;RBBP7	Q09028;Q16576	WT	1	3,23337
RBBP4;RBBP7	Q09028;Q16576	ΔIBB	1	2,66485
RPL14	P50914	WT	2	1,02103
SLC25A13	Q9UJS0	WT	3	n.a.
SMARCA4;SMARCA2	P51532;P51531	ΔIBB	2	n.a.
SMARCA5	O60264	ΔIBB	10	1,56394
SMARCC2	Q8TAQ2	ΔIBB	1	n.a.
SPTBN1	Q01082	WT	4	2,20215
TAF4	O00268	WT	1	n.a.
TGFBRAP1	Q8WUH2	ΔIBB	1	n.a.
TRIM28	Q13263	WT	8	1,29490
TRIM28	Q13263	ΔIBB	8	1,53192

Table 39: Gene Ontology (GO) enrichment analysis of importin-α7 (WT, ΔIBB) interaction partners in uninfected cells (Mock). Shown are the Top10 enriched GO terms for *Molecular Function*, *Biological Process* and *Cellular Component*, each sorted by their respective *p* values.

Molecular function

ID	Name	*p* value
GO:0031491	nucleosome binding	3,38E-08
GO:0008139	nuclear localization sequence binding	3,86E-08
GO:0005048	signal sequence binding	1,98E-06
GO:0031492	nucleosomal DNA binding	4,61E-06
GO:0003682	chromatin binding	3,18E-05
GO:0017056	structural constituent of nuclear pore	6,68E-04
GO:0031490	chromatin DNA binding	7,18E-04
GO:0016866	intramolecular transferase activity	1,63E-03
GO:0035326	cis-regulatory region binding	2,39E-03
GO:0044877	protein-containing complex binding	3,49E-03

Biological process

ID	Name	*p* value
GO:0075733	intracellular transport of virus	8,51E-10
GO:0046794	transport of virus	1,51E-09
GO:0034504	protein localization to nucleus	4,12E-09
GO:0006606	protein import into nucleus	5,16E-09
GO:0044766	multi-organism transport	7,53E-09
GO:1902579	multi-organism localization	7,53E-09
GO:0051170	import into nucleus	1,70E-08
GO:0043044	ATP-dependent chromatin remodeling	3,44E-08
GO:0006913	nucleocytoplasmic transport	6,26E-08
GO:0051169	nuclear transport	6,85E-08

Cellular component

ID	Name	*p* value
GO:0016581	NuRD complex	6,00E-15
GO:0090545	CHD-type complex	6,00E-15
GO:0090568	nuclear transcriptional repressor complex	1,78E-14
GO:1904949	ATPase complex	1,29E-12
GO:0070603	SWI/SNF superfamily-type complex	2,24E-12
GO:0017053	transcriptional repressor complex	4,59E-10
GO:0000118	histone deacetylase complex	5,07E-09
GO:0018995	host cellular component	7,10E-09
GO:0043657	host cell	7,10E-09
GO:0005643	nuclear pore	3,81E-08

Table 40: Gene Ontology (GO) enrichment analysis of importin-α7 (WT, ΔIBB) interaction partners in influenza (A/WSN/33, $PB2_{627K}$) infected cells. Shown are the Top10 enriched GO terms for *Molecular Function*, *Biological Process* and *Cellular Component*, each sorted by their respective *p* values.

Molecular function

ID	Name	*p* value
GO:0031491	nucleosome binding	3,34E-06
GO:0008139	nuclear localization sequence binding	8,22E-06
GO:0031492	nucleosomal DNA binding	8,53E-06
GO:0042623	ATPase activity, coupled	1,01E-05
GO:0030898	actin-dependent ATPase activity	5,03E-05
GO:0003682	chromatin binding	1,05E-04
GO:0005048	signal sequence binding	2,05E-04
GO:0003713	transcription coactivator activity	3,38E-04
GO:0044877	protein-containing complex binding	4,19E-04

GO:0016887	ATPase activity	5,37E-04

Biological process

ID	Name	*p* value
GO:0043044	ATP-dependent chromatin remodeling	1,60E-09
GO:0075733	intracellular transport of virus	1,38E-07
GO:0046794	transport of virus	2,26E-07
GO:0006606	protein import into nucleus	4,34E-07
GO:0044766	multi-organism transport	9,09E-07
GO:1902579	multi-organism localization	9,09E-07
GO:0006338	chromatin remodeling	1,20E-06
GO:0051170	import into nucleus	1,25E-06
GO:0016032	viral process	3,09E-06
GO:0017038	protein import	4,86E-06

Cellular component

ID	Name	*p* value
GO:1904949	ATPase complex	7,28E-14
GO:0070603	SWI/SNF superfamily-type complex	8,63E-14
GO:0016581	NuRD complex	5,58E-12
GO:0090545	CHD-type complex	5,58E-12
GO:0090568	nuclear transcriptional repressor complex	8,38E-12
GO:0017053	transcriptional repressor complex	6,11E-08
GO:0005635	nuclear envelope	3,28E-07
GO:0000118	histone deacetylase complex	6,44E-07
GO:0018995	host cellular component	8,63E-07
GO:0043657	host cell	8,63E-07

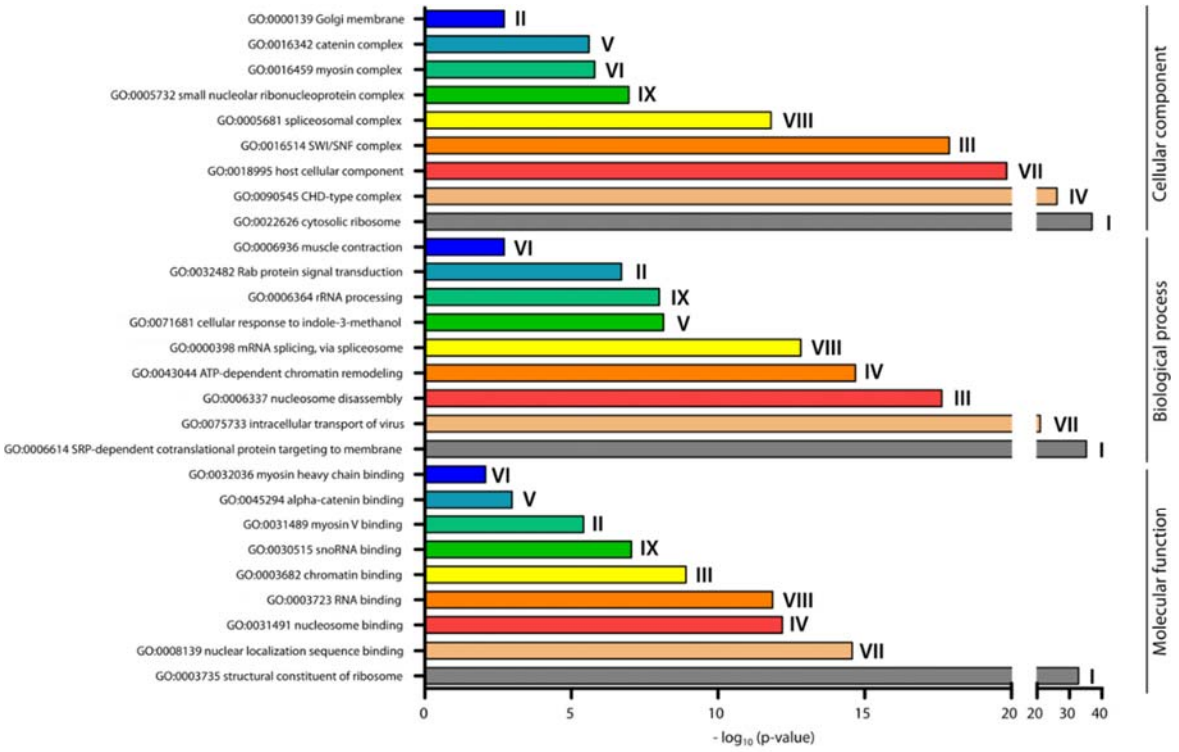

Figure 45: Gene ontology (GO) enrichment analysis of clusters of importin-α1, -α5 and -α7 interacting cellular proteins in uninfected cells. Cellular proteins presented in the identified clusters of importin-α interaction partners (I – IX) were subjected to GO analysis (Molecular function, Biological process, Cellular component). GO terms (and identifiers) were sorted according to the associated *p*-value.

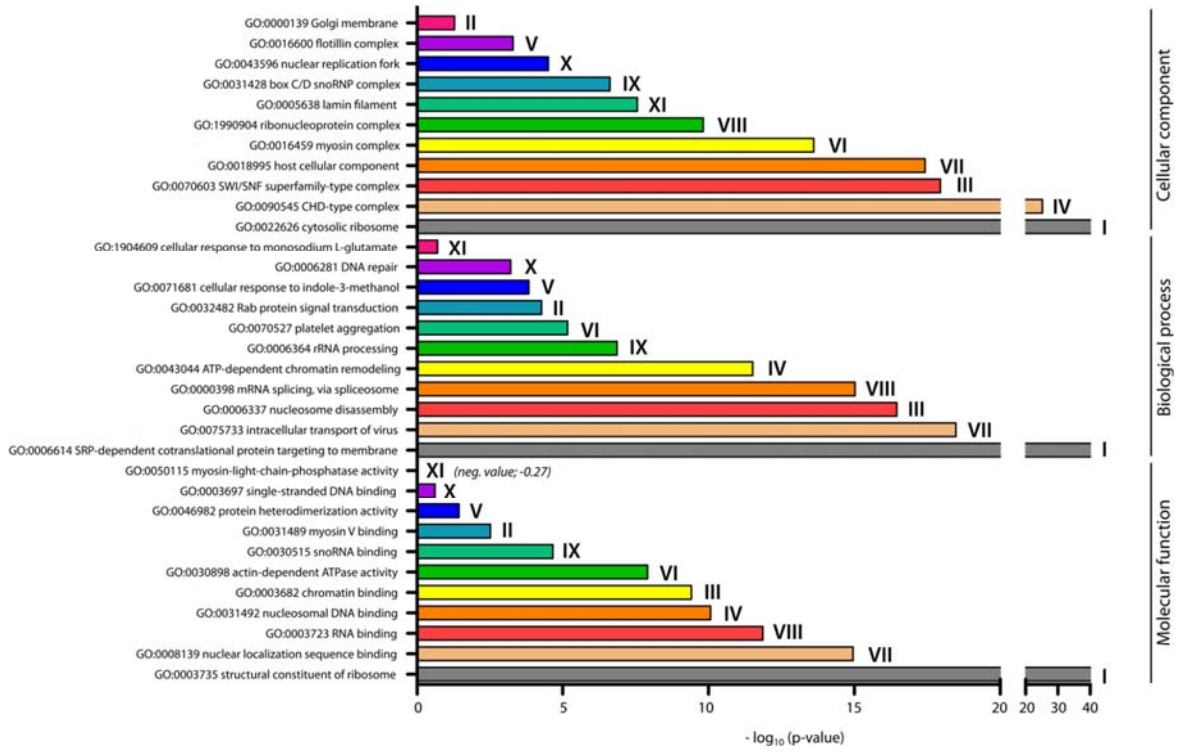

Figure 46: Gene ontology (GO) enrichment analysis of clusters of importin-α1, -α5 and -α7 interacting cellular proteins in influenza infected cells. Cellular proteins presented in the identified clusters of importin-α interaction partners (I – XI) were subjected to GO analysis (Molecular function, Biological process, Cellular component). GO terms (and identifiers) were sorted according to the associated *p*-value.

8.3 Supplemental information accompanying chapter 5.3

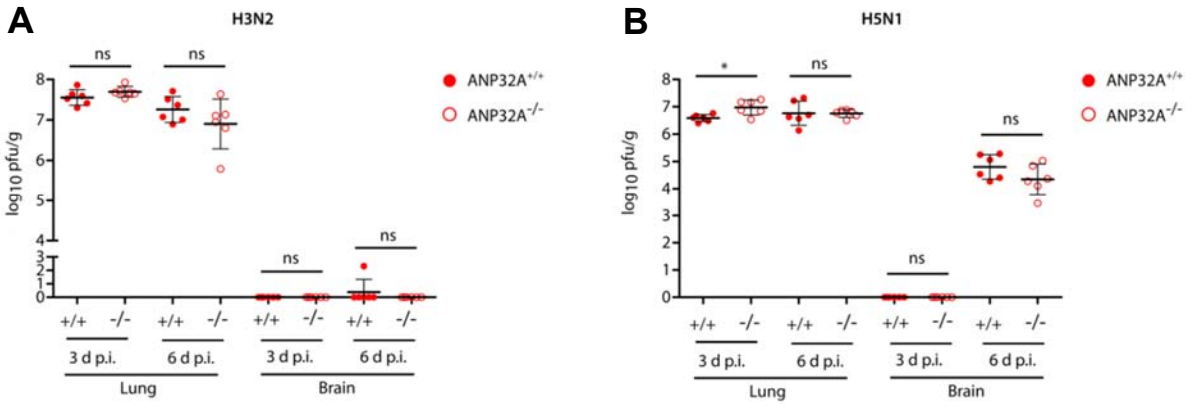

Figure 47: Knockout of ANP32A does not affect influenza A virus replication in mice. ANP32A$^{+/+}$ and ANP32A$^{-/-}$ mice were either control treated with PBS or infected with 10^3 pfu of a seasonal H3N2 subtype (**A**) or a highly pathogenic H5N1 human isolate (**B**). Viral titers were determined 3 and 6 days p.i. in lung and brain of infected animals. No virus was detected in PBS infected mice (n = 5). Presented are individual organ titers for each animal as well as the means ± SD for each group (n = 5-6). Statistically significant differences were calculated using the two-tailed Student's *t*-test (*p < 0.05; ns, not significant).

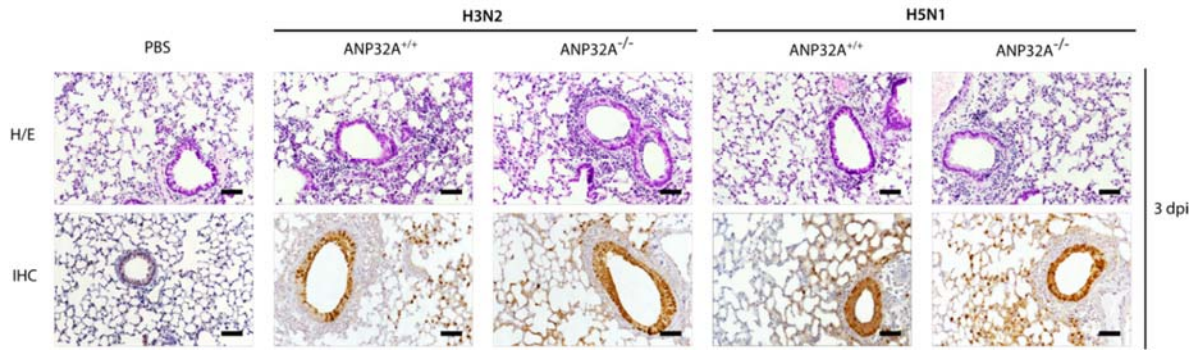

Figure 48: Absence of ANP32A does not affect viral replication or cell tropism in the murine lung. ANP32A$^{+/+}$ and ANP32A$^{-/-}$ mice were either control treated with PBS or infected with 10^3 pfu of a seasonal H3N2 subtype or a highly pathogenic H5N1 human isolate. At 3 d p.i., lungs from infected animals were removed and immunohistochemically (IHC) stained for viral NP antigen. Additionally, hematoxylin and eosin (H/E) staining was performed. Shown are representative images for each group (n = 5). Scale bar represents 10 µm. Original magnification, 10x**.**

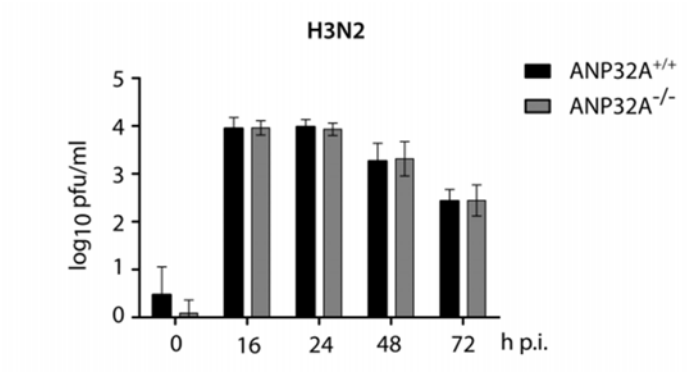

Figure 49: H3N2 IAV replication in ANP32A$^{+/+}$ and ANP32A$^{-/-}$ murine lung fibroblast cells. Murine lung fibroblasts with a deleted ANP32A gene were infected with H3N2 IAV over a time period of 72 h. Viral titers were determined by plaque test on MDCK cells at the indicated time points. n = 3 independent experiments. No statistical significant differences were observed.

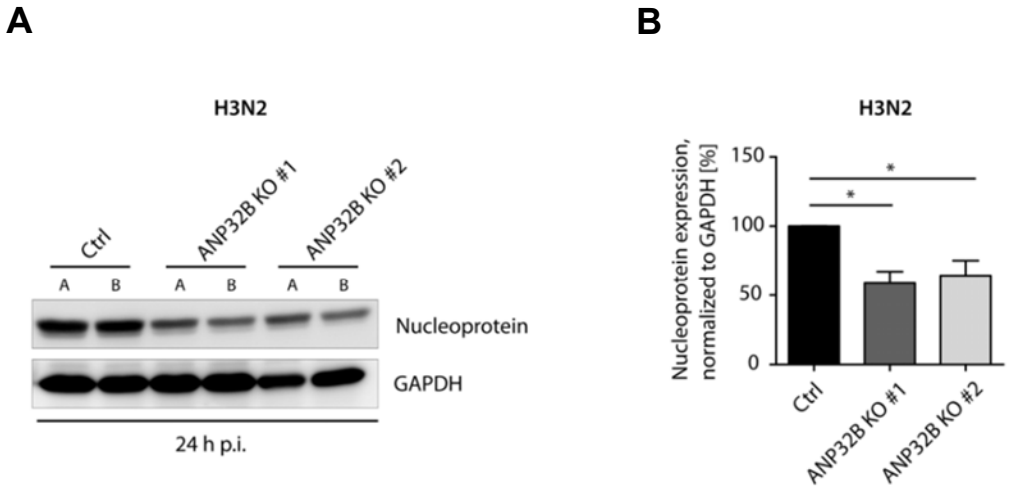

Figure 50: Viral nucleoprotein expression is reduced in ANP32B knockout human HeLa cells. **A**, Expression of viral nucleoprotein (NP) in H3N2 infected HeLa cell lines deficient for ANP32B was analyzed by Western blotting at 24 h p.i. (in duplicates, A and B). Two different knockout cell lines were used to exclude clonal artefacts (ANP32B KO #1 and ANP32B KO #2, respectively). Cells treated with a CRISPR/Cas construct expressing a non-targeting guide RNA were used as control (Ctrl). GAPDH was detected as loading control. **B**, Quantification of viral NP expression from two independent experiments was performed using ImageJ software and normalization to the GAPDH loading control. Statistical significant differences were determined using the two-tailed Student's *t*-test (*p < 0.05). n = 2 independent experiments.

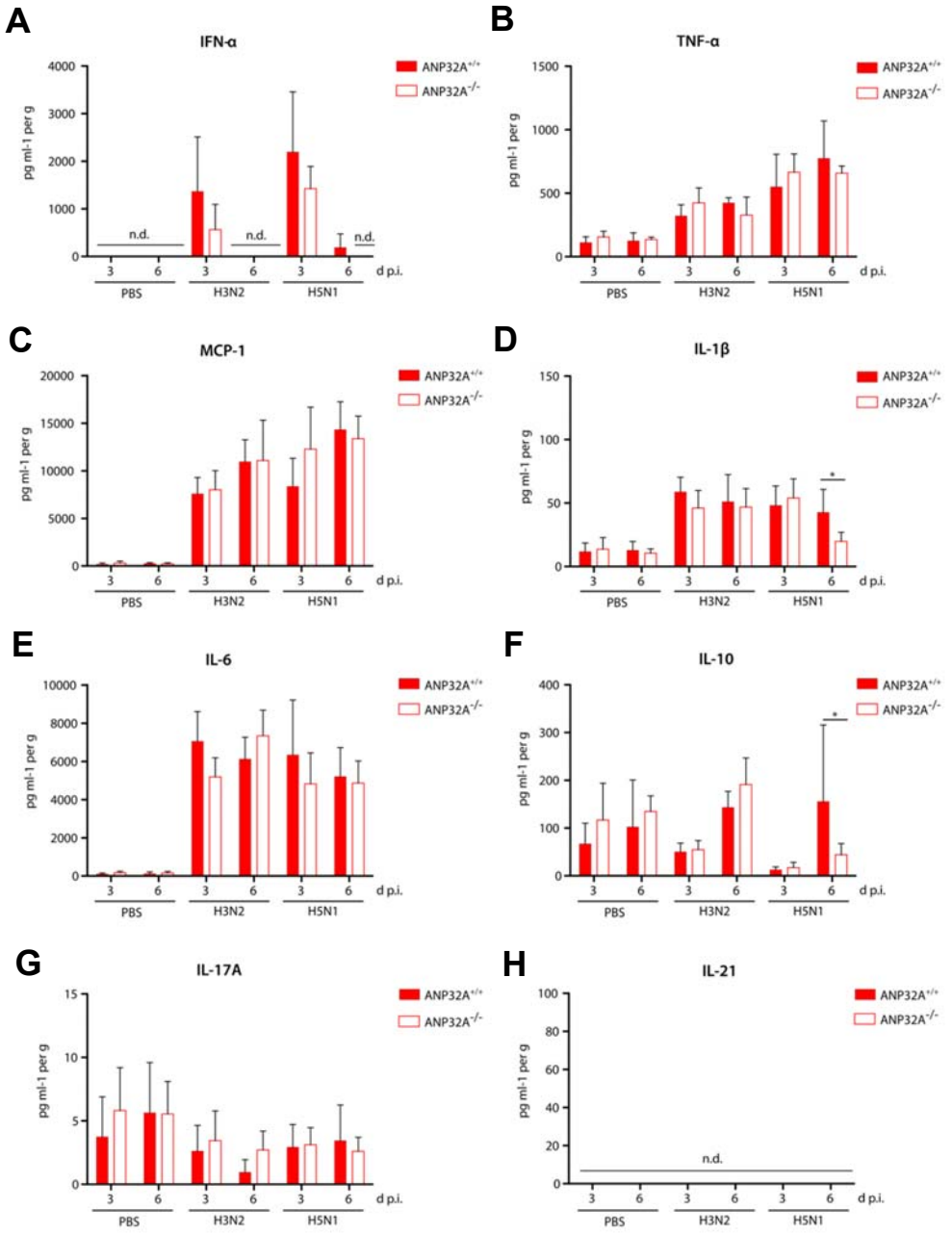

Figure 51: Comparable cytokine and chemokine response in IAV infected ANP32A$^{+/+}$ and ANP32A$^{-/-}$ mice. A-H, ANP32A$^{+/+}$ and ANP32A$^{-/-}$ mice were either control treated with PBS or infected with 10^3 pfu of a seasonal H3N2 subtype or a highly pathogenic H5N1 human isolate. At 3 and 6 d p.i., cytokine/chemokine expression levels were determined in lung homogenates using a multiplex immunoassay. Interferon-α (**A**, IFN-α), tumor necrosis factor α (**B**, TNF-α), monocyte chemotactic protein 1 (**C**, MCP-1), interleukin 1β (**D**, IL-1β), interleukin 6 (**E**, IL-6), interleukin 10 (**F**, IL-10), interleukin 17A (**G**, IL-17A), and interleukin 21 (**H**, IL-21). Presented are the concentrations measured for each cytokine/chemokine as mean ± SD for each group (n = 5-7). Statistical significance was calculated using two-way ANOVA with Bonferroni post-test (* $p < 0.05$; n.d., not detected).

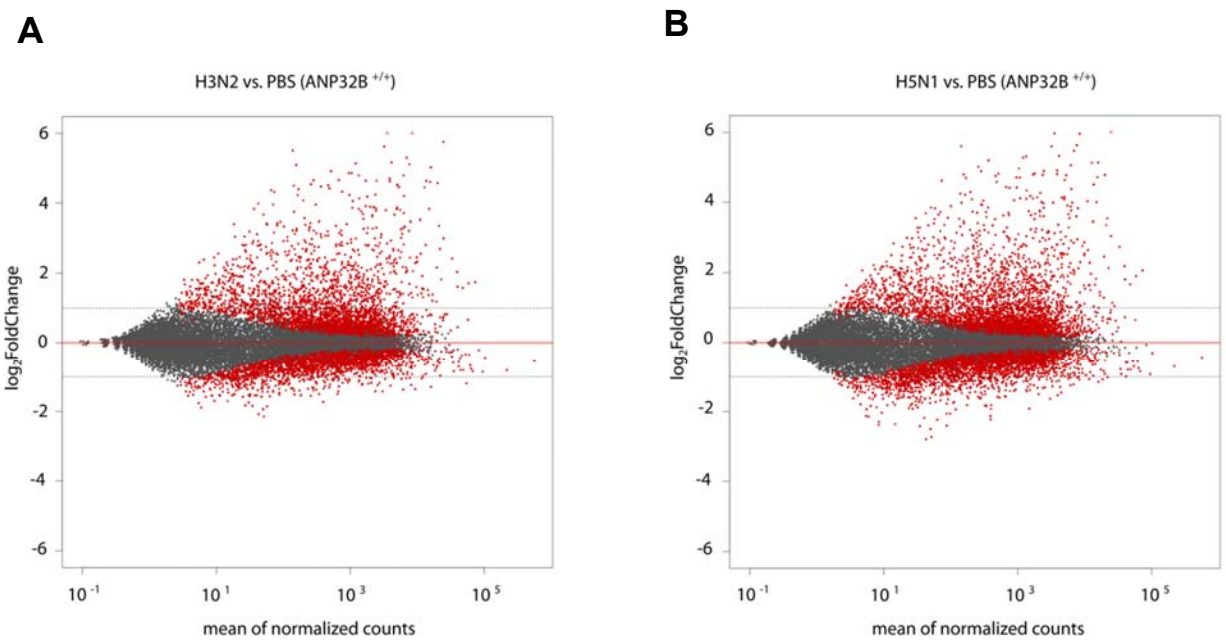

Figure 52: Differentially regulated genes in influenza A virus infected ANP32B$^{+/+}$ mice. A and B, ANP32B$^{+/+}$ mice were either control treated with PBS or infected with 10^3 pfu of a seasonal H3N2 subtype (**A**) or a highly pathogenic H5N1 human isolate (**B**). At 3 d p.i., lungs were removed, total RNA was isolated and subjected to next generation sequencing. Shown is a MA plot analysis of all differentially regulated genes in PBS vs. IAV infected ANP32B$^{+/+}$ mice at 3 d p.i., plotted as log2FoldChange over the mean of normalized counts for each experimental group (n = 3 animals per group). Cut-off (log2FoldChange ≥ 1 or ≤ -1) for significantly disregulated genes is indicated with dashed lines. (**A**) H3N2 infection vs. PBS control in ANP32B$^{+/+}$ mice; (**B**) H5N1 infection vs. PBS control in ANP32B+/+ mice.

Table 41: Significantly upregulated genes (Top20) in PBS vs. H3N2 infected ANP32B$^{+/+}$ mice at 3 days post infection, sorted by log2FoldChange (log2FC).

No.	Gene	Entrez ID	Uniprot ID	log2FC (≥ +1)
1	Mx1	4599	P09922	6,114
2	Cxcl10	15945	P17515	6,010
3	Irf7	54123	Q92985	5,748
4	Oasl1	231655	Q8VI94	5,617
5	Ifnb1	15977	P01575	5,504
6	Isg15	100038882	Q64339	5,294
7	Oas3	246727	Q8VI93	5,158
8	Ccl7	20306	Q03366	5,135
9	Apod	11815	P51910	5,106
10	Sectm1a	209588	Q921W8	5,086
11	Ifit1	15957	Q64282	5,016
12	Apol9a	223672	Q6PF90	4,910
13	Mx2	17858	Q9WVP9	4,855
14	Ifi211	381308	P0DOV1	4,853
15	Zbp1	58203	O88477	4,787
16	Tgtp1	21822	Q62293	4,786
17	Ifit1bl1	667373	E9PXF7	4,696
18	Trim30c	434219	D3YVI9	4,654
19	Ifi205	226695	Q8CGE8	4,637
20	Ccl2	20296	P10148	4,636

Table 42: Significantly downregulated genes (Top20) in PBS vs. H3N2 infected ANP32B$^{+/+}$ mice at 3 days post infection, sorted by log2FoldChange (log2FC).

No.	Gene	Entrez ID	Uniprot ID	log2FC (≤ -1)
1	Gsg1l	269994	D3Z7H4	-2,145
2	Cd209a	170786	Q91ZX1	-2,076
3	Hepacam2	101202	Q4VAH7	-1,936
4	Vstm2b	58188	Q9JME9	-1,886
5	Calml3	70405	Q9D6P8	-1,861
6	Acaa1b	235674	Q8VCH0	-1,842
7	Cd209c	170776	Q91ZW9	-1,764
8	Zmat4	320158	Q8BZ94	-1,743
9	Scn3a	20269	A2ASI5	-1,725
10	Cntn4	269784	Q69Z26	-1,700
11	Pck1	18534	Q9Z2V4	-1,575
12	Ces2b	234669	Q6PDB7	-1,561
13	Sept3	24050	Q9Z1S5	-1,558
14	Wfdc16	277345	Q5DQQ4	-1,551
15	Bex2	12069	Q9WTZ8	-1,548
16	Angptl7	654812	Q8R1Q3	-1,540
17	Lsamp	268890	Q8BLK3	-1,539
18	Fabp1	14080	P12710	-1,539
19	Wnt10b	22410	P48614	-1,535
20	Ces2e	234673	Q8BK48	-1,528

Table 43: Significantly upregulated genes (Top20) in PBS vs. H5N1 infected ANP32B$^{+/+}$ mice at 3 days post infection, sorted by log2FoldChange (log2FC).

No.	Gene	Entrez ID	Uniprot ID	log2FC (≥ +1)
1	Irf7	54123	Q92985	6,062
2	Mx1	4599	P09922	5,966
3	Cxcl10	15945	P17515	5,960
4	Apod	11815	P51910	5,626
5	Orm2	18406	P07361	5,603
6	Oasl1	231655	Q8VI94	5,595
7	Isg15	100038882	Q64339	5,472
8	Oas3	246727	Q8VI93	5,321
9	Tgtp1	21822	Q62293	5,313
10	Ccl7	20306	Q03366	5,273
11	Gbp10	626578	Q000W5	5,196
12	Ifit1	15957	Q64282	5,134
13	Saa3	20210	P04918	5,124
14	Zbp1	58203	O88477	5,058
15	Sectm1b	58210	Q9JL59	5,012
16	Ifi211	381308	P0DOV1	4,963
17	Ifi204	15951	P0DOV2	4,913
18	Ifi205	226695	Q8CGE8	4,891
19	Trim30c	434219	D3YVI9	4,887
20	Apol9a	223672	Q8VDU3	4,816

Table 44: Significantly downregulated genes (Top20) in PBS vs. H5N1 infected ANP32B$^{+/+}$ mice at 3 days post infection, sorted by log2FoldChange (log2FC).

No.	Gene	Entrez ID	Uniprot ID	log2FC (≤ -1)
1	Cd209a	170786	Q91ZX1	-2,794
2	Gsg1l	269994	D3Z7H4	-2,725
3	Hepacam2	101202	Q4VAH7	-2,504
4	Acaa1b	235674	Q8VCH0	-2,419
5	Ackr4	252837	Q924I3	-2,406
6	Cd209f	69142	Q4KL16	-2,364
7	Cd209d	170779	Q91ZW8	-2,297
8	Sept3	24050	Q9Z1S5	-2,235
9	Scn3a	20269	A2ASI5	-2,224
10	Fabp1	14080	P12710	-2,185
11	Vstm2b	58188	Q9JME9	-2,142
12	Nptx1	18164	Q62443	-2,131
13	Cd209c	170776	Q91ZW9	-2,127
14	Cr2	12902	P19070	-2,058
15	Cntn4	269784	Q69Z26	-2,037
16	Gdf10	14560	P97737	-1,940
17	Crabp1	12903	P62965	-1,935
18	Colq	382864	O35348	-1,926
19	Hmcn1	545370	D3YXG0	-1,917
20	Ano5	233246	Q75UR0	-1,901

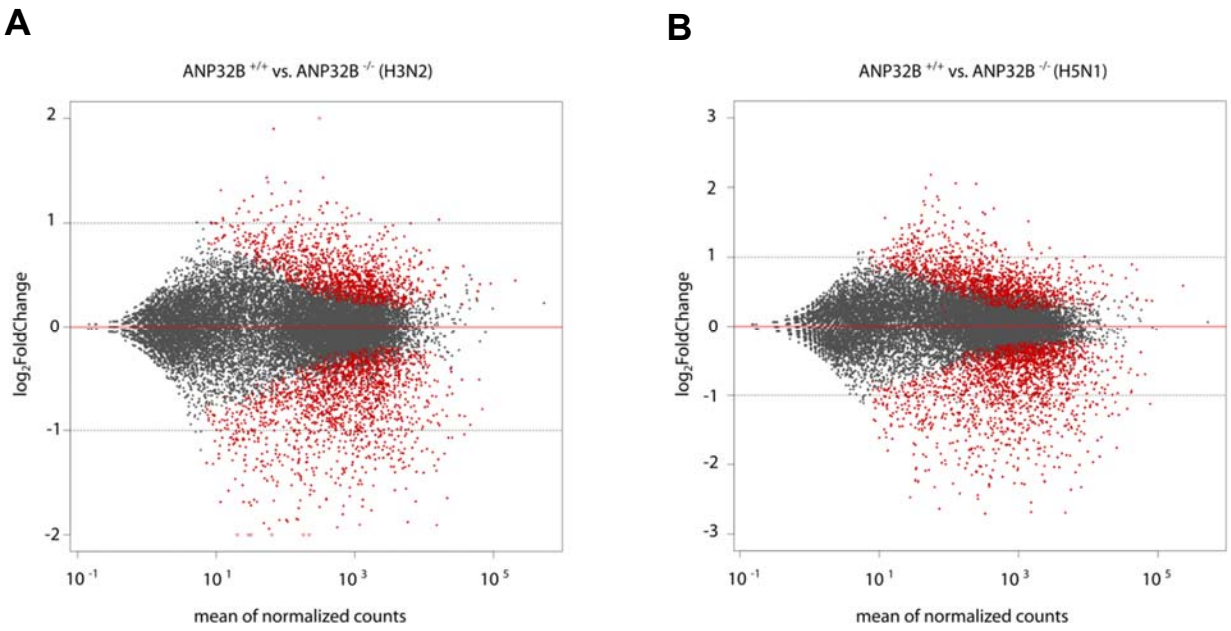

Figure 53: Differentially regulated genes in influenza A virus infected ANP32B$^{+/+}$ versus ANP32B$^{-/-}$ mice. A and B, ANP32B$^{+/+}$ and ANP32B$^{-/-}$ mice were either control treated with PBS or infected with 10^3 pfu of a seasonal H3N2 subtype (**A**) or a highly pathogenic H5N1 human isolate (**B**). At 3 d p.i., lungs were removed, total RNA was isolated and subjected to next generation sequencing. Shown is a MA plot analysis of all differentially regulated genes in IAV infected ANP32B$^{+/+}$ and ANP32B$^{-/-}$ mice at 3 d p.i., plotted as log2FoldChange over the mean of normalized counts for each experimental group (n = 3 animals per group). Cut-off (log2FoldChange ≥ 1 or ≤ -1) for significantly disregulated genes is indicated with dashed lines. (**A**) H3N2 infection in ANP32B$^{+/+}$ vs. ANP32B$^{-/-}$ mice; (**B**) H5N1 infection in ANP32B$^{+/+}$ vs. ANP32B$^{-/-}$ mice.

Table 45: Significantly upregulated genes (Top20) in H3N2 infected ANP32B$^{+/+}$ vs. ANP32B$^{-/-}$ mice at 3 days post infection, sorted by log2FoldChange (log2FC).

No.	Gene	Entrez ID	Uniprot ID	log2FC (≥ +1)
1	Esr1	13982	P19785	2,076
2	Cd209a	170786	Q91ZX1	1,898
3	Hykk	235386	Q5U5V2	1,431
4	Gsg1l	269994	D3Z7H4	1,430
5	Hes2	15206	O54792	1,386
6	Fam124b	241128	Q8BLQ0	1,383
7	Crabp1	12903	P62965	1,314
8	Cttnbp2	30785	B9EJA2	1,309
9	Adamts17	233332	D3YX90	1,281
10	Gprasp2	245607	Q8BUY8	1,256
11	Akr1b7	11997	P21300	1,215
12	Ackr4	252837	Q924I3	1,209
13	Tet1	52463	Q3URK3	1,205
14	Tril	66873	Q9DBY4	1,198
15	Glp1r	14652	O35659	1,192
16	Scn3a	20269	A2ASI5	1,190
17	Cyp26b1	232174	Q811W2	1,183
18	Cyp1a1	13076	P00184	1,170
19	Colgalt2	269132	Q6NVG7	1,163
20	Pgr	18667	Q00175	1,161

Table 46: Significantly downregulated genes (Top20) in H3N2 infected ANP32B$^{+/+}$ vs. ANP32B$^{-/-}$ mice at 3 days post infection, sorted by log2FoldChange (log2FC).

No.	Gene	Entrez ID	Uniprot ID	log2FC (≤ -1)
1	Syt8	55925	Q9R0N6	-2,437
2	Rasl10b	276952	Q5SSG5	-2,412
3	Ifna4	15967	P07351	-2,252
4	Serpina3m	20717	Q03734	-2,140
5	Ubd	24108	P63072	-2,118
6	Pou3f1	18991	P21952	-2,081
7	Cngb3	30952	Q9JJZ9	-1,940
8	Alpl	11647	P09242	-1,928
9	Retnla	57262	Q9EP95	-1,906
10	Anp32b	67628	Q9EST5	-1,901
11	Ifnl2	330496	Q4VK74	-1,887
12	Apod	11815	P51910	-1,879
13	Cxcl3	330122	Q6W5C0	-1,872
14	Orm2	18406	P07361	-1,858
15	Chl1	12661	P70232	-1,855
16	Sectm1a	209588	Q921W8	-1,854
17	Rtn4rl2	269295	Q7M6Z0	-1,846
18	Serpina3f	238393	Q80X76	-1,801
19	Il18bp	16068	Q9Z0M9	-1,763
20	Pla1a	85031	Q8VI78	-1,741

Table 47: Significantly upregulated genes (Top20) in H5N1 infected ANP32B$^{+/+}$ vs. ANP32B$^{-/-}$ mice at 3 days post infection, sorted by log2FoldChange (log2FC).

No.	Gene	Entrez ID	Uniprot ID	log2FC (≥ +1)
1	Cd209a	170786	Q91ZX1	2,176
2	Igkv6-15	108022	A0A140T8M5	2,054
3	Esr1	13982	P19785	2,048
4	Gsg1l	269994	D3Z7H4	1,995
5	Ackr4	252837	Q924I3	1,872
6	Ighv1-64	380823	A0A075B5X3	1,826
7	Hepacam2	101202	Q4VAH7	1,805
8	Ighv1-18	28468	A0A0A6YXN4	1,755
9	Pla2g2d	18782	Q9WVF6	1,737
10	Itgae	16407	Q60677	1,711
11	Glp1r	14652	O35659	1,701
12	Sept3	24050	Q9Z1S5	1,652
13	Nptx1	18164	Q62443	1,649
14	Snhg11	319317	Q4G0K9	1,620
15	Sptssb	66183	Q925E8	1,603
16	Cd209d	170779	Q91ZW8	1,565
17	Ighv5-17	780794	A0A075B5R1	1,527
18	Hmcn1	545370	D3YXG0	1,516
19	Slc7a10	53896	P63115	1,512
20	Gdf10	14560	P97737	1,512

Table 48: Significantly downregulated genes (Top20) in H5N1 infected ANP32B$^{+/+}$ vs. ANP32B$^{-/-}$ mice at 3 days post infection, sorted by log2FoldChange (log2FC)

No.	Gene	Entrez ID	Uniprot ID	log2FC (≤ -1)
1	Il1r2	16178	P27931	-2,702
2	Slfn4	20558	Q3UV10	-2,690
3	Acod1	16365	P54987	-2,678
4	Ccl2	20296	P10148	-2,541
5	Ido1	15930	P28776	-2,487
6	Pou3f1	18991	P21952	-2,465
7	Adamts4	240913	Q8BNJ2	-2,435
8	Tarm1	245126	B6A8R8	-2,410
9	Ly6c2	100041546	P0CW03	-2,356
10	Apod	11815	P51910	-2,319
11	Ifnb1	15977	P01575	-2,319
12	Serpina3m	20717	Q03734	-2,308
13	Serpina3f	238393	Q80X76	-2,277
14	Adgrb1	107831	Q3UHD1	-2,267
15	Ccl7	20306	Q03366	-2,264
16	Il1b	16176	P10749	-2,262
17	Ifi205	226695	Q8CGE8	-2,240
18	Rhcg	56315	Q9QXP0	-2,225
19	Gbp10	626578	Q29RG2	-2,191
20	Clec4e	56619	Q9R0Q8	-2,178

9. Danksagung

In erster Linie möchte ich mich ganz herzlich bei Prof. Dr. Gülşah Gabriel für die Aufnahme in die Arbeitsgruppe und die Bereitstellung dieses hochinteressanten Forschungsprojekts bedanken. Ich habe mich jederzeit sehr wohl gefühlt und unglaublich viel gelernt, was im Laufe meiner angestrebten akademischen Karriere von großer Bedeutung sein wird. Die Förderung als junger Wissenschaftler war stets exzellent - sei es durch das Ermöglichen der Teilnahme an wissenschaftlichen Kongressen im In- und Ausland oder durch stetige Motivation und Ratschläge in jeder Situation. Ich weiß das sehr zu schätzen. In diesem Sinne: Vielen Dank für alles, Gülşah!

Dr. Stephanie Stanelle-Bertram möchte ich in aller Form meine Dankbarkeit für die exzellente Betreuung seit meiner Masterarbeit aussprechen. Mir wurde zu jeder Tages- und manchmal auch Nachtzeit immer ein offenes Ohr zuteil, trotz manchmal doch sehr knapp bemessener Zeit. Das detaillierte Einarbeiten ins Labor, die unzähligen, teilweise stundenlangen wissenschaftlichen Diskussionen, die geduldige Beantwortung aller meiner Fragen, sowie die kritische Korrektur meiner Doktorarbeit sind dabei nur ein Bruchteil der unermüdlichen Unterstützung, die ich erfahren habe. To cut a long story short: Thank you, Steffi, for everything!

Prof. Dr. Gülşah Gabriel, Prof. Dr. Michael Kolbe und Prof. Dr. Martin Schwemmle danke ich herzlich für die Bereitschaft zur schriftlichen Begutachtung dieser Arbeit.

Prof. Dr. Wolfram Brune, Prof. Dr. Nina Schützenmeister und Prof. Dr. Gülşah Gabriel möchte ich herzlich danken für die Bereitschaft in der Prüfungskommission meiner Disputation mitzuwirken.

Bei Martin Zickler möchte ich mich in aller Form für die Unterstützung bei Experimenten im Labor bedanken. Darüber hinaus bedanke ich mich für die unzähligen Diskussionen, auch manchmal komplett unwissenschaftlicher Natur, die die Arbeit so wunderbar aufgelockert haben. Herzlichen Dank auch für die Korrektur von Teilen meiner Doktorarbeit.

Ein großes Dankeschön möchte ich an Annette Gries aussprechen, die mich bei unzähligen Tierexperimenten sowie darüber hinaus tatkräftig unterstützt hat – immer mit einem Grinsen auf dem Gesicht, auch nach 4-5 Stunden Arbeit im BLS-3 Labor. Annette, du bist ne‘ coole Socke!

Weiterhin möchte ich mich ganz herzlich bei Ulla Müller und allen Mitarbeitern der Technologie-Plattform „*Small Animal Models*“ bedanken. Ohne eure unermüdliche Arbeit wäre ein großer Teil dieser Studie nicht möglich gewesen. Vielen Dank!

Hanna Jania, Gundula Pilnitz-Stolze und insbesondere Zacharias Müller möchte ich für die hervorragende experimentelle Unterstützung bei den durchgeführten Versuchen bedanken. Ohne euch wären meine Arbeitszeiten vermutlich noch um ein Vielfaches länger ausgefallen. Danke, dass ihr mich davor bewahrt habt.

Dr. Vinícius Pinho dos Reis möchte für das große Engagement und die tatkräftige Unterstützung bei der Auswertung von Histologie-Bildern bedanken.

Ganz herzlich möchte ich mich bei allen Kolleginnen und Kollegen der Arbeitsgruppe *Virale Zoonosen – One Health* für die wundervollen Jahre der Zusammenarbeit bedanken - und natürlich für die stetige Bereitschaft als BSL-3 Backup zu fungieren, auch am Wochenende. Dazu zählen natürlich auch unsere ehemaligen Labormitglieder: Patricia, Swantje, Carola – Ihr seid nicht vergessen!

Ich bedanke mich zudem bei der Technologie-Plattform „*Next Generation Sequencing*“ und allen dahinterstehenden Mitarbeiterinnen und Mitarbeitern für die Unterstützung der in dieser Arbeit durchgeführten Transkriptom-Analysen.

Unseren HPI-internen Kollegen Prof. Dr. Joachim Hauber und PD Dr. Jan Chemnitz danke ich für die Bereitstellung der ANP32B-Knockout-Mäuse.

Für die exzellente Durchführung und Auswertung der Massen-Spektrometrie-Analysen möchte mich ganz herzlich bei Prof. Dr. Hartmut Schlüter sowie insbesondere Dr. Christoph Krisp vom Universitätscampus Hamburg-Eppendorf (UKE) bedanken. Weiterhin gilt mein Dank unseren Kollaborationspartnern Dr. Thorsten Klingen und Prof. Dr. Alice McHardy vom Helmholtz Zentrum für Infektionsforschung in Braunschweig für die Durchführung des *in silico* Modellings.

Für die Förderung und Finanzierung meiner Doktorarbeit möchte ich mich ganz herzlich bei der Studienstiftung des Deutschen Volkes bedanken. Zudem gebührt mein Dank Prof. Gabriel für den überaus fairen Aufstockungsvertrag, den ich erhalten habe. Dies ist keine Selbstverständlichkeit, daher vielen Dank dafür.

Zu guter Letzt möchte ich mich bei den Personen bedanken, die mir im Leben am Wichtigsten sind:

Mein größter Dank geht dabei an meine Eltern sowie meine Großeltern, die mich seit Beginn meines Studiums finanziell aber auch mit Wort und Ratschlag unterstützt haben. Ihr habt immer an mich geglaubt, mich stets motiviert, und mich auch mal gebremst, wenn mein Dickkopf die Überhand zu gewinnen drohte. Ohne euch wäre ich nicht dort, wo ich heute bin, und dafür bin ich unendlich dankbar!

Bei meiner Lebensgefährtin Nadja Bork bedanke ich mich aus tiefstem Herzen für ihre Liebe, Zuneigung und Unterstützung, ihren Zuspruch und Trost, sowie ihr Verständnis und ihre Geduld über den gesamten Zeitraum meiner Promotion. Vielen Dank auch dafür, dass du mir immer wieder meine kleinen Macken verzeihst und mich stets auf den Boden der Tatsachen zurückholst.

Abschließend möchte ich mich bei meinem Bruder Fabian bedanken, von dem ich leider viel zu früh Abschied nehmen musste. Während ich dir ein Vorbild sein konnte, so hast du mir immer wieder gezeigt, was wirklich im Leben wichtig ist: Hilfsbereitschaft, Kampfgeist und niemals aufzugeben, egal wie viele Steine einem auch in den Weg gelegt werden. Und dazu noch immer mit einem Lächeln auf dem Gesicht.

Fabi, diese Doktorarbeit widme ich dir. Ich werde dich nie vergessen. *RIP, little brother!*

10. Affidavit

Hiermit versichere ich an Eides statt, die vorliegende Dissertation selbst verfasst und keine anderen als die angegebenen Hilfsmittel benutzt zu haben. Die eingereichte schriftliche Fassung entspricht der auf dem elektronischen Speichermedium. Ich versichere, dass diese Dissertation nicht in einem früheren Promotionsverfahren eingereicht wurde.

05.04.2020 

Sebastian Beck